UNIVERSITY OF SOUTHAMPTON

AN INVESTIGATION INTO THE WAVE WASH AND WAVE RESISTANCE OF HIGH SPEED DISPLACEMENT SHIPS

SATTAYA CHANDRAPRABHA

Thesis submitted for the degree of Doctor of Philosophy

FLUID-STRUCTURE INTERACTION GROUP
SCHOOL OF ENGINEERING SCIENCES
FACULTY OF ENGINEERING AND APPLIED SCIENCE

March 2003

UNIVERSITY OF SOUTHAMPTON

ABSTRACT

FACULTY OF ENGINEERING AND APPLIED SCIENCE
SCHOOL OF ENGINEERING SCIENCES

Doctor of Philosophy

AN INVESTIGATION INTO THE WAVE WASH AND WAVE RESISTANCE OF HIGH SPEED DISPLACEMENT SHIPS

by Sattaya Chandraprabha

In recent years, high speed displacement ships, especially high speed displacement catamarans, have been highly utilised in many countries. As a result, the design concept of high speed displacement craft, including concerns of safety and the environment due to the impact of ship generated wave wash, has received considerable attention. This thesis investigates influences on wave resistance and wave wash generated by high speed displacement craft using experimental and numerical methods. The hull form parameters, speed, water depth and sinkage and trim were investigated.

Experimental tests on model of high speed craft have been carried out in deep and shallow water. The models used were of round bilge form with transom sterns derived from the NPL and the Series 64 round bilge series. Longitudinal wave cuts, model total resistance, sinkage and trim were measured. The effects of length to displacement ratio ($L/\nabla^{1/3}$), catamaran separation to length ratio (S/L), speed, transom immersion, shallow water and propulsion systems on wave wash and resistance were investigated. The data can be used directly for assessing the influence of the main hull parameters, speed and water depth, for the validation of theoretical wash prediction methods and for input into wave propagation models.

For the theoretical investigation, thin ship theory was used and developed in order to predict the wave pattern resistance and wave wash of slender hulls with transom sterns. In particular, the theory was extended to cover the supercritical speed range. The theoretical work included the investigation and use of transom stern corrections, establishment of a regression analysis of dynamic sinkage and trim and the investigation and use of the thin ship theory to estimate the wave profile around the hull. The theory was validated for the physical wave patterns and profiles, especially in shallow water and at supercritical speeds using the experimental results. The validation included the effects of hull form parameters, trim changes and depth Froude number on wave pattern resistance and wave profiles. It is found that numerical methods, based on the thin ship theory, can be satisfactorily employed as a simple and effective means of estimating wave pattern resistance and wave profiles with low computational effort.

The experimental and numerical investigations provide a better understanding of the basic physics of wash waves and wave resistance of high speed displacement craft, and a numerical tool which facilitates the prediction of wave wash properties for the assessment of new designs and the effects of wash on ship operation.

TABLE OF CONTENTS

ACKNOWLEDGEMENTS

The author would like to thank the following for their help:

Professor A.F. Molland, who supervised this research, for his guidance, support, encouragement, and patience.

Dr. D. J. Taunton for his help in computer programming, experiments and discussions.

Professor P.A. Wilson for his help in the experiments.

Dr. S.R. Turnock for his advice on the panel code, PALISUPAN.

Royal Thai Navy for their financial support throughout the project.

My family and in-laws for their love, patience and understanding.

Finally, my beloved wife for her love, generous support, patience and understanding.

NOMENCLATURE

A	Wetted surface area [m^2]
A_W	Wave amplitude [m]
B	Ship breadth [m]
C_F	Coefficient of frictional resistance
C_R	Coefficient of residuary resistance
C_T	Coefficient of total resistance
C_W	Coefficient of wave resistance
C_{WP}	Coefficient of wave pattern resistance
E	Wave energy
Fn	Froude Number $[U/(gL)^{1/2}]$
Fn_H	Depth Froude Number $[U/(gH)^{1/2}]$
H	Water depth [m]
k_n	Wave number
$(1+k)$	Form factor
L	Length on waterline [m]
R_R	Residuary resistance [N]
R_T	Total resistance [N]
R_W	Wave resistance [N]
S	Separation between catamaran demihull centrelines [m]
T	Ship draught [m]
U	Ship speed [m/s]
W	Channel breadth
X	Longitudinal distance [m]
Y	Transverse distance [m]
g	Acceleration due to gravity [$9.81 m/s^2$]
ρ	Density of water [kg/m^3]
σ	Source strength
θ	Wave angle
ζ	Wave elevation

ϕ	Velocity potential
∇	Displacement volume [m^3]

1. INTRODUCTION

1.1 Background to Work

In the last two to three decades, high speed craft, especially high speed displacement catamarans, have been highly utilised in many countries. As a result, the high speed craft design concept has received considerable attention in order to satisfy the design criteria of these vessels. Wave resistance plays an important role in total resistance and power prediction, which influences the design. The hull form parameters, speed and water depth can have significant effects on the wave resistance.

In addition to the wave resistance, wash generated by fast craft is also important for the design concept due to concerns of safety and the environment, such as erosion of the coastline, risk for people on beaches and for small boats in harbours, and changes in the local ecology. This has led to the need for research into the analysis of the characteristics of wash waves. The generation of ship waves is affected by speed, hull form, sinkage and trim, and shallow water and it is apparent that these effects on ship generated wash, particularly for high speed craft, need to be investigated.

Although there have been several experimental and theoretical investigations specifically into the power prediction of high speed craft, when wash is considered there are still a number of questions due to insufficient information on aspects such as the effects of hull form, speed, water depth, sinkage and trim and transom sterns. Additionally, the amount of published information available on the prediction of ship-generated wash for high speed craft is limited. As a result, these effects need further investigation both theoretically and experimentally, together with the development of tools for predicting the wave resistance and ship generated wave wash, both for applications at the preliminary design of the ship and during ship operation.

As a result of the need for more information on the wash of high speed craft, an extensive investigation has been carried out into wash waves and wave resistance of these vessels. This has entailed a number of experimental tests on models of high speed craft in deep and shallow water, together with the assessment and development of theoretical methods. The theoretical approach adopted for the wash investigation was to use thin ship theory which had already been used successfully to estimate wave resistance.

The thin ship theory is outlined in Chapter 2 together with the manner in which wave characteristics may be described. In Chapter 3, the experimental results are analysed and discussed. The effects of hull form parameters, speed, shallow water and trim changes on resistance and wave profiles have been investigated together with the effects of propulsion systems on the wave profile and running trim and sinkage.

Refinements to the theory are described in Chapter 4. The transom stern can have a significant effect on wave pattern resistance and hence wave wash, and the effect is found to depend on the transom immersion. The use of transom stern corrections for the improvement of the prediction of the wave resistance and wave profiles of ships with transom sterns has therefore been investigated and assessed. This has included the use of a virtual stern and the use of local sources and sinks near the transom. A regression analysis of existing experimental dynamic sinkage and trim has been established to provide rapid estimates, and this is described. An outline description is also given of a hybrid model of sinkage/trim which is under development in a complimentary research programme and which uses a prediction of the wave profile along the hull using thin ship theory.

Validation of the theory is described in Chapter 5. Three hull forms: a Wigley hull, Series 64 hull, and NPL hull forms, are used. The Wigley hull form is a mathematical parabolic hull form which was chosen because it has been widely tested by a number of researchers and it has no transom. It can therefore be used to

validate the theoretical model. The other two hull forms have transom sterns which are used for investigations of transom stern effects. Chapter 5 also includes a number of examples which demonstrate the applications of the theory.

Chapter 6 provides an overall discussion of the experimental and theoretical work and applications of the developed numerical methods. Conclusions are drawn in Chapter 7 together with recommendations for further possible work.

1.2 Literature Review

Wave pattern resistance:

Extensive research into the powering of fast displacement craft has been carried out at the University of Southampton, Refs. 1 to 15. Insel [1, 2] investigated the resistance components of high speed displacement catamarans over a wide range of speed (up to Fn of 1.0) with a range of separation ratios and length to breadth ratios. Both experimental and theoretical investigations were carried out. Thin ship theory was used for the theoretical investigation on wave resistance. A hydrostatic correction was used with the theory for the transom effect. The effect of demihull separation was also investigated by Doctors [16, 17] and Millward [18]. The results showed the same trends as those obtained by Insel and Molland [2].

The effects of length to displacement ratio and breadth to draught ratio on resistance components were investigated experimentally by Molland [3] in 1996. The results indicated that the length to displacement ratio has significant effect on resistance whereas the breadth to draught ratio hardly affects the resistance. The increase in length to displacement ratio causes a reduction in resistance. For practical scaling, the total resistance of catamarans was expressed as:

$$C_{Tmono} = (1+k)C_F + C_W \qquad \text{(monohull)}$$

$C_{Tcat} = (1+\phi k)\sigma C_F + \tau C_W$ (catamaran)

C_F : obtained from ITTC 1957 correlation line

C_W : Wave resistance coefficient for the demihull in isolation

$(1+k)$: Form factor for the demihull in isolation

ϕ : to take account of pressure field change around the demihull

σ : to take account of the velocity augmentation between the hulls and would be calculated from an integration of local frictional resistance over the wetted surface

τ : Wave resistance interference factor (C_{Wcat}/ C_{Wmono})

For practical convenience, ϕ and σ can be combined into an overall viscous resistance interference factor β.

For catamarans, $C_{Tcat} = (1+\beta k)C_F + \tau C_W = R_{Tcat}/(0.5\rho AV^2)$

and for monohulls, $C_{Tmono} = (1+k)C_F + C_W = R_{Tmono}/(0.5\rho AV^2)$

Form factors for some fine vessels, high speed transom stern monohulls and high speed catamarans, were evaluated by Couser [4]. Experimental investigations into the effect of prismatic coefficient on catamaran resistance were carried out by Molland [5, 6] and Lee [7].

The effects of demihull forms and demihull spacing on catamaran resistance were experimentally investigated by Matsui [19]. The uses of stern flaps, anti-wave hydrofoils and bow spray strips were investigated and suggested in order to reduce the resistance.

Three geosim models of high speed hard chine catamarans were tested for the effects of towing line positions on the resistance components by Cassella [20]. The results showed that the differences in trim and total resistance among the different towing directions were not negligible at the operative speed of the catamaran.

Dand [21] carried out model experiments on high speed catamarans in shallow water. The aim was to highlight some aspects of shallow water behaviour at sub-, trans- and supercritical speeds on resistance, trim and wash. The results showed that water depth had a significant effect at sub-critical speeds. The resistance increased as the water depth decreased. At about critical speed (depth Froude number about 1.0), the resistance coefficients increased dramatically. The water depth hardly affected the resistance at super-critical speed, i.e. depth Froude number greater than one. The effect of water depth on the resistance was also investigated by Zibell [22], Millward [18, 23] and Everest [24].

With regard to theoretical wave resistance prediction, thin ship theory has been used successfully for theoretical wave resistance prediction by a number of researchers. The theory was originally introduced by Michell in 1898, Ref.25. The theory was developed by Insel [1] using a far field wave energy approach, in which the far field wave system and far field wave coefficients (Eggers coefficients) of a Kelvin source were presented using linearised theory, to derive the wave resistance. The effects of a canal width and depth were included. The approach gives acceptable results especially for very slender ships, which are generally the case for high speed vessels.

As the thin ship approach represents a body with a source-sink distribution over the centreline plane of the hull, which is a function of the slope of the waterline, the wave resistance for ships with transom sterns is underpredicted. This is because of the undefined slope of the waterline on the transom. Modifications have been introduced for the transom effect such as a hydrostatic correction, transom sources by Molland [6] and Lee [7] and Virtual Appendage by Couser [9]. Thin ship theory with a hydrostatic transom correction was used to investigate wave resistance and interference effect of catamarans and trimarans with various factors by Wijaya [14].

Doctors [26] investigated simplified non-linear corrections and viscous corrections to thin ship theory, but only small improvement were shown. Steen [27] predicted the resistance of fast displacement catamarans using empirical methods in the early

stage, an advanced numerical method as a tool for hull shape optimization, and model tests for final optimization and verification.

Cong [28, 29] investigated the wave resistance of a surface ship with a transom stern by using thin ship and flat ship theories. The method represented the whole ship by three singularity terms: a source system distributed on the longitudinal centreplane, a sink line along the bottom edge of the transom stern and a sink plane on the bottom of the over hang aft body. Gadd [30] applied second-order theory for the wave resistance prediction. There were some improvements at low speeds, especially for the case of a mathematical model.

Wave wash:

The concern of ship generated waves, known as wash, caused by high speed craft in coastal waters has been increased due to the impact on safety and the environment. A number of research investigations have been carried out in order to determine the properties of wash waves created by ships. Various factors have been considered such as hull form parameters, water depth and sinkage and trim.

The model experiments for high speed catamarans in shallow water carried out by Dand [21] also studied the generation of wash. The attention concentrated on wash at speeds in the sub-, trans, and super-critical regimes. It was found that the largest waves were obtained in the trans-critical region whereas small waves were obtained in the sub-critical region and a virtually constant wave height was found in the super-critical conditions. The effect of hull design was also investigated. The results showed that the more slender the hull form, the lower the wash height.

Full scale/ site measurements in confined waters were carried out and compared with CFD methods by Whittaker [31] and Kofoed-Hansen [32, 33]. The results showed that model results and full-scale measurements were in general in good agreement.

The results also indicated that the highest waves appeared in the trans-critical speed range.

Stumbo [34, 35] carried out full-scale measurements of different ships. It was found that as length to breadth ratio increases, wave wash decreases, Ref. 34. The effect of water depth was also investigated and the results showed that not only depth Froude number but also length Froude number could affect the wave pattern, Ref. 35. The use of a flap at the bottom of transom for optimising trim was suggested due to a marked reduction in wake wash height and energy density in deep water.

Model and full-scale measurements of wave wash were also carried out by Macfarlane [36, 37]. Wash waves created by multihull and monohull vessels were measured and compared at the same displacement, waterline length and speed, Ref. 37. It was found that multihull vessels generate less maximum wave height than monohull vessels but with longer wave period. However, it was found that the energy in the wave, generated by both monohull and multihull vessels, is more or less the same. Ship displacement and ship length were found to have an influence on wave height and wave energy. As the displacement increases, both wave height and wave energy increase but it hardly affects the wave period. The investigations also showed that the more slender the hull forms, the lower the wash height and wave energy. As a result of the investigation, it was suggested that ships should be designed to generate moderate wave height but short wave period.

Thin ship theory can also be used for the prediction of ship generated wash. The use of thin ship theory for the prediction of wash is discussed in Ref. 9. The theory was used to investigate the wash of pleasure craft on inland waterways by Edwards [10]. The experimental results of a Wigley hull form were compared with the theoretical results. The results showed very good agreement, especially in the near field. Further investigations on ship generated near-field wash waves using thin ship theory have been carried out by Molland [38, 39]. The effects of hull form, shallow water, and speed were investigated. Three hull forms: a Wigley hull, Series 64 catamaran hull,

and NPL catamaran hull were used as case studies and the predictions were promising, especially the Wigley parabolic hull which has no transom.

Various methods for the prediction of far field waves, distant from the ship, were used by Gadd [40, 41]. Gadd [40] used panel methods, conventional tank wave analysis and surface pressure distribution to predict far-field waves made by high speed ferries and compared them with experimental results. It was found that the panel method approach combined with a fitted surface pressure distribution could give realistic results. Janson [42] used a combined Rankine/Kelvin source method to predict the far-field wash wave. It was found that the combined method gave better prediction than the Rankine method and gave good prediction of wave profiles compared to measured results. However, only deep water calculations were carried out.

In addition to above methods for the prediction of wave wash, a boundary element method was used by Brizzolara [43], and a Boussinesq type model was used by Jiang [44] to simulate ship waves at sub-, trans-, and supercritical speeds. The Boussinesq model is more typically used by coastal engineers for wave propagation over large distances. Raven [45] has set up a coupled wave making/wave propagation model, which is based on coupling a steady free-surface potential flow code, RAPID, used for the prediction of wave generation with a non-linear Boussinesq type model used for the prediction of wave propagation. Leer-Anderson [46] used a CFD code, SHIP FLOW, for the prediction of wash waves in order to optimise hull forms for wave wash reduction. Reasonable results were achieved except at critical speed. Hughes [47] used CFD methods to examine the unsteady effects on the wake wash as a ship moves from deep water into shallow water.

Some possible solutions to the wash problem of high speed craft, such as speed and route restrictions, hull design and remedial measures on shore were suggested by the ITTC Specialist Committee on safety of high speed marine vehicles, Ref. 48. The Danish Maritime Authority [49] has proposed wash height restrictions. The

acceptable height of a long period wash wave was limited to 0.35 metres in 3 metres water depth.

Day and Doctors [50] investigated theoretically four different concepts for high speed low-wash craft: a conventional catamaran, a semi-SWATH, a hovercraft, and a surface-effect ship (SES). They found that hovercraft could offer some improvement at certain speed and depth combinations, whilst SES and semi-SWATHs did not offer any significant improvement over conventional catamarans. Feldtmann and Garner [51] introduced a Critical Speed Step in the seabed to avoid operation near critical speed in sensitive areas.

The literature review and survey of research has indicated a number of areas and issues in the field of ship wave resistance and wave wash for high speed craft which require further attention. The objectives of the current research programme have been to address a number of these areas and issues.

1.3 Overall Objectives

The objectives of the research programme are:

- To provide better understanding of the basic physics of wash waves, using experimental and numerical methods.

- To determine the influence on wash of parameters such as hull form, speed, trim and shallow water.

- To carry out experiments to provide a further understanding of, and data relating to, shallow water, transom immersion, trim and wave wash measurements.

- To compare and validate the numerical methods with the experimental data.

- To develop a practical numerical tool for the prediction of wave resistance and ship generated near-field wave wash (taken, say, as within 0.5 to 1.0 ship lengths from the ship centreline). This will include the prediction of the influences of changes in hull form, speed, and water depth, and the assessment of the likely wave wash of new designs, together with operational effects on the wash of ships in service.

- To show how the numerical method may be applied to identify low-wash and/or novel designs and to identify acceptable operational patterns.

2. OUTLINE OF THEORY

2.1 Available Theories

Ship wave resistance can be calculated from either the far-field wave system or pressure integration over the wetted surface of the hull. In general, potential methods are used to calculate wave resistance. Most of them use a linear approximation to the free surface boundary condition.

A number of methods have been used for the prediction of wave resistance. For simple parabolic hull forms such as Wigley, the wave resistance can be obtained by integrating the appropriate Green's functions such as Kelvin or Rankine sources. Thin ship or slender body theory has been used by a number of researchers as it provides fast and accurate solutions for slender hull forms. In this theory, the body is represented by an array of sources on the centreline plane (y=0). The main disadvantage of using thin ship theory is that the hulls must be slender. However, the hull forms of interest in this investigation are generally very slender, with L/B in the order of 10-12.8. Additionally, there are a number of panel methods such as double body panel method, non-linear free surface panel method, integral boundary methods, Navier Strokes formulations, and Zonal models. These methods are, for example, reviewed and discussed in Ref.13.

In addition, CFD techniques have also been used by a number of investigators such as Ship Flow [46] and RAPID [45] for the prediction of wave system. Ship Flow uses a zonal approach to compute the flow. Only the potential flow and thin boundary layer solver are used to predict wave wash. RAPID (Raised-Panel Iterative Dawson) is a nonlinear free-surface potential flow code used by Raven [45] to predict wave making. The flow model is that of a steady 3D incompressible potential flow around the ship hull.

For the present investigation, thin ship theory has been developed and used. It builds on the theory described by Insel [1, 2] and Molland [3]. The theory was developed in order to calculate the wave pattern resistance of slender hulls with transom sterns and is applicable up to the supercritical speed range. The thin ship method provides an alternative to the higher order panel methods and, when applied strictly to thin or slender hulls, has been found to provide a similar degree of accuracy at a fraction of the computational effort, Couser [13]. Thin ship theory is described in the next section.

2.2 Thin Ship Theory

The thin ship theory of wave resistance was originally introduced as a purely theoretical approach for predicting the wave resistance of a ship by J.H. Michell in 1898 [25]. The dependence of wave resistance on ship's hull form was established. The velocity potential and wave resistance for a sufficiently narrow ship moving on the surface of an infinitely deep fluid were found. Insel, Ref.1, developed the far field wave system for a Kelvin source in a shallow water canal and applied it to thin ship theory. In the basic thin ship theory, the following assumptions are made:

a) The ship hull(s) is slender i.e. high length to breadth ratio.
b) The fluid is inviscid, incompressible and homogeneous.
c) The fluid motion is steady and irrotational.
d) Surface tension can be neglected.
e) The wave height at the free surface is small compared with the length.

A Cartesian coordinate system moving with the model is used. The origin is on the free surface at the centre of the model. Ox is in the direction of motion, Oy is to the starboard and Oz is to vertical upwards. The tank centreline is at y=0 and the

undisturbed free surface is at z=0. The model moves in the positive direction of the x-axis at a constant speed, U, in a finite channel of width B and uniform depth H.

Ship bodies are represented by planar arrays of Kelvin sources on the local hull centreline, together with the assumption of linearised free surface conditions. The theory includes the effects of a channel of finite breadth and shallow water.

The source strength is:

$$\sigma = -\frac{U}{2\pi}\frac{dy}{dx} \qquad (2.1)$$

As seen from equation (2.1), the local source strength is proportional to the longitudinal waterline slope. Hence, it can be calculated from a given offset of hull definition at a given constant speed. The centreline plane of the hull can be divided into a grid of rectangular panels. The contribution of each panel is calculated by replacing the uniform source distribution over each of the panels with a point source located at the centre of each panel. Therefore, the strength of the source on each panel can be calculated from the local slope of the local waterline, as follows:

$$\sigma = -\frac{U}{2\pi}\frac{dy}{dx}\mathrm{dA} \qquad (2.2)$$

Where dA is the panel area. The hull waterline offsets in the current procedure can be obtained directly and rapidly as output from a commercial lines faring package, Ship Shape, Ref. 52.

2.3 Theoretical Wave Elevation

The far field velocity potential is expressed by Insel [1] as:

$$\phi_{FF} = \frac{g}{U}\sum_{m=0}^{\infty}\left[\begin{matrix}-\eta_m \\ -\beta_m\end{matrix}\cos(k_m x\cos\theta_m) + \begin{matrix}\xi_m \\ \alpha_m\end{matrix}\sin(k_m x\cos\theta_m)\right]\frac{1}{k_m\cos\theta_m} * \frac{\cosh(k_m(z+H))}{\cosh(k_m H)}\begin{matrix}\cos(m\pi y/W) \\ \sin(m\pi y/W)\end{matrix} \quad (2.3)$$

Where the last cosine term applies to even m and sine term applies to odd m.

The wave elevation found from linearised free surface condition is expressed as:

$$\zeta = \sum_{m=0}^{\infty}\left[\begin{matrix}\xi_m \\ \alpha_m\end{matrix}\cos(xk_m\cos\theta_m) + \begin{matrix}\eta_m \\ \beta_m\end{matrix}\sin(xk_m\cos\theta_m)\right]\begin{matrix}\cos(\frac{m\pi y}{W}) \\ \sin(\frac{m\pi y}{W})\end{matrix} \quad (2.4)$$

Where ξ_m,η_m and cosine term are applied to even m whilst α_m, β_m and sine term are applied to odd m. The term m=0 is halved. The wall reflection condition and the wave speed condition including shallow water effects are also satisfied.

$k_m\sin\theta_m = \pi m/W$ (Wall reflection) (2.5)

$k_m\cos^2\theta_m = \bar{k}\tanh(k_m H)$ (Wave speed condition) (2.6)

where $\bar{k} = g/U^2$

The wave coefficients are:

$$\left|\begin{matrix}\xi_m \\ \eta_m\end{matrix}\right| = \frac{16\pi U}{Wg}\frac{\bar{k} + k_m\cos^2\theta_m}{1+\sin^2\theta_m - \bar{k}H\,\mathrm{sech}^2(k_m H)}$$

$$\sum_{\sigma}\left[\sigma_\sigma e^{-k_m H}\cosh(k_m(H+z_\sigma))\cos\left(\frac{m\pi y_\sigma}{W}\right)\left|\begin{matrix}\cos(k_m x_\sigma\cos\theta_m) \\ \sin(k_m x_\sigma\cos\theta_m)\end{matrix}\right|\right] \text{ for even m} \quad (2.7)$$

$$\left|\begin{matrix}\alpha_m \\ \beta_m\end{matrix}\right| = \frac{16\pi U}{Wg}\frac{\bar{k} + k_m \cos^2\theta_m}{1+\sin^2\theta_m - \bar{k}H\,\mathrm{sech}^2(k_m H)}$$

$$\sum_\sigma \left[\sigma_\sigma e^{-k_m H}\cosh\left(k_m(H+z_\sigma)\right)\sin\left(\frac{m\pi y_\sigma}{W}\right)\left|\begin{matrix}\cos(k_m x_\sigma \cos\theta_m) \\ \sin(k_m x_\sigma \cos\theta_m)\end{matrix}\right|\right] \quad \text{for odd m} \qquad (2.8)$$

If the ship model is symmetric relative to the tank centreline, the wave elevation at a longitudinal cut, y, can be expressed by taking the even terms only and substituting n=2m as follows:

$$\zeta = \sum_{n=0}^{n}\left[\xi_n \cos(xk_n \cos\theta_n) + \eta_n \sin(xk_n \cos\theta_n)\right]\cos\frac{n\pi y}{W} \qquad (2.9)$$

The wave coefficients (ξ_n and η_n) can be derived theoretically using Equations (2.7), and they can also be derived experimentally from physical measurements of wave elevation, ζ, in Equation (2.9).

The wave number at n^{th} harmonic, k_n, can be found by combining the square of equation (2.5) with (2.6).

$$k_n^2 = \frac{g}{U^2}k_n \tanh(k_n H) + \left(\frac{n\pi}{W}\right)^2$$

In the current work, θ_n can then be found by substituting k_n into equation (2.6) in order to satisfy the wave speed condition including shallow water effects. It is noted that in the original version of the theoretical approach, θ_n was found by substituting k_n into equation (2.5) which does not satisfy the wave speed condition at supercritical speeds. For example, at supercritical speed, if θ_n is obtained from equation (2.5), the smallest value of θ_0 will be zero, which is not correct.

From the wave speed condition (2.6), for small k_nH i.e. shallow water, k_nH is greater than $\tanh k_nH$. Hence;

$$k_n Cos^2\theta_n = (g/U^2).\ \tanh k_n H < k_n(gH/U^2)$$

therefore;

$$Cos\theta_n < \sqrt{(gH)}/U$$

If $U < \sqrt{(gH)}$, the wave speed condition will be satisfied for all values of θ_n, i.e. no restriction as $Cos\theta_n \leq 1$ for 0-90°. On the other hand, if $U \geq \sqrt{(gH)}$, the largest value of $Cos\theta_n$ is given by $Cos\theta_n = \sqrt{(gH)}/U$ in order to satisfy the wave speed condition. Hence, the smallest value of θ_n becomes $\theta = Cos^{-1}(\sqrt{(gH)}/U)$. Speeds $U < \sqrt{(gH)}$ are called sub-critical speeds whereas speeds $U > \sqrt{(gH)}$ are called supercritical speeds.

Since gravity waves cannot travel at speeds greater than $\sqrt{(gH)}$, if the ship is running at a higher speed than the critical depth speed $\sqrt{(gH)}$, the transverse waves disappear and waves can only exit at angles greater than $\theta_0 = Cos^{-1}(\sqrt{(gH)}/U)$, Lunde [53]. It is noted that θ_n increases as the speed increases.

For a catamaran, the wave elevation can be found from equation (2.4) by calculating wave coefficients from equation (2.7) and (2.8) over a distribution of sources for both demihulls. For a catamaran made up two symmetric demihulls relative to the tank centreline, the wave elevation can be expressed as follows [1]:

$$\zeta = \sum_{n=0}^{\infty}[2\xi_n C_S \cos(xk_n \cos\theta_n) + 2\eta_n C_S \sin(xk_n \cos\theta_n)]\cos\frac{n\pi y}{W} \qquad (2.10)$$

Where $C_S = Cos(k_n\ S/2\ Sin\theta_n) = Cos(n\pi S/W)$.

Thus equations (2.9) and (2.10) can be used to fully describe the wave patterns for monohulls and multihulls.

2.4 Theoretical Wave Resistance

From the considerations of momentum changes, Appendix A, the resistance components of a ship model can be derived. The total resistance can then be expressed as follows:

$$R_T = \frac{\rho g}{2}\int_{-W/2}^{W/2} {\zeta_B}^2 dy + \frac{\rho}{2}\int_{-W/2}^{w/2}\int_{-H}^{\zeta_B}\left(v^2 + w^2 - u^2\right)dzdy + \int_{-W/2}^{W/2}\int_{-H}^{\zeta_B}\Delta P dzdy \tag{2.11}$$

Where B represents down stream.

The first two terms in equation (2.11) represent the wave resistance and the third term represents the viscous resistance.

Therefore, the wave resistance can be expressed as follows:

$$R_W = \frac{\rho g}{2}\int_{-W/2}^{W/2} {\zeta_B}^2 dy + \frac{\rho}{2}\int_{-W/2}^{W/2}\int_{-H}^{\zeta_B}\left(v^2 + w^2 - u^2\right)dzdy \tag{2.12}$$

or

$$R_W = \frac{\rho g}{2}\int_{-W/2}^{W/2}\zeta^2 dy + \frac{\rho}{2}\int_{-W/2}^{W/2}\int_{-H}^{0}\left(\left(\frac{\partial\phi}{\partial y}\right)^2 + \left(\frac{\partial\phi}{\partial z}\right)^2 - \left(\frac{\partial\phi}{\partial x}\right)^2\right)dzdy \tag{2.13}$$

Where ζ is the wave elevation in the far field and $(\partial\phi/\partial x)^2$, $(\partial\phi/\partial y)^2$, $(\partial\phi/\partial z)^2$ can be obtained from the derivatives of the far field velocity potential ϕ_{FF} with respect to x, y, z, see Ref. 1. The wave resistance can then be expressed in terms of the Eggers coefficients as follows:

$$R_W = \frac{\rho g W}{4}\left\{(\xi_{m=0}^2 + \eta_{m=0}^2)(1 - \frac{2k_{m=0}H}{\sinh(2k_{m=0}H)}) + \sum_{m=1}^{\infty}(\frac{\xi_m^2 + \eta_m^2}{\alpha_m^2 + \beta_m^2})\left[1 - \frac{\cos^2\theta_m}{2}\left(1 + \frac{2k_mH}{\sinh(2k_mH)}\right)\right]\right\}$$

(2.14)

Where ξ_m and η_m are applied for even m whilst α_m and β_m are applied for odd m.

It is noted that $k_{m=0}$ is k_m at 0^{th} harmonic, which is not the same as $\bar{k}$ which is g/U^2, especially at supercritical speeds. It is obtained from the combination of the wave speed condition (2.6) and wall reflection condition (2.5), as follows:

$$k_m^2 = \frac{g}{U^2}k_m \tanh(k_mH) + (\frac{m\pi}{W})^2$$

at m=0;

$$k_{m=0} = \frac{g}{U^2}\tanh(k_{m=0}H)$$

Noting that $k_{m=0} = \bar{k}$ if deep water is assumed.

For a ship model symmetric to the tank centreline the wave resistance can be simplified as:

$$R_W = \frac{\rho g W}{4}\left\{(\xi_{n=0}^2 + \eta_{n=0}^2)(1 - \frac{2k_{n=0}H}{\sinh(2k_{n=0}H)}) + \sum_{n=1}^{\infty}(\xi_n^2 + \eta_n^2)\left[1 - \frac{\cos^2\theta_n}{2}\left(1 + \frac{2k_nH}{\sinh(2k_nH)}\right)\right]\right\}$$

(2.15)

The wave resistance of a catamaran with symmetric demihulls can be expressed as:

$$R_W = \frac{\rho g W}{4}\left\{(2\xi_{n=0}^2 + 2\eta_{n=0}^2)(1 - \frac{2k_{n=0}H}{\sinh(2k_{n=0}H)}) + \sum_{n=1}^{\infty}(2\xi_n^2 C_S + 2\eta_n^2 C_S)\left[1 - \frac{\cos^2\theta_n}{2}\left(1 + \frac{2k_nH}{\sinh(2k_nH)}\right)\right]\right\}$$

(2.16)

Where $C_S = \mathrm{Cos}(\pi nS/W)$.

A schematic overview of the modelling procedure is shown in Fig.2.2. It is noted that the theory provides an estimate of the proportions of transverse and diverging

content in the wave system and that the theoretical predictions of the wave pattern and wave resistance can be compared directly with values derived from physical measurements of the wave elevation.

An outline of the computer program incorporating the theory is shown in Appendix B. The program calculates the wave resistance and wave profiles of a ship model moving along a rectangular tank, having finite width and depth, with a constant speed. The program allows up to 3 hulls to be calculated. The hull offsets data are generated by a hull faring program, Shipshape [52], and are then converted into the format required by the thin ship theory program using a Fortran program called Convert2.

The thin ship theory program has been developed by the author to allow extra source(s) with desired strength to be added at suitable positions in the program for the purpose of transom stern corrections. The program has also been modified to satisfy the wave speed condition at supercritical speeds, as mentioned in Section 2.3.

2.5 Refinements to Thin Ship Theory

It has been noted from model tests and full-scale operation that trim and hence transom immersion can have a significant influence on the wave pattern and consequently on the wave resistance and wave wash, Ref.9. An important refinement to the basic theory, and a requirement of all theories, does therefore concern the need to model the transom stern in a satisfactory manner. As the thin ship approach represents a body with a source-sink distribution over the centreline plane of the hull, the wave resistance of a ship with a transom stern is underpredicted. This is due to the undefined slope of the waterline on the transom. As a result, there is need for refinements to the theory for transom stern effects in order to improve the potential for predicting wave resistance and near-field wave wash. These refinements are discussed in Chapter 4.

As a result of the significance of the transom stern immersion and its effect on resistance and wash, it is important to be able to incorporate suitable estimates of running sinkage and trim in the theoretical model. This was highlighted by the work reported in Refs. 9 and 13 which showed that, whilst reasonably large changes in trim can have relatively small effects on wave resistance arising from the hull source distribution, the resulting changes in the wave resistance due to changes in the transom immersion can be very significant. A number of investigators have employed an experimentally derived sinkage and trim input to their theoretical models, which is not unreasonable if data from a fairly wide range of geosim hull forms are employed, such as those described in Ref. 3. In order to facilitate data for this use, regression analysis of dynamic sinkage and trim has been carried out using the experimental deep water data obtained from Insel [2] and Molland [3, 11]. This is discussed in Chapter 4.

A hybrid model has also been developed which facilitates improvements in the estimates of sinkage and trim based on changes in the dynamic pressure around the hull. The model links the thin ship theory to a panel method. This technique can provide reasonable first order approximations to sinkage and trim and might be suitable for new developments in hull forms for which acceptable trim and sinkage data is not available. The model is described in Chapter 4.

2.6 Validation of Thin Ship Theory

The theory has been well validated for wave resistance in deep water, Refs. [1, 7, 9, and 13]. Little work has been carried out so far on the validation of the theory in respect of wave profiles for wave wash purposes. In particular, there is a need for validation of the theory in shallow water and at supercritical speeds. This has been held up mainly by the lack of experimental measured wave elevations in shallow

water. Chapters 4 and 5 describe the validation of the theory for super critical speeds using new shallow water data presented and described in Chapter 3.

2.7 Description of Wave Characteristics

The wave system can be described using some or all of the following wave properties at sub-critical, trans-critical and supercritical speeds.

The overall characteristics of sub-critical and supercritical wave pattern are shown in Fig.2.1. At sub-critical speed (Fn_H<1.0), the basic Kelvin wave with both transverse and divergent waves is generated. The direction of propagation of diverging waves is about 35° to the ship's track. At supercritical speed (Fn_H>1.0), the transverse waves disappear and the divergent wave angle becomes larger. The effect of depth Froude number, Fn_H, on the direction of propagation of divergent waves is discussed in Chapters 3 and 5.

Basic properties of the wave system are given in Fig.2.2 which shows a typical (predicted) wave pattern, a longitudinal cut through the wave pattern, the typical distribution of wave energy (sub-critical in this example) within the wave system and the wave resistance. Further descriptions are given in Figs.2.3 and 2.4 which show the propagation angles of the leading divergent waves and wave resistance relative to deep water as speed passes from sub-critical, through trans-critical to supercritical. A typical predicted wave pattern and wave cut is illustrated in Fig.2.5.

2.8 Wave Propagation and Decay

In order to predict the likely size of the waves as they approach some other area or the shore, and hence their likely impact, the rate of decay of ship waves need to be estimated. The basic properties of the wave system mentioned above may typically be used for wave transformation / propagation studies from ship to shore. This can

entail extensive computer modelling using, for example, Boussinesq-type equations for the prediction of the propagation and decay of the waves. Alternatively, a much simpler approach, but with practical applications, is to use theoretical and experimental methods to predict the decay of the waves as they propagate. In deep water, the rate of decay can be described by Havelock's theoretical prediction of decay, Ref. 54, which is:

$$H \propto \gamma.y^{-n}$$

Where n=0.5 for transverse wave components and n=0.33 for divergent waves. y is the distance perpendicular to the ship's track. γ can be determined experimentally based on a wave height at an initial value (offset) of y and as a function of the speed of the vessel.

Hence, once the maximum wave height is measured close to the ship's track, it can be calculated at any required distance from the ship.

In shallow water, smaller values of n in the above equation between 0.2 and 0.4 may be applicable, Ref. 55. This depends on wave period and water depth/ship length ratio. The decay rates for shallow water waves (supercritical) are less than for deep water and, consequently, the wave height at a given distance from the ship is greater than that of the equivalent height of a wave in deep water (sub-critical).

The energy in the first two or three waves can be used as a good representation of the potential damaging effects of the waves because it combines the effects of wave height and period. The energy is given, Ref.55, by:

$$E = \rho g^2 H^2 T^2 / 16\pi \qquad \text{for deep water}$$

$$E = \rho g H^2 \lambda / 8 \qquad \text{for shallow water}$$

Where $\lambda = (gT^2/2\pi).\tanh(2\pi h/L)$. H is wave height, T is wave period, h is water depth and L is wavelength.

In shallow water, most of wave energy is contained in a single long period wave and the decay of the wave height and energy with distance from the ship is relatively small, Ref. 55. It is recommended that the description of wash waves in shallow water should include both maximum wave height and maximum wave energy as if the energy alone is used, the individual components of wave height and period are lost.

The current investigation concentrates on the generation of the waves and their properties within about one ship length off the centreline of the ship.

3. EXPERIMENTAL INVESTIGATIONS

3.1 Introduction

An extensive experimental investigation has been carried out which would establish a database that could be used for design and investigation purposes, for the validation of theoretical models and for input to wave propagation models. Whilst the experiments formed part of a wider EPSRC funded programme of research, the author of this thesis was directly involved with the actual running of the experiments and the acquisition and analysis of the measured data.

The basic aims of the experimental investigations were to assess the effects of hull form parameters, transom immersion, shallow water and propulsion systems on wave wash and resistance and to validate the theoretical model. The NPL round bilge series [56 and 3] and Series 64 hull forms [57] were chosen for the investigation. Models for these forms were available and had been tested at the University of Southampton for resistance and seakeeping over a number of years. The models broadly represent the underwater form of a number of monohulls and catamarans in service or currently under construction.

The resistance data in deep water used in the investigation were obtained from the earlier tests on the resistance of high speed displacement monohulls and catamarans carried out over a number of years at the University of Southampton, Refs. 1-3, 11, and 12. These tests included the measurement of total and wave pattern resistance, running sinkage and trim and a limited number of wave profiles along the hull. The models used were derived from the NPL round bilge series, designated models 4b, 5b, and 6b and Series 64, designated model 5s. The tests covered a range of length to displacement ratios ($L/\nabla^{1/3}$) and catamaran separation to length ratios (S/L).

An extensive series of wave wash measurements for monohull and catamaran models travelling in both deep and shallow water has been carried out as part of the wider research programme, funded by EPSRC and industry. The models were tested in deep water in the Towing Tank at Southampton Institute and in shallow water at the GKN Westland tank on the Isle of Wight. Overall, the tests covered a range of length Froude Number of 0.25-1.2 and depth Froude Number of 0.5-3.2. Longitudinal wave cuts, model total resistance, sinkage and trim were measured and used in this investigation.

The tests also covered a range of catamaran separation to length ratios (S/L), two shallow water depths and significant bow and stern trim. These allowed the effects of separation to length ratio, water depth and trim changes or transom immersion on total resistance and wave wash to be investigated. The effects of separation to length ratio and water depth on running sinkage and trim were also examined.

Two separate model 5s catamarans, one self-propelled by propellers and the other by water jets, were tested in shallow water in order to investigate the effect of propulsion systems on the generation of wave wash.

3.2 Description of Models

Details of the models used are given in Table 1.

The models were constructed using an epoxy-foam sandwich skin. Models 4b, 5b, and 5s are 1.6m in length. The length of model 6b was increased to 2.1m in order to achieve satisfactory weight – displacement balance.

The models were of round bilge form with transom sterns, Fig. 3.1, and were derived from the NPL round bilge series [56] and the Series 64 round bilge series [57]. The

models were tested as monohull and catamaran configurations with separation to length ratios (S/L) of 0.2, 0.3, 0.4, and 0.5.

The model towing force was in the horizontal direction. The towing point in all cases was situated at the longitudinal centre of gravity and at a height of 1.5 times the draught above the baseline. No compensation was made for the vertical separation of the tow point and the propeller thrust line. The tow fitting allowed free movement in sinkage and trim while movements in surge, sway, roll and yaw were not allowed.

The models were fitted with turbulence stimulation comprising trip studs of 3.2mm diameter and 2.5mm height at a spacing of 25mm. The studs were situated 37.5mm aft of the bow. No underwater appendages were attached to the towed models.

Two model 5s catamarans were built and equipped with propulsion systems in order to investigate the effect of propulsion systems on wave wash. One was propelled by a pair of propellers and the other was propelled by two pairs of waterjets. The propellers provided a speed up to about 3 m/s while the waterjets gave a speed up to 4 m/s.

3.3 Facilities and Tests

3.3.1 General

The deep water experiments were carried out in the Southampton Institute towing tank. The tank has the following principal particulars:

Length	:	60.0m
Breadth	:	3.7m
Water Depth	:	1.85m

Maximum Carriage Speed : 4.6m/s

The shallow water experiments were carried out in the GKN-Westland Aerospace test tank on the Isle of Wight, which has principal particulars as follows:

Length : 200m
Breadth : 4.6m
Water Depth (deep water) : 1.7m
Maximum Carriage Speed : 14m/s
In the current tests, water depths of 200mm and 400mm were used.

Both tanks have a manned carriage which is equipped with a dynamometer for measuring total resistance together with various computer and instrumentation facilities for automated data acquisition.

Total resistance, running trim, sinkage and wave elevation were measured in calm water. The tests were carried out over a speed range up to Fn of 1.0 for deep water cases and the shallow water tests were carried out at a speed range of 1m/s – 4m/s corresponding to a length Froude Number range of 0.2 to 1.0 and a depth Froude Number range of 0.2 to 2.8.

For the shallow water self-propulsion tests, a special frame, fitted under the carriage, was used as a guide to keep the models travelling on the tank centreline and also parallel to the centreline of the tank. During the run, model propeller revolutions were adjusted until the model speed was the same as the carriage set speed.

3.3.2 Wave pattern measurement

The wave profiles were measured using resistance type wave probes with a length of 300mm coupled to Churchill wave probe monitors. The data were acquired and stored using a laptop computer.

The tests on wave wash measurement in deep water were carried out at the Southampton Institute towing tank. Model 5s was used and tested in catamaran configurations with separation to length ratios (S/L) of 0.2, 0.3 and 0.4. During each test run, four longitudinal wave profiles were measured, with transverse position (Y) relative to the tank centreline to the model length ratios (Y/L) of 0.694, 0.77, 0.86, and 1.028. These spaces were chosen to suit the wave pattern resistance analysis [1]. The longitudinal position of the wave probes was about halfway down the tank which allowed adequate time for the wave system to settle before measurements commenced.

For the shallow water tests, models 4b, 5b, 6b, and 5s were used and tested at GKN-Westland Aerospace test tank. Seven longitudinal wave profiles were measured at the transverse position to model length ratios (Y/L) of 0.43, 0.55, 0.68, 0.80, 0.93, 1.05, and 1.18 for models 4b, 5b, and 5s and Y/L of 0.33, 0.42, 0.52, 0.61, 0.71, 0.80, and 0.90 for model 6b. The longitudinal position of the probes was 62.5m from the model starting point.

The wave wash tests using self-propelled models 5s were also carried out in shallow water in GKN-Westland Aerospace test tank. Three sets of wave probes were placed at three different longitudinal positions. Eight longitudinal wave probes were measured at the transverse position to model length ratios (Y/L) of 0.43, 0.55, 0.68, 0.80, 0.93, 1.05, 1.18, and 1.32 and were placed between the other two at the longitudinal position of 62.5m from the model starting point.

Two sets of four longitudinal wave probes were also measured at the same transverse position to the model length ratios (Y/L) of 0.89, 1.02, 1.14, and 1.27. The longitudinal positions of these two sets of wave probes were approximately at 41m and 87m from the model starting position. These positions allowed adequate time for the wave system to settle before measurements were commenced. The schematic layout of the GKN test tank is shown in Fig. 3.2. Routine repeat tests demonstrated that the wave profile measurements were repeatable within 1% of the typical measured maximum wave heights. Examples can be found in Refs.58 - 60.

3.3.3 Total resistance and side force measurements

Total resistance and side force were measured using a dynamometer provided by the Wolfson Unit for Marine Technology and Industrial Aerodynamics. The total resistance was recorded every test run while the side force was monitored to ensure that the model yaw angle was negligible. i.e. the side force is 10% less than the total drag, which is reasonable assumption based on the results of Ref. 61.

3.3.4 Running trim and sinkage measurements

Running trim and sinkage were measured for every test run. The running trim was measured by means of a potentiometer mounted on the tow fitting. The accuracy of the measurement was within ±0.05°. The running trim was measured as angle in degrees and taken positive for bow up.

The sinkage was measured by means of a potentiometer and a track on the tow post. The accuracy of the measurement was within ±0.1mm. The sinkage was taken positive for vertical motion downward and non-dimensionalised using the draught of the model.

3.3.5 Trim changes

A limited series of tests with changes in static trim were carried out using models 5b and 5s as catamaran configurations with a separation to length ratio (S/L) of 0.2. The tests were carried out at 200mm water depth for the cases of significant bow and stern trim. These would provide information on the effect of trim changes on the resistance and wave wash.

3.3.6 Self-propulsion tests

In order to investigate the influence of propulsion systems on wave wash, two model 5s catamarans: one propelled by a pair of propellers and the other propelled by two pairs of waterjets were used. Sixteen longitudinal wave probes were used to measure the wave elevations at various longitudinal and transverse positions as described in section 3.3.2.

The models were tested as catamaran configurations with separation to length ratios (S/L) of 0.2, 0.3 and 0.4 at the water depths of 400mm and 200mm. The tests were carried out at the speed range between 1-3m/s for the one propelled by propellers and between 1-4m/s for the one propelled by waterjets. The series of tests covered a range of length Froude Number of 0.25-1.0 and depth Froude Number of 0.7-2.85.

Self-propulsion tests were also carried out on 4.5m and 1.6m free-running models in the QinetiQ (Haslar) model basin, and wave measurements were carried out.

3.4 Data Reduction and Corrections

3.4.1 Coefficients

The resistance data were reduced to coefficient form as follows:

$$\text{Resistance Coefficient} = \frac{\text{Resistance}}{0.5\rho AU^2}$$

Where ρ : Fresh water density (1000 kg/m^3).

A : Static wetted surface area (m^2).

U : Model speed (m/s^2).

3.4.2 Temperature correction

The total resistance measurements were corrected to the standard temperature of 15°C by modifying the frictional resistance component as follows:

$$C_{T15}=C_{Ttest} - C_{Ftest} + C_{F15}$$

Although the correction should be slightly larger due to the form factor being greater than one, the correction is small in any case. Hence, the above equation is considered to be sufficiently accurate.

3.4.3 Resistance due to turbulence studs

Turbulence studs were attached to all models as described in Section 3.2. The influence of turbulence studs on model resistance was investigated and described in Ref. 11. It was found that the resistance due to the studs might be neglected since the laminar region upstream is counterbalanced by the boundary layer momentum thickness increase down stream of the studs.

3.4.4 Wetted surface area

Static wetted surface area was used to non-dimensionalise the resistance measurements. Although the use of running wetted surface area may provide a better understanding of the physical components of resistance, it was found in Ref. 11 that the use of static wetted area does not have a significant effect on model to ship extrapolation providing both model and full scale coefficients are based on static wetted surface area. Furthermore, the running wetted surface area is difficult to measure experimentally and will not be available for a new design. It is, therefore, more practical and generally satisfactory to use the static wetted surface area.

3.5 Presentation of Data

The residuary resistance coefficient C_R, rather than total resistance coefficient C_T, is used for the presentation of experimental resistance data as the residuary resistance consists mainly of wave resistance. It is obtained from the following:

$$C_T = C_F + C_R$$

Where C_T is total resistance coefficient measured from the tests.

C_R is residuary resistance coefficient.

C_F is frictional resistance coefficient calculated from ITTC:

$$C_F = 0.075/[\log (Rn)-2]^2$$

The wave profiles are presented in terms of wave height (m) to a base of longitudinal distance, X (m) for a given model or ship speed. The running trim was presented in degrees and taken positive for bow up. The sinkage was taken positive for vertical movement downward and non-dimensionalised using the draught of the model.

For the investigation of shallow water effects, the depth Froude number is used and defined as $Fn_H = V/(g.H)^{0.5}$ where H is water depth in meters. The wave wash is defined as sub-critical, critical or supercritical as $Fn_H <, =,$ or > 1.0 respectively.

The data are presented in Figs. 3.3 - 3.90 in terms of the influence of $L/\nabla^{1/3}$, S/L, shallow water and trim changes on the residuary resistance and the wave characteristics.

3.6 Discussion of the Results

3.6.1 Residuary resistance

3.6.1.1 Effect of length to displacement ratio ($L/\nabla^{1/3}$)

The effect of length to displacement ratio ($L/\nabla^{1/3}$) on residuary resistance is illustrated in Figs. 3.3 - 3.5. The figures show plots of residuary resistant coefficients of model 4b, 5b, and 6b as monohull and catamaran configurations at the water depth of 0.4m. As the length to displacement ratio ($L/\nabla^{1/3}$) increases (moving from model 4b to 6b), the residuary resistance coefficient decreases, especially at the hump. A similar trend was also obtained in deep water by Molland [3].

3.6.1.2 Effect of separation to length ratio (S/L)

The effects of S/L are shown in Figs. 3.6 - 3.11. The residuary resistance coefficients of the catamarans are greater than that of monohull, especially at the Fn between 0.4 and 0.6. This is due to the interference effects between the demihulls. It is noted that $C_{Rcat} = R_{Rcat}/(0.5\rho AU^2)$ where A is the wetted surface area of both demihulls. For catamarans, the general trend is that as the hull separation reduces, the residuary resistance increases. The effect is significant at the hump i.e. Fn between 0.4 and 0.6 for the deep water case. In the higher speed range, changes in hull separation tend to have a relatively small effect. The trend is also the same as that of models 3, 4 and 6

which have different length to breadth ratios (L/B) and breadth to draught ratios, see Ref. 3.

In shallow water, the resistance hump may occur at lower Fn as it also depends on depth Froude number Fn_H. For instance, at the water depth of 0.2m, the peak is at the Fn of 0.35 where the depth Froude number, Fn_H, is about 1.0 which is the critical depth speed. The effect of water depth on residuary resistance is discussed in section 3.6.1.4.

3.6.1.3 Effect of speed

The deep water results were used to illustrate the effect of model speed. As seen from Figures 3.6 and 3.9, as the speed increases, the residuary resistance coefficient gradually increases and peaks at a Froude number of about 0.45 and then decreases.

3.6.1.4 Effect of water depth

Figures 3.12 - 3.23 present the influence of water depth on residuary resistance coefficient at a range of length Froude number, Fn. The ratios of the residuary resistance in shallow water to the residuary resistance in deep water of model 5b and 5s as monohulls and catamarans are plotted against a range of depth Froude number Fn_H, Figures 3.24 - 3.29. The residuary resistance for the deep water case is the residuary resistance obtained from the tests at the water depth of 1.85m, taken from Molland [11] and Wellicome [12].

It can be seen from Figs. 3.12 - 3.23 that the resistance coefficients in shallow water are much higher than those in deep water at the length Froude numbers of about 0.35 and 0.5 for the water depths of 0.2m and 0.4m respectively. It is noted that the depth

Froude number is about 1.0 at the length Froude number of 0.35 for the water depth of 0.2m and 0.5 for the water depth of 0.4m.

Figures 3.24 - 3.29 show the curves of resistance ratio ($R_R/R_{R\infty Depth}$) against depth Froude number, Fn_H with two different water depths. It can be seen that the shallow water effect on the resistance is significant in the critical depth speed region ($Fn_H \cong 1.0$). The resistance ratio increases dramatically as the depth Froude number is close to one. The resistance ratio then decreases sharply just below the value of 1.0 i.e. the shallow water resistance is slightly less than the deep water resistance. In the supercritical speed region, as the depth Froude number increases the resistance ratio gradually increases to the value of about 1.0, the resistance in shallow water being about the same as the resistance in deep water i.e. the effect of water depth disappears.

Moreover, the water depth also influences the resistance at a given depth Froude number around the critical speed. As might be expected, the reduction in water depth causes an increase in the effect of shallow water. For instance, at the depth Froude number around 1.0 the resistance at the water depth of 0.2m is much higher than that of 0.4m. This is probably due to the effect of clearance under the hull. The similar trend was also obtained by Dand [21] and Millward [23, 62]. It is noted that at the critical speed, the length Froude numbers at the water depth of 0.2m and 0.4m are 0.35 and 0.5, respectively. For the case of model 5s (Figs. 3.27 - 3.29) at the water depth of 0.4m, this trend cannot be seen due to lack of data points near critical depth speed.

3.6.1.5 Effect of trim changes

The residuary resistance coefficients of model 5b and 5s catamarans with separation to length ratio (S/L) of 0.2 starting with level trim, 2° bow up and 2° bow down are compared in Figures 3.30 and 3.31.

It can be seen that bow down trim hardly affects the residuary resistance whilst bow up trim causes an increase in residuary resistance coefficient at a range of Fn between 0.25 and 0.45 in this case. The increase is significant at the peak (Fn of 0.35) where the depth Froude number is about unity for the water depth of 0.2m i.e. critical depth speed. At higher speed, the bow up trim has a small effect on the residuary resistance.

3.6.2 Running sinkage and trim

The measured sinkage and trim data of model 5b and 5s as monohull and catamaran configurations over a range of length Froude number are presented in Figures 3.32 - 3.41 at different water depths.

3.6.2.1 Effect of separation to length ratio (S/L)

The interference effects on the running trim and sinkage in both deep and shallow water can be seen in Figs. 3.32 - 3.35. The overall results and trends for deep water are broadly similar to other round bilge hulls such as those reported in Ref. 3.

For the deep water cases, trim angle interference is significant between Fn of 0.4 and 0.7 where the catamaran shows higher trim angles than the monohull, but generally approaches the monohull trim angle as S/L is increased. For shallow water cases, the interference is significant at around critical depth speed where Fn = 0.5 and 0.35 for the depth of 0.4m and 0.2m respectively. This will be discussed in section 3.6.2.3.

With regard to running sinkage, the catamaran shows significantly higher running sinkage than the monohull at Fn between 0.3 and 0.5 for deep water cases and at lower Fn for shallow water cases. In general, the sinkage is increased as the

separation to length ratio (S/L) is reduced. At higher speed, the trends change to the opposite. The monohull has higher sinkage than the catamaran and the catamaran with S/L of 0.2 has the lowest sinkage.

3.6.2.2 Effect of speed

The effect of speed can be seen from Figs. 3.32 and 3.33. Similar to the effect on the resistance, the running trim and sinkage increases and peaks at about a Fn of 0.45 and then decreases as the speed increases.

3.6.2.3 Effect of water depth

Figs. 3.36 - 3.41 illustrate the effect of water depth on the running sinkage and trim for models 5b and 5s. Similar to the effect of water depth on the resistance, there is a significant increase in running trim and sinkage at the critical depth speed where Fn is around 0.5 and 0.35 for water depths of 0.4m and 0.2m respectively. At higher speeds (supercritical speed), the sinkage and trim of the catamarans in shallow water are less than that in deep water and then gradually approach the values of deep water as the speed increases. For the case of model 5s at the water depth of 0.4m, the effect cannot be seen clearly due to lack of data points near critical depth speed. It is noted that there is probably an error in trim measurement for model 5s in deep water as the trim seems too high when compared with the results of model 5b in deep water.

3.6.2.4 Effect of propulsion system

Figs. 3.42 and 3.43 illustrate the effect of propulsion system on running trim and sinkage of model 5s catamaran with S/L of 0.2 and 0.4 travelling in shallow water (H=0.2m). It is seen that the values of running trim of both propeller and water jet are similar. Their trends agree with that of the towed model although the values for

the towed case is higher for S/L=0.2. It is noted that the tow line for the towed model in shallow water did not have a trim correction. It is also seen that the propulsion systems have little influence on the running sinkage.

3.6.3 Wave profiles

In the QinetiQ (Haslar) Ocean Basin, the 4.5m and 1.6m free running catamarans were tested in deep water at one speed for hull separation to length ratios (S/L) of 0.2 and 0.4. Multiple wave cuts were made with two wave probe arrays and two Wavetector buoys.

Example wave cuts are given in Fig. 3.44 which shows a comparison between the wave cuts for the 4.5m and 1.6m models for the same (non-dimensional) lateral wave cut position (Y/L). The results are very similar, verifying the suitability of the results from the smaller 1.6m models and the absence of any significant scale effects. Actual differences are likely to be due to the small difference in test Fn, model displacement and Y/L value.

3.6.3.1 Effect of length to displacement ratio ($L/\nabla^{1/3}$)

Figs. 3.45-3.47 illustrate the effect of length to displacement ratio ($L/\nabla^{1/3}$) on the wave profiles. Some of the measured wave cuts of models 4b, 5b, and 6b are taken as examples and compared at the same speeds and at the water depth of 0.4m. It is noted that the length of model 6b is 2.1m whilst the length of the other models is 1.6m. Therefore, the wave profiles are non-dimensionalised with the model length and presented in terms of wave height/L to a base of longitudinal distance (X)/L. The wave cuts are compared at the transverse position (Y/L) of 0.55 for models 4b and 5b and at the Y/L of 0.52 for model 6b.

It is seen that the effect on the wave profiles is similar to the effect on the resistance, namely, an increase in length to displacement ratio ($L/\nabla^{1/3}$) (from model 4b to 6b) results in a reduction of the wave height, as also seen later in Figs. 3.53a and 3.54a. The wave phases of model 4b and 5b are almost identical whilst model 6b has shorter wavelength. It is noted that models 5b and 6b are compared at the same speed but not the same Fn as model 6b, which has a longer length, whilst models 4b and 5b are compared at the same speed and Fn. At a given speed, the Fn of model 6b is 13% less than that of models 5b and 4b.

Comparison of different hull forms:

The wave profiles of models 5b and 5s are compared at the water depth of 0.2m in Fig. 3.48. Both models have the same length to displacement ratio ($L/\nabla^{1/3}$) and breadth to draught ratio (B/T) but different draught (T) and hull shape. The details are given in Table 1 and the model body plans can be seen in Fig. 3.1. Model 5b and 5s have the draught to water depth ratio (T/H) of 0.365 and 0.315 respectively. It can be seen that the wave profiles are almost identical. This also agrees with the residuary resistance measurement. The values of residuary resistance of models 5b and 5s are hardly different, as seen in Figs. 3.18 - 3.23. It is noted that model 5s has higher L/B, C_B, C_M but lower draught to water depth ratio (T/H) i.e. shallower draught. It can be clearly seen that $L/\nabla^{1/3}$ has more influence on the resistance and wave profile than L/B, C_B, C_M or T/H. Fig. 3.48b also displays solitons ahead of the model, and this subject is discussed later in section 3.6.5.

3.6.3.2 Effect of separation to length ratio (S/L)

It can be seen from Figs. 3.49 - 3.52 that the effect of hull separation ratio on the generated wave is small although there is an increase in resistance as the hull separation is reduced, noting that the wave resistance is proportional to the square of wave amplitude A_W^2. For instance, Fig. 3.51 shows that the wave cuts of model 5b

catamaran with S/L of 0.2 and 0.4 at Fn of 0.44 and the water depth of 0.4m are almost identical although the residuary resistance of model 5b with S/L of 0.2 is about 20% higher than that of the model with S/L of 0.4, as seen from Fig. 3.7. However, the increase in A_W^2 is about 22% as the hull separation ratio (S/L) is reduced from 0.4 to 0.2, then being similar to the residuary resistance change.

The waves generated by the catamaran are generally bigger than the waves generated by the monohull. This is probably due to interference effects.

3.6.3.3 Effect of speed

Figures 3.49 and 3.50 present the waves generated by model 5s catamaran travelling in deep water at two different speeds. It is seen that an increase in speed in the sub-critical speed region results in increases in wave height and wavelength. This is because wavelength is proportional to U^2 and, for the deep water case, wavelength $\lambda = 2\pi U^2/g$. The wave amplitude also depends on the speed, U as the wave drag is proportional to the terms $0.25\rho g A_w^2$ and $0.5\rho A U^2$. Increasing the speed will therefore increase amplitude and thus the wave resistance, Ref. 63.

3.6.3.4 Effect of shallow water

Figs. 3.53 - 3.56 show the plots of wave height and half wave period of leading wave height against depth Froude number. Trends are similar to the residuary resistance results.

Figures 3.57 - 3.64 illustrate the experimental wave cuts of model 5b and 5s as monohulls and catamarans travelling in shallow water at various speeds and two different water depths of 0.2m and 0.4m. The wave cuts at sub-critical, critical and

supercritical speeds are presented. To investigate the shallow water effects on wave profiles, the following conditions are compared:

1. Same water depth *but* different speed and depth Froude number: Figs. 3.57 - 3.58
2. Same speed *but* different water depth and depth Froude number: Figs. 3.59 - 3.63
3. Same depth Froude number *but* different water depth and speed: Fig. 3.64

Constant water depth:

Figs. 3.57 - 3.58 show the waves generated by the models travelling in shallow water at a constant water depth but different speed i.e. different depth Froude number Fn_H. As the speed increases, the depth Froude number increases. The effect of depth Froude number on the resistance at a constant water depth is shown in Figs. 3.24 - 3.29 and as the depth Froude number approaches the critical depth speed ($Fn_H \cong 1.0$), the wave elevation increases and then decreases when the depth Froude number is greater than one i.e. supercritical depth speed. This is also clearly seen in Figs. 3.53 - 3.56.

Constant Fn:

To investigate the effect of water depth on the wave profiles at a given speed, the waves generated by the same model travelling at the same speed i.e. Fn but at different water depth and hence depth Froude number Fn_H are compared and illustrated in Figs. 3.59-3.63. It was found that the water depth or depth Froude number Fn_H hardly influences the wave in the sub-critical speed region ($Fn_H < 1.0$). The wave phases are almost identical but the wave amplitudes are slightly different, as seen in Figs. 3.59 and 3.62. This agrees with the effect of water depth on the resistance. As seen in Fig. 3.18, the residuary resistance coefficients of model 5b monohull at the Fn of 0.25 for both water depths are little different. In the super-critical speed region ($Fn_H > 1.0$), a decrease in water depth from 0.4m to 0.2m, causing an increase in Fn_H, results in small changes in wave height and wavelength, seen in Figs. 3.60 and 3.61 whereas it hardly affects the resistance, as seen in Figs.

3.18 - 3.20. Fig. 3.63 shows a significant increase in bow wave as the water depth is increased from 0.2m to 0.4m. This is because at the Fn of 0.505 the depth Froude number of the water depth of 0.4m is the critical speed (Fn_H=1.0) whilst that of the depth of 0.2m is supercritical. It is clearly seen that the shallow water effect on the wave profiles is significant at or near the critical speed ($Fn_H \cong 1.0$).

Constant Fn_H:

Wave profiles for the same model travelling at about the same depth Froude number but different speed and water depth are compared in Fig. 3.64. It is seen that at sub-critical depth speed the Froude number or speed has an influence on wave height and wavelength, discussed in 3.6.3.3. As seen in Fig. 3.64, the wave height and length are increased as the speed increases. The resistance is also increased slightly with increasing the speed, as seen in Fig. 3.18.

3.6.3.5 Effect of trim changes

In order to investigate the effect of trim changes on generated waves, the measured wave cuts of model 5b and 5s catamarans with separation to length ratio (S/L) of 0.2 at level static trim, bow up and bow down static trim are presented and compared in Figures 3.65-3.66.

The effect of bow down trim on the wave profiles agrees with the effect on the resistance, as the waves generated by bow down trim are almost identical to the level trim, as seen in Figs. 3.65b and 3.66b. For the effect of bow up trim, the wave phases are about the same but the wave height of the bow up trim is slightly higher than the level trim. The residuary resistance of bow up trim is also higher than that of the level trim, as seen in Figs.3.30 and 3.31. For example, Fig. 3.66a shows that the wave elevation of bow up trim is slightly higher than that of the level trim whereas the increase in residuary resistance due to bow up trim seems to be more significant,

as seen in Fig. 3.31. This is because the wave resistance is proportional to the square of wave amplitude, A_W^2. In this case, the residuary resistance coefficient of bow up trim is about 20% higher than that of level trim whilst the increase in $A_W{}^2$ is about 11%. It is noted that the residuary resistance consists of wave resistance and others.

3.6.3.6 Effect of propulsion systems

Figs. 3.67-3.74 present the influence of the propulsion systems: water jets and propellers on the wave profiles in shallow water. The experimental wave cuts of model 5s catamaran with S/L of 0.4 and 0.2 travelling in shallow water are compared at sub-critical, critical and supercritical speeds. It can be seen from Figs. 3.67 and 3.71 that the water jet causes an increase in wave height at low Fn in the sub-critical depth speed region but has a small effect on the wave profiles at the supercritical depth speed, as seen in Figs. 3.69, 3.70, 3.73 and 3.74. However, the wave height at low speed region is not important as it is very low when compared to those at higher speeds and in critical and supercritical speed regions. At the critical depth speed, the water jet and propeller result in a small increase in wavelength whilst the amplitudes are hardly different, see Fig. 3.68 and 3.72.

It is seen that the differences in wave elevation between the three propulsion methods are small. This is a highly significant result as it implies that the towed case provides realistic wave cuts which compare well with those from propelled models. This further implies that towed data can be used with some confidence for design and validation work.

3.6.4 Direction of wave propagation

The diverging wave angle (θ), the angle between wave direction and the direction of the model, of the bow and stern waves was determined from the wave cuts measured

at the same longitudinal position but different transverse positions (Y/L), see Fig. 3.75. The diverging wave angles (θ) of model 5b monohull and catamaran in shallow water are plotted against depth Froude number, Fn_H in Figs. 3.76 – 3.88.

It can be seen from Figures 3.76 – 3.81 that when the depth Froude number moves toward the critical depth speed ($Fn_H \cong 1.0$), the diverging bow wave angle reduces close to zero i.e. the wave propagation's direction is almost parallel to the model's direction. The wave angle increases sharply as the depth Froude number moves to greater than one i.e. the wave pattern becomes steeper. This trend was also obtained by Whittaker [31] and Kofoed-Hansen [32].

The experimental results agree satisfactorily with the theoretical diverging wave angles calculated from the following equations, Ref. 32:

$$\theta = 35.267\left(1 - \exp\left(12\left(Fn_H - 1\right)\right)\right) \quad \text{for } Fn_H < 1$$

$$\theta = \cos^{-1}\left(\frac{1}{Fn_H}\right) \quad \text{for } Fn_H > 1$$

A physical description is offered by Whittaker [31] in that as depth Froude number increases, the longer wave components in the wash begin to feel the bottom and the wave properties start to change. The long waves become steadily less dispersive between depth Froude number of 0.57 and 1.0. At critical speed region (Fn_H at or near 1.0), the energy is being pumped into a few transverse waves with front perpendicular to the direction of the ship. The waves, therefore, travel at the same speed as the ship and parallel to the direction of the ship. At supercritical speed, the transverse waves are left behind, as they can not keep the pace with the ship because their velocity is limited by water depth. The wave crests are concave close to the ship as they are pulled along at a greater speed than they can sustain due to the limited water depth.

It is also found from the experiments that the stern wave travels at a higher angle than the bow wave at the supercritical speeds. This is because the wave crest length increases whilst the wave height reduces as the waves propagate toward the tank wall, as seen in Fig.3.75. The similar trend was also obtained by Whittaker [64]. In addition, as the depth Froude number increases, the difference between the bow and stern wave propagation directions becomes smaller.

It can be seen from Figs. 3.82 - 3.88 that the water depth and hull separation hardly affect the direction of wave propagation.

3.6.5 Solitons

3.6.5.1 Effect of longitudinal distance (x)

As the model travels along the towing tank in shallow water at the near or critical depth speed ($Fn_H \cong 1.0$), solitons are built up and spill out ahead of the model. Their amplitudes are very high when compared to the waves at sub- and supercritical speeds and are above the still water level. The wave direction of propagation of the solitons is almost parallel to the direction of the model, as seen in Figs. 3.76 - 3.81. The number of solitons increases as the model travels along the tank, as seen in Figs. 3.89 - 3.90. It can be seen from the Figures that when the model passes the front probes, there are about 1.5 solitons. Then when the model passes the back probes, there are 3 solitons. The longitudinal distance between the front and back probes is about 46 meters.

It is generally considered that the production of solitons, at or near critical speed, is increased due to the finite width of the tank. Solitons are therefore not considered further in the present investigation. Studies into the physical properties of solitons have been carried out, such as those reported in Refs.65 and 66.

3.7 Summary

3.7.1 An extensive data base has been established which shows the effects of length to displacement ratio, hull separation, speed, water depth, and significant trim changes on resistance and wave wash.

3.7.2 The database included the effects of hull separation and shallow water on the direction of the wave propagation and running sinkage and trim.

3.7.3 The results show that an increase in length to displacement ratios causes a decrease in residuary resistance and wave height.

3.7.4 For catamarans, the hull separation to length ratio (S/L) was found to have an influence on resistance and running sinkage and trim, especially at the hump speed. It hardly affects the wave wash and direction of wave propagation.

3.7.5 Significant changes in model behaviour occurred at or near the critical speed, Fn_H=1.0. There were large increases in resistance and wave height and significant changes in sinkage and trim and the direction of wave propagation.

3.7.6 At around the critical speed, the resistance increases as the water depth is decreased. This implies that the shallow water effect at the critical speed depends on the water depth. This may be due to the effect of clearance under the hull.

3.7.7 The effect of significant static trim changes on resistance and wave was examined. It was found that the bow up trim causes an increase in resistance especially at the hump speed but it hardly affects the wave height.

3.7.7 The effect of the propulsion system on wave profiles is found to be small. This implies that the towed case provides realistic wave cuts which compare well with those from propelled models. This further implies that the data obtained from towed models can be used with some confidence for design and validation work.

3.7.8 The data should prove useful for assessing the influence of the main hull parameters, speed and water depth, for the validation of theoretical wash prediction methods and for input into wave propagation models.

4. REFINEMENTS TO THE THEORY

4.1 Introduction

Basic thin ship theory requires a number of refinements in order to improve its potential for predicting wave pattern resistance and wave wash in a reliable manner over the whole range of likely ship operation and requirements. For instance, the transom stern which is used by most high speed displacement ships is known to have a significant effect on wavemaking, and hence on wash. The effects of the transom are also known to be sensitive to changes in the operational trim of the vessel, Ref. 9. As a result, running sinkage and trim are needed to be estimated.

4.2 Transom Stern Corrections

As described in Chapter 2, thin ship theory represents a body with a source-sink distribution over the centreplane of the hull. The calculated source strength in each panel depends on the slope of the waterline (dy/dx). For a ship with a transom stern, the waterline slope on the transom is, therefore, undefined causing the under-prediction of wave resistance and wave wash. As a result, there is need for a transom correction to improve the potential for predicting wave resistance and wave wash.

For the prediction of wave resistance, a hydrostatic ($\rho g H_T$) transom resistance correction, Ref. 8, has been a popular and reasonably satisfactory procedure. It gives a reasonable correction to the resistance but it is important to note that it does not do so by correcting the wave system and is therefore not suitable for correctly predicting the wave wash. The use of sources/sinks placed in the vicinity of the transom, Refs. 67 and 7, has been used with reasonable success for correcting the wave pattern resistance, whilst the creation of a virtual stern and associated source strengths, Refs.

9, 13 and 68, has been found to provide the best results in terms of the wave pattern resistance. Typical examples, from Refs. 7 and 9, of the predicted wave pattern resistance using a single source correction and a virtual stern correction are shown in Figs. 4.1 and 4.2.

In view of the proposed use of the thin ship theory to predict wave wash, the use of a virtual stern based on Couser [9] and source corrections based on Lee [7] are investigated for wave wash prediction for ships with transom sterns. In order to provide a better understanding and obtain the best predictions, the use of different positions of a single source and a single trailing line of sources with various numbers of sources is also investigated.

4.2.1 Virtual Stern Transom Correction.

The Virtual Stern approach was introduced by Couser [9&13] in order to improve the prediction of wave pattern resistance of a ship with a transom stern. It was found that the approach gave very good prediction for wave pattern resistance. In this method, the virtual stern is added to the transom which encloses the separated flow in the low speed range and the air pocket in the high speed range, see Fig. 4.3.

From physical observations, it is found that the length of the hollow varies with speed. Fig. 4.4 shows typical experimentally derived values of re-attachment length for different speeds (Fn), compared with values of re-attachment length of the virtual stern (L_{VS}) from Couser [9] and from Doctors [68] used in theoretical methods to achieve a suitable correction. Some full-scale measurements of the length of the hollow in the water behind the transom on two wave piercing catamarans with hard-chine hull forms were carried out by Armstrong and discussed in Ref. 69. These are shown in Fig. 4.4 and it is interesting that the full-scale results are reasonably close to the values used by Doctors in the theoretical methods.

In Ref. 9, the re-attachment length of the virtual stern (L_{VS}) was obtained by choosing the length which gave the best results for wave pattern resistance over a specific range of Froude number. The re-attachment length was found to be dependent on Froude number and Breadth to Draught ratio (B/T). The experimental values were obtained by physical observation during the experimental tests in shallow water, Chapter 3. It can be seen from Fig. 4.4 that in order to obtain a good prediction of wave pattern resistance using the virtual stern correction, the theoretical values need to be higher than those obtained from physical observations. The reasons for this are not altogether clear.

From the observations and Fig. 4.4, it is seen that the length of the hollow depends on the speed. The length increases as the speed increases. This agrees with the trend of deficit of source strength required by the theory to give a net source strength of zero, as discussed later in section 4.2.2. It was also found from the tests that bow up trim tends to shorten the length of the hollow whilst bow down trim increases the length of the hollow.

The virtual stern can be easily created and added to the transom of the ship by using a typical commercial lines faring package such as ShipShape [52]. In the current model, these lines are established as parabolas. The offsets for the ship with a virtual stern are created and then used as an input file for source strength calculations within the thin ship theory program.

The effect of re-attachment length on the wave pattern and wave pattern resistance at a given speed has been investigated. The model used is 5b monohull travelling at Fn of 0.785. It is seen from Fig. 4.4 that at Fn of 0.785 the length of the hollow behind transom observed from the experiment is 3 times half transom breadth whilst the re-attachment length recommended by Doctors [68] and Couser [9] are 6 and 8 times half transom breadth respectively. Three different re-attachment lengths: 3, 6 and 8 times half transom breadth were, therefore, chosen for the investigation.

The wave pattern resistance is found to be reduced as the re-attachment length is increased, as shown in Fig. 4.6. Increasing the re-attachment length of the virtual stern from 3 to 8 times the half transom breadth causes a reduction of 20% in wave pattern resistance for this case. This brings it much closer to the measured wave pattern resistance, as discussed later.

Fig. 4.7 shows the effect of the re-attachment length on the wave profile at Fn of 0.785 in shallow water with a depth of 0.4m. It is seen that when the re-attachment length is increased, the wavelength is increased whereas the amplitude and phase are hardly changed. The distribution of total source strength of the three re-attachment lengths is shown in Fig. 4.8a. The net source strength of the hull with the virtual stern of these three cases is zero. Fig. 4.8b shows the vertical distribution of source strength at positions near the bow and within the virtual stern, with the reattachment length 3 times half transom breadth. It is interesting to note the distinct increase in source strength near the surface and the implications of this are discussed again later.

The theoretical wave cuts for three different re-attachment lengths, plotted against an experimental wave cut, at Y/L of 0.55 in shallow water (0.4m), are shown in Figs. 4.9 a-c. The theoretical wave cut using the virtual stern with L_{VS} of 3 times half transom breadth is compared with a theoretical wave cut with no correction at Y/L of 0.55, Fig. 4.10. It can be seen that thin ship theory with a virtual stern correction is considerably less damped than the experiment and the theory with no correction. This tends to arise due to the concentration of source strength near the water surface, Fig. 4.8b. In the case being considered (Fn=0.785, B/T =2.0), it was recommended by Couser [9] to use a re-attachment length of 8 times half transom breadth. The theoretical wave pattern resistance coefficient (C_{WP}) using the virtual stern with L_{VS} of 8(B/2) is 0.00093 compared with 0.0006938 with no correction. The estimated experimental wave resistance coefficient (C_W) is 0.00109 which was obtained using the equation: $C_W = C_T - (1+k)C_F$, Ref. 11. It is clearly seen that using the virtual stern correction gives a distinct improvement in the prediction of the wave pattern resistance.

A similar result is also obtained in deep water, as seen in Fig. 4.11. A theoretical wave cut for model 5b monohull is compared with an experimental wave cut at Fn of 0.44, Y/L of 0.694 with the water depth of 1.85 metres. It is also seen that the theory plus a virtual stern correction gives less damping than the experiment. However, it shows reasonable agreement between the experiment and theory, particularly for the leading waves. The re-attachment length used is 4.55 of half breadth at transom, taken from Couser's line, Fig. 4.4.

It can be clearly seen that using thin ship theory with the virtual stern correction gives less damping for the trailing wave profiles than experiment or using the theory with no correction, although it can give good results for the wave pattern resistance. The length of the virtual stern hardly affects wave amplitude and phase but affects wavelength and wave pattern resistance. In the main, the predictions for the leading waves, which are important from the point of view of wash analysis, are good.

Doctors and Day [26] used the virtual stern with nonlinear free-surface effects by introducing a vertical straining or distortion of the hull for the prediction of the resistance, sinkage and trim. The influence of boundary-layer was also included by means of adding the displacement thickness to the hull. It was found that the nonlinear methods did not improve the predictions for the resistance, sinkage and trim and the boundary-layer model showed hardly any improvement to the prediction.

4.2.2 Single Source Transom Correction.

The use of a single source, or limited number of sources, near the transom has been applied by a number of investigators, Refs. 7, 29, and 67. If a suitable position and strength of a source can be established, then the method can offer a very simple but effective transom correction without the need to create a virtual stern.

A single source correction was used and investigated for the prediction of wave pattern resistance by Lee [7]. He found that placing the single source at the bottom of transom on the centre-plane of the hull gave the best result for wave pattern resistance. To balance out the net positive strength of the hull and produce a closed body, the strength of the source was set as a balancing source to give the net source strength of zero i.e. no water passes through the hull. This approach tends to give a good prediction of wave pattern resistance for Fn greater than about 0.35, Fig. 4.1.

In the current investigation, the effect of the position of a single source on the wave profile and wave pattern resistance was firstly investigated. This would provide some fundamental evidence as to the best position to site a single source. Model 5b monohull is used as an example. Four positions are considered, as illustrated in Fig. 4.12. The strength of the source is the same for all positions. Positions 1 and 2, designated as ss1 and ss2, are close to the transom at the bottom and waterline, respectively. Positions 3 and 4, designated as ss3 and ss4, are further aft of the transom at a longitudinal distance of 10% L_{WL} at the bottom and waterline respectively. The distance between the waterline and the bottom of the transom is 2.4% of L_{WL}.

Fig. 4.13 shows the effect of the position of the single source on wave profiles in shallow water. It can be seen that placing a single source at waterline level (positions 2&4) gives less damping than placing the source at the bottom (position 1&3). In addition, the longitudinal position of the single source at the waterline level has an effect on wave height but a small effect on wave phase whereas moving the source at the bottom of the transom in the longitudinal direction affects the phase but hardly affects the wave profile.

The results of this investigation also help to explain the predicted wave profiles obtained using the virtual stern correction, since the number of sources/sinks near the

waterline is more than that near the bottom, as seen in Fig. 4.8b. This results in less damping of the wave profile, as identified in section 4.2.1.

A similar result is also obtained in deep water, as shown in Fig. 4.14. The single source only affects the wave amplitude. Placing the single source at the waterline close to the transom (ss2) gives less damping than placing the single source at the bottom of transom (ss1).

The position of the single source also affects the wave pattern resistance. As the single source is moved up from the bottom of transom to the waterline level, the wave pattern resistance coefficient increases by about 80% while if the single source is moved longitudinally from a position close to the transom to the position at 10% of L_{WL} aft the transom, the wave pattern resistance coefficient reduces by only about 11%. This agrees with the effect on the wave profile and confirms that the vertical position of the single source has more influence on the wave profile and wave pattern resistance than the longitudinal position.

It is clearly seen that placing a single source at the bottom close to the transom gives the best result for both wave pattern resistance and wave profile for Fn greater than about 0.35.

Fig. 4.15 shows a theoretical wave cut using a single source placed at the bottom of the transom, plotted against a theoretical wave cut with no correction and an experimental wave cut, for model 5b monohull at Fn of 0.785. It can be seen that the theory shows good agreement with the experiment for wave height, although with a slightly different phase. In general, the theory with no correction gives less wave height than the experiment. Using a single source correction can improve the wave height. It is also seen that the single source correction affects the wave amplitude but hardly affects the phase.

In the case of Fn below about 0.35, Fig. 4.16a shows the comparison between a predicted wave profile using thin ship theory with no correction and a measured wave profile at a Fn of 0.22. It can be seen that the thin ship theory with no correction under-predicts the wave amplitude. If the single source is used with value of strength set as a balancing source to give the net source strength of zero i.e. the strength of the single source = – total source strength, the wave profile is over-predicted, as seen in Fig. 4.16b. It can be seen that the predicted wave profile has greater amplitude than the measured one. This agrees with the result for wave pattern resistance, as mentioned above. It is found for this example that the strength of the single source needs to be reduced to about 25% of the total source strength to give a satisfactory result, as seen in Fig. 4.16c. This would tend to indicate that transom effects, and hence transom corrections, tend to diminish at these slower speeds. Lee [7] found a similar result for wave resistance and systematically reduced the hydrostatic correction between Fn = 0.4 and 0.2.

4.2.3 A single trailing line of sources correction

The use of a single trailing line of sources placing at the bottom of transom on the centreplane for the prediction of wave pattern resistance was investigated by Lee [7]. The strength of sources was determined by extrapolating values from the total source strength of the hull. The number of sources was determined by the requirement to achieve zero net source strength. The results in Ref. 7 showed that using the single line of sources gave less wave pattern resistance than using the single source. This is probably due to a large number of sources used.

In the current study, the effect of number of sources on wave profiles and wave pattern resistance was, therefore, investigated. The number of sources used is 5, 10 and 15 sources. The single line of sources is placed at the bottom of transom on the centreplane of the hull, as seen in Fig. 4.17. The sources are of equal strength and the sum of all the sources gives the net source strength over the hull of zero.

It is found that the number of sources has little effect on wave profile. Increasing the number of sources results in a small reduction in wave height, as seen in Fig. 4.18a and 4.18c. The theoretical wave profiles are compared with the experimental wave profile in Fig. 4.18b and reasonable agreement is found.

With regard to wave pattern resistance, the wave pattern resistance is reduced linearly as the number of sources increases, as seen in Fig. 4.19. Increasing from 5 to 15 sources causes a reduction of 13% in C_{WP}. This agrees very well with the reduction in wave height as the square of the leading wave height is also reduced by 12.9%.

4.2.4 Summary

The use of a virtual stern, a single source and a single line of sources corrections have been investigated for the prediction of the wave profiles of high speed displacement catamarans with transom sterns. It is found that the virtual stern correction gives less damping for the trailing wave profiles. Using a single source increases the wave amplitude but hardly affects the phase. The single source gives more damping than the virtual stern and good agreement with the experiment for Fn greater than about 0.35. The single line of sources gives little improvement on the single source correction.

Overall, in terms of wave profiles, the use of a single source placed at the bottom close to the transom is deemed to be the most effective, as it gives the best results and is the simplest to apply. The use of a single source correction will, therefore, be further investigated and validated in Chapter 5.

4.3 Dynamic Sinkage and Trim

Changes in dynamic sinkage and trim affect the immersion of transom, which is known to have a significant effect on wave pattern resistance, and hence wave wash [9]. It is, therefore, important to be able to incorporate suitable estimates of running sinkage and trim in the theoretical model. In the present investigation, a regression analysis of available data has been carried out which allows rapid estimates of sinkage and trim to be made. This analysis is described in the next section.

4.3.1 Regression analysis of dynamic sinkage and trim

A predictive technique is established by regression analysis using experimental data from Refs. 2, 3 and 11. Length to displacement ratio ($L/\nabla^{1/3}$) was found to have a significant effect on sinkage and trim, Ref. 3. Therefore, dynamic sinkage and trim are considered as dependent variables while length to displacement ratio ($L/\nabla^{1/3}$) is considered as an independent variable.

In 1992 models 3b, 4b and 5b were tested at the University of Southampton. Model 6b and some of the previous models were re-tested in 1996. The experiments were carried out in the Southampton Institute test tank, for which dimensions are shown in Chapter 3. The models were of round bilge form with transom stern and derived from the NPL round bilge series with the range of $L/\nabla^{1/3}$ between 6.27-9.50. The details of the models are given in Table 2.

As seen from Table 2, length to displacement ratio ($L/\nabla^{1/3}$) is increased when going from models 3b to 6b. The models were tested as monohulls and catamarans with separation to length ratios (S/L) of 0.2, 0.3, 0.4, and 0.5 at a range of Fn between 0.2 and 1.0. The total resistance, running trim and sinkage were measured. The results were published in Refs. 2, 3 and 11. Hence, the effect of length to displacement ratio on running trim and sinkage can be investigated at each configuration and speed.

It was found that between Fn of 0.3 and 0.7 the catamaran shows higher trim angles than the monohull and generally comes near the monohull trim angle as the separation to length ratio (S/L) is increased, Ref. 3. As the length to displacement ratio ($L/\nabla^{1/3}$) is increased the running trim is decreased, as seen in Fig. 4.20. The positive value of trim represents bow up. The effect of length to displacement ratio ($L/\nabla^{1/3}$) is significant at a Fn between 0.4 and 0.7.

The trim angle can be considered as a function of length to displacement ratio ($L/\nabla^{1/3}$) and can be put into the equation: Trim angle = $a[L/\nabla^{1/3}]^n$. The values of a and n are shown in Table 3. It is noted that, at Fn below 0.4, the trim angles seem to be independent of the length to displacement ratio ($L/\nabla^{1/3}$). The R^2 values are shown in Table 5. It is seen that the R^2 values are very close to 1.0.

With regard to running sinkage at Fn between 0.3 and 0.5, as the length to displacement ratio ($L/\nabla^{1/3}$) is increased, the running sinkage is decreased and the catamaran shows higher sinkage than the monohull and generally approaches the monohull sinkage as the separation to length ratio (S/L) is increased, as seen in Figs. 4.21a-c. The positive value of sinkage means an increase in draught or downwards and its unit is in percentage of draught. At Fn of 0.6, where its direction begins to change to the opposite, the monohull has higher sinkage than the catamaran and the catamaran with S/L of 0.2 has the lowest sinkage, see Fig. 4.21d. Above Fn of 0.7, the relation between sinkage and length to displacement ratio ($L/\nabla^{1/3}$) is opposite compared with lower speeds. As length to displacement ratio ($L/\nabla^{1/3}$) is decreased the running sinkage is reduced (ie. The models rise.), as seen in Figs. 4.21e-h.

The relation between running sinkage and length to displacement ratio ($L/\nabla^{1/3}$) can be represented as Sinkage (%draught) = $a(L/\nabla^{1/3})^n$ - m. The values of a, n and m of each case at a given speed are shown in Table 4. It is noted that the equation is for Fn greater than 0.4 as the running sinkage at Fn below 0.3 seems to be independent of length to displacement ratio ($L/\nabla^{1/3}$), Ref. 3. The R^2 values are indicated in Table 6.

Most of the values are close to one except the cases of Fn=0.3 and Fn=0.7, Catamaran with S/L=0.2 and 0.5 where the data are scattered.

The predicted sinkage and trim are compared with the experimental sinkage and trim in Figs. 4.22a&b. It is seen that the agreement between the experiment and prediction is acceptable.

It is noted that this regression analysis is valid only for deep water case. As discussed in Chapter 3, shallow water has an effect on sinkage and trim at or near critical depth speed ($Fn_H \cong 1$) although at sub-critical and supercritical the effects are not significant. The regressions are therefore also suitable for shallow water for sub-critical and supercritical speeds. At or near critical speed, the large increases in sinkage and trim have to be considered separately.

4.3.2 Hybrid Model

A hybrid model is under development in the Fluid-structure Interaction Research Group, University of Southampton. The author has been partly involved.

An important feature of the hybrid model is that it facilitates improvements in the estimates of dynamic sinkage and trim based on changes in the dynamic pressures around the hull. The model links the thin ship wave prediction procedures to an existing well proven panel code, PALISUPAN, Ref. 70. In the current version of the procedure, a fixed horizontal waterline is used in the panel code and the hydrostatic moment resulting from the actual wave elevation around the hull is derived by numerical integration of the wave.

This technique provides reasonable first order approximations to sinkage and trim and should be suitable for new developments in hull forms for which acceptable trim and sinkage data are not available. In order to improve the robustness of the method,

further work is ongoing by another research team to use the theoretical estimate of hull wave profile directly in the panel code. Fig. 4.23 shows an outline of the overall approach which is still under development.

4.4 The Prediction of Wave Profiles along the Hull

An estimate of the hull wave profile over the hull is required in order to provide the limits of the integration of pressures over the hull. These in turn may be used to estimate dynamic sinkage and trim or hydrostatic forces and moments, as discussed in section 4.3.2.

Linear thin ship theory has been used to predict the wave pattern resistance and wave elevations with some success. The potential convenience of using the same theory to estimate the wave profile around the hull was also investigated.

Based on the generated wave pattern, the wave elevation was calculated firstly around the hull waterline shape and then using longitudinal cuts at B/4 and B/2 off the centreline, as seen in Fig. 4.24. The technique was investigated for the Wigley parabolic hull and the round bilge hulls.

It has been found that using the longitudinal cuts at B/4 off the centreline gives the best agreement with the experimental wave profiles. However, the theoretical wave cuts need to be shifted forward in order to match the phase with the experimental ones. This is probably because the wave pattern close to the hull is non-linear, see Fig. 4.25. Linearlised thin ship theory is not able to predict these non-linear effects, unless artificial sources are placed ahead of the bow, see Hogben [71]. The distance required to shift the waves forward was found to be dependent on Froude Number and was investigated.

Wigley Hull:

Figs. 4.26 and 4.27 show the comparisons between theoretical wave cuts and experimental wave profiles along the Wigley hull at Fn of 0.35 and 0.5 respectively. The experimental wave profiles are taken from Insel [1] and Shearer [72]. In order to match the phase with the experimental wave profiles, the theoretical wave cuts were required to be moved forward for a distance of 32% and 16% of ship length for Fn of 0.35 and 0.5 respectively. It can be seen that the theory gives promising agreement with the experiment, especially at a Fn of 0.5. The wavelength and phase are well predicted. The amplitude of the bow wave is found to be under-predicted. The under-prediction of the bow wave was also obtained by Zhang [73] and Stern [74]. As was discussed by Stern, this may be because of the existence of a thin film and beads of fluid at the bow region. He also found that CFD was unable to predict them.

Apart from the bow wave, the stern wave is overestimated and the hollow is exaggerated by the theory. These features were also obtained by Gadd [30, 75]. In Ref. 30, a second order method where sources were placed on the centre-plane of the hull was introduced. The theoretical wave profiles of Wigley hull obtained from the second order method were compared with Michell theory and Guilloton's method. It was found that the second order method gave a reduction in amplitude for stern crest and hollow. He suggested that the over-predicted stern crest was probably due to viscous effects on the experimental wave.

Round Bilge Hull:

A limited number of wave profiles along an NPL hull were measured by Spencer [76]. The model was equivalent to model 4b used at the University of Southampton. The model's parameters are shown in Table 1. The model was tested in monohull and catamaran configurations with the hull separation to length ratio (S/L) of 0.4. The wave profiles were measured and plotted relative to the model, whereas the theoretical wave cuts are relative to earth or static waterline. Due to dynamic sinkage

and trim, these two references are angled to each other. In order to compare the experiment with the theory it was necessary to adjust the experimental wave profiles to be relative to earth by rotating the wave profiles about LCF.

Figs. 4.28 – 4.30 show the comparison between the experimental wave profiles along the NPL (model 4b) as monohull and the theoretical wave cuts at B/4 at Fn of 0.4, 0.6 and 0.9 respectively. It can be seen that the theory can give promising agreement with the experiment, although the theory underpredicts the trough at about amidship at Fn of 0.4 and 0.6 and the amplitude of the bow wave at Fn of 0.9. These also agree with the case of Wigley hull.

Fig. 4.31 shows the theoretical wave profiles at B/4 compared with the experimental wave profiles of the catamaran with the separation to length ratio (S/L) of 0.4 at Fn of 0.4 for both inboard and outboard. It was found from the experiment that the inboard wave profile has a little higher amplitude than the outboard wave profile. This is due to the interference effects between demihulls. This can also be obtained from the theory, Fig. 4.31c. The comparison of the outboard wave profiles between theory and experiment at Fn of 0.6 and 0.9 are shown in Figs. 4.32 and 4.33. The agreement between experiment and theory is acceptable.

In order to match the phase of theoretical wave cuts with the experimental wave profiles, the theoretical wave cuts were shifted forward by 20%, 10% and 5% of ship length at Fn of 0.4, 0.6 and 0.9 respectively for both monohull and catamaran configurations.

As there were limited data available for the wave profiles along the NPL hull forms, the data for a similar hull form, the Athena, taken from Brizzolara [77] were therefore used to compare with model 4c. Although the Athena does not have the same hull form, its length to displacement ratio ($L/\nabla^{1/3}$) which tends to be the important parameter in the case of resistance, is similar to that of model 4c, Table 7.

It can be seen from Figs. 4.34, 4.35 that the agreement between experiment (Athena) and theory (model 4c) is reasonable although the bow wave is a little overestimated and the stern wave is a little underestimated. Brizzolara [77], found that the numerical wave profile for the Athena, obtained from a linear boundary element method, had a lower bow wave amplitude than the experimental wave profile at Fn of 0.65 but at Fn of 0.48 they were well matched except for the stern wave which agree very well with the case of model 4b. It was suggested that the bow wave was breaking at higher speeds and the non-linear methods could be used for high speed hulls. The wave profile of the Athena model at Fn of 0.48 was also predicted by Cong [28] using thin ship theory with a sink line along the bottom edge and flat ship theory on the bottom of the overhang aftbody. It was compared with Michell (equivalent to thin ship theory), Rankine source and Guilloton methods. The prediction was found to be more or less the same as Michell's method except with lower stern wave amplitude.

The theoretical wave cuts of model 4c were shifted forward for 15% and 10% of ship length at Fn of 0.48 and 0.65. These agree very well with the previous cases.

It can be seen from all three cases that as the speed is increased, the distance needed for shifting the theoretical waves forward is decreased. The trend in forward shift of the theoretical waves is shown in Fig. 4.36. The distance required to move forward is suitably represented by

$$\text{forward shift (\%L)} = 4.176/\text{Fn}^{1.709}$$

It is seen that all three cases follow the numerical trend well, except for the case of the Wigley hull at Fn of 0.35.

It is clearly seen that thin ship theory can provide acceptable approximations to the wave profiles along the ship hull for the intended uses. This is important in that it will allow the incorporation of this in future hybrid developments.

4.5 Summary

4.4.1 The use of a virtual stern, single source and a single trailing line of sources corrections were investigated for wave wash prediction of ships with transom sterns. In terms of wave profiles, the single source correction was found to be satisfactory and the simplest to apply.

4.4.2 The effect of the position of the single source on wave pattern resistance and wave profiles was investigated. It was found that changing the source in the vertical direction has a significant effect on wave pattern resistance and wave profiles. Using a single source near the base of the transom gives the best result for wave profiles.

4.4.3 The virtual stern correction gives best result for the wave pattern resistance but not for the wave profiles, as it causes less damping in the trailing wave profiles than the experiment. This is due to the number of sources/sinks positioned near the waterline, as discussed in 4.2.2.

4.4.4 A regression analysis of dynamic sinkage and trim of NPL hull form with the range of $L/\nabla^{1/3}$ between 6.27-9.50 in deep water was established. Other than near the critical speed, this analysis was found to be also suitable for shallow water.

4.4.5 Thin ship theory can provide an acceptable approximation to the wave profiles along the ship hull.

4.4.6 A hybrid model is under development. An important feature of the hybrid model is that it facilitates improvements in the estimates of dynamic sinkage and trim based on changes in the dynamic pressures around the hull. This

technique provides reasonable first order approximations to sinkage and trim and should be suitable for new developments in hull forms for which acceptable trim and sinkage data are not available.

5. VALIDATION OF THE THEORY AND EXAMPLE APPLICATIONS

5.1 Introduction

The theory has been well validated for wave pattern resistance in deep water, Refs. 1, 7, 9, and 13. In this chapter, the theory will be validated for the physical wave patterns and profiles, especially in shallow water and at supercritical speeds, using the new shallow water experimental data presented and described in Chapter 3. In order to cover typical ship operating regimes, the cases of a ship travelling in deep water, shallow water at sub-critical speed and shallow water at supercritical speed are considered. The validation includes the effects of length to displacement ratio, hull separation ratio, trim changes and depth Froude number on wave pattern resistance and wave profiles. For this part of the investigation, the thin ship theory with a single source correction and with no correction is used for theoretical validation of wave profiles of ships with transom sterns. The theory with a single source correction is used for the prediction of wave pattern resistance. The distribution of the component of wave pattern resistance and the propagation direction of the diverging waves are also investigated and presented.

5.2 Validation

5.2.1 Wigley Hull: Deep Water

The Wigley hull, Fig. 5.1, is a mathematical parabolic hull form with no transom. It therefore forms a good example for validation of the theoretical program and a transom correction is not needed. The hull surface was defined by the equation y/b =

$(1-x^2/l^2).(1-z^2/d^2)$ adopted by Wigley [78] where the origin lies at the intersection of the median, midsection and water planes. x, y, and z are the longitudinal, transverse and vertical ordinates of the hull surface and l, b, and d are the half length, half breadth and draught respectively. The principal particulars of the model used in the investigation are L= 1.8, L/B= 10, B/T= 1.6, $L/\nabla^{1/3}$= 7.116, C_B= 0.44, C_P= 0.667 and C_W= 0.607. These are the same as those for the experimental model used by Insel [1].

Fig. 5.2 shows the comparison of theoretical and experimental wave pattern resistance over a wide range of speeds. The experimental results were taken from Insel [1] and it is seen that good agreement is achieved. Figs. 5.3a&b show the comparison of distribution of the components of the computed and measured wave pattern resistance. The parameter θ is the direction of propagation of each component wave mode. It is noted that the transverse part of the Kelvin wave system corresponds to $\theta < 35°$. As was found by Insel [1], the theory tends to overestimate the transverse waves.

Theoretical and experimental wave cuts at Fn of 0.331 at two different transverse positions are shown in Fig. 5.4. They also show good agreement. The good agreement between experimental and theoretical results of wave resistance and wave profiles for the Wigley model has also been found by other researchers such as Millward [23], Everest [24], Gadd [30], Shearer [72] and Zhang [73]. This is perhaps not surprising, as there is no need for any form of transom correction.

5.2.2 Round Bilge Hull: Deep Water

Model 5s which has round bilge form with transom stern, Fig. 3.1, derived from the Series 64 round bilge series [57], was tested as a catamaran configuration in deep water in the towing tank at Southampton Institute. The dimensions of the model are in Table 1. Figs. 5.5 - 5.7 illustrate the comparison of the theoretical and experimental wave cuts of model 5s catamaran travelling at medium to high speeds

in deep water (sub-critical speeds). It can be seen that the theory can provide reasonable results for wave wash prediction for a ship with transom stern. The thin ship theory with a single source correction overestimates the bow wave for all speeds. Apart from the bow wave, the theory with a single source correction generally gives better prediction than the theory with no correction, which slightly under-predicts the wave height. It was noted in Chapter 4 that from the aspect of overall wave pattern resistance, more realistic results are achieved when the single source transom correction is applied.

5.2.3 Round Bilge Hull: Shallow Water

Shallow water (Sub-critical speed):

Fig. 5.8 shows the comparison of measured and predicted wave cuts of model 5b monohull at Fn of 0.22 and Fn_H of 0.44 at Y/L of 0.93. The theory with no transom correction underestimates the wave height although the wave phase is well predicted. It can be seen that the theory with a single source correction gives an acceptable result. It is noted that the strength of a single source for this case was reduced to 25% of the deficit of total source strength, as discussed in Chapter 4.

Figs. 5.9 - 5.10 show the predicted wave cuts compared with the experimental wave cuts of 5b monohull at the water depth of 0.4m and Fn of 0.38 and 0.44 respectively. Fig. 5.11 illustrates the comparison of the wave cuts of model 5b catamaran with S/L of 0.4 at the water depth of 0.4m and Fn of 0.435. The theory shows an acceptable agreement with the experiment. As seen from Fig. 5.9, the theory with a single source correction gives a better prediction, particularly at the rear of the wave system. Some wave phase shift is seen in Fig. 5.9 and 5.11, which is likely to arise from non-linearlities in the actual (experimental) wave system. The shift of the theoretical is forward in the case of the monohull (Fig. 5.9) and aft in the case of the catamaran (Fig. 5.11).

It is noted that the theory overestimates the leading bow waves at a Fn higher than about 0.38. It can be seen from Figs. 5.10 and 5.11 that at a Fn of 0.435 and 0.44, the theory over-predicts the bow wave which is similar to the case of high Fn in deep water (sub-critical speeds), as seen in Figs. 5.5 - 5.7. It is noted that the case of 5b monohull at Fn of 0.38 and water depth of 0.4m (Fig. 5.9) has the value of Fn_H = 0.76 which is higher than those in deepwater (high Fn, sub-critical speeds) case. The overestimated bow waves, therefore, seem to depend on Fn rather than Fn_H.

In a similar manner to the deepwater (high speed) case, the theory with no correction gives better prediction of the leading wave for the case of Fn = 0.435 and 0.44, but in general it underestimates the wave height. Apart from the over-predicted leading wave at the Fn of 0.435 and 0.44, the theory with a single source gives better results.

Shallow water (Supercritical speed):

Figs. 5.12 - 5.19 show the comparison between the experimental and theoretical wave profiles of model 5b as monohull and catamaran configurations travelling at supercritical speeds with two different water depths. In general, the theory provides an acceptable agreement with the experiment, especially at very high speeds. The theory with no transom correction underestimates the wave height. The theory with a single source correction gives better results, including the prediction of the leading bow waves.

However, it has been found that at the supercritical speeds the theory with a single source creates a hollow in front of the bow wave. The size of the hollow seems to depend on Fn. As Fn increases, the size of the hollow is reduced. It is seen from Figs. 5.18 and 5.19 that the two conditions have the same Fn but different water depth and, hence, Fn_H. The size of the hollow of both conditions is about the same. From Figs. 5.12 and 5.13, the two cases have about the same Fn_H but different Fn. It is seen that

the one with Fn of 0.511 has a bigger hollow. This is probably because at Fn about 0.5 the wave height is more significant, as is also the case for C_{WP}.

Overall, the single source correction helps to improve the prediction of the wave profiles, and it generally gives a better prediction than the theory with no correction. This type of single source correction does therefore offer a practical method for the transom correction. However, there are some limitations. At very low speeds (Fn < 0.35) in the sub-critical speed region, in order to get acceptable correction the strength of the single source must be reduced to less than 100% of the deficit of total source strength. This needs further investigation. For Fn > 0.35, the strength of the single source should be set equal to 100% of the deficit of total source strength, as discussed in Chapter 4. At sub-critical speeds with Fn > 0.44, the theory with a single source correction over-predicts the bow wave although it gives good prediction in general.

In the supercritical speed region, the single source correction can also be used as it gives better predictions than the case with no correction. However, it should be used with care as it creates the hollow in front of the bow wave, especially at Fn about 0.5. The hollow becomes less significant as the speed increases.

5.2.3.1 The effect of length to displacement ratio

Fig. 5.20 shows the influence of length to displacement ratio on wave pattern resistance using thin ship theory with a single source correction. It is seen that an increase in length to displacement ratio causes a reduction in wave pattern resistance coefficients. The trend is similar to the experimental wave resistance coefficients, Fig. 5.21, which were derived from the equation $C_W = C_T - (1+\beta k)C_F$. The form factor $(1+\beta k)$ was obtained from Ref. 11 and C_F was derived using the ITTC formulation. It is noted that the experimental wave pattern resistance coefficients were not derived from the shallow water wave cuts. Whilst the analysis program

works well for deep water, it is currently not able to produce a close enough fit to the measured shallow water wave cuts.

Fig. 5.22 illustrates the effect of length to displacement ratio on the wave profiles. The examples are compared at the same speeds and at the water depth of 0.4m. It is noted that the length of model 6b is 2.1m whilst the length of the other models is 1.6m. Therefore, the wave cuts are compared at the Fn of 1.02 and transverse position (Y/L) of 0.93 for models 4b and 5b and at the Fn of 0.89 and Y/L of 0.71 for model 6b. The wave profiles are non-dimensionalised with the model's length and presented in terms of wave height/L to a base of longitudinal distance (X)/L.

It can be seen that an increase in length to displacement ratio causes a reduction in wave height. This agrees with the experimental results, Figs. 3.45 - 3.47. The wave phases of model 4b and 5b are almost identical whilst model 6b has shorter wavelength. This is because model 6b is compared at the same speed but not the same Fn as models 4b and 5b, as mentioned above.

The theoretical wave profiles of models 4b, 5b, and 6b are compared with the experimental wave cuts in Figs. 5.23, 5.24 and 5.25 respectively. The comparisons show an acceptable agreement between theory and experiment.

5.2.3.2 The effect of hull separation in shallow water

Fig. 5.26 shows the predicted wave pattern resistance coefficients C_{WP} of model 5b catamaran with S/L of 0.2 and 0.4 at the water depth of 0.4m. It is seen that reducing the separation causes an increase in wave pattern resistance at Fn around 0.5. This trend is similar to the experimental wave resistance coefficients C_W, as seen in Fig. 5.27. The trend also agrees with the experimental residual resistance coefficients obtained from the tests in shallow water, as shown in Fig. 3.7.

The predicted wave profiles of model 5b catamaran with S/L of 0.2 and 0.4 are compared with the experimental wave profiles at Fn of 1.02 and water depth of 0.4m in Figs. 5.28 and 5.29. It can be seen that the thin ship theory with a single source correction provides acceptable predictions of the effect of hull separation ratio on wave profiles. This compliments the acceptable prediction of the influence of hull separation on wave pattern resistance, seen in Figs. 5.26 and 5.27.

5.2.3.3 The effect of trim changes

The model used for the investigation is 5b catamaran with S/L of 0.2 at the waterdepth of 0.2m. The model was trimmed 2 degree by stern using the line faring package, ShipShape [52]. The offsets of the hull underwater with new maximum draught and static wetted surface area were obtained and used as input for the theoretical program. The single source correction is used and its strength is equal to the deficit required to balance net source strength of zero. The strength of the single source depends on speed and trim, Fig. 5.30. The single source is placed at the bottom of the transom, which is lower than the case of level trim as the transom submerges deeper due to bow up trim.

Fig. 5.31 shows the theoretical prediction of the effect of static trim changes on wave pattern resistance coefficients, C_{WP}. It can be seen that bow up trim results in an increase in wave pattern resistance around the peak. The trend is similar to the experimental wave resistance coefficients, C_W, in Fig. 5.32.

Fig. 5.33 illustrates the effect of trim changes on wave profile predicted by the theory. It can be seen that the predicted wave profiles of level and bow up trim are hardly different. This agrees with the experimental results, as shown in Fig. 5.34.

It was also found that applying the experimental dynamic sinkage and trim hardly improves the wave profiles. The predicted wave profile using thin ship theory with

dynamic sinkage and trim is compared with the predicted wave profile using the theory with static setup waterline (level trim) in Fig. 5.35. The model used is 5b catamaran with S/L of 0.4 at Fn of 1.02 and Fn_H of 2.04. The values of dynamic sinkage and trim obtained from the experiments for this example were 1.8% draught and 1.338° bow up respectively. It is noted that the wave profile along the hull causing dynamic sinkage and trim was not applied to the theoretical model.

5.2.3.4 The effect of shallow water on wave pattern resistance, diverging wave angle, wave height and wave energy

Wave pattern resistance:

The effect of shallow water on wave pattern resistance and divergent wave angle can be predicted by thin ship theory. Fig. 5.36 shows the plot of theoretical wave pattern resistance ratio ($C_{WP}/C_{WP\infty}$) of model 5b catamaran with S/L of 0.2 at the water depths of 0.2m and 0.4m with changes in depth Froude number. It is seen that the trend agrees with the experimental wave resistance ratio ($C_W/C_{W\infty}$), as seen in Fig. 5.37, although the theoretical wave pattern resistance ratio of the water depth of 0.2m is much higher than the experimental wave resistance ratio at the critical speed. It is noted that the experimental wave resistance coefficients C_W were derived from the equation $C_W = C_T - (1+\beta k)C_F$ which is not the same as C_{WP} predicted by thin ship theory. The similar trend was also obtained by Dand [21] and Millward [23, 62].

As can be seen from the figures, the effect of shallow water is significant in the critical speed region. The wave pattern resistance dramatically increases as the depth Froude number is close to critical speed and then sharply reduces, when the depth Froude number is greater than unity.

Diverging wave angle:

Fig. 5.38 shows the comparison of the predicted diverging wave angles obtained from the thin ship theory approach, from Kofoed-Hansen [32] and experiments. It is noted that the diverging wave angle (θ) is the angle between ship's direction and the direction of wave propagation, as seen in Fig. 2.1. The predicted diverging wave angles using thin ship theory were determined by calculating the angle (θ) from the position of the bow wave at various transverse positions (Y/L). It is seen that the values of the diverging wave angle, modelled using the thin ship theory, are close to those obtained by the experiments and broadly similar to those obtained theoretically by the following equations taken from Ref. 32.

$$\theta = 35.267\left(1 - \exp\left(12\left(Fn_H - 1\right)\right)\right) \quad \text{for } Fn_H < 1$$

$$\theta = \cos^{-1}\left(\frac{1}{Fn_H}\right) \quad \text{for } Fn_H > 1$$

These results show promise for further development although the very small angles expected at or near Fn_H=1.0 were not achieved with the theory in its current form.

It can be seen that as the depth Froude number moves close to critical speed region, the diverging wave angle reduces close to zero i.e. the direction of the wave propagation is almost paralell to the ship's track. Then, the wave angle increases again in supercritical speed region and greater than the wave angle in sub-critical speed region. This was also obtained by Whittaker [31] and Kofoed-Hansen [32].

Wave height, wave period and wave energy:

Figs. 5.39 - 5.41 show the influence of depth Froude number on wave height, wave period and wave energy of the first leading wave of model 5b monohull travelling at the waterdepth of 0.2m and 0.4m and 5b catamaran with S/L of 0.4 travelling at the

waterdepth of 0.2m respectively. The wave enery is derived from the following equation for shallow water:

$$E = \rho g H^2 \lambda / 8$$

Where $\lambda = (gT^2/2\pi).\tanh(2\pi h/L)$. H is wave height, T is wave period, h is water depth and L is wavelength.

It can be seen that the wave height, wave period, and wave energy increase sharply in the critical speed region. The trends are similar to the wave pattern resistance.

The theoretical results are compared with the experiment in Figs. 5.39 - 5.41. The theoretical results were obtained using thin ship theory with a single source correction. Apart from the under-predictions of the wave height, wave period and wave energy at or near critical speed, it is seen that the theory gives a reasonable agreement with the experiment, especially for the wave energy. At supercritical speeds for the case of monohull, the theory over-predicts the wave height and under-predicts the wave period but it gives rather good prediction for the wave energy. For the case of the catamaran, the theory gives better predictions, as seen in Fig. 5.41.

5.2.4 Summary

The validation examples have demonstrated that the theory is suitable for predicting and investigating the changes in wave pattern resistance and wave profiles due to the influences of length to displacement ratio, hull spacing, trim changes, speeds and water depth.

5.3 Example Applications

General:

The results, shown in Figs. 5.42 - 5.46, which might be representative of say a 60m to 80m catamaran or monohull travelling at various Froude number and water depths, are used to illustrate the use of the theory for predicting the influences of speed and water depth and for example, a typical 60m catamaran travelling at 25 knots in 6m depth of water would have a length Froude number Fn of 0.53 and a depth Froude number Fn_H of 1.68, i.e. supercritical speed. In the supercritical speed range, the leading divergent waves will dominate, Fig. 5.46, and in this particular case the leading wave will be propagated at an angle about 55°, Fig. 5.38. The decay rate of these waves will be less than those in sub-critical speeds in deep water, as discussed in Section 2.7.

The effects of Fn and Fn_H:

Fig. 5.42 shows the wave patterns at different speeds in deep water, and the changes from diverging plus transverse waves to predominantly diverging waves can be seen. It can be seen that as the speed increases, the diverging wave angle becomes steeper. According to the figure, at the Froude number of about 0.7, the transverse wave begins to disappear.

Fig. 5.43 shows the influences of changes in depth Froude numbers (Fn_H) at a given set speed. It is seen that at a constant speed Froude number of 0.5, as the depth Froude number increases close to critical speed the diverging wave angle reduces close to zero i.e. the wave propagation's direction is almost parallel with the ship's direction. Then, the wave angle increases again at supercritical speed. From Fig. 5.43, it can be seen that at the constant Froude number of 0.8 this phenomenon is not seen so clearly. The diverging wave angle can also be seen from the contour plots, Fig. 5.44.

The results show that not only depth Froude number but also length Froude number will affect the wave pattern. This was experimentally obtained by Stumbo [35]. He found that the wave pattern of displacement vessels operating at a subcritical speed (Fn_H <1.0) i.e. in deep water and length Froude number less than about 0.65 produced the standard Kelvin wave pattern with the existence of both diverging and transverse waves. At or near the critical speed, the direction of wave propagation was almost parallel with the ship's direction. At a supercritical speed (Fn_H >1.0) and Fn less than about 0.65, the diverging wave angle became larger and transverse waves disappeared. For the case of vessels operating at a very high speed (Fn >0.9) and at any supercritical (Fn_H >1.0), subcritical (Fn_H <1.0) or critical speeds ($Fn_H \cong 1.0$), the wave pattern would be the same for all depth Froude numbers. Transverse waves disappeared and diverging waves became steeper. For vessels operating in the range of length Froude numbers between about 0.65 and 0.9, the wave pattern could be somewhere between the two conditions.

Fig. 5.45 shows the predicted wave patterns and the distribution of wave pattern resistance at different speeds in deep water. It can be seen that as the speed increases, the diverging wave angle becomes steeper and the distribution of wave pattern resistance also changes. It is seen that at high Froude number, where the transverse waves almost disappear, most of the wave resistance components lie in the diverging waves.

Fig. 5.46 illustrates the predicted wave pattern and the distribution of wave pattern resistance (or wave components) with changes in depth Froude number. It is seen that at supercritical speeds the transverse waves disappear and waves can only be propagated at an angle of direction greater than $\theta_0 = \mathrm{Cos}^{-1}(\sqrt{(gH)}/\ U)$, as discussed in Chapter 2. These results, which describe wave patterns and their associated distribution of wave components within that pattern, e.g. high transverse or divergent content, are of value for input to wave propagation models.

It can be noted that when a vessel travels at a given speed but at different water depth, the generated wave patterns can be different whilst the wave resistance is about the same. Fig. 5.47 shows the wave pattern of model 5b catamaran with S/L of 0.2 travelling at Fn of 0.5 in deep and shallow water with Fn_H of 0.465 and 1.155 respectively. It is clearly seen that the wave patterns are different. It is also seen from Fig. 5.48 that the heights of the first leading wave of the two conditions are different although the maximum wave heights are close. However, the wave resistance is calculated from the integration of the whole wave system. It is noted that the wave resistance of the two conditions is about the same, as seen in Fig. 5.49. This would imply that wave resistance alone is not adequate to describe changes in wash, and that there is a need to consider actual wave elevations for wash purposes.

The effect of draught to water depth ratio (T/H):

In order to investigate the effect of water depth in terms of under hull clearance, or draught to water depth ratio (T/H), three NPL monohull models, 5a, 5b, and 5c, were used. The three models have the same water line length and length to displacement ratio but have different length to breadth and breadth to draught ratios, as seen in Fig. 5.50 and diagrammatically in Fig. 5.51. The details of their dimensions are indicated in Table 8. The wave cuts of the three models were compared at sub-critical and supercritical speeds, shown in Figs. 5.52 and 5.53. It is seen that the wave cuts are hardly different. This might infer that under hull clearance is not important at sub-critical and supercritical speeds.

These results tend to agree with the comparison of the experimental wave profiles of models 5b (T/H = 0.365) and 5s (T/H = 0.315), as discussed in section 3.6.3.1. Both models have the same length to displacement ratio ($L/\nabla^{1/3}$) and breadth to draught ratio (B/T) but different draught (T) and hull shape. The details are given in Table 1 and the model body plans can be seen in Fig. 3.1. In this case also, although the draught and hence under hull clearances were different, their wave resistance and wave profiles were similar.

However, as seen from Figs. 5.36 and 5.37, the water depth can have a significant effect on the resistance at around critical speed. The reduction in water depth causes an increase in resistance at the critical speed. This implies that the effect of clearance under the hull may have a particular influence at or around the critical speed.

The effect of tank breadth:

Fig. 5.54 shows the effect of tank breadth on predicted wave pattern resistance ratio ($C_{WP}/C_{WP\infty}$). The model used was 5b monohull travelling at a constant water depth of 0.4m. Three different sizes of tank breadth were used: 1.856m (b/L=0.58), 3.7m (b/L=1.156) and 4.6m (b/L=1.438), where b is the distance between tank wall and the hull centreline.

It is found that the tank wall can have an effect on the resistance, particularly around the critical speed, Fig. 5.54. The effect of the wall decreases very rapidly as the distance from the wall gets bigger, as seen in Fig. 5.55, which shows the effect of tank wall on maximum resistance ratio at Fn_H=0.9. If the distance between the hull and tank wall is more than approximately 1.5 hull lengths the effect is negligible. These trends are similar to those obtained experimentally and theoretically by Rich [79]. The effect of tank wall in deep water was also investigated theoretically by Rich [79] and found that the effect of the tank wall was small.

The breadth of the tank has little influence on wave wash at sub-critical and supercritical speeds, as can be seen in Figs. 5.56a&c. The wave profiles are hardly different as the breadth of the tank is increased from 4.6m (b/L=1.438) to 9.6m (b/L=3). The tank breadth has an effect on wave profiles at around critical speed, as seen in Fig. 5.56b. It is seen that the wave profile of the narrow tank (b/L=0.58) has a larger wave height than that of the wider tank (b/L=1.438). These results agree with the effects on resistance.

5.4 Discussion

The examples have illustrated the wide scope and applications of thin ship theory in the prediction of wave pattern resistance, wave patterns and wave wash and, in particular, the relative effects due to changes in the design and operational features. Potential limitations in the application of the theory have also been illustrated. In particular, there is a need for great care in the use of single source transom correction and the need to incorporate reliable sinkage/trim estimates. There is also the need for further refinements to improve the predictions around the critical depth speed.

5.5 Summary

5.5.1 The theory has been validated in deep water at low and high speeds and in shallow water at sub-critical and supercritical speeds using the experimental results presented and described in Chapter 3.

5.5.2 The single source correction can improve the prediction of the wave profiles and wave pattern resistance for ships with transom stern with some limitations.

5.5.3 Thin ship theory can be used to predict the wave pattern resistance and wave profiles at sub-critical and supercritical speeds.

5.5.4 The theory is proved to be useful for predicting and investigating the changes in wave pattern resistance and wave profiles due to the influences of length to displacement ratio, hull spacing, trim changes, speed and water depth.

5.5.5 It was demonstrated that changes in wave resistance alone may not be adequate to describe changes in wave wash since, with changes in water

depth, the vessel can have the same resistance but different wave systems.

5.5.6 The output of the thin ship theory program such as the wave pattern, the direction of wave propagation and the distribution of wave energy has applications for input to wave propagation models.

6. OVERALL DISCUSSION

6.1 General

Experiments:

Extensive experiments including resistance measurements and wave cuts have been carried out in deep and shallow water. The experimental results are useful for validation purposes, or design and operational purposes in their own right.

Validation of the experiments included comparing the results for 1.6m and 4.5m models for a practical case. The results were very similar, confirming the suitability of the models employed.

Further investigation and validation involved testing a model with different methods of propulsion, namely towed, or propelled with conventional propellers or with waterjets. The results were broadly similar, confirming the suitability of the methods and procedures employed.

Theory:

Various validation exercises have demonstrated that thin ship theory can be usefully employed as a simple and effective means of estimating wave pattern resistance and wave profiles with low computational effort. Part of its effectiveness relies on the ship hull(s) being slender or thin, which is generally the case for high speed vessels.

The theory has been shown to work effectively for deep and shallow water. The theory was validated using the experiments and covered the aspects of hull parameters, speed, trim and water depth.

Wave cuts:

It has been noted that for a given speed, and different water depths, a vessel can have similar resistance but different wave patterns. This would indicate that relating wave wash simply to wave resistance is not adequate and that wave cuts and wave criteria are required for wash investigations.

6.2 Transom Stern Corrections

The use of virtual stern and a single source transom corrections have been investigated for the prediction of wave wash. The virtual stern correction introduced by Couser [9] was found to give good prediction for wave pattern resistance. The virtual stern can be easily created and added to the transom using a typical commercial lines faring package. In the current model, these lines are established as parabolas. The offsets for the ship with a virtual stern are created and then used as an input file for source strength calculations within the thin ship theory program.

The thin ship theory program has been modified to be able to insert a single source with desired strength at a suitable position. Firstly, the thin ship theory program was run at a set Fn with no correction. The total source strength was then obtained. The strength of the source was set as a balancing source to give the net source strength of zero i.e the strength of the single source = – total source strength.

In terms of wave profiles, the single source correction was found to be satisfactory and the simplest to apply. The thin ship theory program with a single source correction has been validated in deep water and shallow water sub-critical and supercritical speeds using the experimental results. The single source correction can improve the prediction of wave profiles. The effects of $L/\nabla^{1/3}$, S/L and shallow water can be predicted. However, there are some limitations such as the over-prediction of

the bow wave for Fn > 0.44 and the hollow created in front of the bow wave at supercritical speed. These were discussed in detail in Chapter 5.

When trim is applied to the model, the hull shape under water is changed. The total source strength is changed. The strength and position of the single source must then be changed. This causes changes in C_{WP} and slight changes in wave profiles. The prediction of the effect of trim changes has been validated in Chapter 5 and found to give an acceptable agreement with the experiments.

It is noted that using different transom corrections may give the same wave resistance but different wave wash, as seen in Chapter 4. The virtual stern correction can give good prediction for wave pattern resistance but poor predictions for the wave profiles. Whilst in principle the wave resistance is proportional to the square of wave height, this may not always be the case as there could be a different combination of wave heights for the same resistance. Again, this illustrates the need to consider actual wave elevations for wash purposes.

6.3 Critical Speed

Information at speeds at or near critical is difficult to assess due to the significant changes in resistance, wave height and trim in this speed range. The experiments suffered from the presence of solitons which made the acquisition of consistent results difficult, and the theory is not effective at Fn_H=1.0. Generally, ships will try to avoid operating at or near critical speed and should if possible pass through the trans-critical speed range as quickly as possible. However, there remains the need for reliable data at or near critical speed.

6.4 Applications

(i) Design Parameters:

The effects of length to displacement ratio ($L/\nabla^{1/3}$) and hull separation ratio (S/L) (for catamarans) on wave resistance and wave wash have been investigated experimentally and numerically for different speeds and water depths. A change in hull form was also investigated. The results and developed techniques provide the facility to investigate the main design parameters when taking wave wash into account.

(ii) Operational Parameters:

The effects of speed, trim, and water depth on wave wash have been investigated using experiments and the thin ship theory program. The results and the developed prediction techniques provide the facility to offer guideline for ship operation when taking wave wash into account.

6.5 Numerical Predictions

The computer program based on the thin ship theory provides a means of predicting wave resistance and wash by numerical methods in a rapid and computationally efficient manner.

The numerical program has applications to:

- Low-wash design

As discussed in Chapter 5, wash waves with different wave height and period may have the same wave resistance and energy. As a result, both wave height and wave energy should be used as criteria.

It is clearly seen from the experimental and theoretical investigations that the effect of length to displacement ratio ($L/\nabla^{1/3}$) on wave wash and wave resistance is significant. An increase in $L/\nabla^{1/3}$ causes a reduction in wave height and wave resistance. The effect of hull separation ratio (S/L) is significant at around main hump speed. As the hull separation ratio is increased, the wave resistance and wave height are decreased. As a result, the length to displacement ratio ($L/\nabla^{1/3}$) and hull separation ratio (S/L) should be as high as possible in order to reduce wave resistance and wave wash. At the same time, the numerical method allows the assessment of the increase in wave wash and resistance if these low wash hull parameters cannot be achieved.

- Operational guidelines

It is found from the experimental and theoretical investigations that an increase in speed or Fn in the sub-critical speed region results in increases in wave height and wavelength. In deep water, the resistance coefficient peaks at hump speed around Fn of 0.5. The water depth is also important. It is found that the shallow water has a pronounced effect on wave resistance and wave height at about critical speed ($Fn_H \cong 1.0$). The wave resistance and wave height increase sharply at the depth Froude number close to one. Moreover, the depth of water in the critical speed region is also important as a reduction in water depth causes an increase in the effects of shallow water. As seen from the investigations, the effects at the water depth of 0.2m are more significant than the effects at the water depth of 0.4m at around critical speed.

This implies that the shallow water effect at the critical speed depends on the water depth. This is probably due to the effects of clearance under the hull. If a vessel travels at around critical speed in much deeper water, the effect of Fn_H may not be seen. However, the vessel would have to travel at a very high speed.

An increase in transom immersion due to stern trim causes an increase in resistance and changes in the wave wash pattern. This can be tracked using the numerical program in order to assess the effects on the generation of wash and on the ship operation.

Shallow water has an effect on the direction of wave propagation. At or near the critical speed, the direction of wave propagation is almost parallel to the direction of a ship. The ability of the numerical model to predict the wave propagation direction is important as it allows assessments to be made of the direction of wave travel and the potential damage to people on beaches, small boats in harbour or marine ecology.

- Inputs for wave propagation models

In order to predict the likely size of the waves as they approach some other area or the shore, and hence their likely impact, the rate of decay of ship waves need to be estimated. Basic wave properties such as wave height, wave period, direction of wave propagation and distribution of wave energy may be used for wave transformation / propagation studies from ship to shore. These properties can be obtained using the thin ship theory program.

The rate of decay of ship waves can be estimated using the wave height predicted by thin ship theory and, for example, Boussinesq-type equations used for the prediction of the propagation and decay of the waves. Alternatively, a much simpler approach, but with practical applications, is to use the rate of decay described by Havelock's theoretical prediction of decay, Ref. 54, shown in Chapter 2. Apart from the wave

height, the direction of wave propagation is also needed and it can be derived using the thin ship theory program.

The energy of the first two or three waves can be used as a good representation of the potential damaging effects of the waves. The wave energy can be estimated using wave height and period, which can be obtained from the thin ship theory program, as shown in Chapter 5. The theory can also provide the distribution of wave energy at a set condition which indicates the likely level of energy at a particular wave propagation angle. This is particularly true in shallow water where much of the energy is in the leading diverging waves.

6.6 Summary

Potential applications of the experimental results and developed numerical model have been brought together and discussed. It is seen that many useful applications of the wash prediction procedures exit in their fields of ship design and operation.

7. CONCLUSIONS AND RECOMMENDATIONS

7.1 General

7.1.1 The literature review and survey of research identified a number of areas and issues in the field of ship wave resistance and wave wash for high speed craft which require further attention.

7.1.2 An extensive investigation has been carried out experimentally and numerically into wash waves and wave resistance of high speed displacement craft. The current work has focused on the investigation of the effects of hull form parameters, speed, trim and water depth. The experimental and theoretical investigations have shown that hull form parameters, speed, trim and water depth can have significant effects on wave resistance and wave wash.

7.1.3 The current investigations have demonstrated that not only wave resistance but also wave wash should be considered both for applications at the preliminary design of high speed craft and during their operation.

7.1.4 It has been determined that at a particular speed and two water depths a vessel can have the same resistance but a different wave pattern, depending on the depth of water. It is concluded that wave wash should be assessed from a knowledge of the wave profile and its properties, and not by assessing wave wash as a function of the wave resistance.

The principal findings and conclusions drawn from the investigations are outlined as follows.

7.2 Experiments

7.2.1 Experiments were carried out at various tank test facilities in both deep and shallow water in order to establish an extensive database and to provide a further understanding of the influence of hull form parameters, speed, water depth, and trim changes on resistance and wave wash. The effects of hull separation and shallow water on direction of the wave propagation and running sinkage and trim have also been studied. The experimental results, particularly those covering shallow water and its effects, provide one of the most extensive sets of experimental data currently available.

7.2.2 The effect of the propulsion system on the wave profiles was investigated experimentally and found to be small. It can be concluded that the extensive wash data obtained from towed models can be used with some confidence for design and validation work.

7.2.3 The influences of hull form parameters, speed, trim and shallow water on wash and wave resistance have been determined using the experimental results. It was found that an increase in length to displacement ratio results in a decrease in wave height and wave resistance. This is consistent with earlier wave resistance tests.

For catamarans, the hull separation ratio (S/L) was found to have an influence on running sinkage and trim, especially at the hump speed. It was found to have a small effect on the wave wash and direction of wave propagation.

Significant changes in model behaviour were found to occur at or near the critical speed, $Fn_H = 1.0$. There were large increases in resistance and wave height and significant changes in sinkage and trim and the direction of wave propagation.

From the investigations into changes in static trim, it was found that stern trim causes an increase in resistance, particularly at hump speed, but the effects on the wash height tend to be relatively small.

7.2.4 It is concluded that the experimental data is in a suitable form to be used directly for the assessment of the influence on wash of the main hull parameters, speed, trim changes and water depth, for the validation of theoretical wash prediction methods and directly as input to wave propagation models.

7.3 Theory

7.3.1 A thin ship theory program has been developed for the prediction of wave resistance and ship generated near-field wave wash, including the case of shallow water. It is found that thin ship theory can be satisfactorily employed as a simple and effective means of estimating wave pattern resistance and wave profiles with low computational effort. Parts of its effectiveness rely on the ship hull(s) being slender or thin, which is the case for high speed vessels.

7.3.2 The thin ship theory model has been validated in deep water and in shallow water at sub-critical and supercritical speeds using the experimental data. Limitations of the theoretical approach are centred mainly on speeds at or around critical speed.

7.3.3 The uses of a virtual stern, a single source and a single trailing line of sources corrections to the thin ship theory were investigated for wave wash prediction of ships with transom sterns. In terms of wave profiles, the single source correction was found to be satisfactory and the simplest to apply.

7.3.4 A regression analysis of existing experimental dynamic sinkage and trim has been established. This provides rapid estimates of sinkage and trim for input to the thin ship model.

7.3.5 It has been demonstrated that thin ship theory is able to provide an acceptable approximation to the wave profiles along the ship hull. This is achieved using a suitable longitudinal wave cut and an empirical correction to the phasing of the wave. Such wave profiles may be used for enhancing models of the prediction of dynamic sinkage and trim.

7.3.6 Thin ship theory is proved to be useful for predicting and investigating the effects of hull form parameters, speed, trim and shallow water on wash and wave resistance. The distribution of wave components, diverging wave angle, wave height, wave period, and hence wave energy can also be determined. These provide the necessity information for input to wave propagation models.

7.3.7 The theory can be used as a preliminary design tool or as a means of developing operational guidelines for ship's operators. The current work has shown how the numerical method may be applied to identify low-wash designs and to identify the effects on wash of speed, trim and water depth in order to develop acceptable operational patterns.

7.4 Achievement of the objectives

7.4.1 It is considered that the objectives, outlined in Chapter 1, have been achieved. The experimental and numerical investigations provide a better understanding of basic physics of wash waves and wave resistance of high speed displacement craft. This includes basic wave cuts and the properties of the waves, the distribution of wave energy content and typical angles of wave propagation from the ship.

Thin ship theory has been developed and extended to cover vessels operating in shallow water. The theory has been validated using extensive experimental measurements covering changes in speed and water depth.

A numerical tool, based on the thin ship theory, has been developed which facilitates the prediction of wave wash properties for the assessment of new designs and the effects of wash on ship operation.

7.5 Recommendations for further work

As a result of the research programme using experiments and the thin ship theory approach, the following recommendations are put forward:

7.5.1 Due to the significant changes in resistance, wave height, wave pattern and trim at around critical speed, further model tests should be carried out to provide a better knowledge at this speed. The thin ship theory program also needs further improvement as it is not fully effective at around critical speed.

7.5.2 The single source correction offers a practical method for the transom correction and it gives satisfactory improvements in wave resistance and wave wash predictions and is the simplest to apply. However, it has some limitations, such as the need for arbitrary reductions in source strength at lower speeds. The method therefore needs further investigation and improvement.

7.5.3 Further development is recommended of the hybrid model, which intends to facilitate improvements in the estimates of sinkage and trim based on changes in the dynamic pressures around the hull.

7.5.4 Full-scale measurements of wave wash should be carried out to provide much needed reliable data for validation of the experimental and theoretical predictions.

7.5.5 Experimental tests on different hull shapes should be carried out including other types of multi-hull vessels such as trimarans, pentamarans, SWATH and SES.

The thin ship theory approach should also be enhanced in its performance in order to be able to predict the wave resistance and wave wash of such vessels.

REFERENCES

1. Insel, M., *An Investigation into the Resistance Components of High Speed Displacement Catamarans*, PhD Thesis, Ship Science, University of Southampton, 1990.

2. Insel, M., and Molland, A.F., *An Investigation into the Resistance Components of High Speed Displacement Catamarans*, Transactions of RINA, Vol. 134, 1992.

3. Molland, A.F., Wellicome, J.F., and Couser, P.R., *Resistance Experiments on a Systematic Series of High Speed Displacement Catamaran Forms: Variation of Length – Displacement Ratio and Breadth – Draught Ratio*, Transactions of RINA, Vol. 138, 1996.

4. Couser, P.R., Molland, A.F., Armstrong, N.A., and Utama, I.K.A.P., *Calm Water Powering Predictions for High Speed Catamarans*, Proc. Fourth International Conference on Fast Sea Transportation, FAST' 97, Sydney, 1997.

5. Molland, A.F., and Lee, A.R., *An Investigation into the Effect of Prismatic Coefficient on Catamaran Resistance*, Transactions of RINA, Vol. 139, 1997.

6. Molland, A.F., and Lee, A.R., *The Theoretical Investigation of a Series of High Speed Displacement Catamaran Forms: Variation of Prismatic Coefficient*, Ship Science Report No. 87, February 1995.

7. Lee, A.R., *A Theoretical and Experimental Investigation of the Effect of Prismatic Coefficient on the Resistance of High Speed Displacement Catamarans*, MPhil Thesis, Ship Science, University of Southampton, March 1995.

8. Insel, M., Molland, A.F., and Wellicome, J.F., *Wave Resistance Prediction of a Catamaran by Linearised Theory*, Proceedings of Fifth International Conference on Computer Aided Design, Manufacturing and Operation in the Marine and Offshore Industries, CADMO'94, Southampton, September 1994.

9. Couser, P.R., Wellicome, J.F., and Molland, A.F., *An Improved Method for the Theoretical Prediction of the Wave Resistance of Transom – Stern Hulls Using a Slender Body Approach*, International Shipbuilding Progress, 45, No.444, 1998.

10. Edwards, I.P., *Development of a Method to Investigate the Wash of Pleasure Craft on Inland Waterways*, M.Eng. 3rd year project report, Ship Science, University of Southampton, May 1995.

11. Molland, A.F., Wellicome, J.F., and Couser, P.R., *Resistance Experiments on a Systematic Series of High Speed Displacement Catamaran Forms: Variation of Length – Displacement Ratio and Breadth – Draught Ratio*, Ship Science Report No.71, University of Southampton, March 1994.

12. Wellicome, J.F., Molland, A.F., Cic, J., and Taunton, D.J., *Resistance Experiments on a High Speed Displacement Catamaran of Series 64 form*, Ship Science Report No.106, University of Southampton, January 1999.

13. Couser, P.R., *An Investigation into the Performance of High-Speed Catamarans in calm water and waves*, Ph.D. Thesis, Ship Science, University of Southampton, 1996.

14. Wijaya, I.S., *Development of New Hull Shapes for Commercial Multihulls using Thin-Ship Theory*, MSc. Dissertation, Ship Science, University of Southampton, December 1997.

15. Mitchel, A.R., Lawrence, R.A., Mosnier, A., and Cheshire, R., *An Innovative Ferry for Rapid Transportation around the Purbeck Coast*, M.Eng. Group Marine Project

Report, School of Engineering Sciences, Ship Science, University of Southampton, 2000.

16. Doctors, L.J., and Renilson, M.R., *The Influence of Demihull Separation and River Banks on the Resistance of a Catamaran*, Proc. Second International Conference on Fast Sea Transportation, FAST'93, Yokohama, Japan, December 1993.

17. Doctors, L.J., Renilson, M.R., Parker, G., and Hornsby, N., *Waves and Wave Resistance of a High-Speed River Catamaran*, Proc. First International Conference on Fast Sea Transportation, FAST'91, Trondheim, Norway, June 1991.

18. Millward, A., *The Effect of Hull Separation and Restricted Water Depth on Catamaran Resistance*, Transactions of RINA, Vol.134, 1992.

19. Matsui, S., Shao, S.M., Wang, Y-C., and Tanaka, K., *The Experimental Investigations on Resistance and Seakeeping Qualities of High-Speed Catamarans*, Proc. Second International Conference on Fast Sea Transportation, FAST' 93, Yokohama, Japan, December 1993.

20. Cassella, P., Coppola, C., Lalli, F., Pensa, C., Scamardella, A., and Zotti, I., *Geosim Experimental Results of High-Speed Catamaran: Co-operative Investigation on Resistance Model Tests Methodology and On Ship–Model Correlation*, Proceedings of the 7th International Symposium on Practical Design of Ships and Mobile Units, PRADS' 98, The Hague, The Netherlands, September 1998.

21. Dand, I.W., Dinham – Peren, T.A., and King, L., *Hydrodynamic Aspects of A Fast Catamaran Operating in Shallow Water*, RINA Conference on Hydrodynamics of High Speed Craft, London, 1999.

22. Zibell, H.G., and Grollius, W., *Fast Vessels on Inland – Waterways*, Proc. International Conference on Coastal Ship and Inland Waterways, RINA, London, February 1999.

23. Millward, A., and Bevan, M.G., *Effect of Shallow Water on a Mathematical Hull at High Subcritical and Supercritical Speeds*, Journal of Ship Research, Vol.30, No.2, pp. 85-93, June 1986.

24. Everest, J.T., and Hogben, N., *An Experimental Study of The Effect of Beam Variation and Shallow Water on 'Thin Ship' Wave Prediction*, Transactions of RINA, Vol.112, 1970.

25. Michell, J.H., *Wave Resistance of A ship*, Philosophical Magazine and Journal of Science, vol. XLV, 5th Series, January – June, V.1, 1898.

26. Doctors, L.J. and Day, A.H., *Nonlinear Free-Surface Effects on the Resistance and Squat of High-Speed Vessels with a Transom Stern*, Twenty-Fourth Symposium on Naval Hydrodynamics, Fukuoka, Japan, July 8-13, 2002.

27. Steen, S., Rambech H.J., Zhao, R., and Minsaas, K.J., *Resistance Prediction for Fast Displacement Catamarans*, Proc. Fifth International Conference on Fast Sea Transportation, FAST'99, Washington D.C., 1999.

28. Cong, L., and Hsiung, C.C., *Computing Wave Resistance, Wave Profile, and Sinkage and Trim of Transom Stern Ships*, Proc. of the Third International Conference on Computer Aided Design, Manufacture and Operation in the Marine and Offshore Industry, Florida, USA, January 1991.

29. Cong, L., and Hsiung, C.C., *A Simple Method of Computing Wave Resistance, Wave Profile, and Sinkage and Trim of Transom Stern Ships*, ITTC 1990.

30. Gadd, G.E., *Ship Wavemaking in Theory and Practice*, Transactions of RINA, Vol.111, 1969.

31. Whittaker, T., Bell, A., Shaw, M., and Patterson, K., *An Investigation of Fast Ferry Wash in Confined Waters*, Proc. of International Conference on the Hydrodynamics of High Speed Craft, RINA, London, November 1999.

32. Kofoed – Hansen, H., Jensen, T., Kirkegaard, J., and Fuchs, J., *Prediction of Wake Wash from High-Speed Craft in Coastal Areas*, Proc. of International Conference on the Hydrodynamics of High Speed Craft, RINA, London, November 1999.

33. Kofoed - Hansen, H., and Mikkelsen, A.C., *Wake Wash from Fast Ferries in Denmark*, Proc. Fourth International Conference on Fast Sea Transportation, FAST'97, Sydney, 1997.

34. Stumbo, S., Fox, K., and Elliott, L., *Hull Form Considerations in the Design of Low Wake Wash Catamarans*, Proc. Fifth International Conference on Fast Sea Transportation, FAST'99, Washington D.C., 1999.

35. Stumbo, S., Fox, K., and Elliott, L., *An Assessment of Wake Wash Reduction of Fast Ferries at Supercritical Froude Numbers and at Optimised Trim*, Proc. International Conference on Hydrodynamics of High Speed Craft, RINA, London, November 2000.

36. Macfarlane, G.J., and Renilson, M.R., *Wave Wake – A Rational Method for Assessment*, Proc. International Conference on Coastal Ship and Inland Waterways, London, February 1999.

37. Macfarlane, G.J., and Renilson, M.R., *When Is Low Wash Low Wash? – An Investigation Using A Wave Wake Database*, Proc. International Conference on Hydrodynamics of High Speed Craft, RINA, London, November 2000.

38. Molland, A.F., Wilson, P.A., and Chandraprabha, S., *The Prediction of Ship Generated Near-Field Wash Waves Using Thin Ship Theory*, Proc. of International Conference on Hydrodynamics of High Speed Crafts: Wake wash and Motion Control, RINA, London, November 2000.

39. Molland, A.F., Wilson, P.A., Turnock, S.R., Taunton, D.J., and Chandraprabha, S., *The Prediction of The Characteristics of Ship Generated Near-Field Wash Waves*, Proc. of the Sixth International Conference on Fast Sea Transportation, FAST'2001, Southampton, September 2001.

40. Gadd, G.E., *Far Field Waves Made by High Speed Ferries*, Proc. Of International Conference on Hydrodynamics of High Speed Craft, RINA, London, November 1999.

41. Gadd, G.E., *The Wash of Boats on Recreational Waterways*, Transaction of RINA, Vol.136, 1994.

42. Janson, C.E., Leer-Andersen, M., and Larsson, L., *A Combined Rankine/Kelvin Source Method for Farfield Wash Wave Calculations*, Proc. 2nd International Euro Conference on High-Performance Marine Vehicles, HIPER'01, Hamburg, May 2001.

43. Brizzolara, S., Bruzzone, D., Cassella, P., Scamardella, A., and Zotti, I., *Wave Resistance and Wave Patterns for High-Speed Crafts; Validation of Numerical Results by Model Test*, Proc. of 22nd Symposium on Naval Hydrodynamics, National Academy Press, Washington D.C., 1998.

44. Jiang, T., *Investigations of Waves Generated by Ships in Shallow Water*, Proc. of 22nd Symposium on Naval Hydrodynamics, National Academy Press, Washington D.C., 1998.

45. Raven, H.C., *Numerical Wash Prediction using A Free-Surface Panel Code*, Proc. International Conference on Hydrodynamics of High Speed Craft, London, November 2000.

46. Leer-Anderson, M., Clason, P., Ottosson, P., Anderson, H., and Svensson V., *Wash Waves – Problems and Solutions*, SNAME Annual Meeting, 2000.

47. Hughes, M., *CFD Prediction of Wake Wash in Finite Water Depth*, Proc. 2nd International Euro Conference on High-Performance Marine Vehicles, HIPER'01, Hamburg, May 2001.

48. The Specialist Committee on Safety of High Speed Marine Vehicles, *Final Report and Recommendations to the 22nd ITTC*, ITTC 1999.

49. *The Impact of High Speed Ferries on the External Environment*, Nautical Division, Danish Maritime Authority, 1998.

50. Day, A. and Doctors, L.J., *Concept Evaluation for High-Speed Low-Wash Vessels*, Proc. of Sixth International Conference on Fast Sea Transportation, Fast'2001, Southampton, September 2001.

51. Feldtmann, M. and Garner, J., *Seabed Modifications to Prevent Wake Wash from Fast Ferries*, Proc. of International Conference on Coastal Ship and Inland Waterways, RINA, London, February 1999.

52. ShipShape User Manual, Wolfson Unit MTIA, University of Southampton.

53. Lunde, J.K., *On the Linearized Theory of Wave Resistance for Displacement Ships in Steady and Accelerated Motion*, Trans. SNAME, Vol.59, 1951.

54. Havelock, T.H., *The Propagation of Groups of Waves in Dispersive Media, with Application to Waves Produced by a Travelling Disturbance*, Proceedings of The Royal Society of London, Series A, Vol.81, pp398-430, 1908.

55. Doyle, R., Whittaker, T.J.T. and Elsaβer, B., *A Study of Fast Ferry Wash in Shallow Water*, Proc. of Sixth International Conference on Fast Sea Transportation, Fast'2001, Southampton, September 2001.

56. Bailey, D., *The NPL High Speed Round Bilge Displacement Hull Series Resistance, Propulsion, Manoeuvring and Seakeeping Data*, Maritime Technology Monograph, No.4, RINA, 1976.

57. Yeh, H.Y.H., *Series 64 Resistance Experiments on High-Speed Displacement Forms*, Marine Technology, July 1965.

58. Molland, A.F., Wilson, P.A. and Taunton, D.J., *A Systematic Series of Experimental Wash Wave Measurements for High Speed Displacement Monohull and Catamaran Forms in Shallow Water*, Ship Science Report No.122, University of Southampton, December 2001.

59. Molland, A.F., Wilson, P.A. and Taunton, D.J., *Further Experimental Wash Wave Measurements for High Speed Displacement Catamaran Forms in Shallow Water*, Ship Science Report No.123, University of Southampton, December 2002.

60. Molland, A.F., Wilson, P.A. and Taunton, D.J., *Experimental Measurement of The Wash Characteristics of A Fast Displacement Catamaran in Deep Water*, Ship Science Report No.124, University of Southampton, December 2002.

61. Couser, P.R., Wellicome, J.F. and Molland, A.F., *Experimental Measurement of Sideforce and Induced Drag on Catamaran Demihulls*, International Shipbuilding Progress, Vol.45, No.443, September 1998.

62. Millward, A., *The Effect of Shallow water on the Resistance of a Ship at High Sub Critical and Super Critical Speeds*, Transactions of RINA, Vol.124, 1982.

63. Newman, J.N., *Marine Hydrodynamics*, Cambridge, Mass: MIT Press, c1977.

64. Whittaker, T.J.T., Doyle, R. and Elsaβer, B., *An Experimental Investigation of the Physical Characteristics of Fast Ferry Wash*, 2nd International Euro Conference on High-Performance Marine Vehicles, HIPER'01, Hamburg, May 2001.

65. Russell, J.S., *Report of the Committee on Waves*, 7th Meeting of the British Association for the Advancement of Science, p.417, 1838.

66. Dinham-Peren, T., *Solitary Wave Generation by Vessels in Shallow Water*, Int. Conf. Hydrodynamic of High Speed Craft, Shanghai, China, 2001.

67. Yim, B., *Analyses of Waves and the Wave Resistance due to Transom-Stern Ships*, Journal of Ship Research, p.155-167, June 1969.

68. Doctors, L.J., and Day, A.H., *Resistance Prediction for Transom-Stern Vessels*, Proc. Fourth International Conference on Fast Sea Transportation, FAST'97, Sydney, 1997.

69. Day, A.H. and Doctors, L.J., *The Survival of the Fittest – Evolutionary Tools for Hydrodynamic Design of Ship Hull Form*, Trans. RINA, Vol.142, 2000.

70. Turnock, S.R., *Technical Manual and User Guide for the Surface Panel Code: PALISUPAN*, Ship Science Report No.100, Ship Science, University of Southampton, October 1997.

71. Hogben, N., *'Equivalent Source Arrays' From Wave Patterns Behind Trawler Type Models*, Transactions of RINA, Vol.113, 1971.

72. Shearer, J.R. and Cross, J.J., *The Experimental Determination of The Components of Ship Resistance for a Mathematical Model*, Transactions of RINA, Vol.107, 1965.

73. Zhang, D. and Chwang, A.T., *On Nonlinear Ship Waves and Wave Resistance Calculations*, Journal of Marine Science and Technology, 1999.

74. Stern, F., Longo, J., Zhang Z.J. and Subramani, A.K., *Detailed Bow-Flow Data and CFD for a Series 60 C_B = 0.6 Ship Model for Froude Number 0.316*, Journal of Ship Research, Vol.40, No.3, September 1996, pp.193-199.

75. Gadd, G.E., *A Method for Calculating the Flow over Ship Hulls*, Transactions of RINA, Vol.112, 1970.

76. Spencer, N., *An Investigation into the Resistance Characteristics of High Speed Catamarans in Calm Water and in Waves*, MPhil. Thesis, Department of Mechanical Engineering, University of Liverpool, 1994.

77. Brizzolara, S. and Bruzzone, D., *Numerical Wave Resistance and Dynamic Trim of High Speed Craft*, NAV2000, International Conference on Ship and Shipping Research, Vol.1, 19-22 September 2000, Venice.

78. Wigley, W.C.S., *Calculated and Measured Wave Resistance of a Series of Forms Defined Algebraically, the Prismatic Coefficient and Angle of Entrance Being Varied Independently*, Trans I.N.A., Vol.84, 1942.

79. Rich, A.J., Sproston, J.L. and Millward, A., *A theoretical Prediction of the Effect of a Wall on the Resistance of a Fast Ship Shape in Water of Uniform Depth*, Trans. of International Shipbuilding Progress, Vol.32, No.376, Dec.1985.

APPENDIX A: TOTAL RESISTANCE FROM CONSIDERATIONS OF MOMENTUM CHANGES

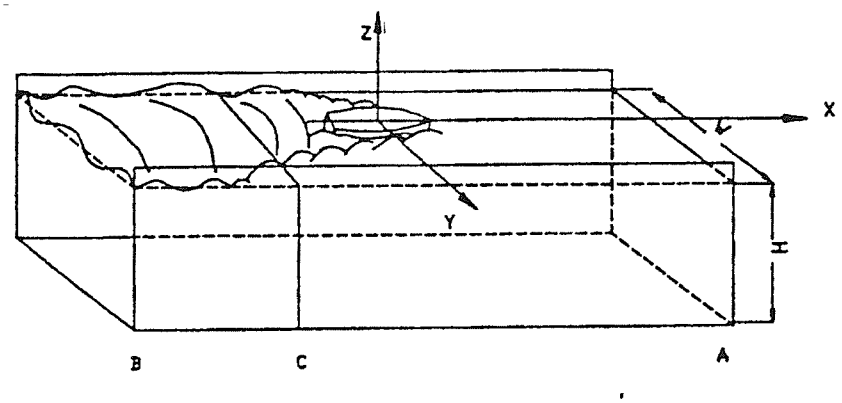

A ship model in towing tank, taken from Insel [1].

The resistance component of a model can be derived from considerations of momentum changes. Consider a model in a control box formed by plane A, plane B, tank walls, tank floor and model surface. Plane A is sufficiently upstream and plane B is far down stream, as seen in the above figure. H and W are depth and breadth of the control box. By applying conservation of momentum, the total forces on the control surface must be equal to the rate of change of momentum of fluid flowing through the control box, hence:

$$M_B - M_A = F_A - F_B - R_T \qquad \text{A1.}$$

Where M_A = Momentum flowing in through plane A per unit time

$$M_A = \rho \int_{-W/2}^{W/2} \int_{-H}^{\zeta_B} U(U + u)\, dz dy \qquad \text{A2.}$$

Momentum flowing out through plane B per unit time:

$$M_B = \rho \int_{-W/2-H}^{W/2} \int^{\zeta_B} (U^2 + 2Uu + u^2)\, dzdy \qquad A3.$$

F_A = pressure force on plane A

$$F_A = \rho / 2\, gWH^2 \qquad A4.$$

F_B = pressure force on plane B

$$F_B = - \int_{-W/2-H}^{W/2} \int^{\zeta_B} [-\rho gz - \rho / 2(2Uu + u^2 + v^2 + w^2) - \Delta P]dzdy \qquad A5.$$

Substituting A2, A3, A4, A5 into A1, total resistance becomes:

$$R_T = \rho g / 2 \int_{-W/2}^{W/2} \zeta_B^2 dy + \rho / 2 \int_{-W/2-H}^{W/2} \int^{\zeta_B} (v^2 + w^2 - u^2)dzdy + \int_{-W/2-H}^{W/2} \int^{\zeta_B} \Delta P dzdy \qquad A6.$$

Perturbation velocity u can be written as $u^2 = u^2 + (u^2 - u^2)$, where u is a fictitious velocity at plane B if viscous head looses were neglected. Hence, equation A6 becomes

$$R_T = \int_{-W/2-H}^{W/2} \int^{\zeta_B} \Delta P dzdy + \rho / 2 \int_{-W/2-H}^{W/2} \int^{\zeta_B} (u^2 - u^2)dzdy$$

$$+\rho g / 2 \int_{-W/2}^{W/2} \zeta_B^2 dy + \rho / 2 \int_{-W/2-H}^{W/2} \int^{\zeta_B} (v^2 + w^2 - u^2)dzdy \qquad A7.$$

by introducing $\underline{u}$, $\underline{v}$, $\underline{w}$ as wave orbital velocities which can be obtained from the measured wave pattern at B and employing linearised wave theory, where:

$$u^2 = \underline{u}^2 + (u^2 - \underline{u}^2)$$
$$v^2 = \underline{v}^2 + (v^2 - \underline{v}^2) \qquad \text{A8.}$$
$$w^2 = \underline{w}^2 + (w^2 - \underline{w}^2)$$

Finally the total wave resistance can be written in the form:

$$R_T = \int_{-W/2}^{W/2}\int_{-H}^{\zeta_B} \Delta P dz dy + \rho / 2 \int_{-W/2}^{W/2}\int_{-H}^{\zeta_B} (u^2 - u^2) dz dy$$

$$+ \rho g / 2 \int_{-W/2}^{W/2} \zeta_B{}^2 dy + \rho / 2 \int_{-W/2}^{W/2}\int_{-H}^{\zeta_B} (\underline{v}^2 + \underline{w}^2 - \underline{u}^2) dz dy$$

$$+ \rho / 2 \int_{-W/2}^{W/2}\int_{-H}^{\zeta_B} [(v^2 - \underline{v}^2) + (w^2 - \underline{w}^2) - (u^2 - \underline{u}^2)] dz dy \qquad \text{A9.}$$

The first line in equation A9 is the resistance due to viscous effect, the second line represents the wave resistance and the third line is the induced drag which may be neglected.

APPENDIX B: FLOW DIAGRAM OF THIN SHIP THEORY PROGRAM

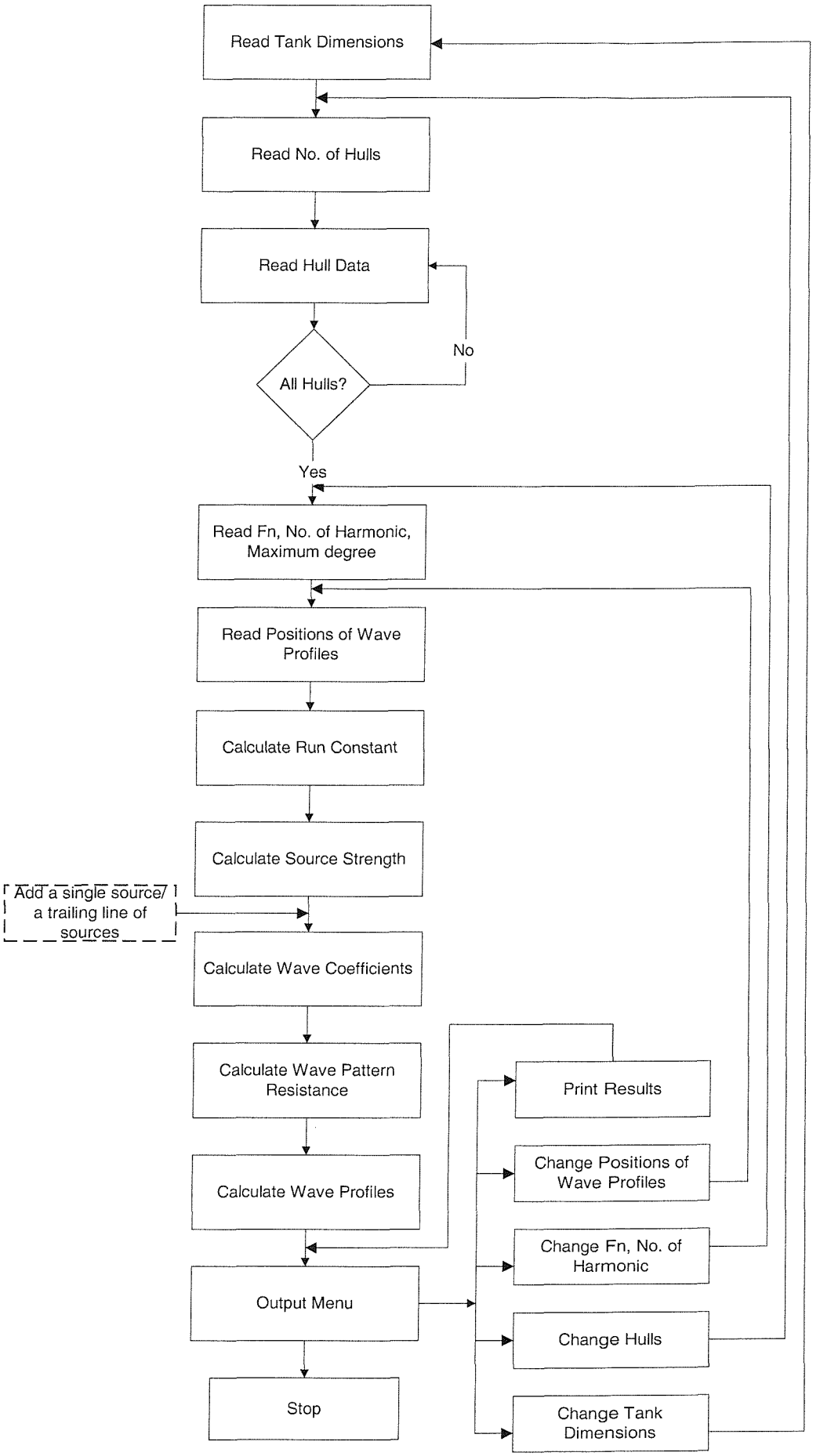

Model	4b	5b	6b	5s
L[m]	1.6	1.6	2.1	1.6
B[m]	0.178	0.146	0.160	0.125
T[m]	0.089	0.073	0.080	0.063
$\nabla[m^3]$	0.0101	0.00667	0.0108	0.00667
Δ[kg]	10.10	6.67	10.75	6.67
$L/\nabla^{1/3}$	7.4	8.5	9.5	8.5
L/B	9.0	11.0	13.1	12.8
B/T	2.0	2.0	2.0	2.0
C_B	0.397	0.397	0.397	0.537
C_P	0.693	0.693	0.693	0.633
C_M	0.565	0.565	0.565	0.848
$A[m^2]$	0.338	0.276	0.401	0.261
LCB[%]	-6.4	-6.4	-6.4	-6.4

Table 1: Principal particulars of models (demihulls) tested in shallow water

Model	L(m)	L/B	B/T	$L/\nabla^{1/3}$	C_B	C_P	C_M	A(m2)	LCB(%amidship)
3b	1.6	7.0	2.0	6.27	0.397	0.693	0.565	0.434	-6.4
4b	1.6	9.0	2.0	7.41	0.397	0.693	0.565	0.338	-6.4
5b	1.6	11.0	2.0	8.50	0.397	0.693	0.565	0.276	-6.4
6b	1.6	13.1	2.0	9.50	0.397	0.693	0.565	0.233	-6.4

Table 2: Principal particulars of models used in regression analysis of dynamic sinkage and trim.

	$TRIM=a(L/V^{1/3})^n$									
Fn	Monohull		S/L=0.2		S/L=0.3		S/L=0.4		S/L=0.5	
	a	n	a	n	a	n	a	n	a	n
0.4	555.06	-3.50	328.00	-2.99	988.28	-3.44	6583.40	-4.48	301.97	-2.90
0.5	5183.70	-4.06	1548.60	-3.18	8799.70	-4.09	5631.00	-3.98	830.40	-3.03
0.6	7722.40	-4.17	3226.40	-3.50	8186.20	-4.03	7183.60	-4.05	1422.40	-3.23
0.7	7583.60	-4.14	2057.30	-3.38	4489.40	-3.79	7010.40	-4.05	1497.70	-3.25
0.8	4760.90	-3.89	2459.10	-3.51	2061.60	-3.42	5498.10	-3.92	1241.60	-3.15
0.9	1777.10	-3.38	1772.10	-3.37	1207.20	-3.14	2687.70	-3.56	825.13	-2.93
1	811.16	-2.98	827.33	-2.99	958.82	-3.04	2068.70	-3.46	419.29	-2.59

Table 3: Dynamic Trim (Degree)

SINKAGE=a(L/V$^{1/3}$)^{n}-m															
Fn	Monohull			S/L=0.2			S/L=0.3			S/L=0.4			S/L=0.5		
	a	n	m	a	n	m	a	n	m	a	n	m	a	n	m
0.3	2.59	0.08	0	8.90	-0.39	0	10.24	-0.50	0	6.91	-0.32	0	11.10	-0.58	0
0.4	19.06	-0.58	0	29.42	-0.61	0	66.53	-1.04	0	18.54	-0.44	0	21.71	-0.57	0
0.5	48.73	-0.96	0	44.31	-0.74	0	87.03	-1.21	0	19.81	-0.49	0	32.37	-0.72	0
0.6	69.52	-1.27	0	7.57	-0.31	0	14.90	-0.65	0	12.10	-0.51	0	18.94	-0.71	0
0.7	14.37	-0.63	0	0.89	-0.16	0	0.59	1.00	3.54	0.30	1.01	0	3.36	-0.11	0
0.8	0.28	1.26	0	1.77	1.00	16.50	1.66	1.00	12.87	1.23	1.00	8.32	0.0022	3.19	0
0.9	0.0004	4.38	0	1.89	1.00	16.97	2.55	1.00	20.68	2.17	1.00	16.62	1.49	1.00	10.50
1	4.00E-08	8.65	0	4.93	1.00	44.16	3.22	1.00	26.49	2.01	1.00	15.61	1.66	1.00	12.58

Table 4: Dynamic Sinkage (% Draught): positive upward

	Fn						
	0.4	**0.5**	**0.6**	**0.7**	**0.8**	**0.9**	**1**
Monohull	0.947	0.9843	0.995	0.9957	0.9952	0.9839	0.9687
S/L=0.2	0.9921	0.9734	0.985	0.9757	0.995	0.9931	0.9821
S/L=0.3	0.9705	0.9987	0.9959	0.999	0.9992	0.9987	0.9748
S/L=0.4	0.6757	0.9146	0.9177	0.9263	0.9624	0.9868	0.9678
S/L=0.5	0.9421	0.9889	0.9896	0.9925	0.9976	0.9981	0.9835

Table 5: R^2 Value of Trim Prediction

	Fn							
	0.3	**0.4**	**0.5**	**0.6**	**0.7**	**0.8**	**0.9**	**1**
Monohull	0.4831	0.8613	0.9457	0.9043	0.5307	0.7457	0.877	0.817
S/L=0.2	0.1957	0.9016	0.7529	0.4843	0.0006	0.9865	0.9973	0.9111
S/L=0.3	0.8871	0.9698	0.9901	0.9871	0.8388	0.9948	0.9422	0.9184
S/L=0.4	0.2108	0.9577	0.7566	0.8274	0.8812	0.968	0.9684	0.9343
S/L=0.5	0.4484	0.5759	0.5152	0.6033	0.1856	0.7878	0.8457	0.8633

Table 6: R^2 Value of Sinkage Prediction

Model	L/B	B/T	$L/\nabla^{1/3}$	C_B	LCB(%amidship)
Model 4b	9.0	2.0	7.410	0.397	-6.4
Model 4c	8.0	2.5	7.390	0.397	-6.4
Athena	6.806	4.57	7.624	0.478	N/A

Table 7: Principal particulars of models used in the prediction of wave profiles along the hull.

Model	L(m)	B(m)	T(m)	$A(m^2)$	$L/\nabla^{1/3}$	L/B	B/T
Model 5a	1.6	0.125	0.0833	0.282	8.51	12.8	1.5
Model 5b	1.6	0.1454	0.0727	0.276	8.50	11	2.0
Model 5c	1.6	0.1616	0.0646	0.277	8.49	9.9	2.5

Table 8: Principal particulars of models (demihulls) used for example applications

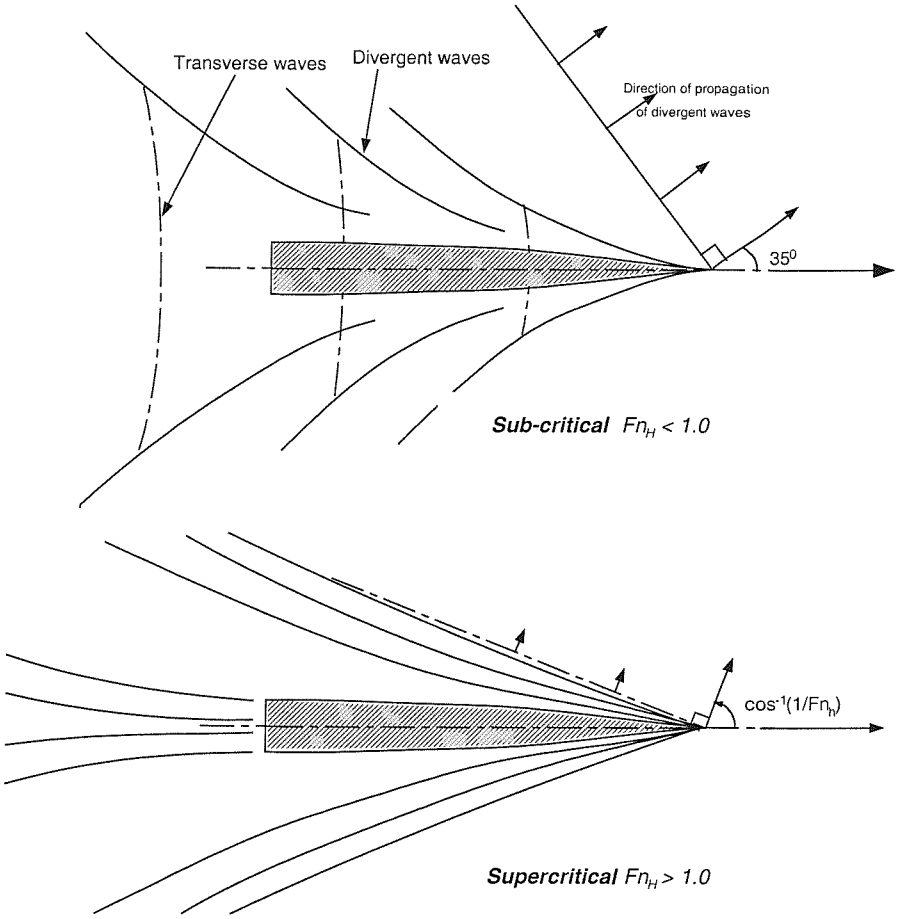

Fig.2.1 Sub-critical and supercritical wave patterns

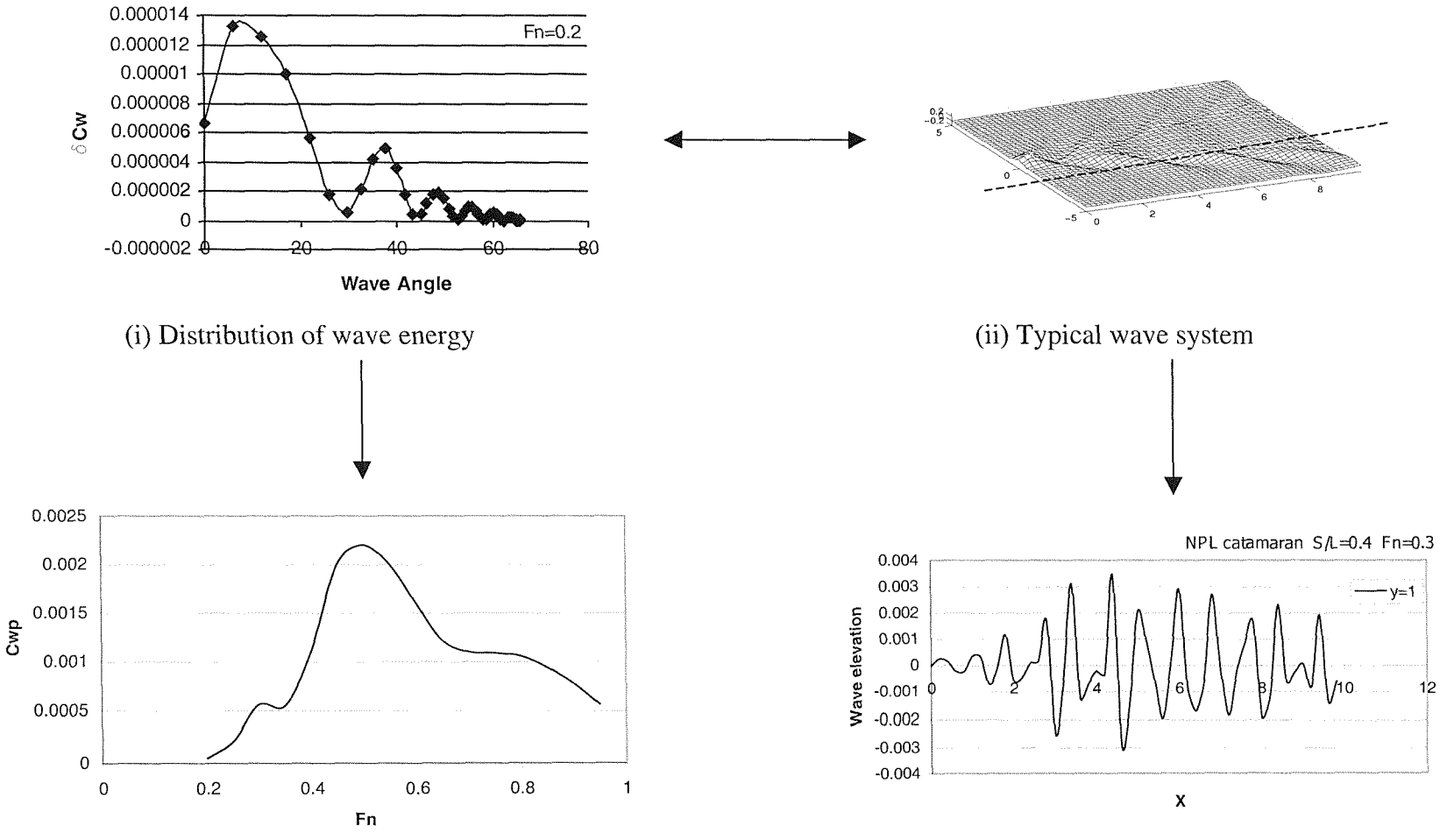

Fig.2.2 Description of wave characteristics: wave pattern, longitudinal wave cut, distribution of wave energy and wave resistance.

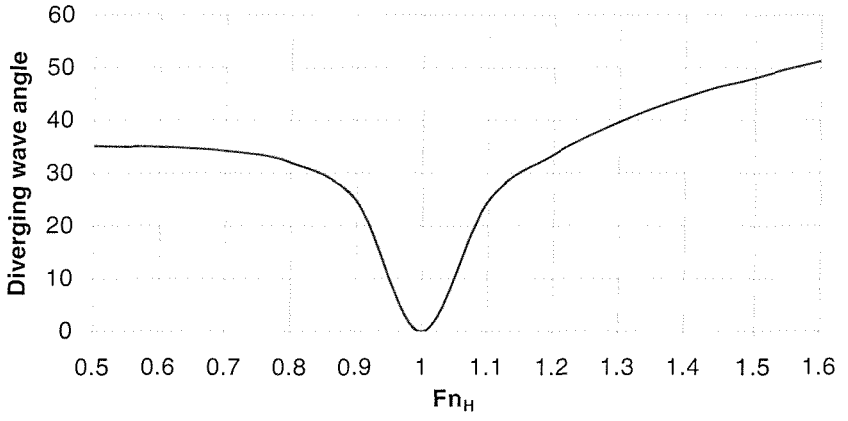

Fig.2.3 Description of wave characteristics: divergent wave angle

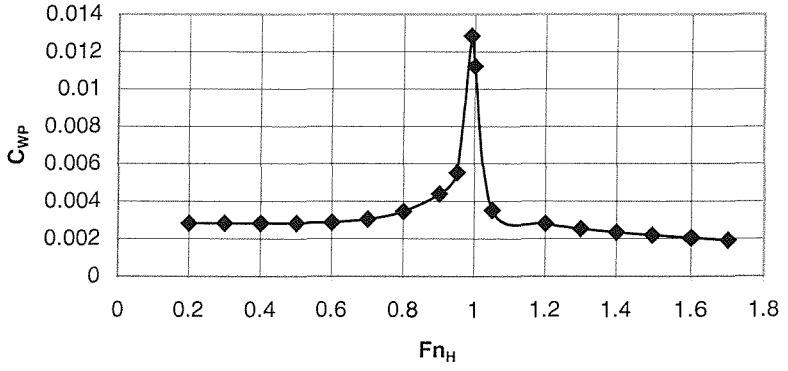

Fig.2.4 Description of wave characteristics: wave pattern resistance coefficients due to the effects of shallow water

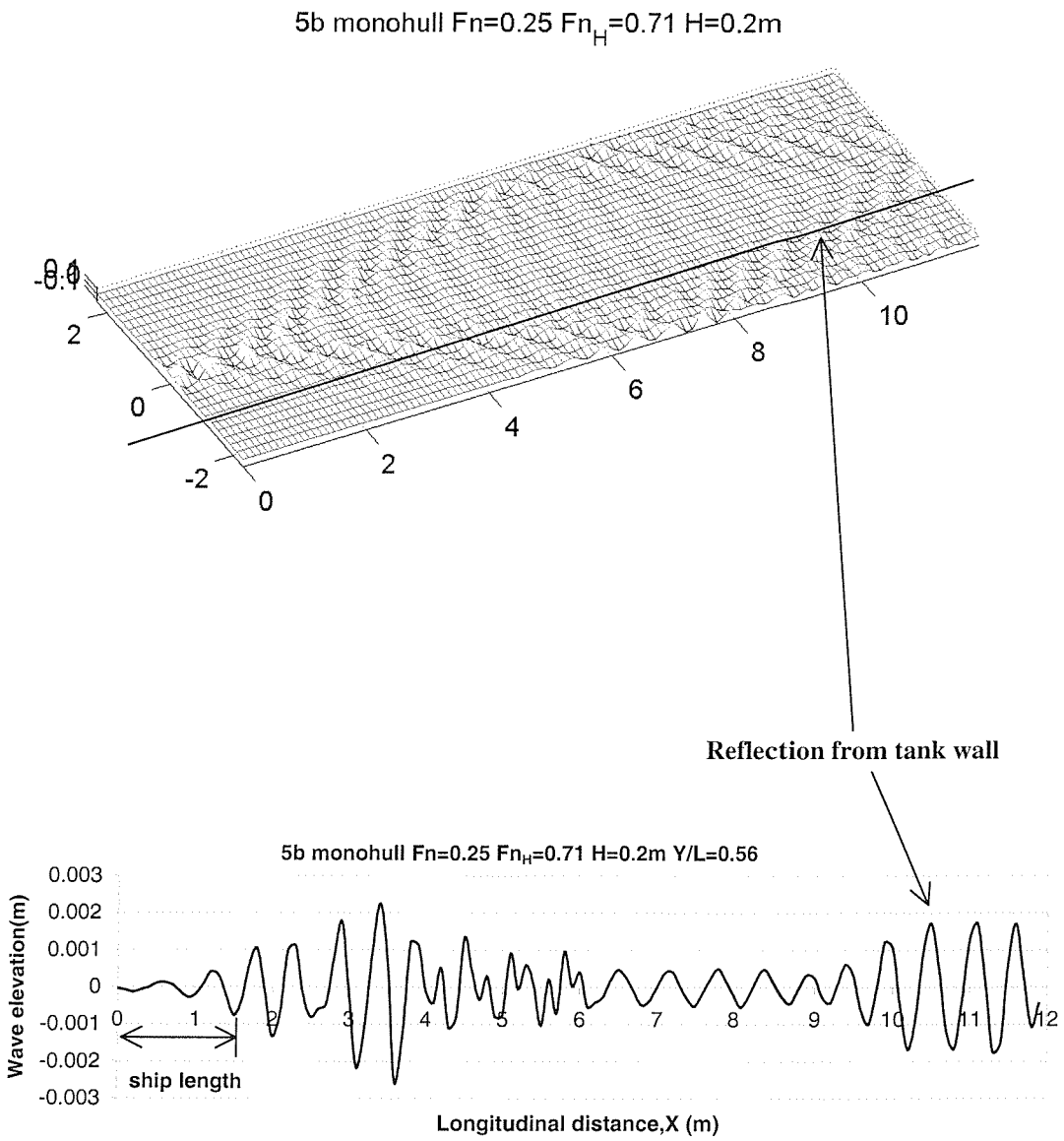

Fig.2.5 Typical wave pattern and wave cut

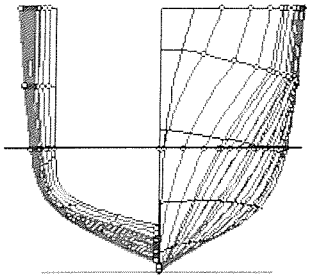

Model 4b

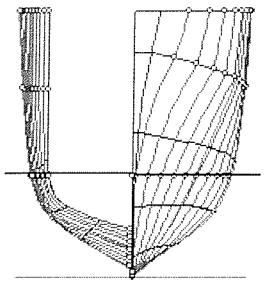

Model 5b

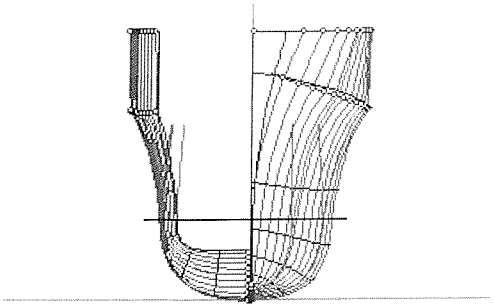

Model 5s

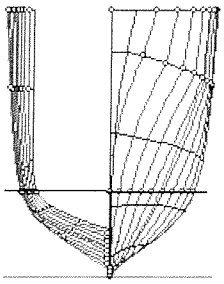

Model 6b

Fig.3.1 Model Bodyplan and Notation

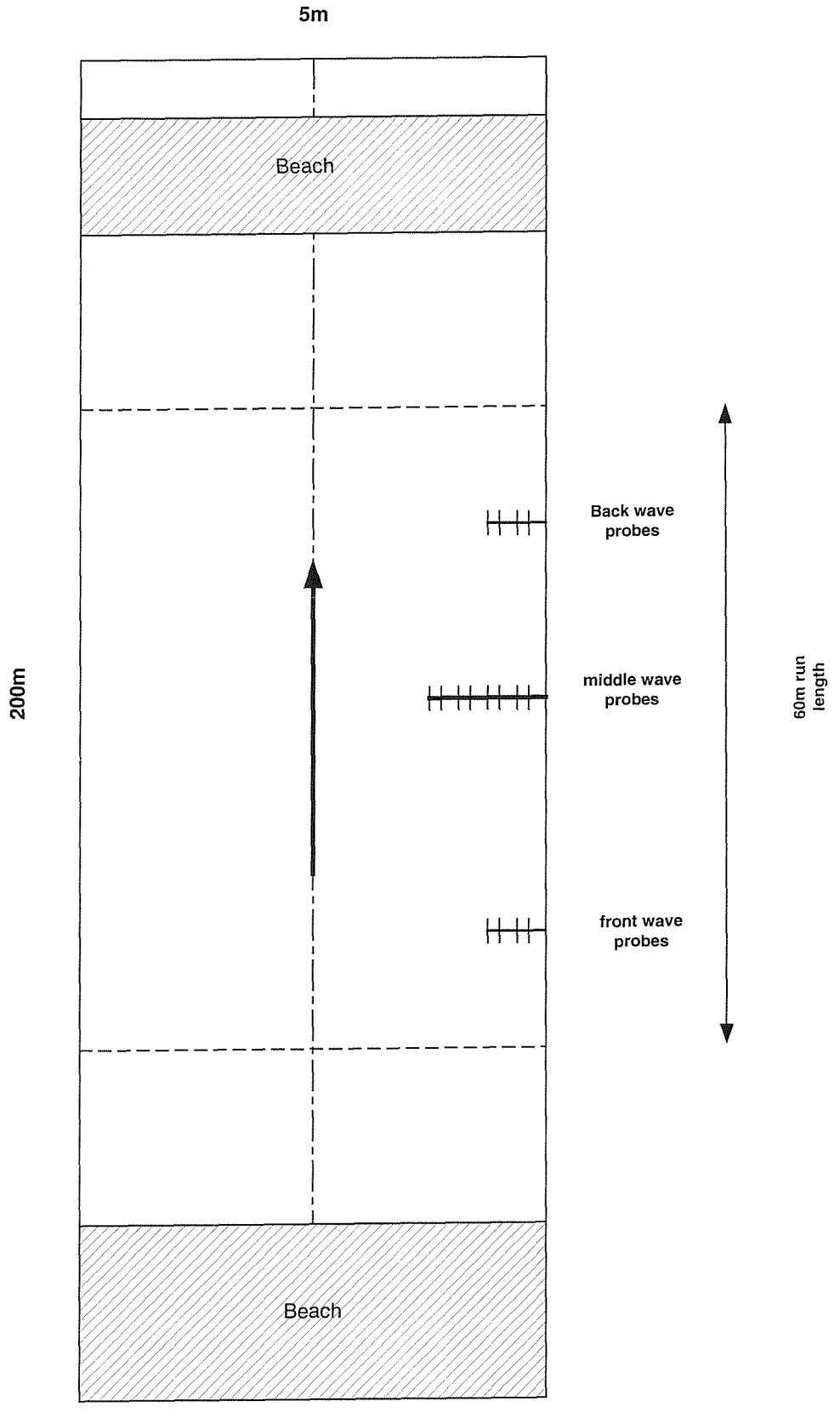

Fig.3.2 Schematic of GKN test tank

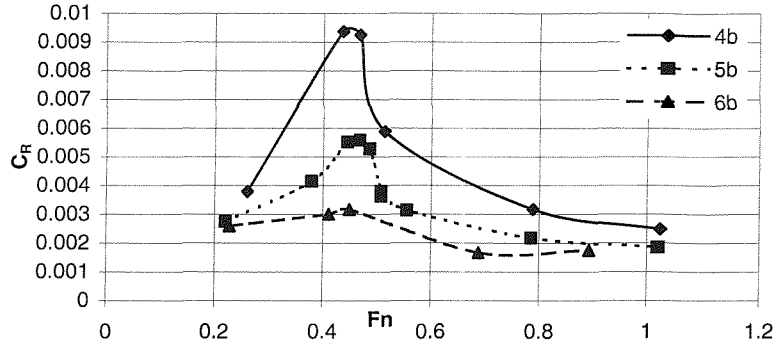

Fig.3.3 Measured residuary resitance coefficients (monohulls, waterdepth=0.4m)

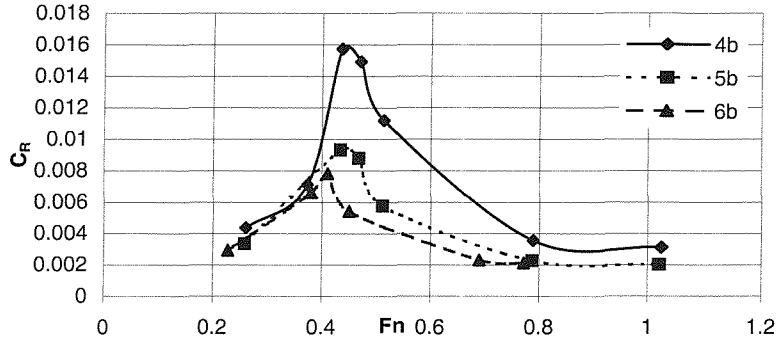

Fig.3.4 Measured residuary resitance coefficients (catamarans S/L=0.2, waterdepth=0.4m)

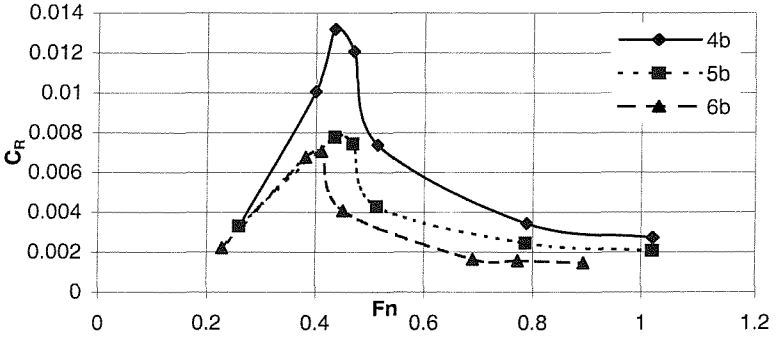

Fig.3.5 Measured residuary resitance coefficients (catamarans S/L=0.4, waterdepth=0.4m)

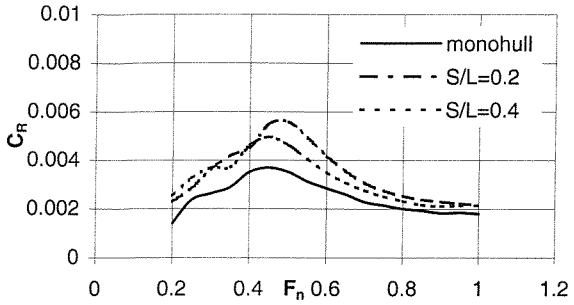

Fig.3.6 Residuary resistance coefficient (5b waterdepth=1.85m)

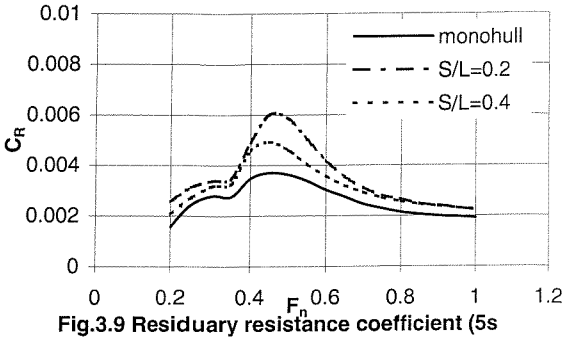

Fig.3.9 Residuary resistance coefficient (5s waterdepth=1.85m)

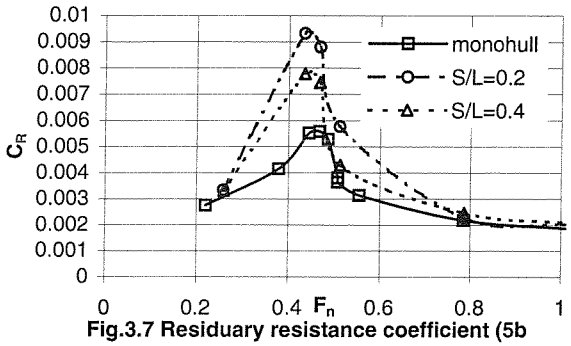

Fig.3.7 Residuary resistance coefficient (5b waterdepth=0.4m)

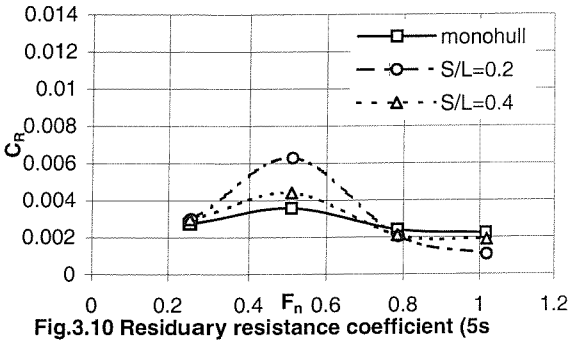

Fig.3.10 Residuary resistance coefficient (5s waterdepth=0.4m)

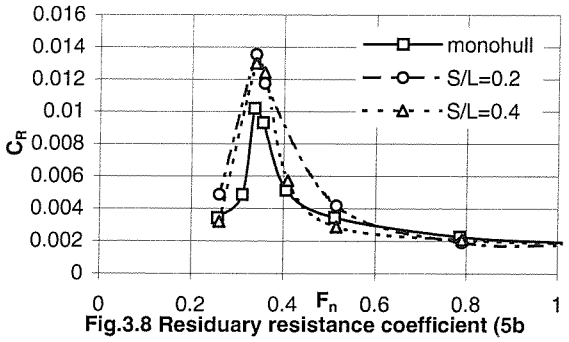

Fig.3.8 Residuary resistance coefficient (5b waterdepth=0.2m)

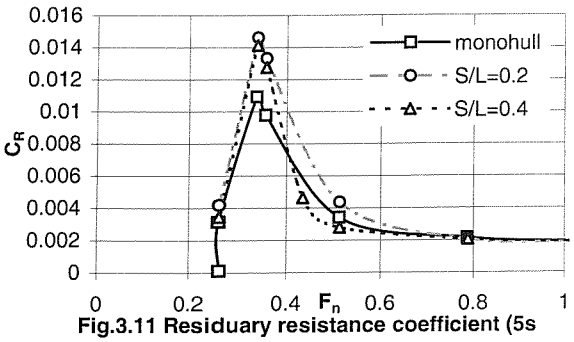

Fig.3.11 Residuary resistance coefficient (5s waterdepth=0.2m)

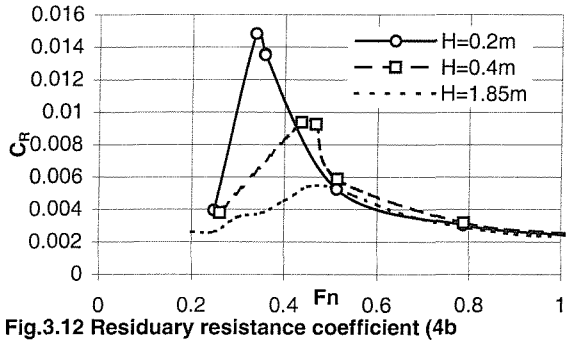

Fig.3.12 Residuary resistance coefficient (4b monohull)

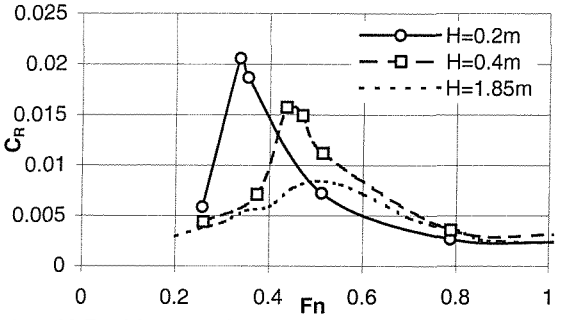

Fig.3.13 Residuary resistance coefficient (4b catamaran S/L=0.2)

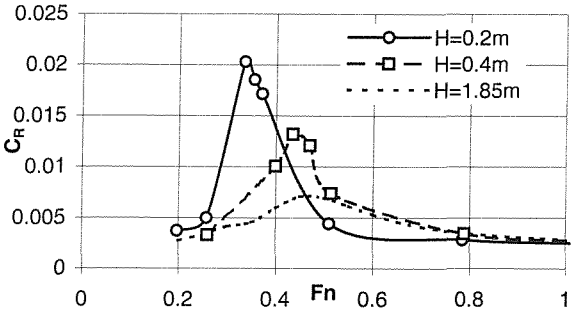

Fig.3.14 Residuary resistance coefficient (4b catamaran S/L=0.4)

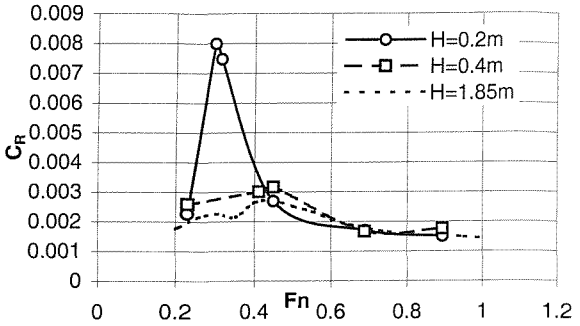

Fig.3.15 Residuary resistance coefficient (6b monohull)

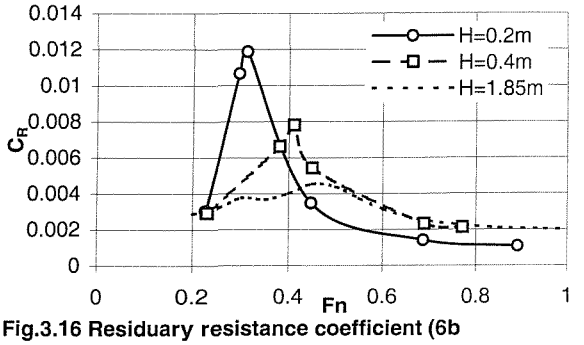

Fig.3.16 Residuary resistance coefficient (6b catamaran S/L=0.2)

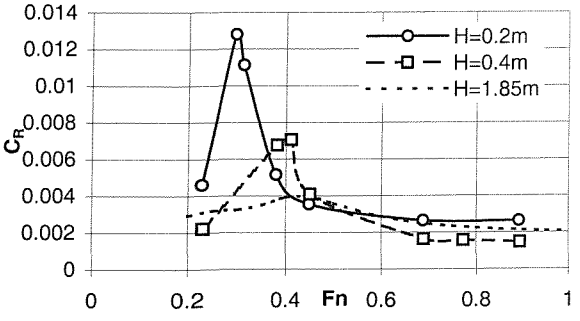

Fig.3.17 Residuary resistance coefficient (6b catamaran S/L=0.4)

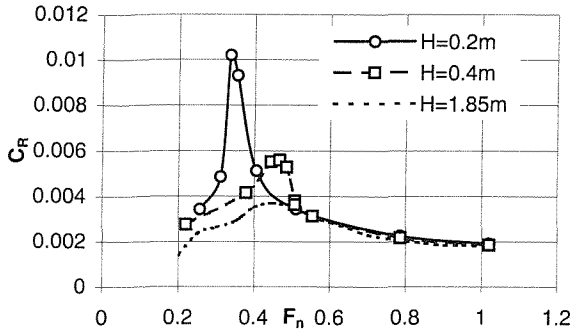

Fig.3.18 Residuary resistance coefficient (5b monohuil)

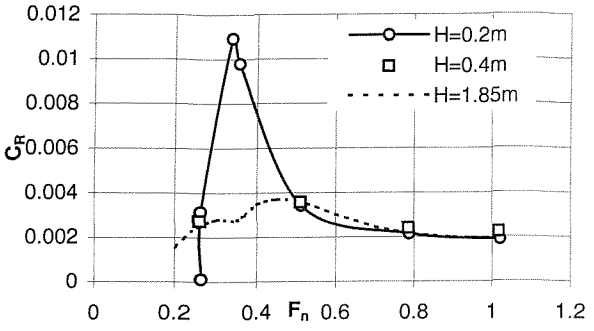

Fig.3.21 Residuary resistance coefficient (5s monohull)

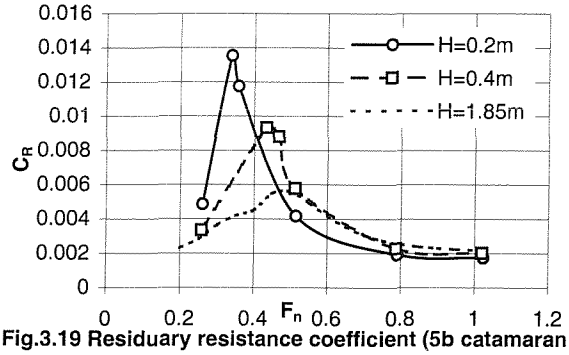

Fig.3.19 Residuary resistance coefficient (5b catamaran S/L=0.2)

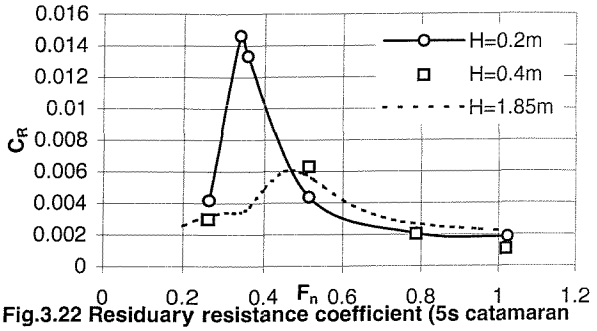

Fig.3.22 Residuary resistance coefficient (5s catamaran S/L=0.2)

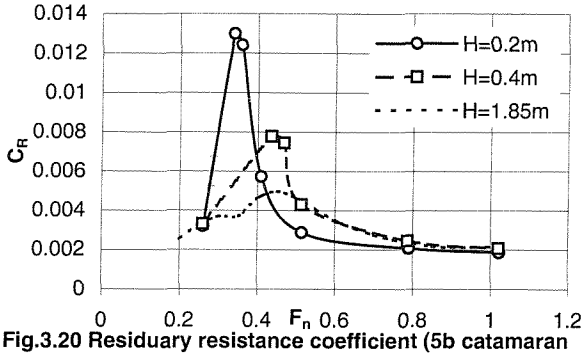

Fig.3.20 Residuary resistance coefficient (5b catamaran S/L=0.4)

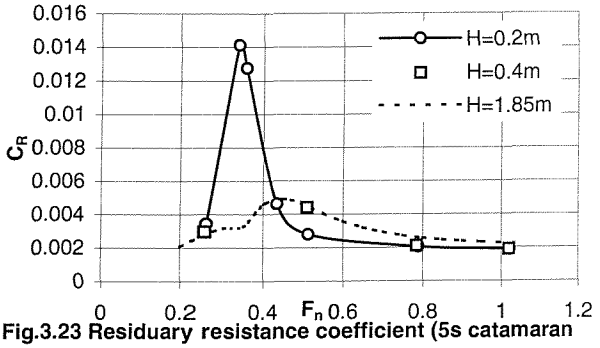

Fig.3.23 Residuary resistance coefficient (5s catamaran S/L=0.2)

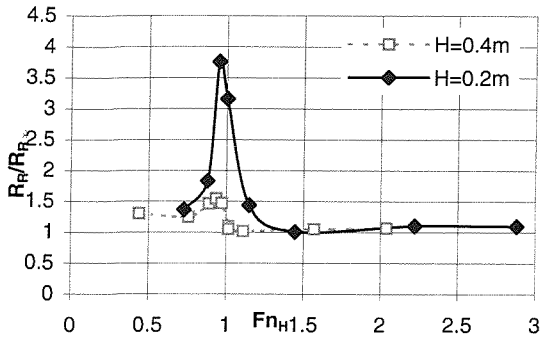

Fig.3.24 Resistance ratio (5b monohull)

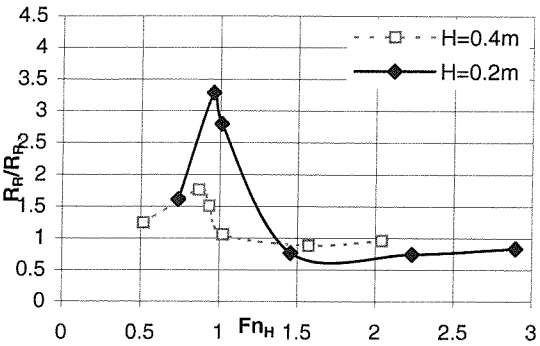

Fig.3.25 Resistance ratio (5b catamaran S/L=0.2)

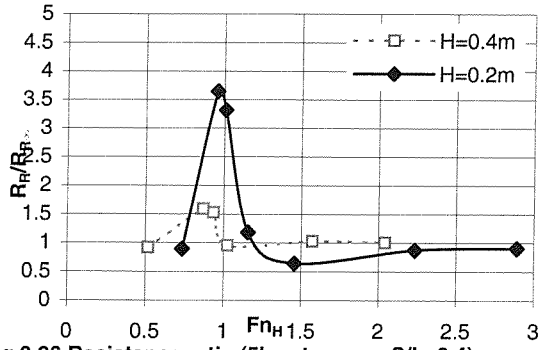

Fig.3.26 Resistance ratio (5b catamaran S/L=0.4)

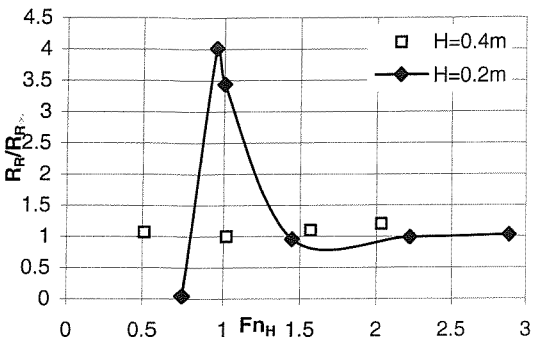

Fig.3.27 Resistance ratio (5s monohull)

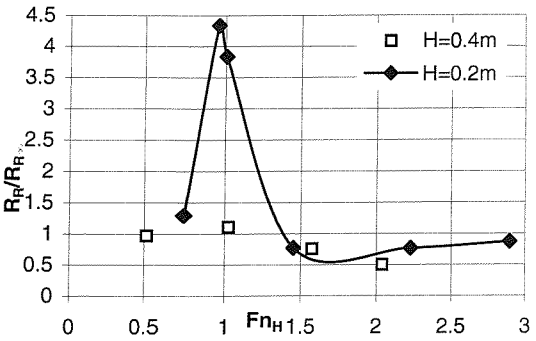

Fig.3.28 Resistance ratio (5s catamaran S/L=0.2)

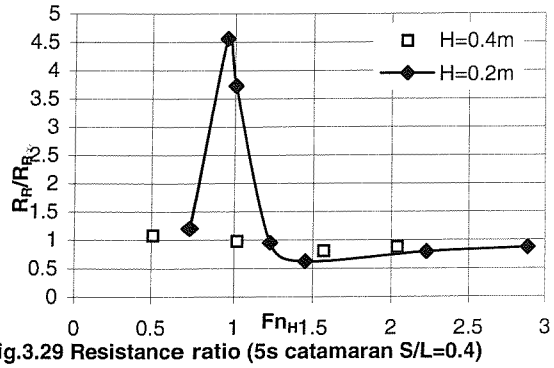

Fig.3.29 Resistance ratio (5s catamaran S/L=0.4)

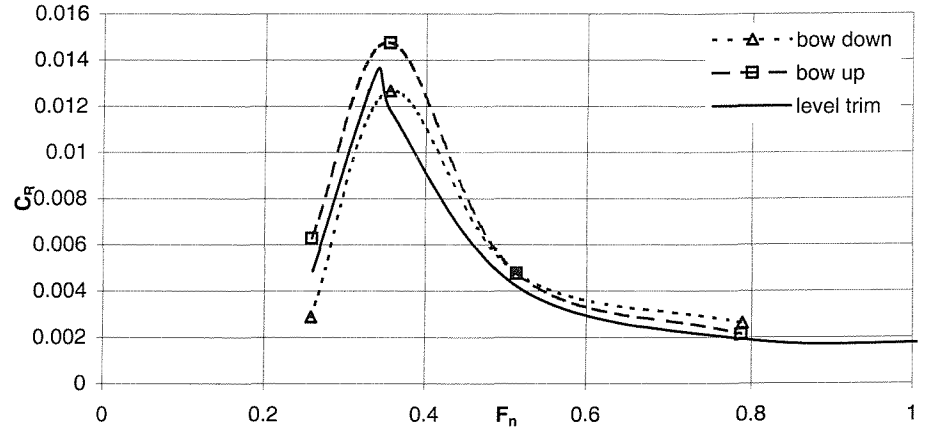

Fig.3.30 Residuary resistance coefficient (5b catamaran, S/L=0.2, water depth=0.2m)

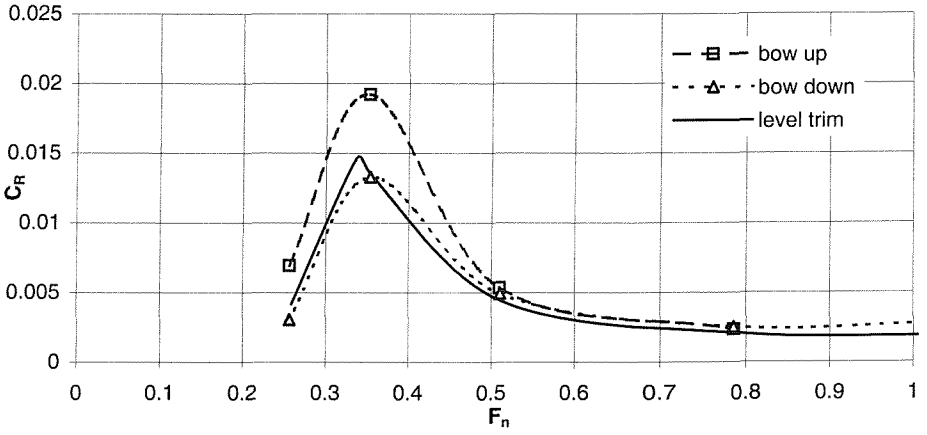

Fig.3.31 Residuary resistance coefficient (5s catamaran, S/L=0.2, water depth=0.2m)

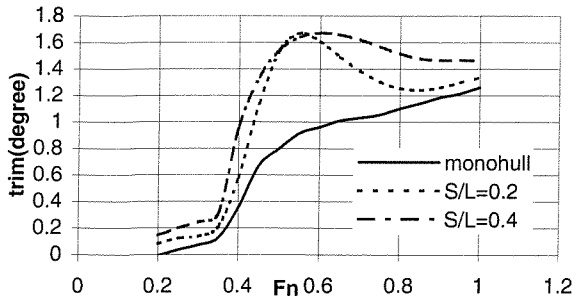

Fig.3.32a Running trim (5b waterdepth=1.85m)

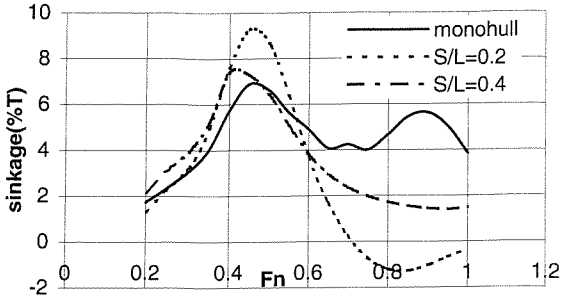

Fig.3.32b Running sinkage (5b waterdepth=1.85m)

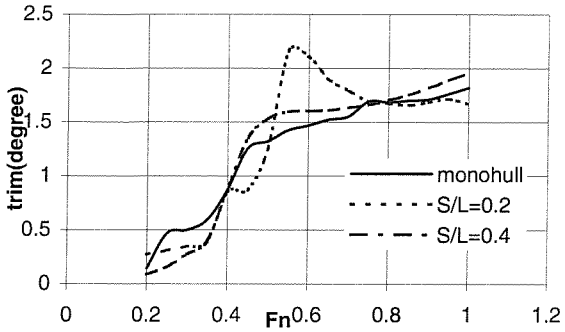

Fig.3.33a Running trim (5s waterdepth=1.85m)

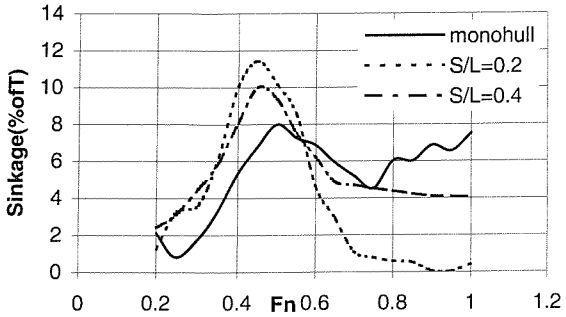

Fig.3.33b Running sinkage (5s waterdepth=1.85m)

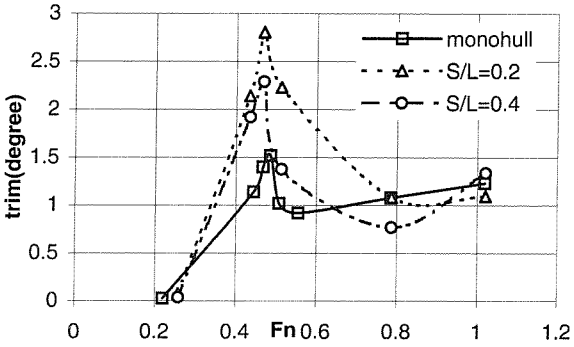

Fig.3.34a Running trim (5b waterdepth=0.4m)

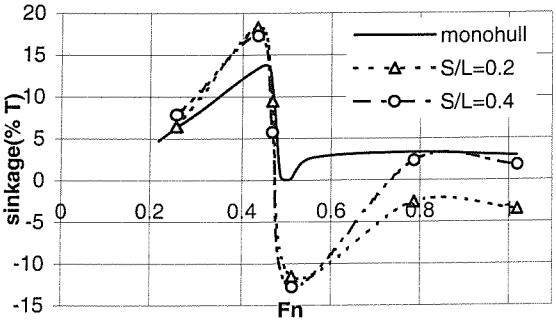

Fig.3.34b Running sinkage (5b waterdepth=0.4m)

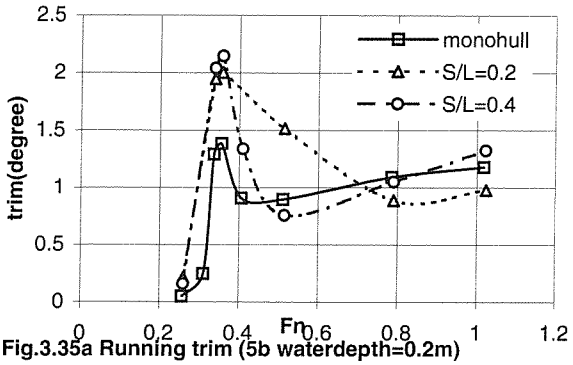

Fig.3.35a Running trim (5b waterdepth=0.2m)

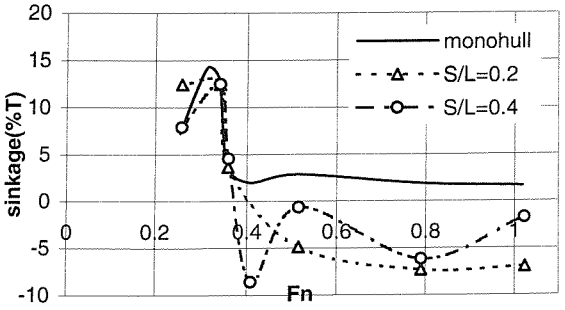

Fig.3.35b Running sinkage (5b waterdepth=0.2m)

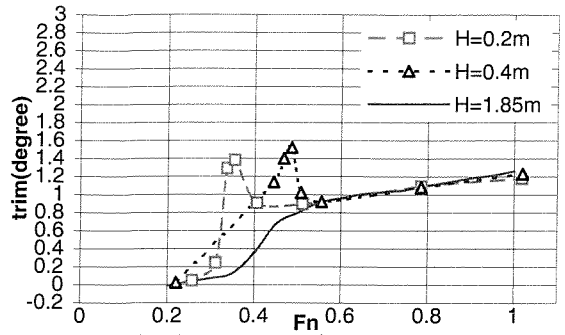

Fig.3.36a Running trim (5b monohull)

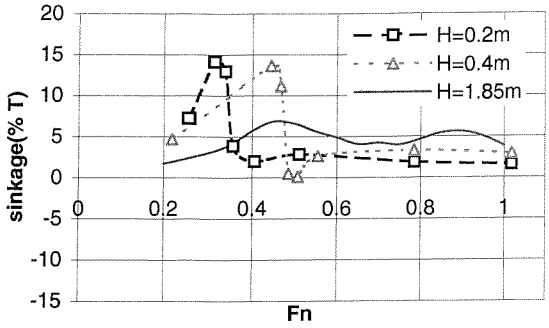

Fig.3.36b Running sinkage (5b monohull)

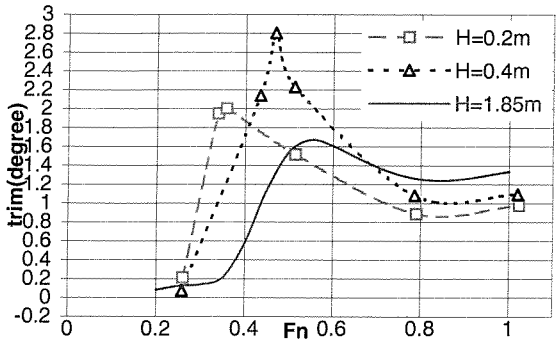

Fig.3.37a Running trim (5b catamaran S/L=0.2)

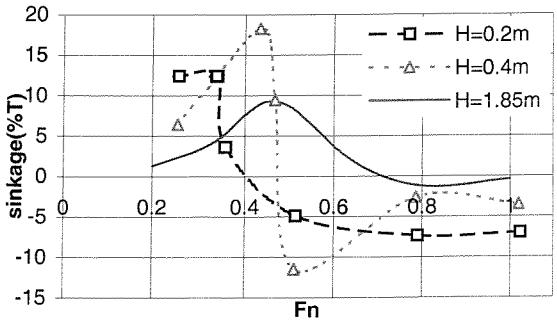

Fig.3.37b Running sinkage (5b catamaran S/L=0.2)

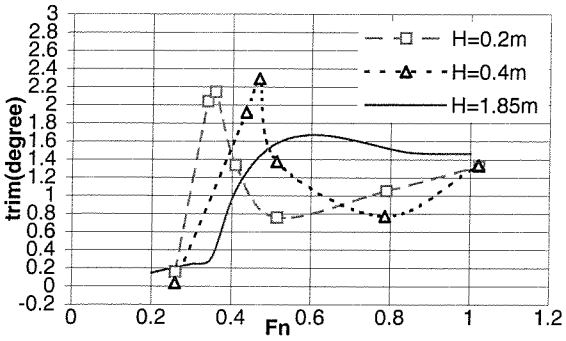

Fig.3.38a Running trim (5b catamaran S/L=0.4)

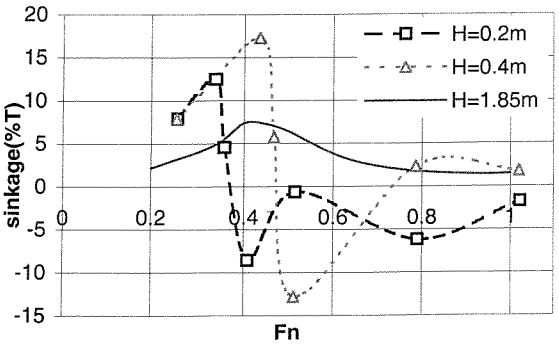

Fig.3.38b Running sinkage (5b catamaran S/L=0.4)

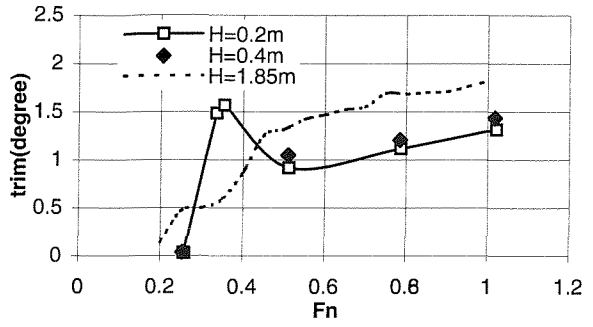

Fig.3.39a Running trim (5s monohull)

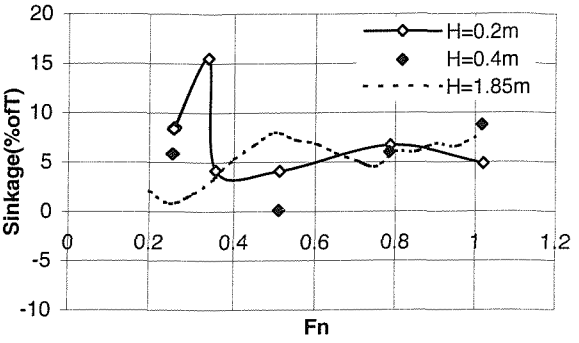

Fig.3.39b Running sinkage (5s monohull)

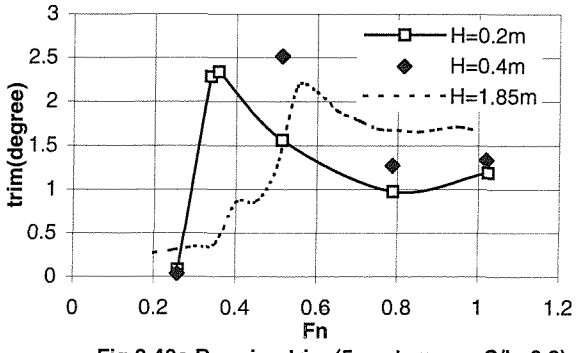

Fig.3.40a Running trim (5s catamaran S/L=0.2)

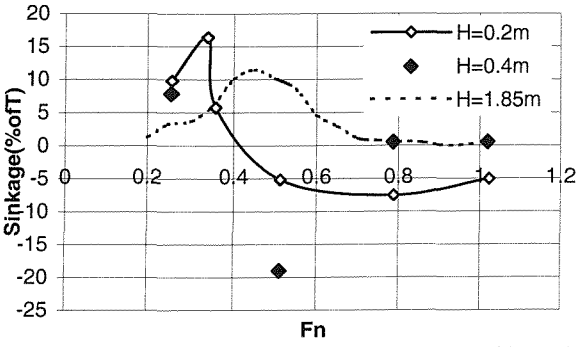

Fig.3.40b Running sinkage (5s catamaran S/L=0.2)

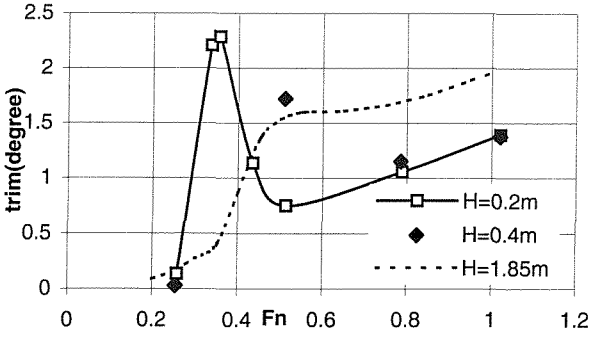

Fig.3.41a Running trim (5s catamaran S/L=0.4)

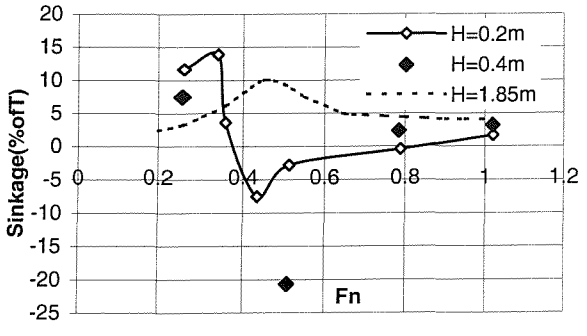

Fig.3.41b Running sinkage (5s catamaran S/L=0.4)

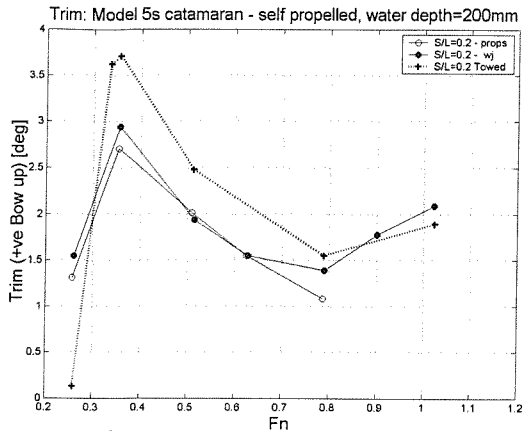

Fig. 3.42a Running Trim: 5s cat S/L=0.2

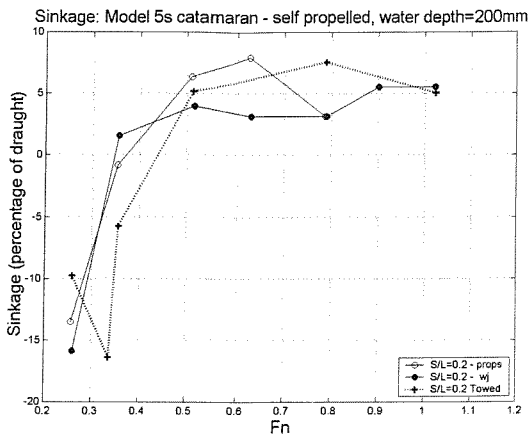

Fig. 3.42b Running Sinkage: 5s catS/L=0.2

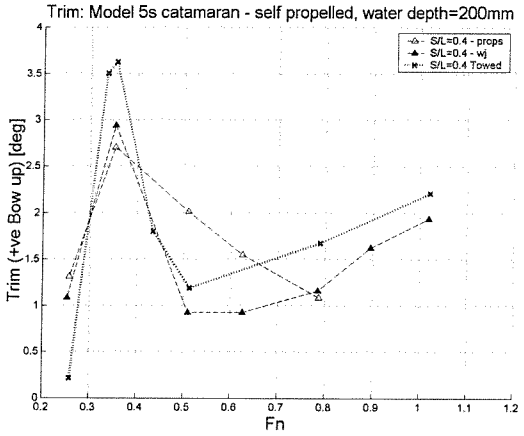

Fig.3.43a Running Trim: 5s cat S/L=0.4

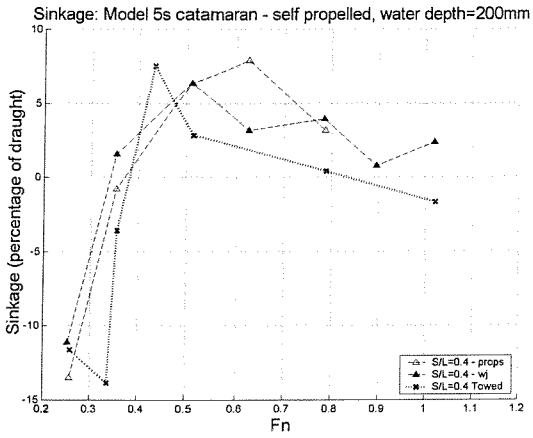

Fig.3.43b Running Sinkage: 5s S/L=0.4

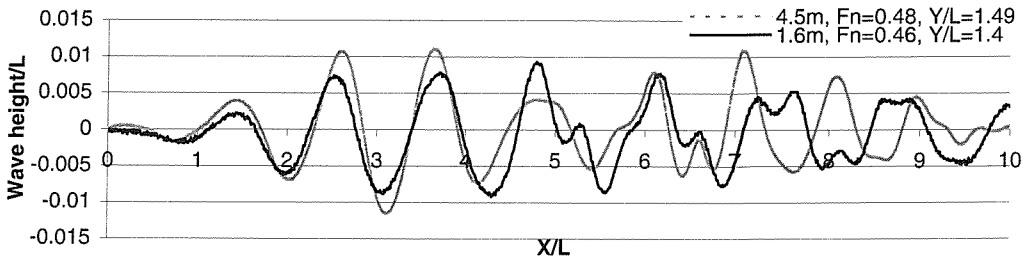

Fig.3.44 Comparison of 4.5m and 1.6m models

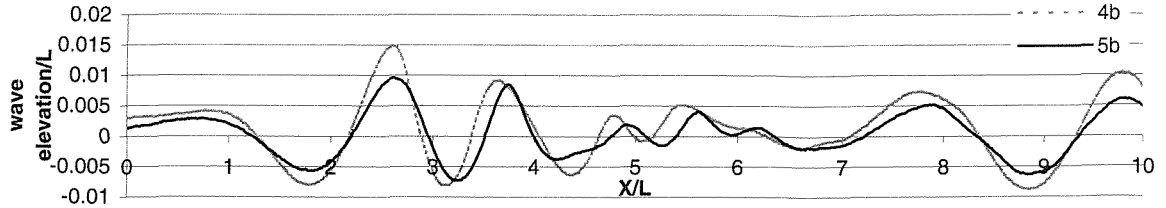

Fig.3.45a Measured wave cuts (monohull H=0.4m Fn=0.785 Y/L=0.55)

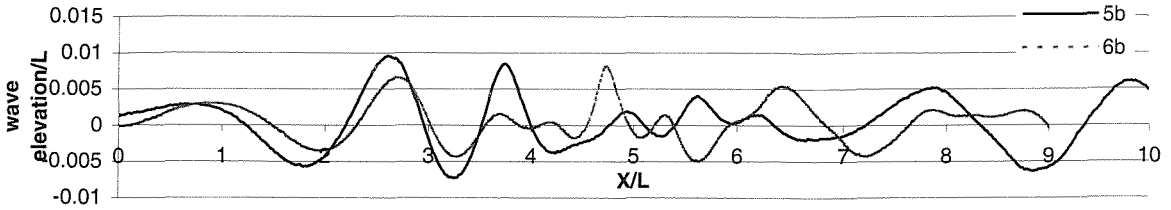

Fig.3.45b Measured wave cuts (monohull H=0.4m Fn=0.785 / 0.685 Y/L=0.55 / 0.52)

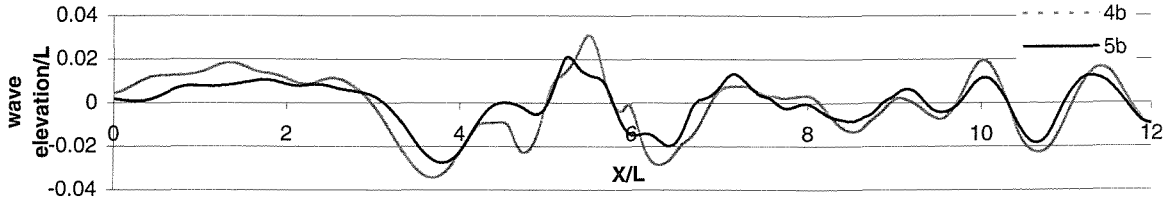

Fig.3.46a Measured wave cuts (catamaran S/L=0.2 H=0.4m Fn=0.47 Y/L=0.55)

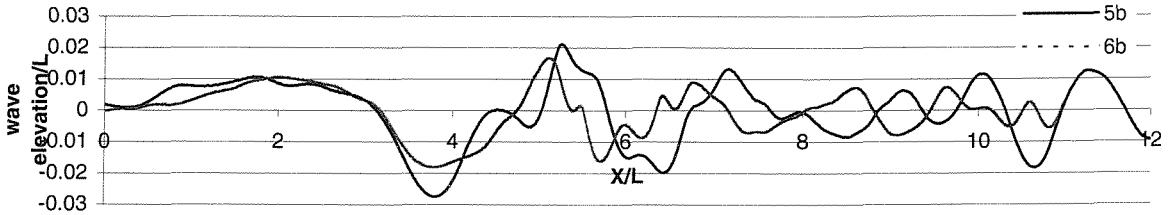

Fig.3.46b Measured wave cuts (catamaran S/L=0.2 H=0.4m Fn=0.47 / 0.41 Y/L=0.55 / 0.52)

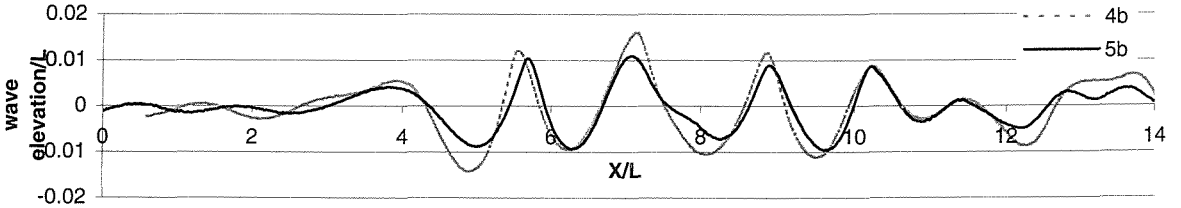

Fig.3.47a Measured wave cuts (catamaran S/L=0.4 H=0.4m Fn=1.0 Y/L=0.55)

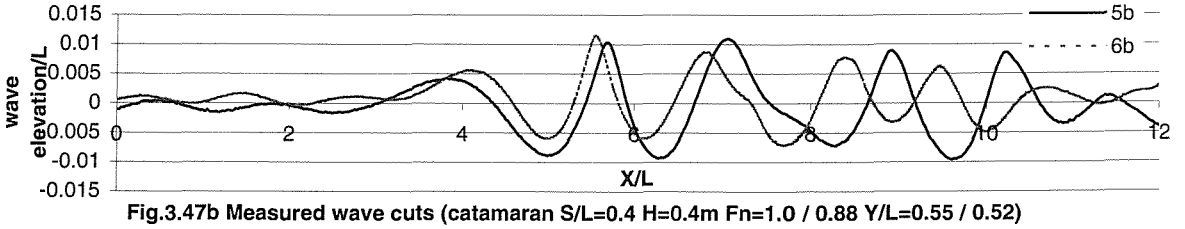

Fig.3.47b Measured wave cuts (catamaran S/L=0.4 H=0.4m Fn=1.0 / 0.88 Y/L=0.55 / 0.52)

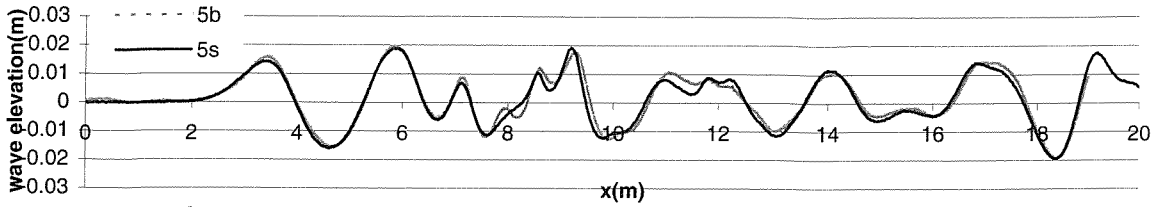

Fig.3.48a Comparison of wave cuts: catamaran S/L=0.2 Fn=0.5 Fn_H=1.43 H=0.2m Y/L=0.68

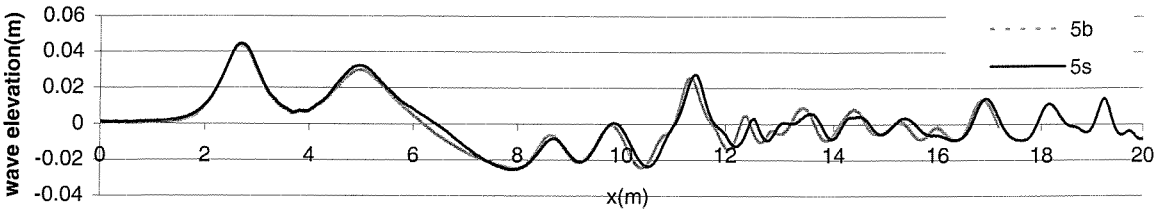

Fig.3.48b Comparison of wave cuts: catamaran S/L=0.2 Fn=0.35 Fn_H=1.0 H=0.2m Y/L=0.93

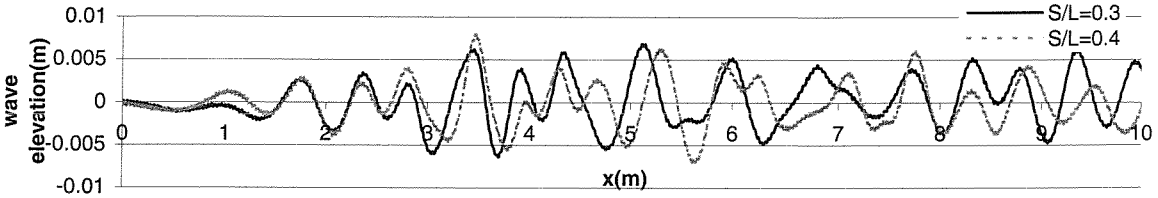

Fig.3.49 Measured wave cuts (5s H=1.85m Fn=0.3 Y/L=0.69)

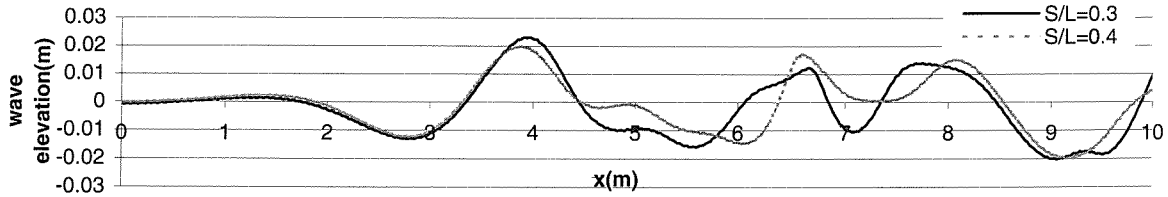

Fig.3.50 Measured wave cuts (5s H=1.85m Fn=0.59 Y/L=0.69)

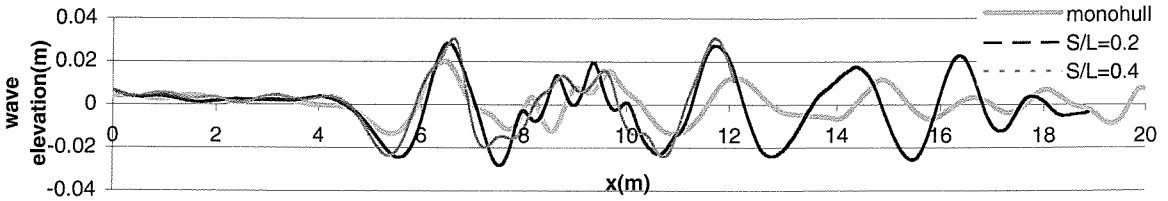

Fig.3.51 Measured wave cuts (5b H=0.4m Fn=0.44 Fn_H=0.88 Y/L=0.55)

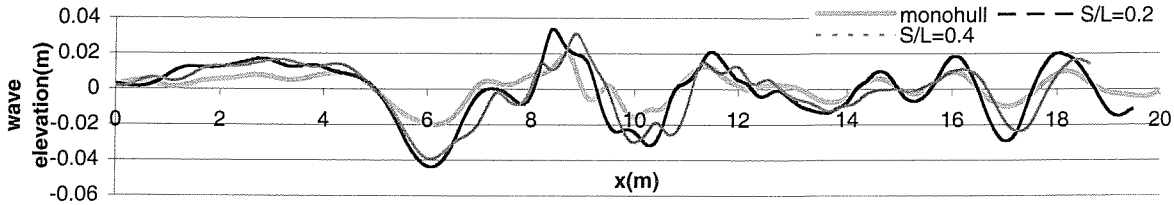

Fig.3.52 Measured wave cuts (5b H=0.4m Fn=0.47 Fn_H=0.93 Y/L=0.55)

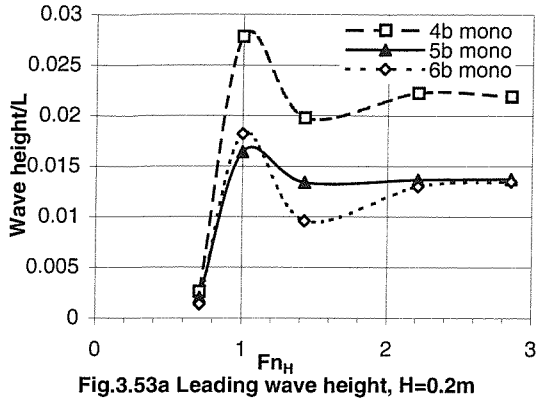

Fig.3.53a Leading wave height, H=0.2m

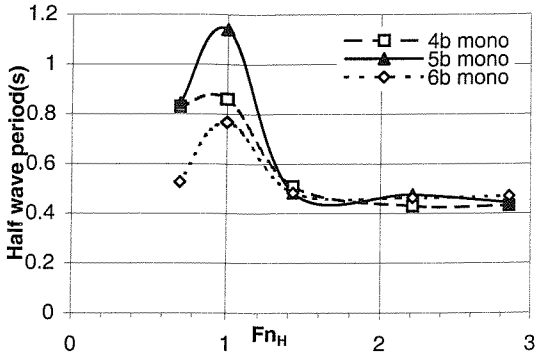

Fig.3.53b Half wave period of leading wave, H=0.2m

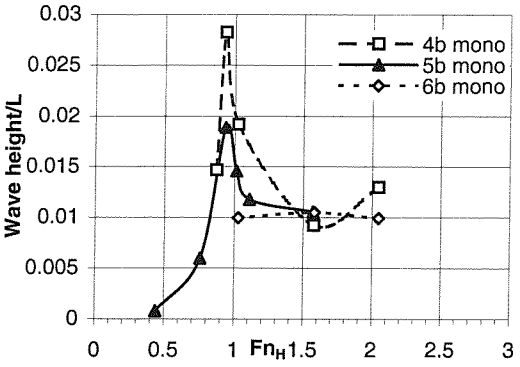

Fig.3.54a Leading wave height, H=0.4m

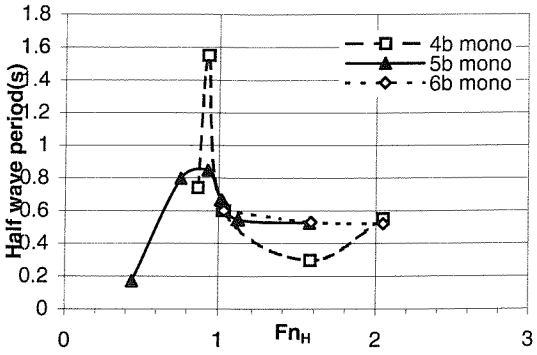

Fig.3.54b Half wave period of leading wave, H=0.4m

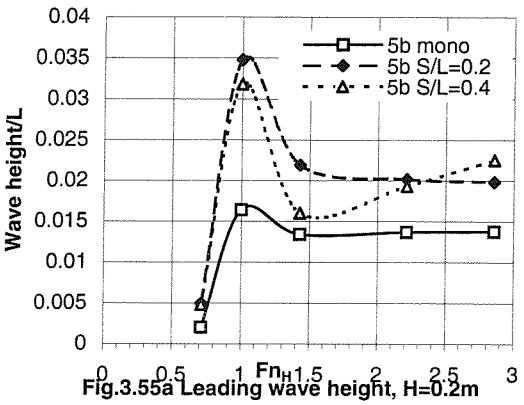

Fig.3.55a Leading wave height, H=0.2m

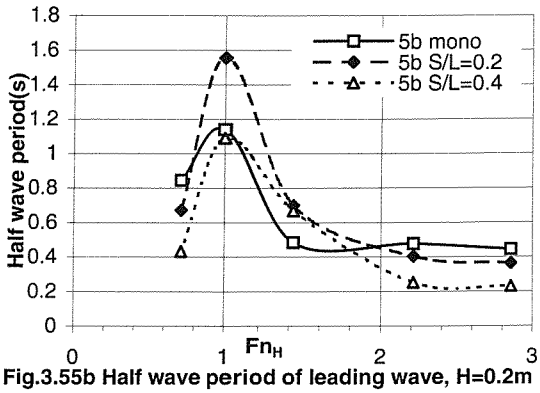

Fig.3.55b Half wave period of leading wave, H=0.2m

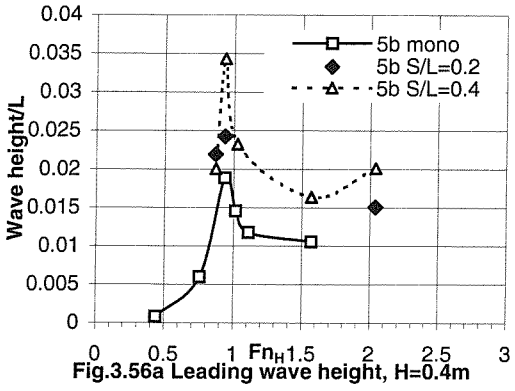

Fig.3.56a Leading wave height, H=0.4m

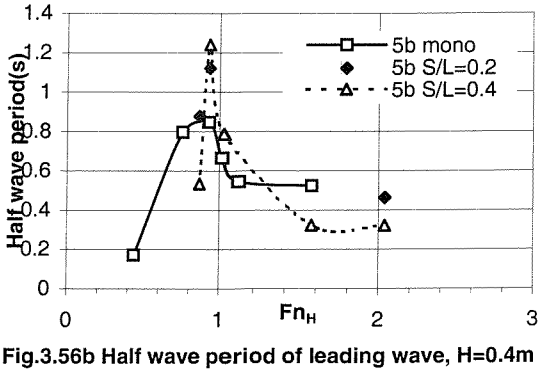

Fig.3.56b Half wave period of leading wave, H=0.4m

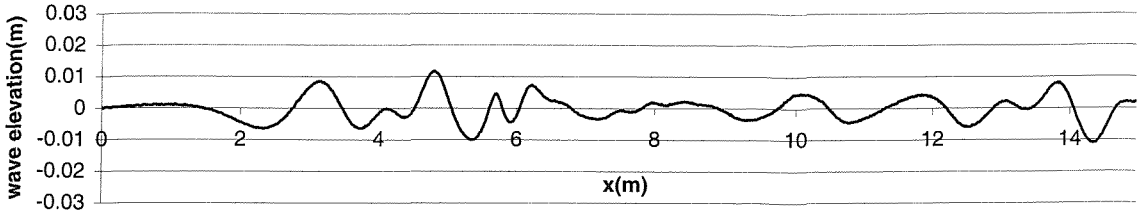

Fig.3.57a Measured wave cut at sub- critical speed (5b monohull H=0.4m Y/L=0.55 Fn=0.38 Fn_H=0.76)

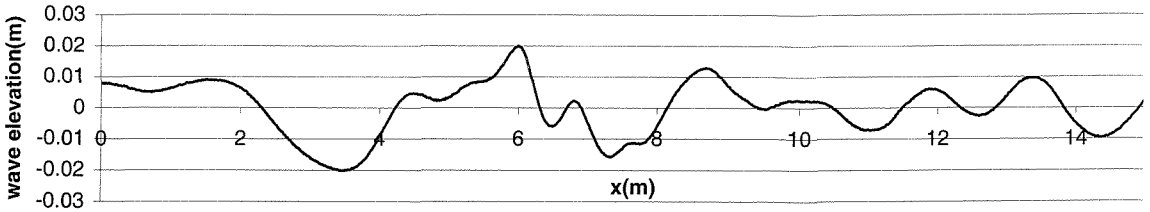

Fig.3.57b Measured wave cut at near critical speed (5b monohull H=0.4m Y/L=0.55 Fn=0.47 Fn_H=0.93)

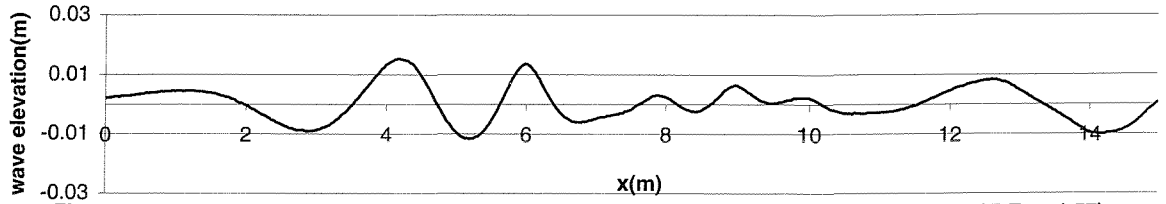

Fig.3.57c Measured wave cut at super-critical speed (5b monohull H=0.4m Y/L=0.55 Fn=0.785 Fn_H=1.57)

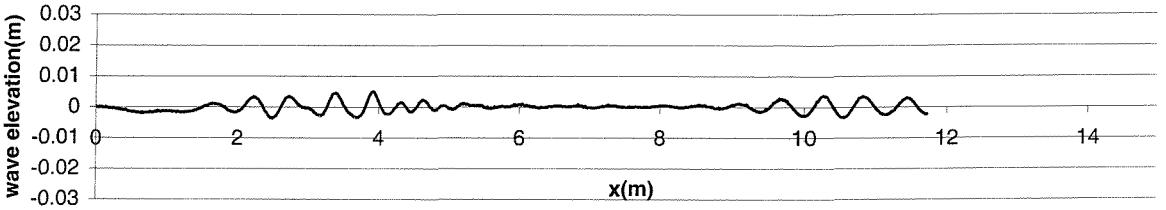

Fig.3.58a Measured wave cut at sub-critical speed (5s monohull H=0.2m Y/L=0.55 Fn=0.25 Fn_H=0.71)

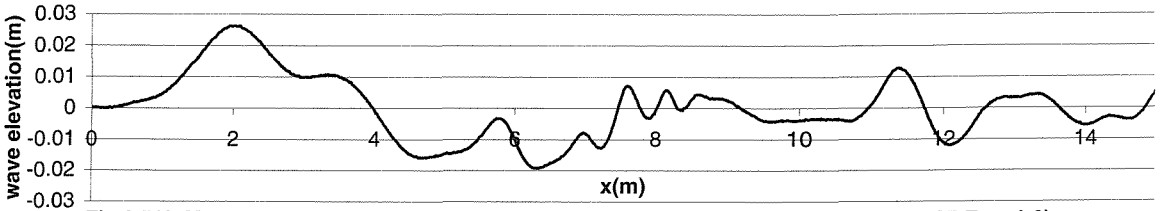

Fig.3.58b Measured wave cut at critical speed (5s monohull H=0.2m Y/L=0.55 Fn=0.35 Fn_H=1.0)

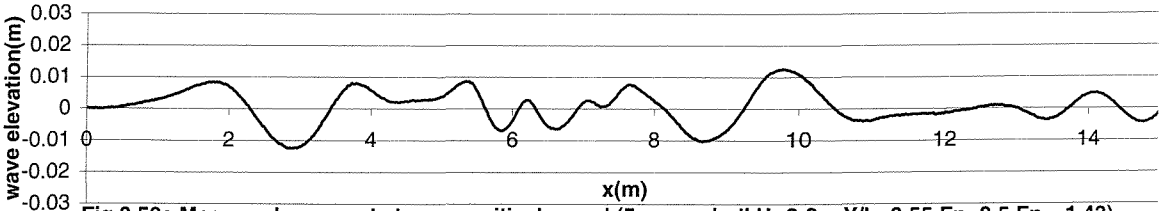

Fig.3.58c Measured wave cut at super-critical speed (5s monohull H=0.2m Y/L=0.55 Fn=0.5 Fn_H=1.43)

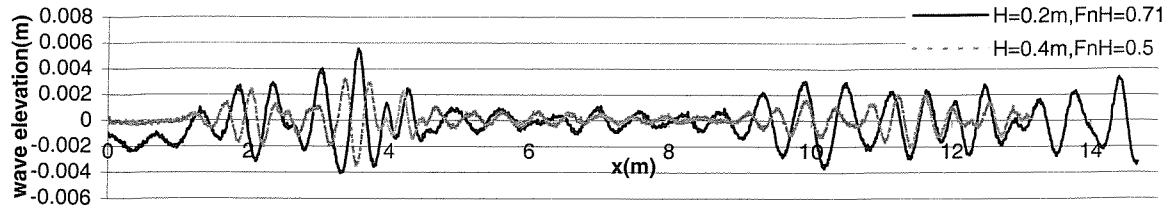

Fig.3.59 Comparison of wave cuts at the same Fn (5b monohull Fn=0.25 Y/L=0.55)

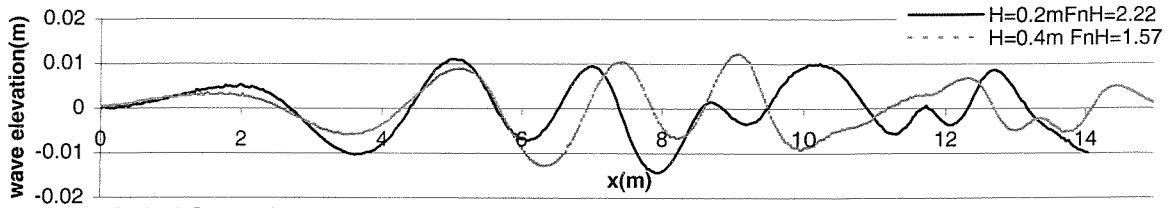

Fig.3.60 Comparison of wave cuts at the same Fn (5b monohull Fn=0.785 Y/L=0.81)

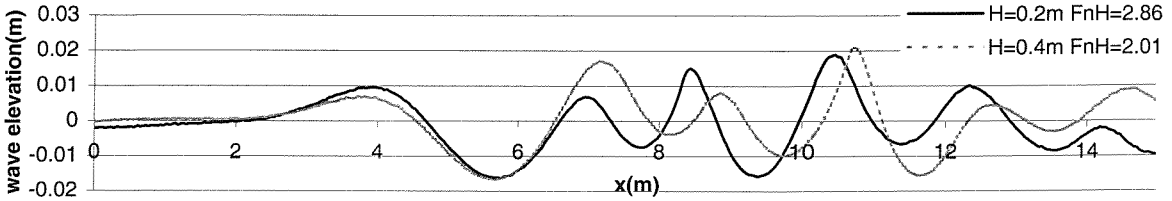

Fig.3.61 Comparison of wave cuts at the same Fn (5b catamaran S/L=0.2 Fn=1.0 Y/L=0.55)

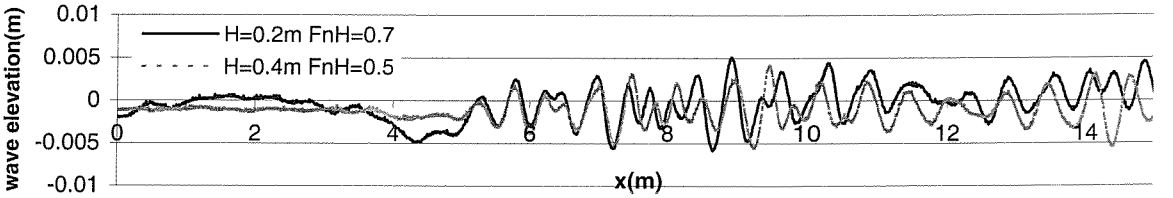

Fig.3.62 Comparison of wave cuts at the same Fn (5b catamaran S/L=0.4 Fn=0.25 Y/L=0.68)

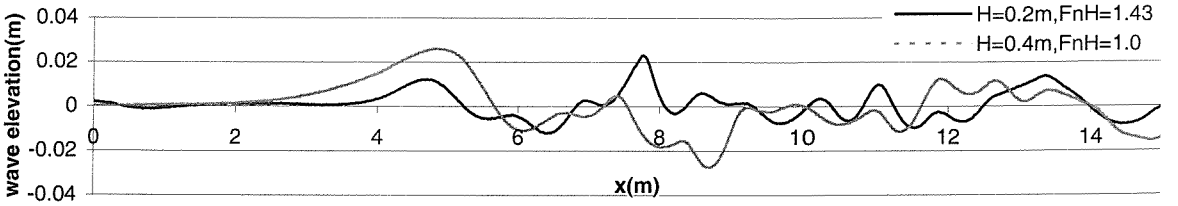

Fig.3.63 Comparison of wave cuts at the same Fn (5b catamaran S/L=0.4 Fn=0.505 Y/L=0.55)

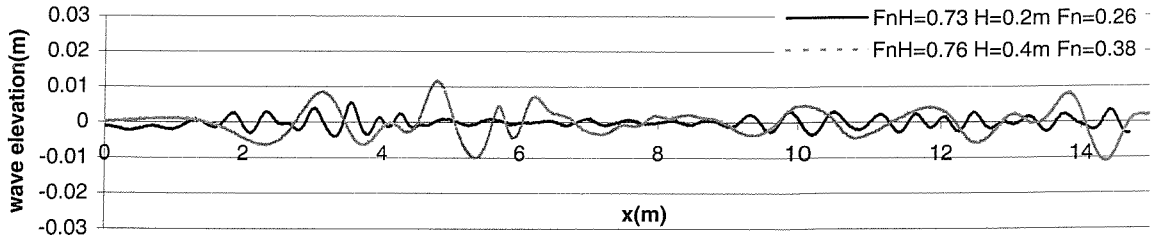

Fig.3.64 Comparison of wave cuts at the same Fn_H (5b monohull Y/L=0.55)

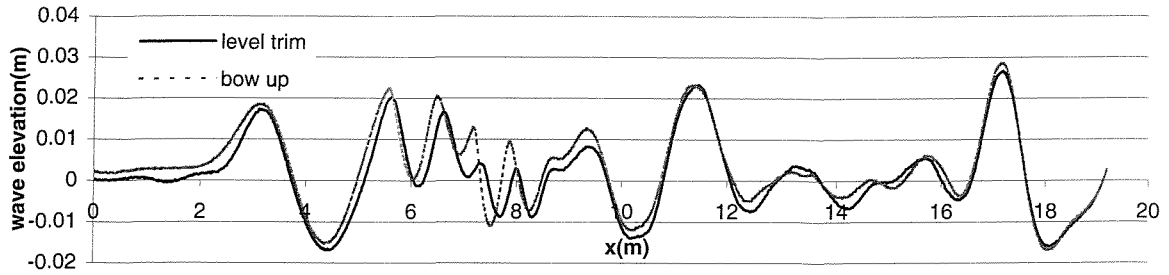

Fig.3.65a Comparison of wave cuts: 5b catamaran S/L=0.2 Fn=0.5 Fn_H=1.43 H=0.2m Y/L=0.55

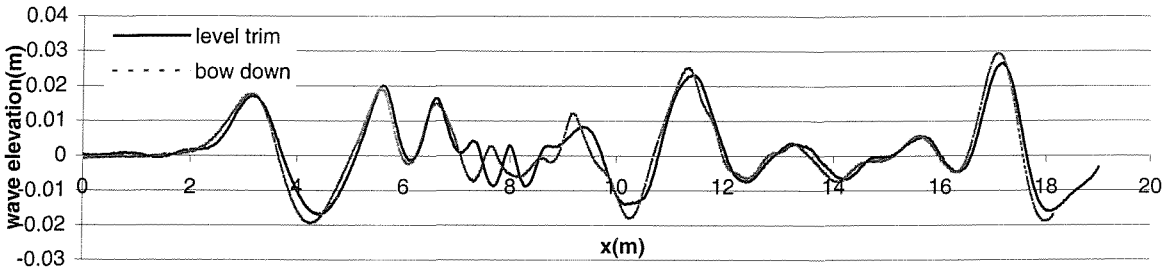

Fig.3.65b Comparison of wave cuts: 5b catamaran S/L=0.2 Fn=0.5 Fn_H=1.43 H=0.2m Y/L=0.55

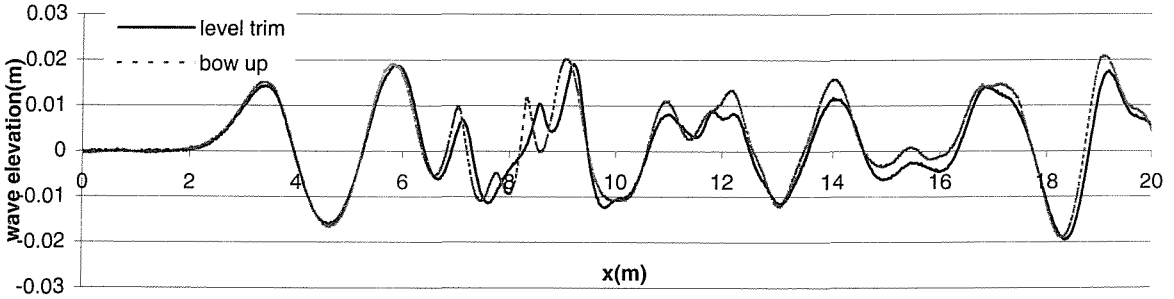

Fig.3.66a Comparison of wave cuts: 5s catamaran S/L=0.2 Fn=0.5 Fn_H=1.43 H=0.2m Y/L=0.68

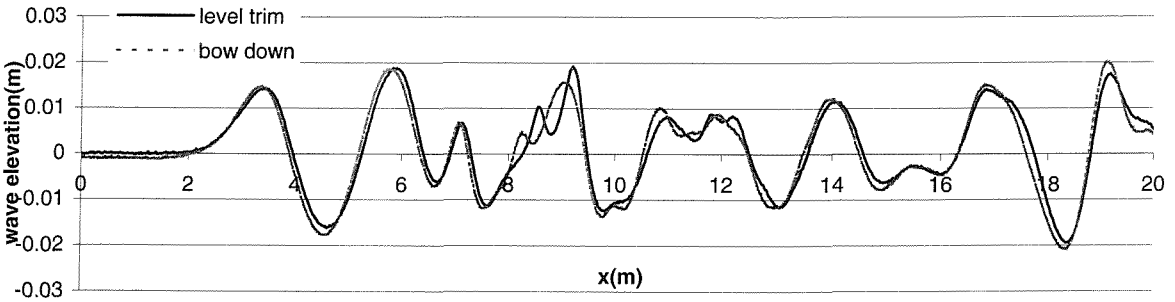

Fig.3.66b Comparison of wave cuts: 5s catamaran S/L=0.2 Fn=0.5 Fn_H=1.43 H=0.2m Y/L=0.68

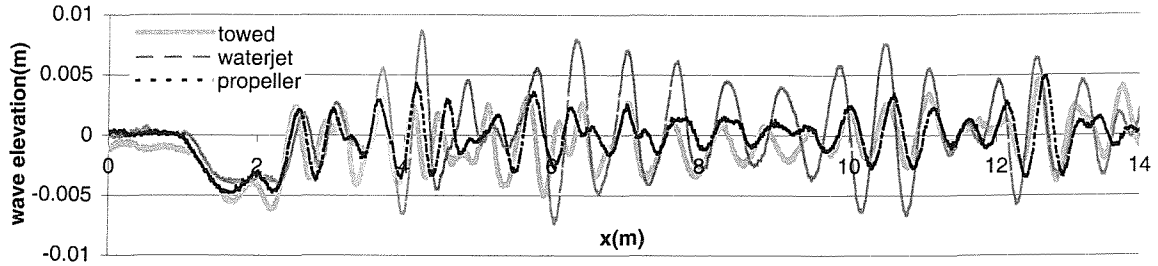

Fig.3.67 Comparison of wave cuts: 5s S/L=0.4 Fn=0.25 Fn_H=0.71 H=0.2m Y/L=0.55

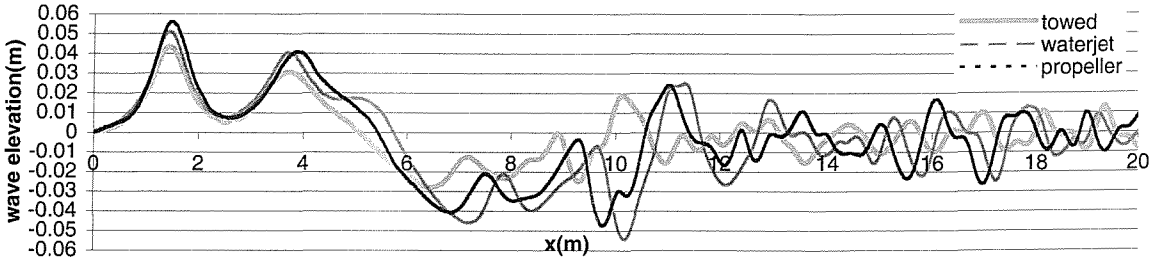

Fig.3.68 Comparison of wave cuts: 5s S/L=0.4 Fn=0.35 Fn_H=1.0 H=0.2m Y/L=0.81

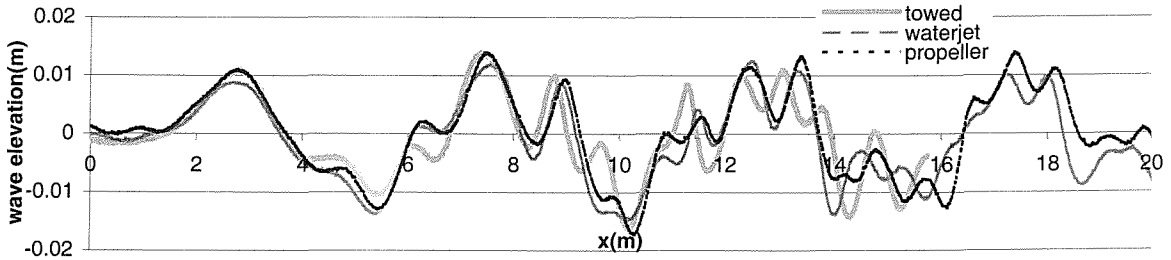

Fig.3.69 Comparison of wave cuts: 5s S/L=0.4 Fn=0.505 Fn_H=1.43 H=0.2m Y/L=1.05

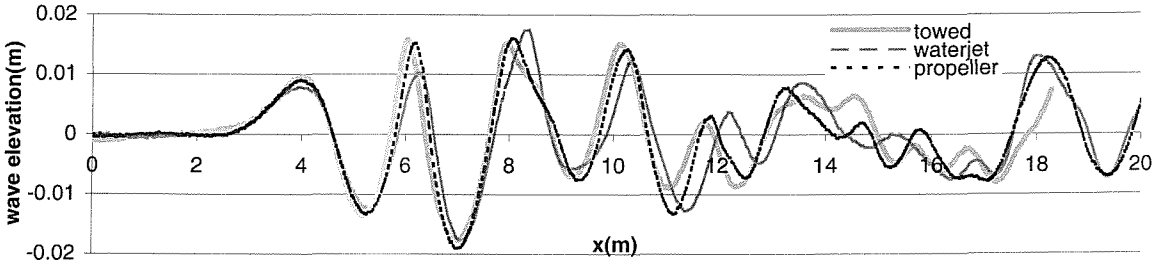

Fig.3.70 Comparison of wave cuts: 5s S/L=0.4 Fn=0.785 Fn_H=2.21 H=0.2m Y/L=0.55

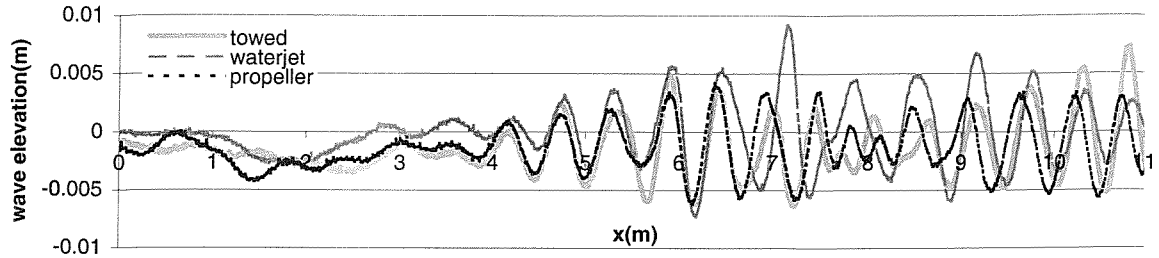

Fig.3.71 Comparison of wave cuts: 5s S/L=0.2 Fn=0.25 Fn_H=0.71 H=0.2m Y/L=0.93

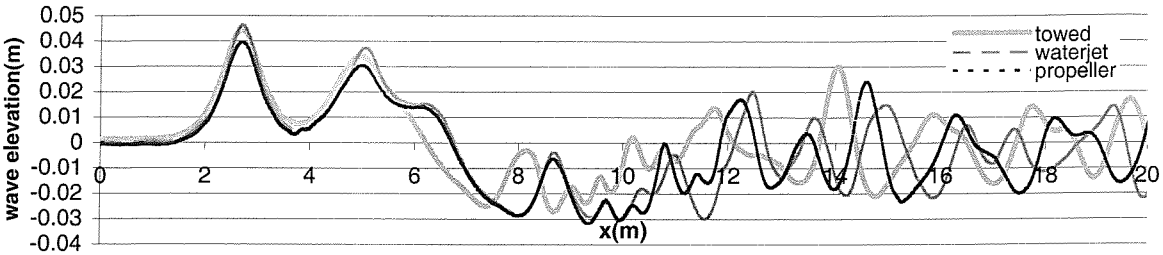

Fig.3.72 Comparison of wave cuts: 5s S/L=0.2 Fn=0.35 Fn_H=1.0 H=0.2m Y/L=0.55

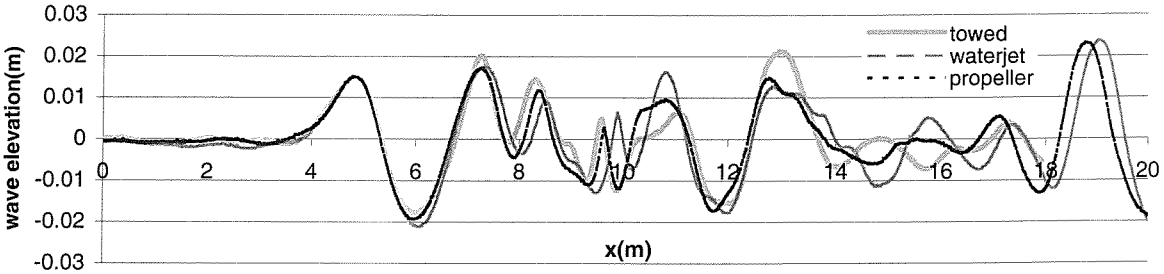

Fig.3.73 Comparison of wave cuts: 5s S/L=0.2 Fn=0.505 Fn_H=1.43 H=0.2m Y/L=0.55

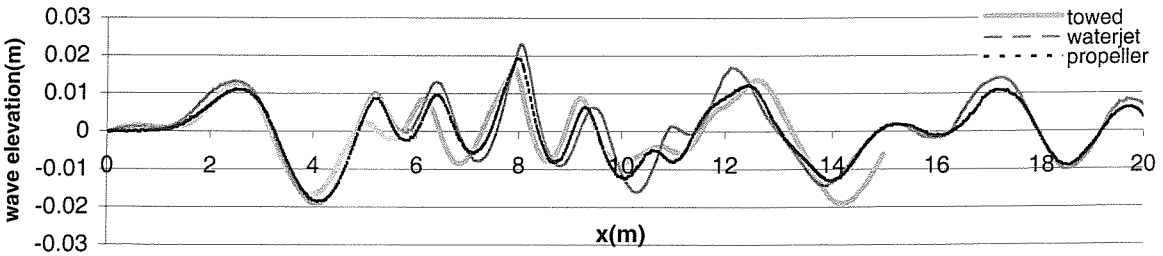

Fig.3.74 Comparison of wave cuts: 5s S/L=0.2 Fn=0.785 Fn_H=2.21 H=0.2m Y/L=0.55

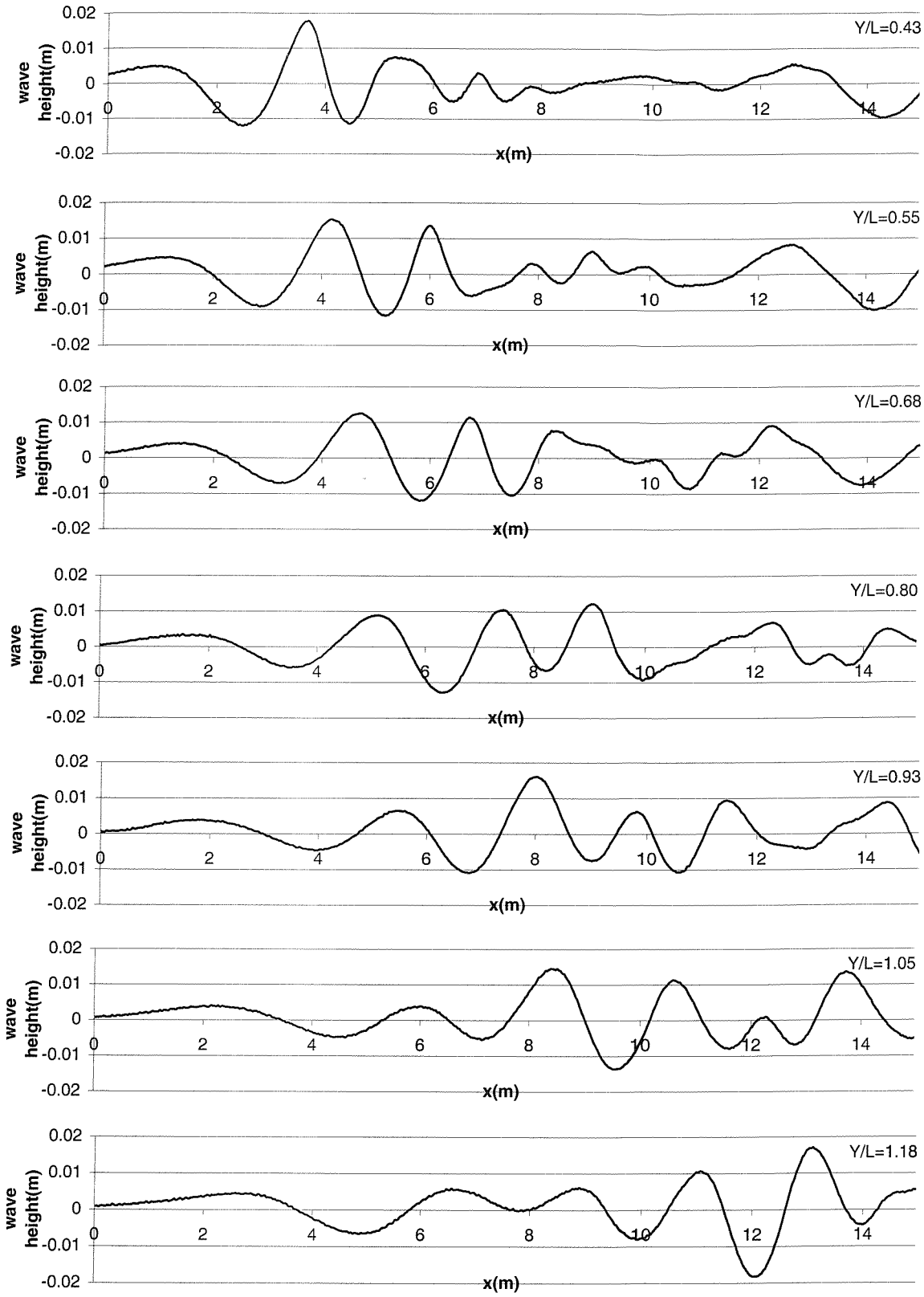

Fig.3.75 Measured wave cuts at varlous transverse positions: 5b monohull Fn=0.785 Fn_H=1.57

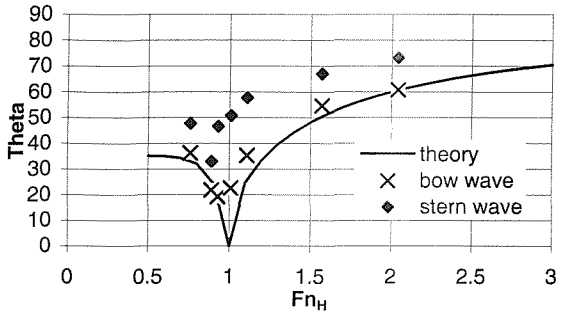

Fig.3.76 Measured wave angle: 5b monohull H=0.4m

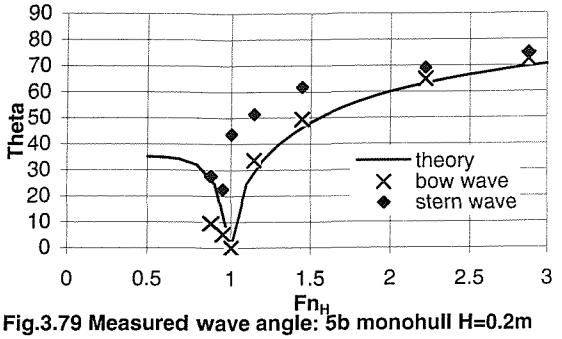

Fig.3.79 Measured wave angle: 5b monohull H=0.2m

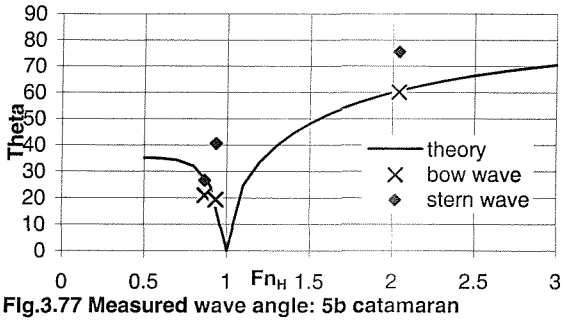

Fig.3.77 Measured wave angle: 5b catamaran S/L=0.2 H=0.4m

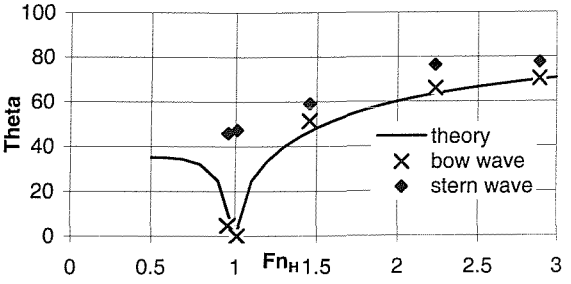

Fig.3.80 Measured wave angle: 5b catamaran S/L=0.2 H=0.2m

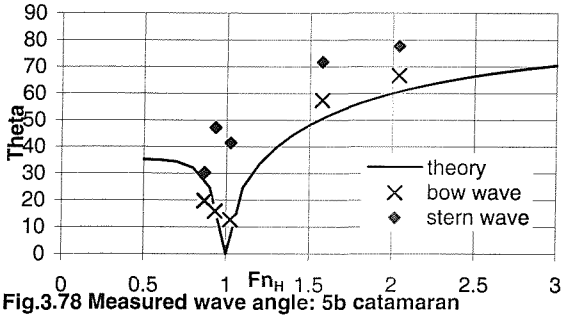

Fig.3.78 Measured wave angle: 5b catamaran S/L=0.4 H=0.4m

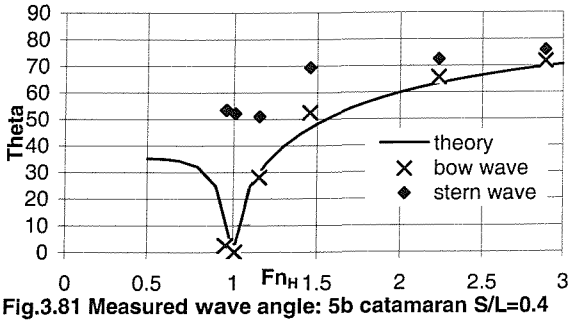

Fig.3.81 Measured wave angle: 5b catamaran S/L=0.4 H=0.2m

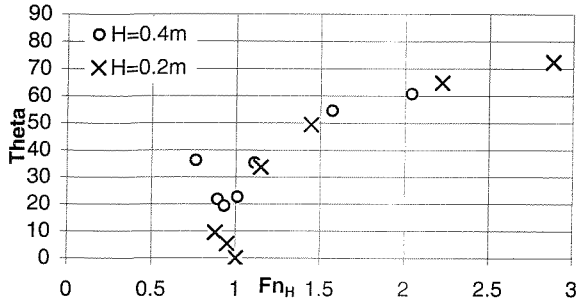

Fig.3.82 Measured bow wave angle: 5b monohull

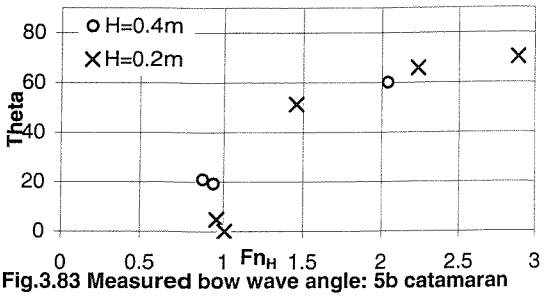

Fig.3.83 Measured bow wave angle: 5b catamaran S/L=0.2

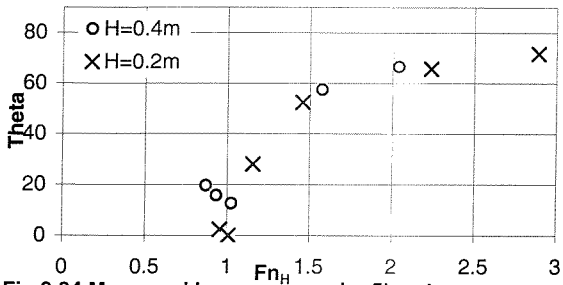

Fig.3.84 Measured bow wave angle: 5b catamaran S/L=0.4

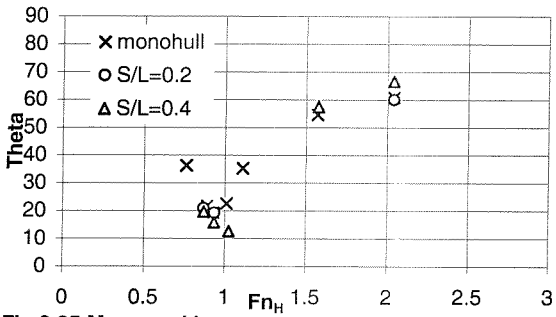

Fig.3.85 Measured bow wave angle: 5b H=0.4m

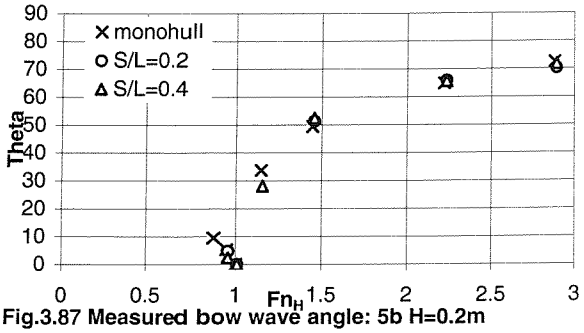

Fig.3.87 Measured bow wave angle: 5b H=0.2m

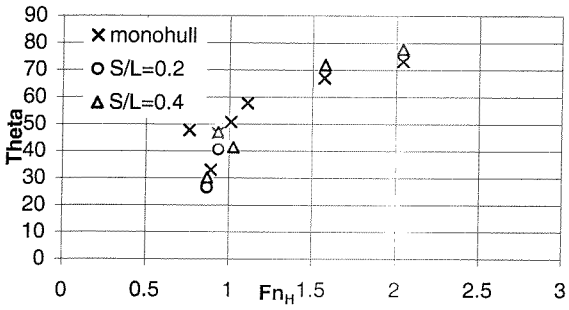

Fig.3.86 Measured stern wave angle: 5b H=0.4m

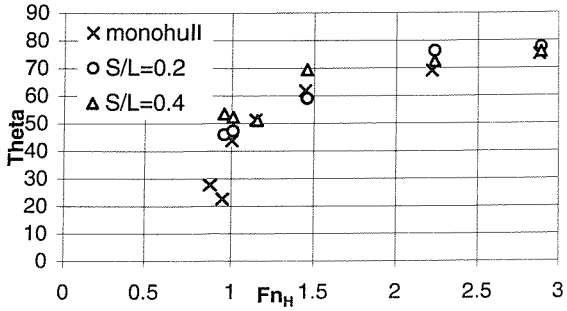

Fig.3.88 Measured stern wave angle: 5b H=0.2m

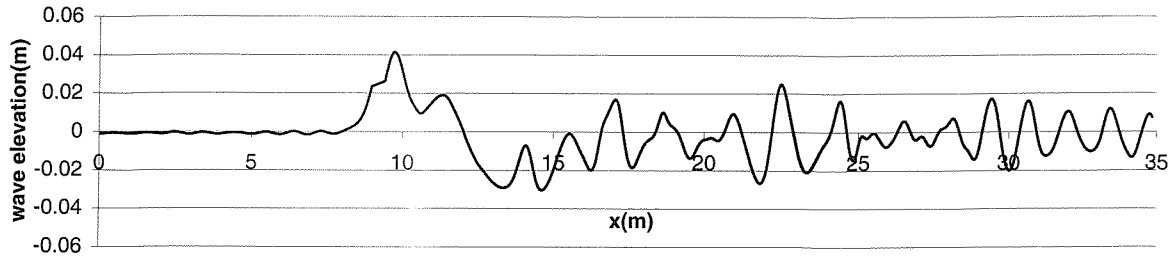

Fig.3.89a Solitons: 5s catamaran S/L=0.2 waterjets, H=0.2m Fn=0.36 Fn_H=1.01 Y/L=0.89 [Front probe]

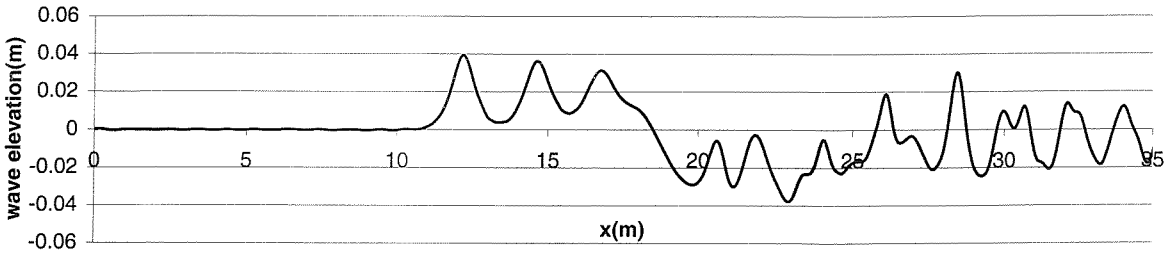

Fig.3.89b Solitons: 5s catamaran S/L=0.2 waterjets, H=0.2m Fn=0.36 Fn_H=1.01 Y/L=0.89 [Back probe]

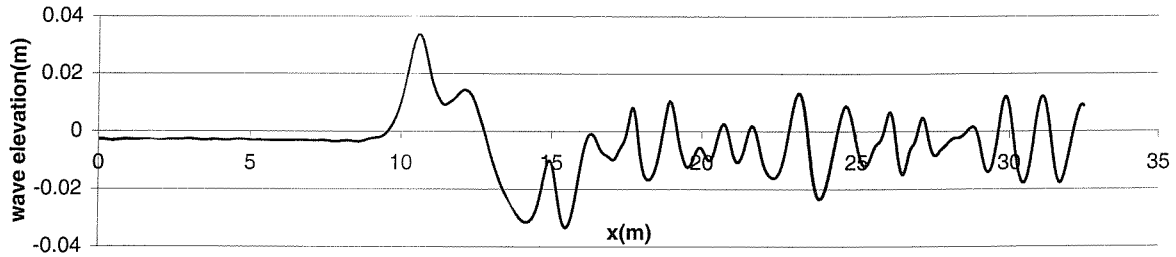

Fig.3.90a Solitons: 5s catamaran S/L=0.2 propellers, H=0.2m Fn=0.36 Fn_H=1.01 Y/L=0.89 [Front probe]

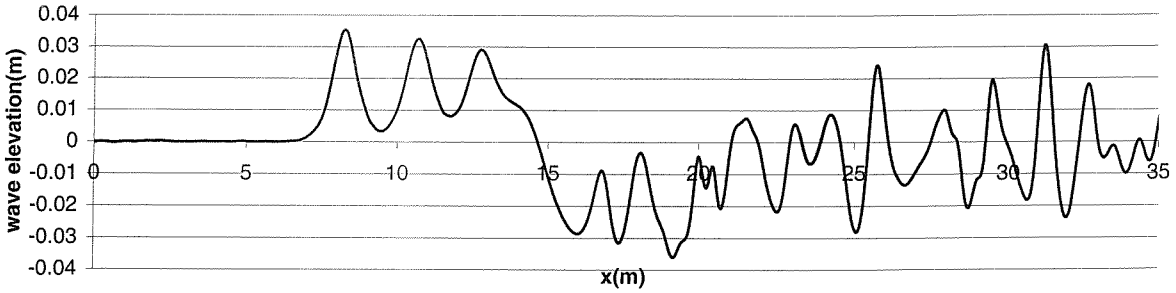

Fig.3.90b Solitons: 5s catamaran S/L=0.2 propellers, H=0.2m Fn=0.36 Fn_H=1.01 Y/L=0.89 [Back probe]

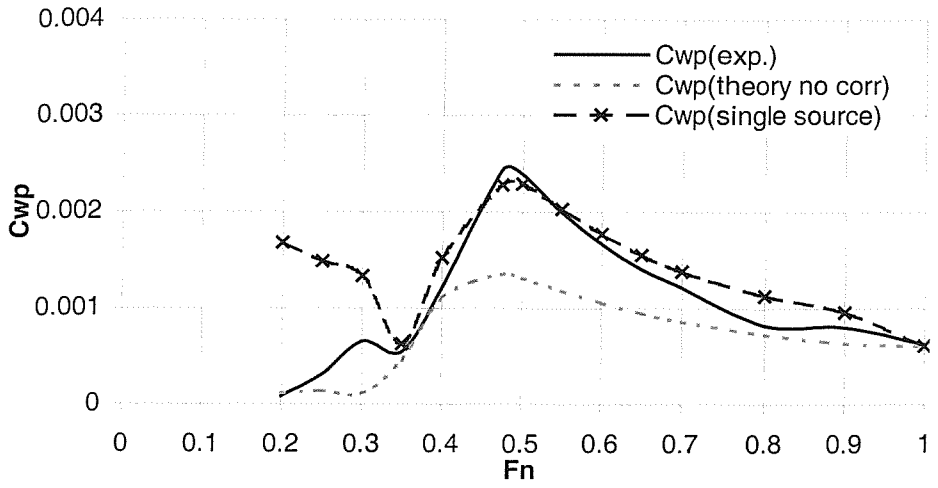

Fig.4.1 Comparison of wave pattern resistance coefficients of 5b catamaran (S/L=0.4)

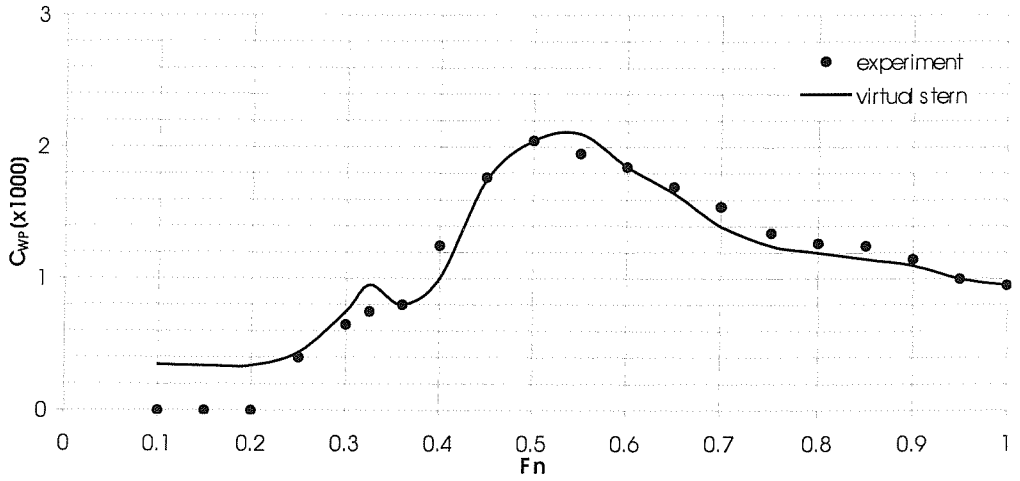

Fig.4.2 Comparison of wave pattern resistance coefficients of 5c monohull

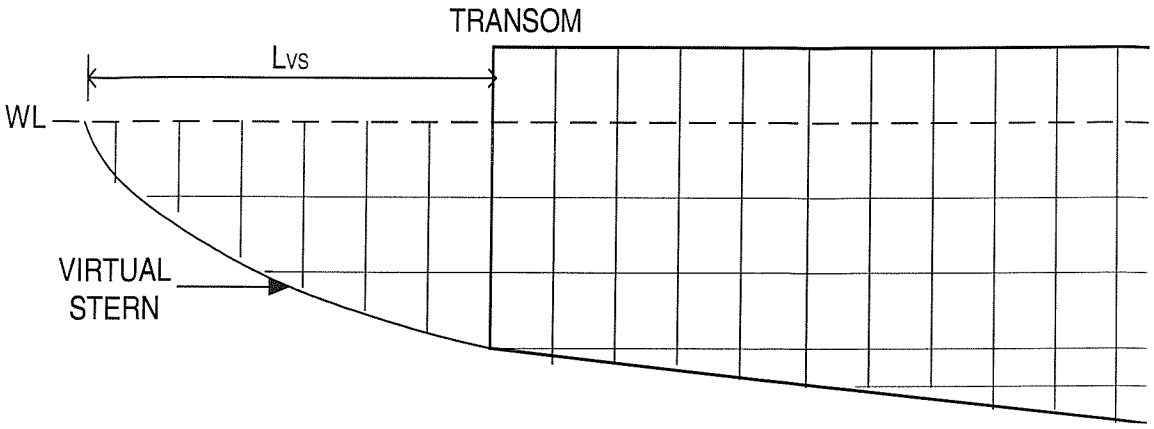

Fig.4.3 Virtual Stern

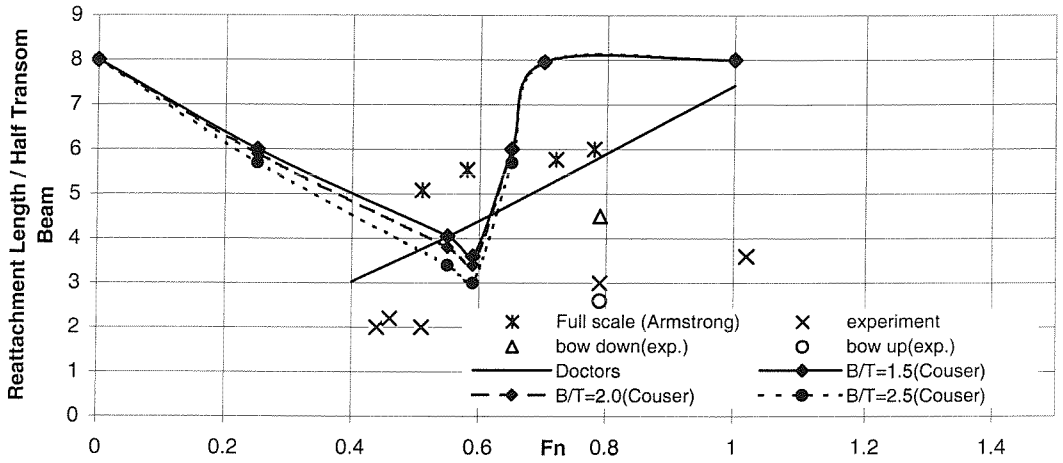

Fig.4.4 Re-attachment length with Fn

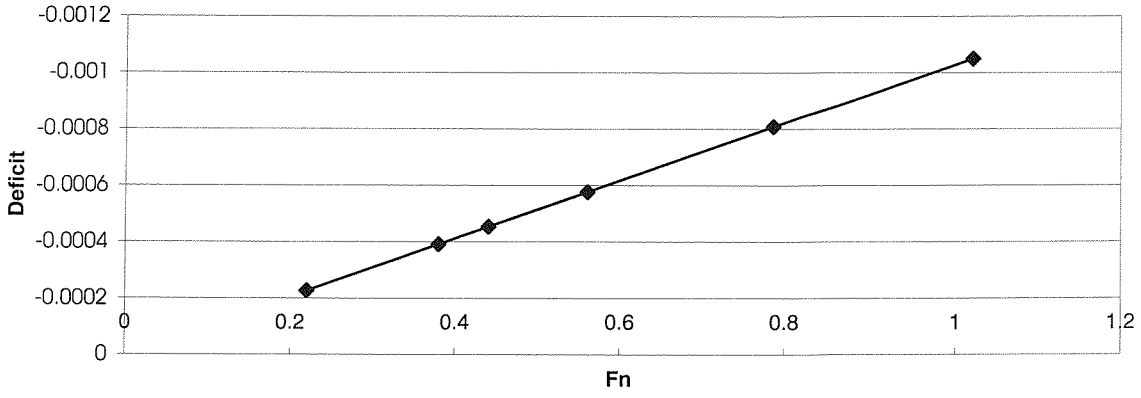

Fig.4.5 Deficit required to balance net source strength of zero: 5b monohull

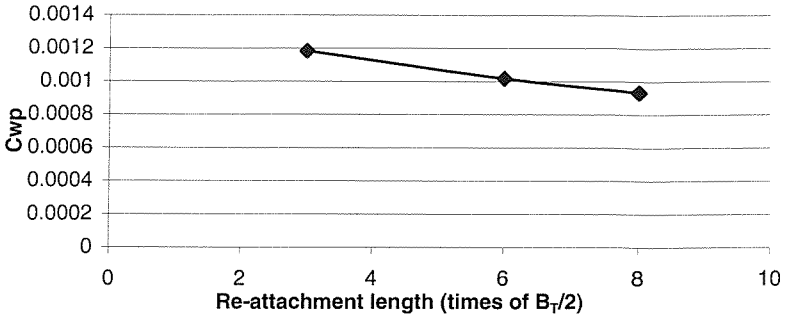

Fig.4.6: The effect of re-attachment length on C_{WP}: 5b monohull Fn=0.785

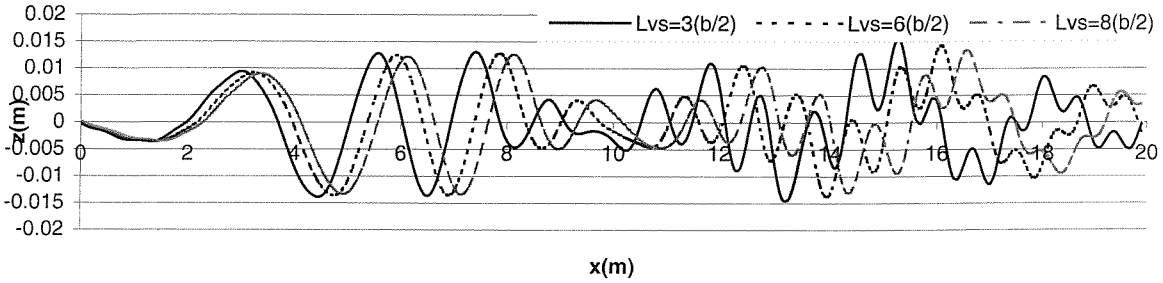

Fig.4.7 Theoretical wave cut using virtual stern with three different re-attachment length model 5b monohull, Fn = 0.785, water depth = 0.4 m Y/L=0.55

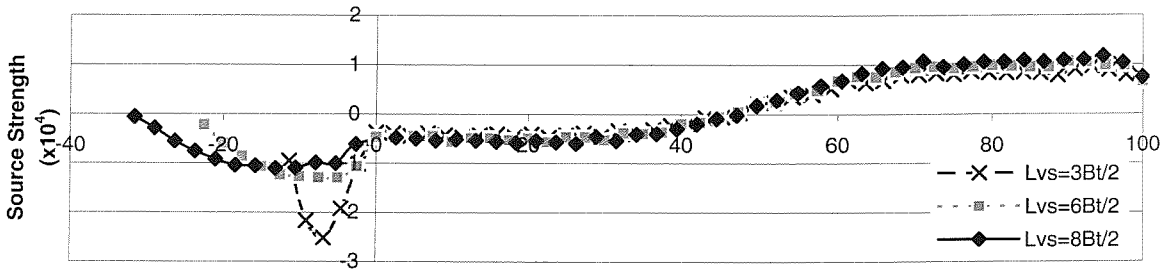

Fig.4.8a Longitudinal plot of source strength along the hull and virtual stern

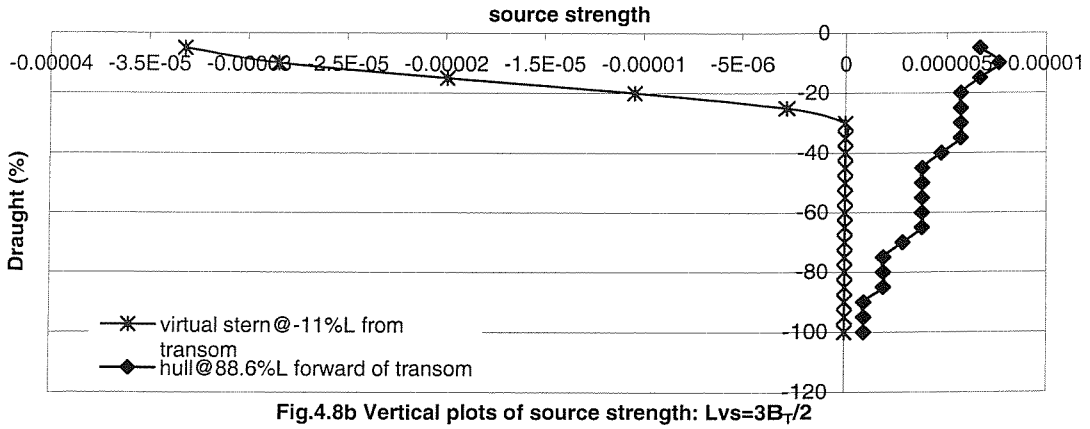

Fig.4.8b Vertical plots of source strength: Lvs=3B_T/2

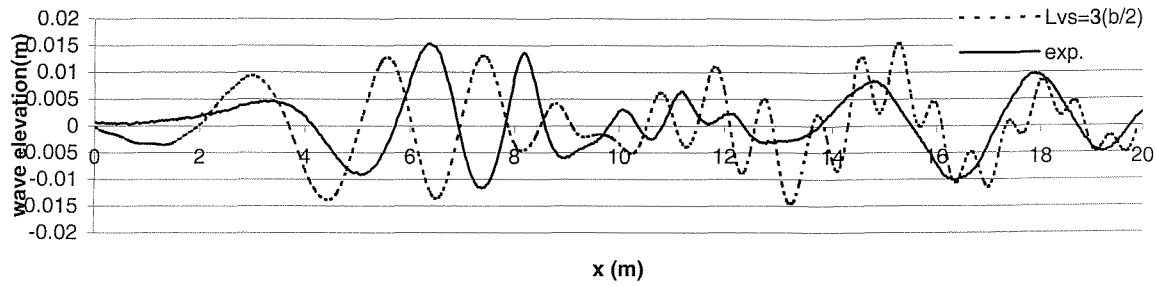

Fig.4.9a Comparison between theory with virtual stern (Lvs = 3(b/2) and experiment: model 5b monohull, Fn=0.785, water depth=0.4 m Y/L=0.55

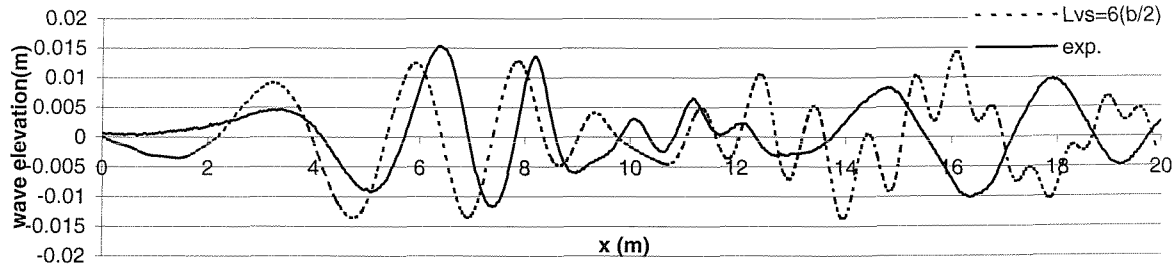

Fig.4.9b Comparison between theory with virtual stern (Lvs = 6(b/2) and experiment: model 5b monohull, Fn=0.785, water depth=0.4 m Y/L=0.55

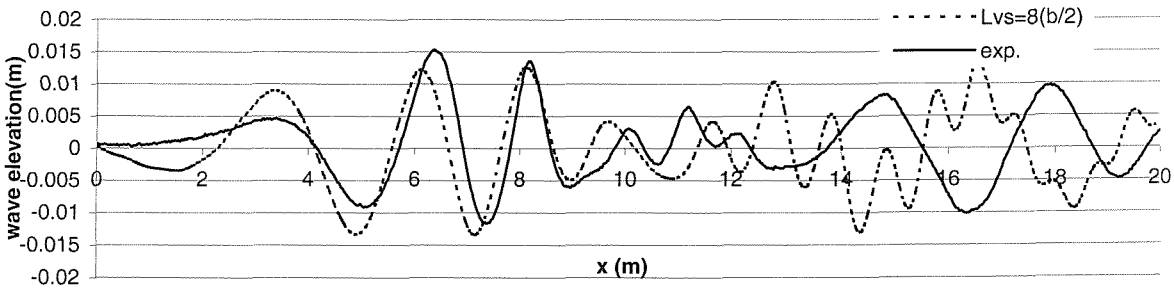

Fig.4.9c Comparison between theory with virtual stern (Lvs = 8(b/2) and experiment: model 5b monohull, Fn=0.785, water depth=0.4 m Y/L=0.55

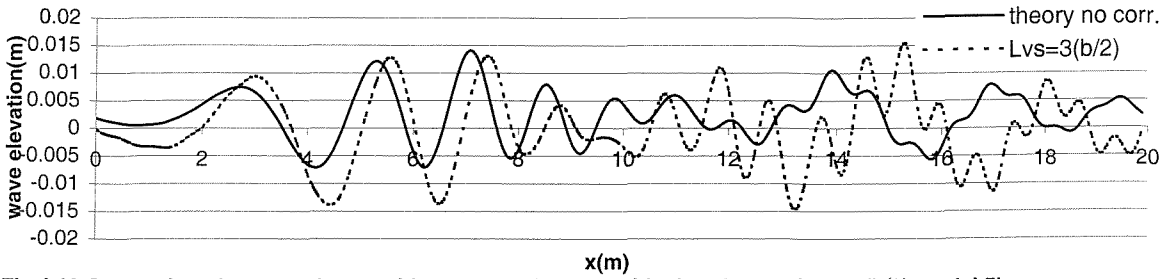

Fig.4.10 Comparison between theory with no correction and with virtual stern (Lvs=3(b/2) model 5b monohull, Fn=0.785, water depth=0.4 m Y/L=0.55

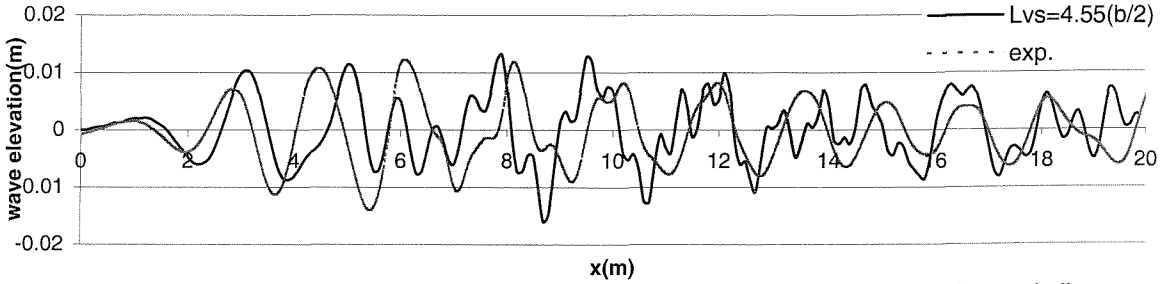

Fig.4.11 Comparison between experiment and theory with virtual stern (Lvs=4.55(b/2) model 5b monohull, Fn=0.44, water depth=1.85 m

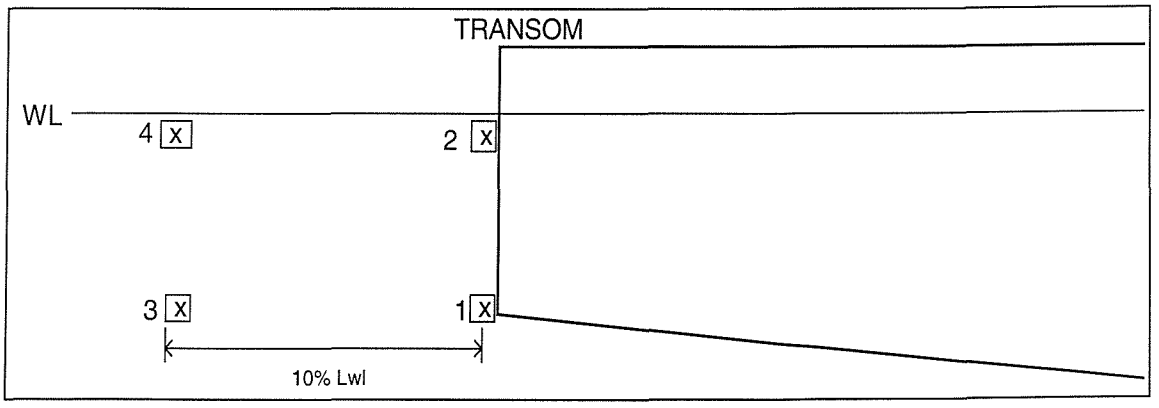

Fig.4.12 Single Source Correction at 4 different positions

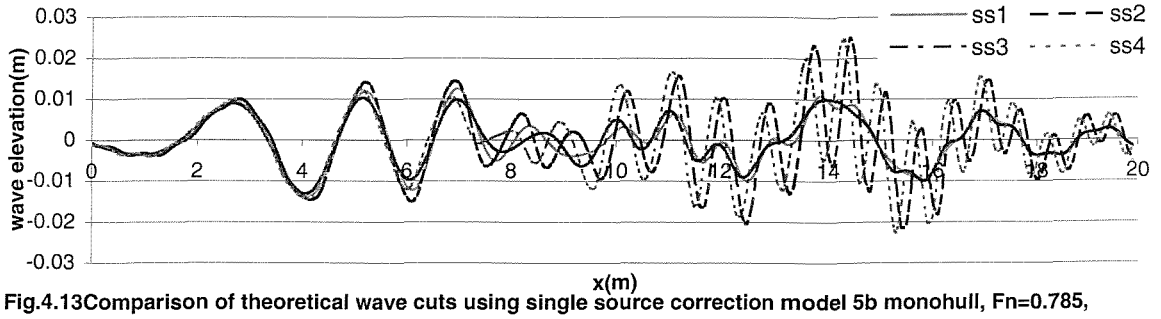

Fig.4.13Comparison of theoretical wave cuts using single source correction model 5b monohull, Fn=0.785, water depth=0.4 m Y/L=0.55

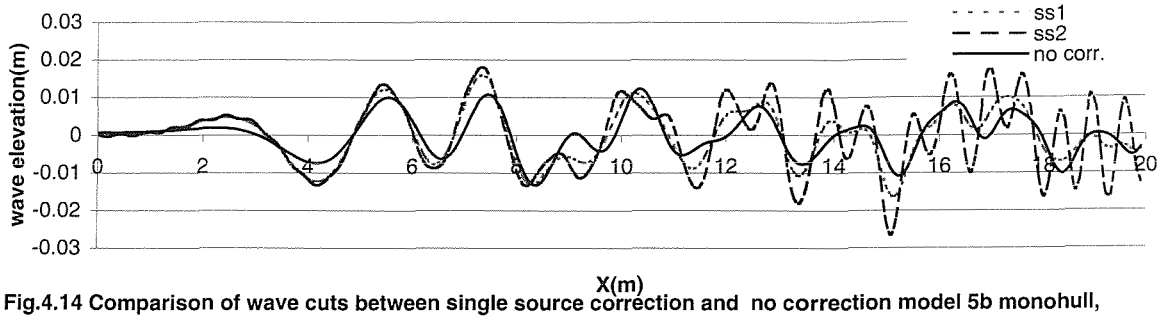

Fig.4.14 Comparison of wave cuts between single source correction and no correction model 5b monohull, Fn=0.714, water depth=1.85 m Y/L=0.77

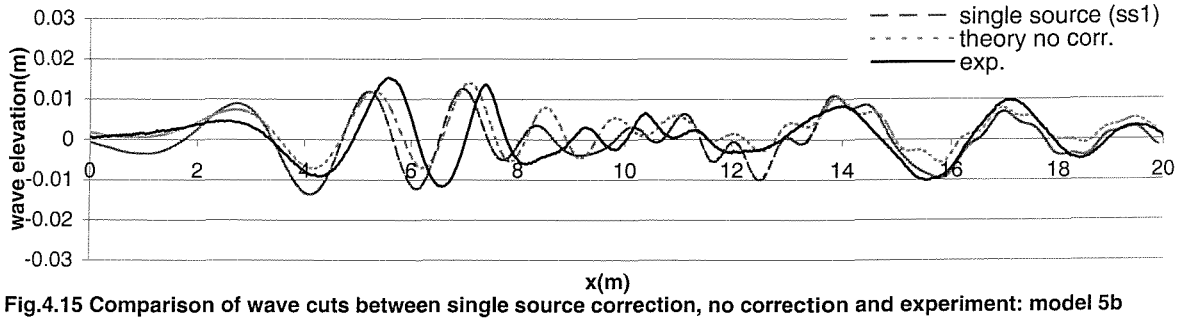

Fig.4.15 Comparison of wave cuts between single source correction, no correction and experiment: model 5b monohull, Fn=0.785, water depth=0.4 m Y/L=0.55

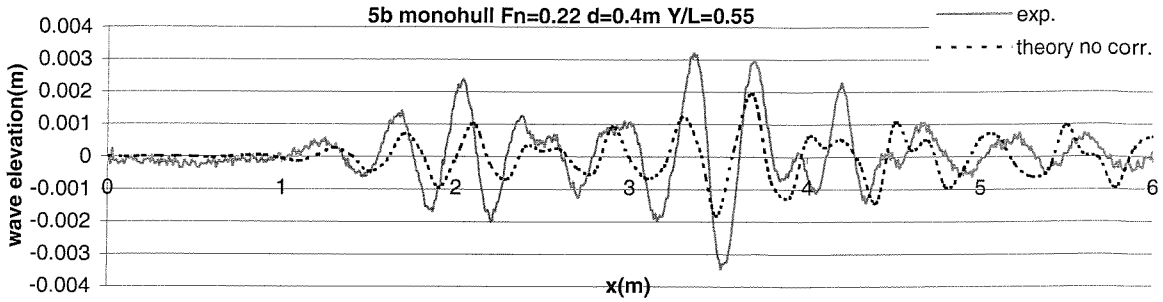

(a)

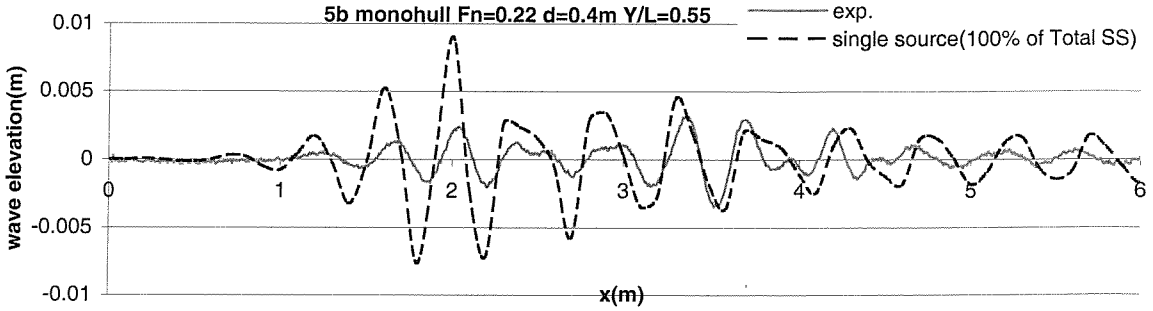

(b)

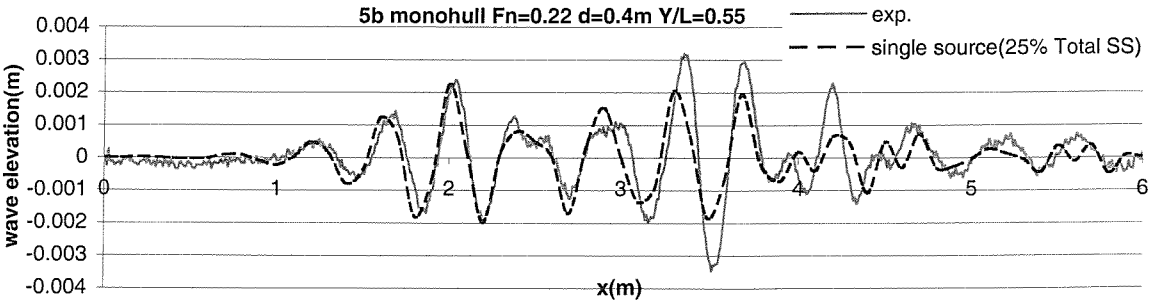

(c)

Fig.4.16 Comparison of wave cuts at low speed: 5b monohull Fn=0.22 H=0.4m Y/L=0.55

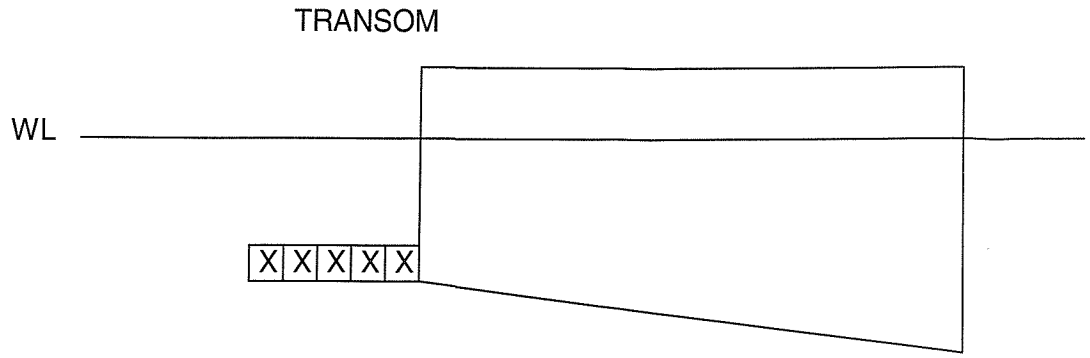

Fig.4.17 Diagram showing a single trailing line of sources

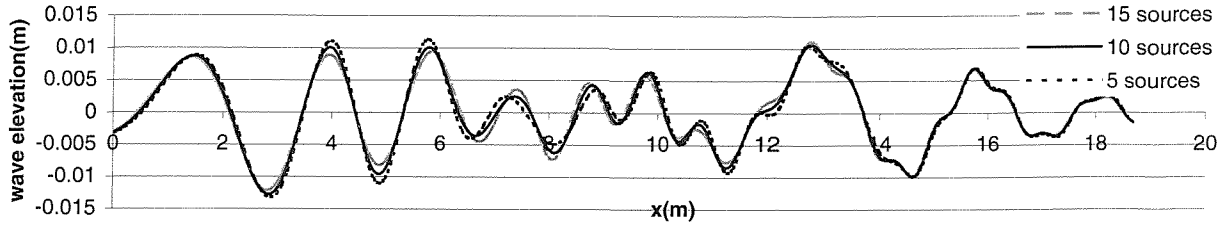

Fig.4.18a Theoretical wave profiles using a single trailing line of sources: 5b monohull Fn=0.785 H=0.4m Y/L=0.55

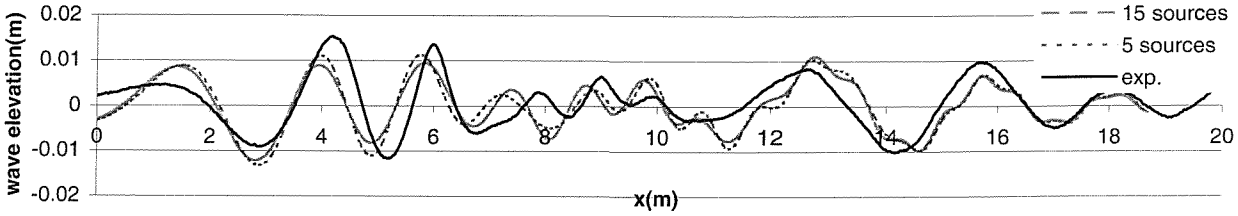

Fig.4.18b Comparison of experimental and theoretical wave profiles: 5b monohull Fn=0.785 H=0.4m Y/L=0.55

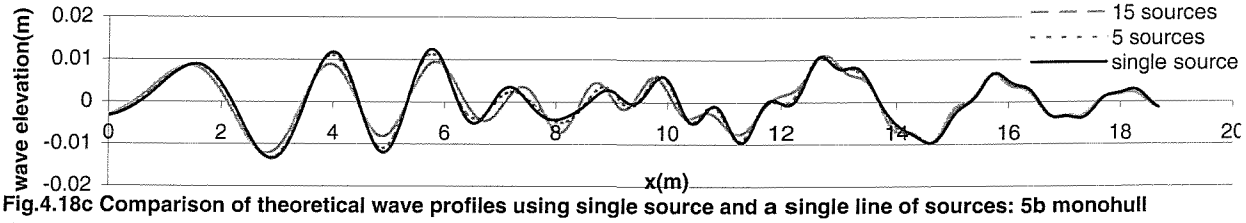

Fig.4.18c Comparison of theoretical wave profiles using single source and a single line of sources: 5b monohull Fn=0.785 H=0.4m Y/L=0.55

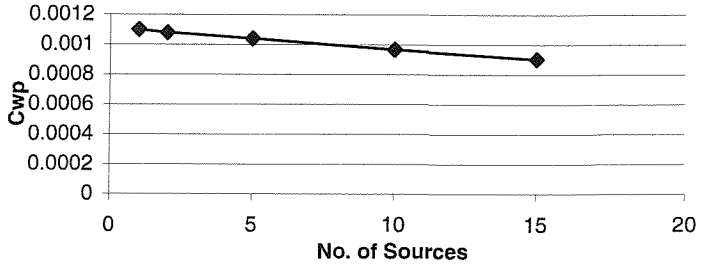

Fig.4.19 The effect of number of sources on C_{WP}: 5b monohull Fn=0.785 d=0.4m

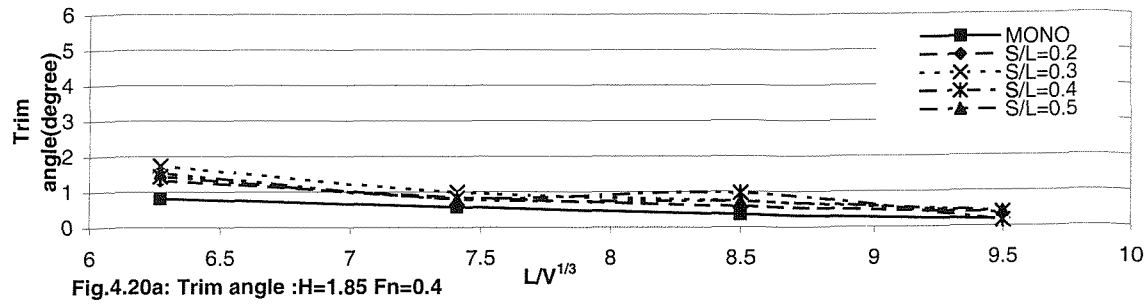

Fig.4.20a: Trim angle :H=1.85 Fn=0.4

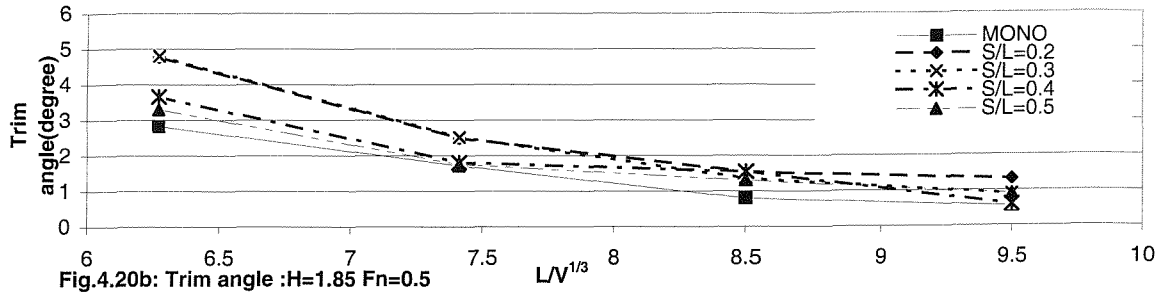

Fig.4.20b: Trim angle :H=1.85 Fn=0.5

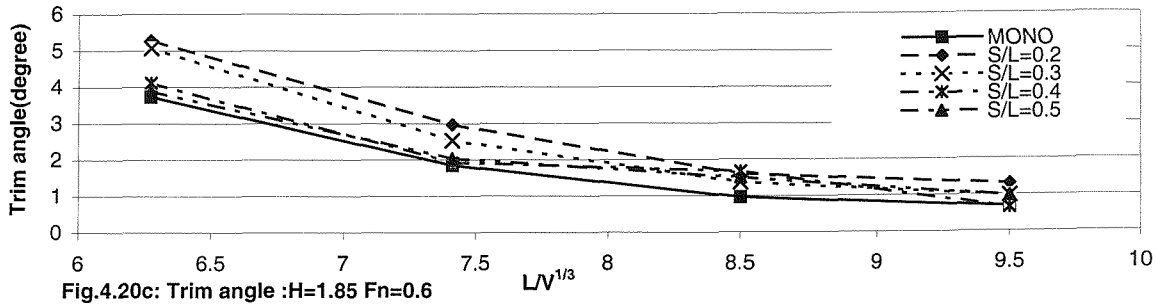

Fig.4.20c: Trim angle :H=1.85 Fn=0.6

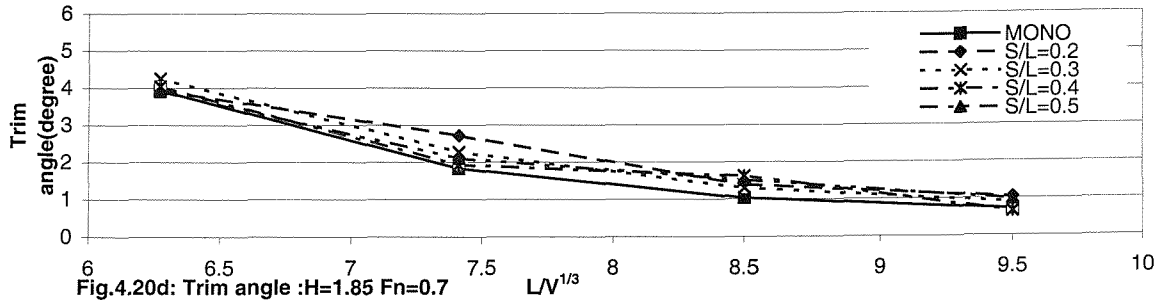

Fig.4.20d: Trim angle :H=1.85 Fn=0.7

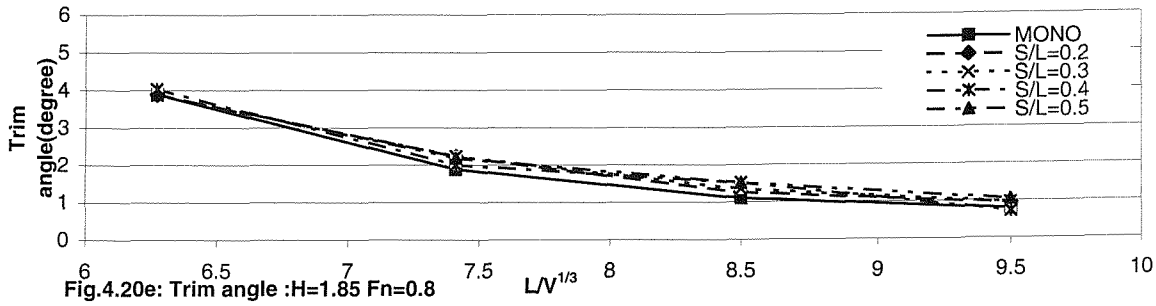

Fig.4.20e: Trim angle :H=1.85 Fn=0.8

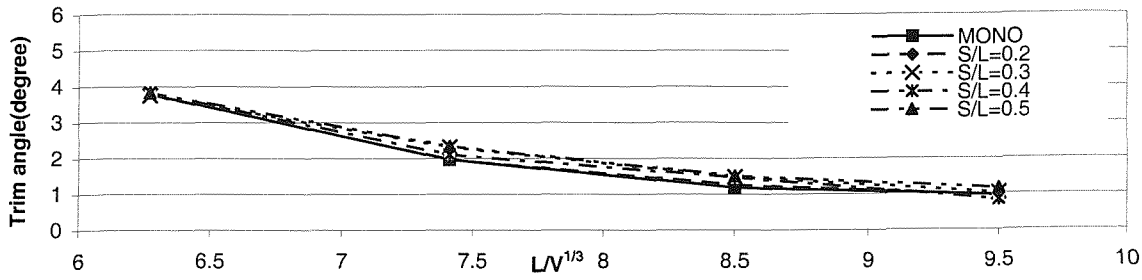

Fig.4.20f: Trim angle :H=1.85 Fn=0.9

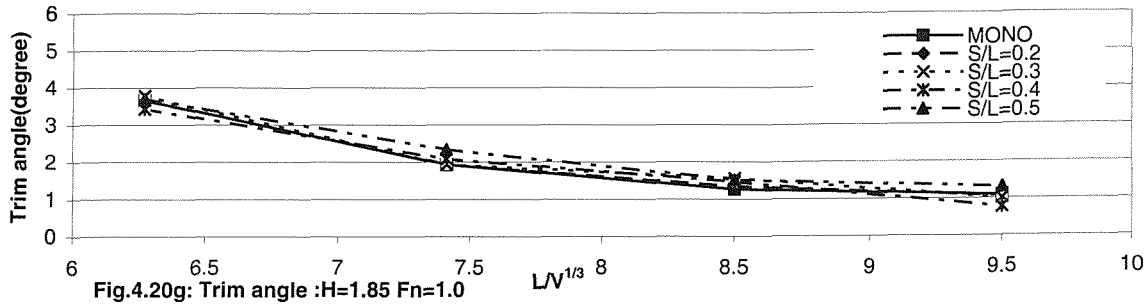

Fig.4.20g: Trim angle :H=1.85 Fn=1.0

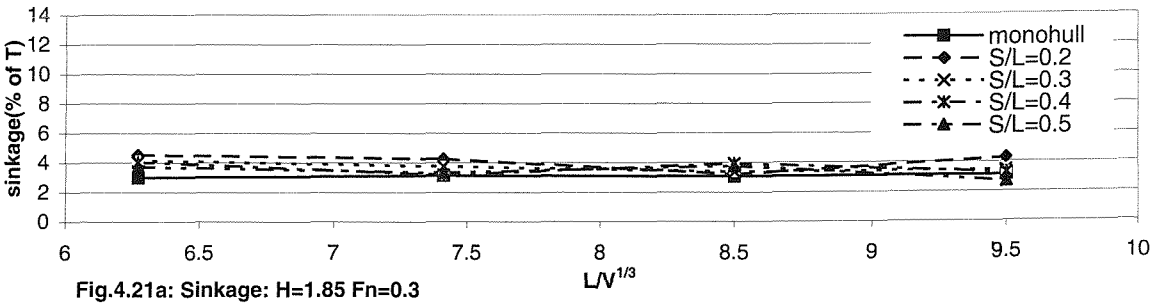

Fig.4.21a: Sinkage: H=1.85 Fn=0.3

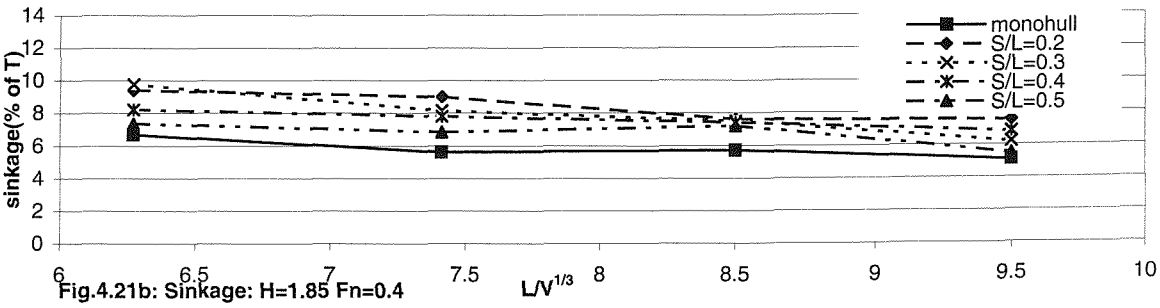

Fig.4.21b: Sinkage: H=1.85 Fn=0.4

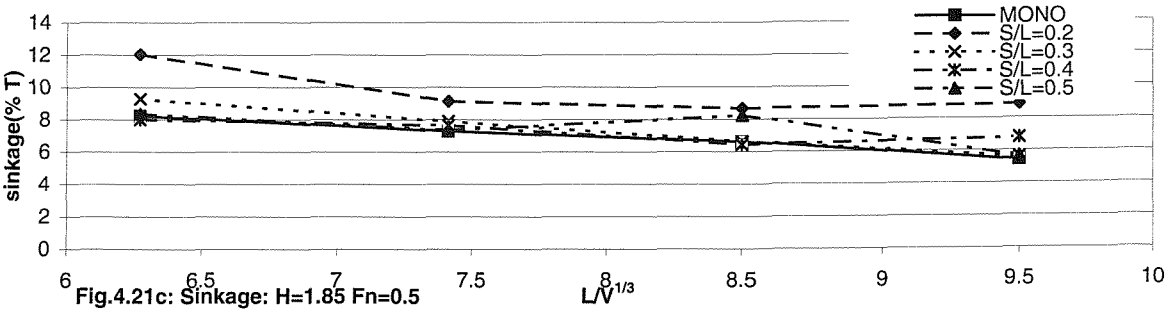

Fig.4.21c: Sinkage: H=1.85 Fn=0.5

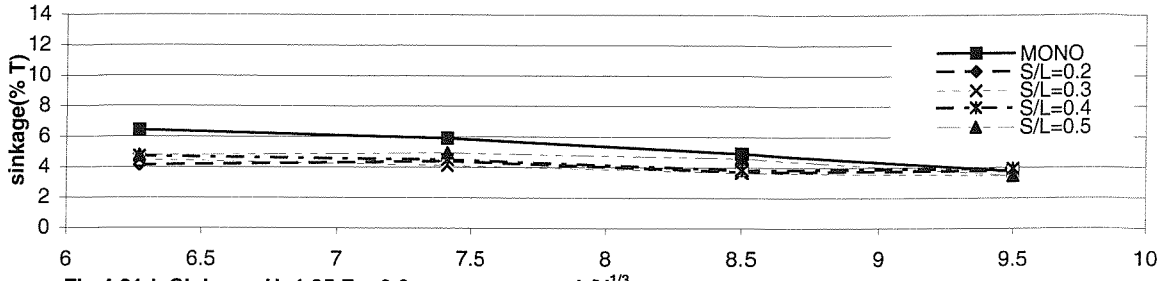

Fig.4.21d: Sinkage: H=1.85 Fn=0.6 $L/V^{1/3}$

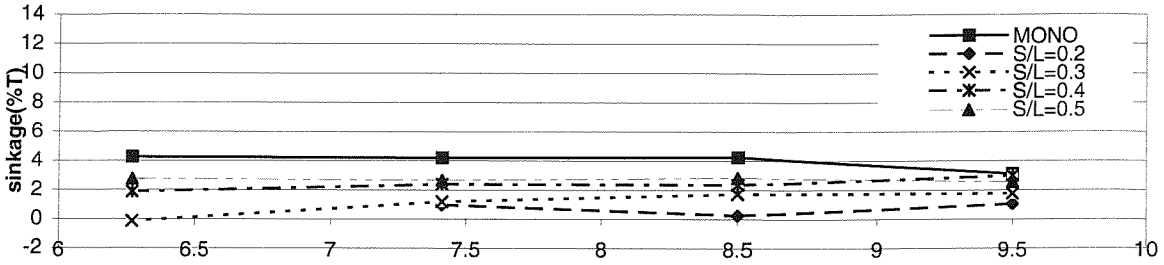

Fig.4.21e: Sinkage: H=1.85 Fn=0.7 $L/V^{1/3}$

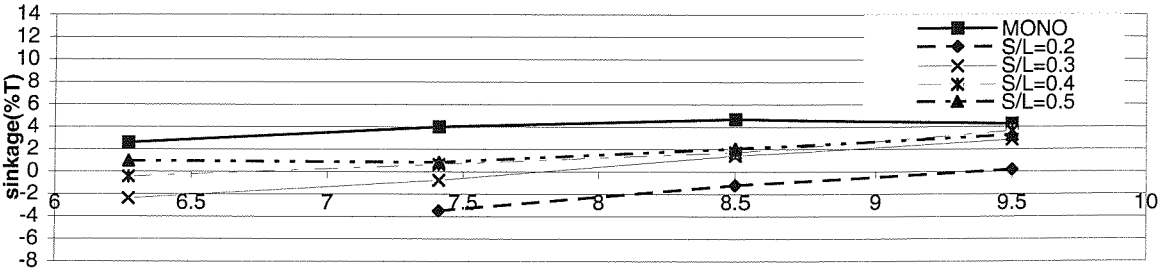

Fig.4.21f: Sinkage: H=1.85 Fn=0.8 $L/V^{1/3}$

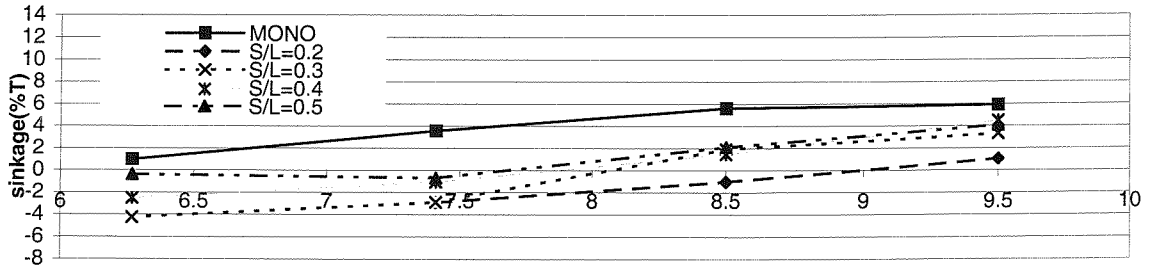

Fig.4.21g: Sinkage: H=1.85 Fn=0.9 $L/V^{1/3}$

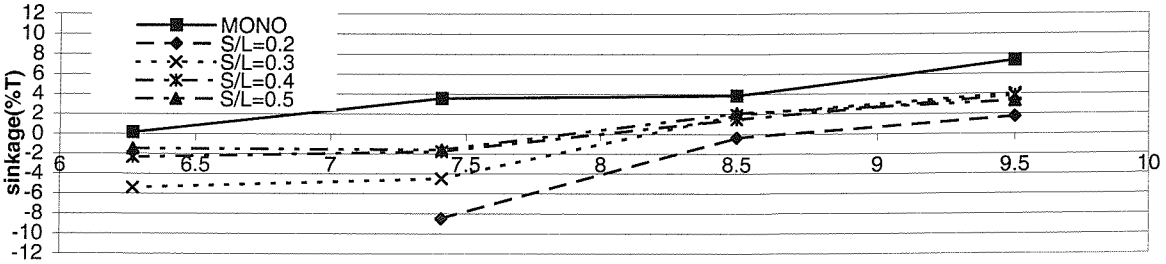

Fig.4.21h: Sinkage: H=1.85 Fn=1.0 $L/V^{1/3}$

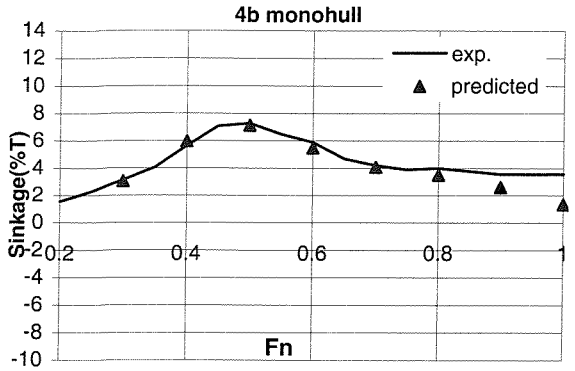

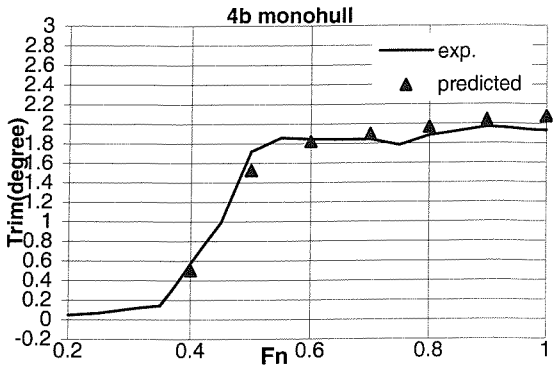

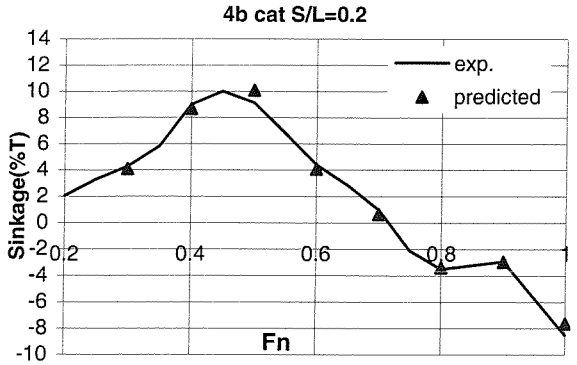

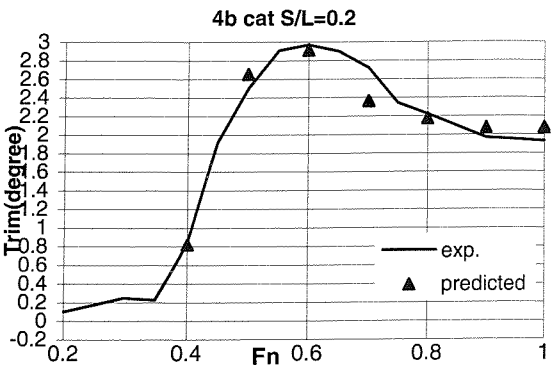

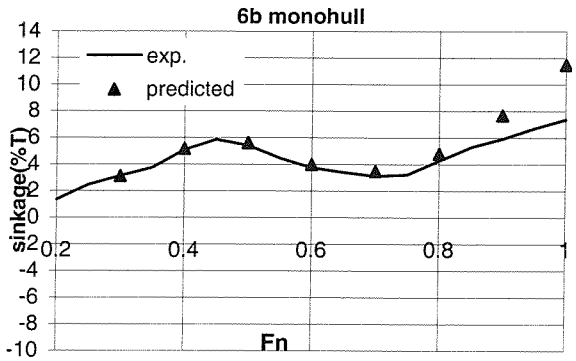

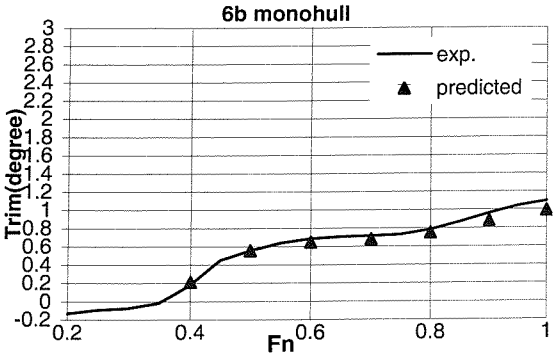

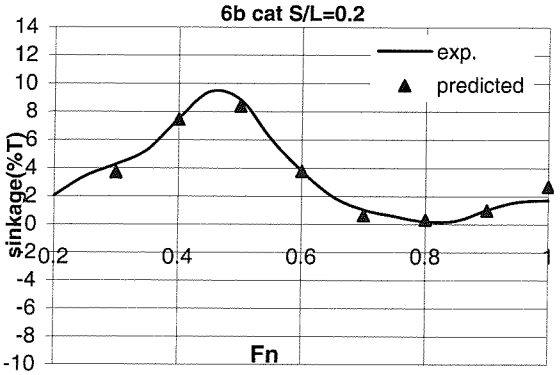

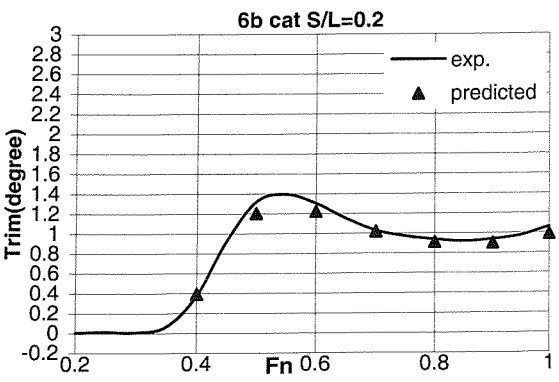

Fig.4.22 a **Dynamic Sinkage**

Fig.4.22 b **Dynamic Trim**

Fig.4.23 Outline of hybrid model

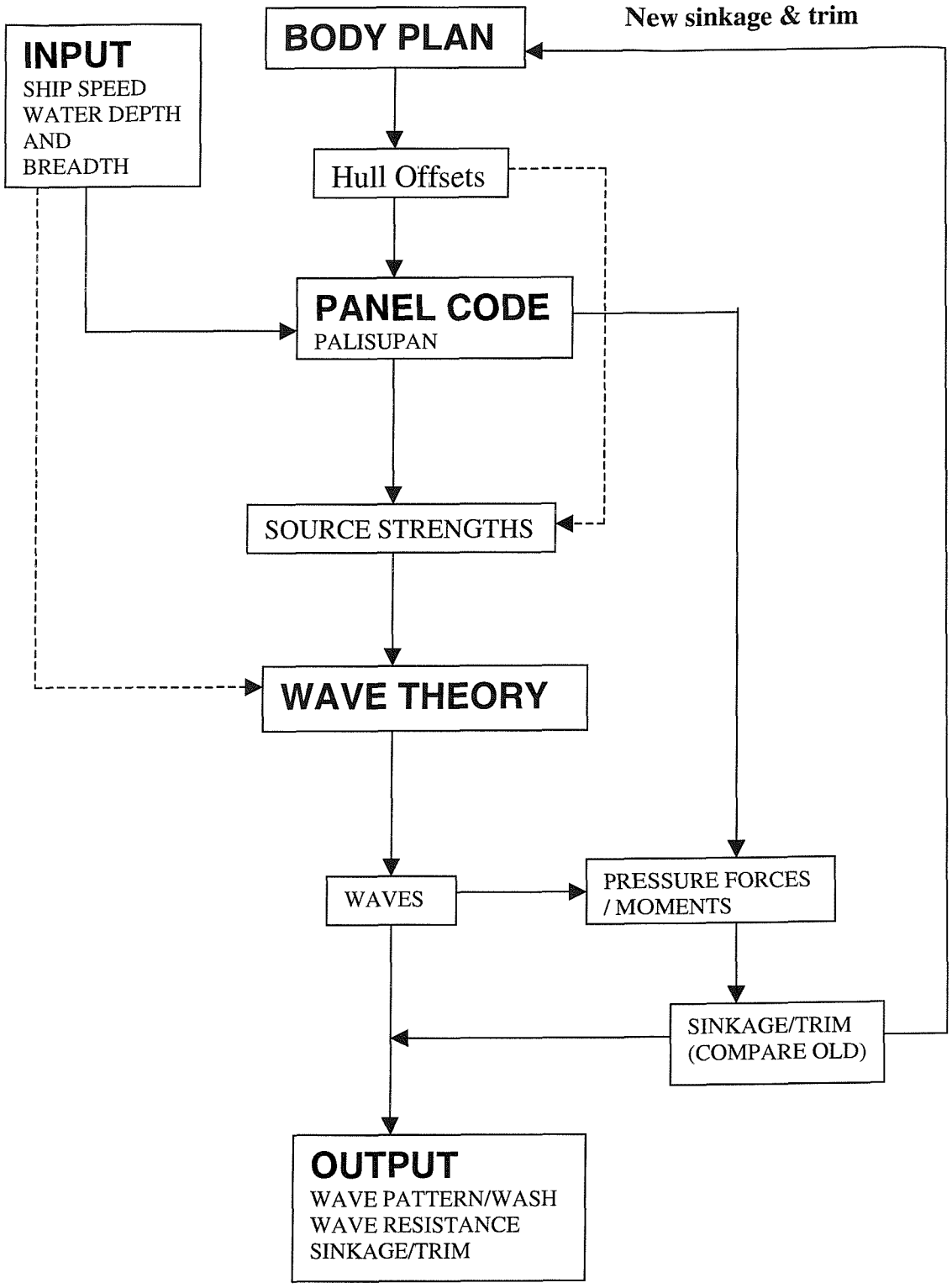

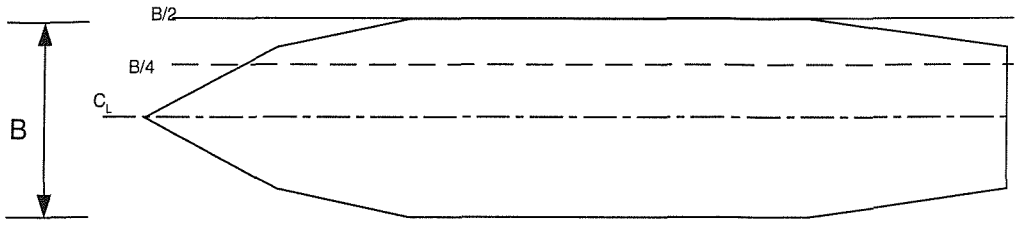

Fig.4.24 Diagram showing positions of longitudinal wave cuts

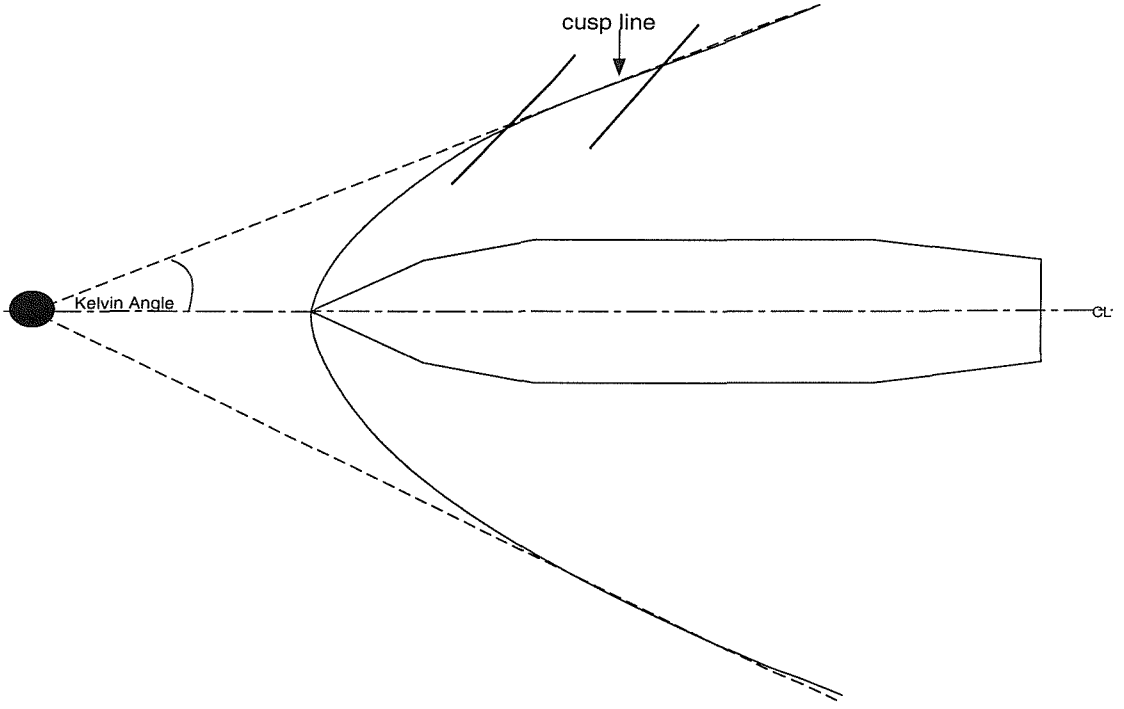

Fig.4.25 Diagram showing Non-Linear Phase Shift Mechanism

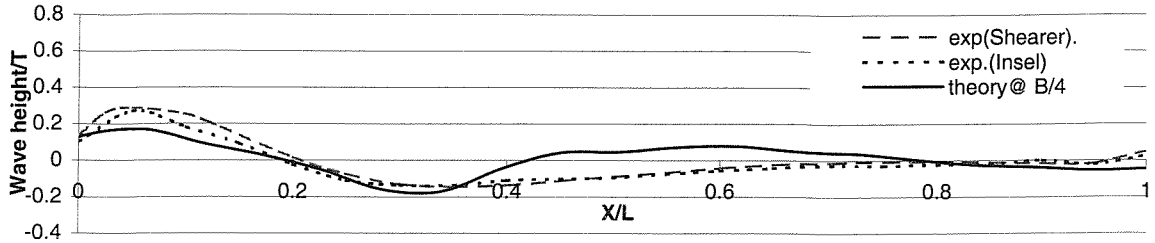

Fig.4.26 Comparison between experimental and theoretical wave profiles: Wigley monohull Fn=0.35

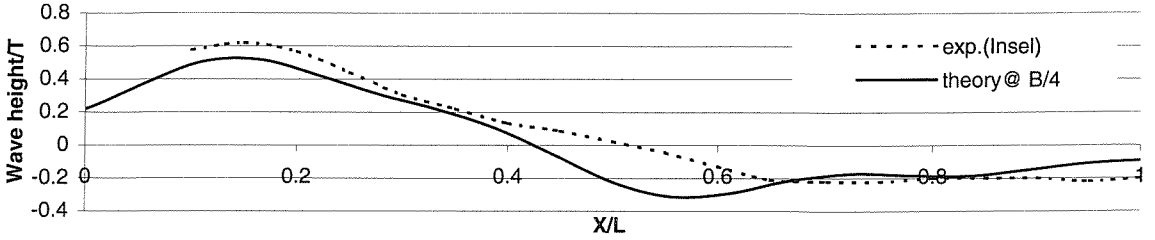

Fig.4.27 Comparison between experimental and theoretical wave profiles: Wigley monohull Fn=0.50

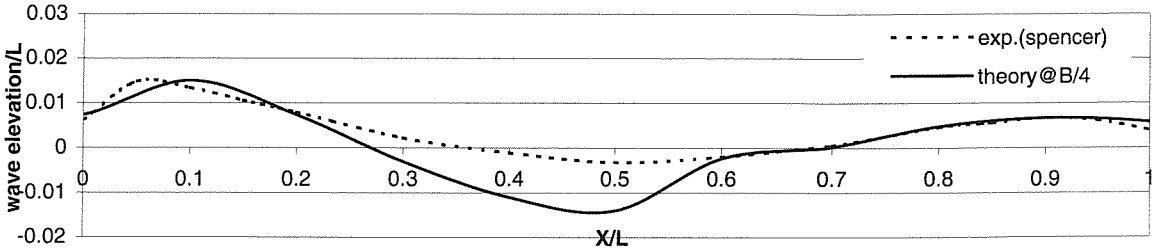

Fig.4.28 Comparison of hull wave profiles of model 4b monohull, Fn=0.4

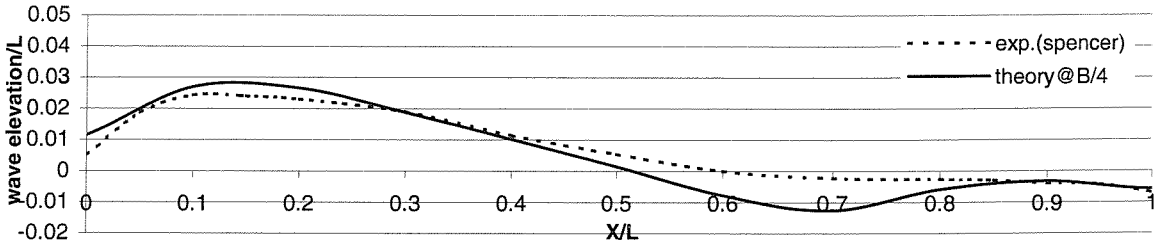

Fig.4.29 Comparison of hull wave profiles of model 4b monohull, Fn=0.6

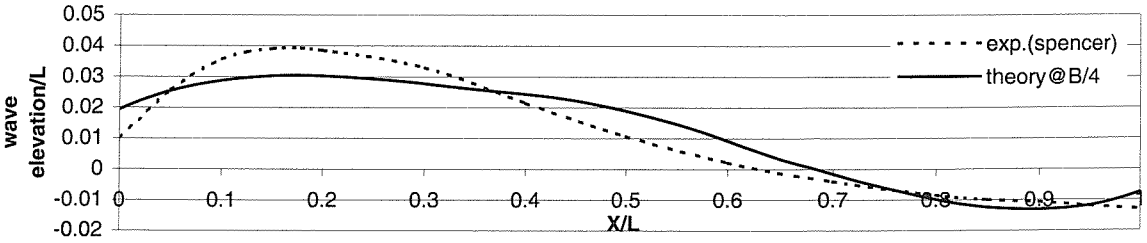

Fig.4.30 Comparison of hull wave profiles of model 4b monohull, Fn=0.9

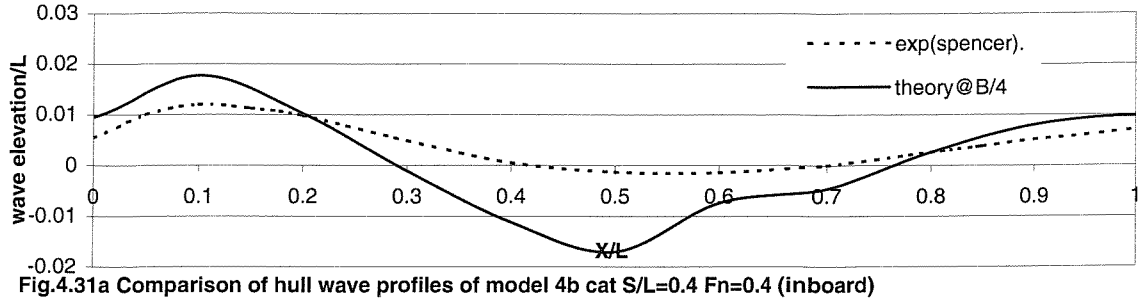

Fig.4.31a Comparison of hull wave profiles of model 4b cat S/L=0.4 Fn=0.4 (inboard)

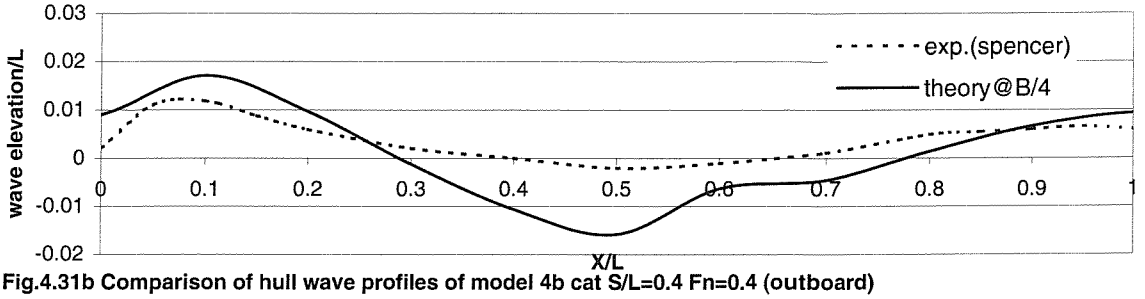

Fig.4.31b Comparison of hull wave profiles of model 4b cat S/L=0.4 Fn=0.4 (outboard)

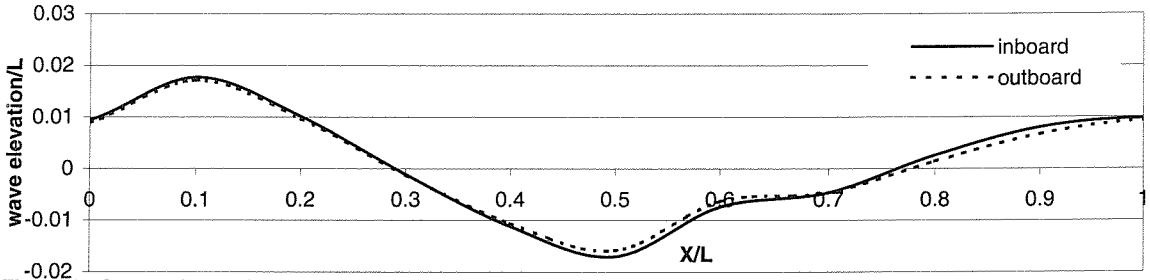

Fig.4.31c Comparison of theoretical hull wave profiles of model 4b cat S/L=0.4 Fn=0.4

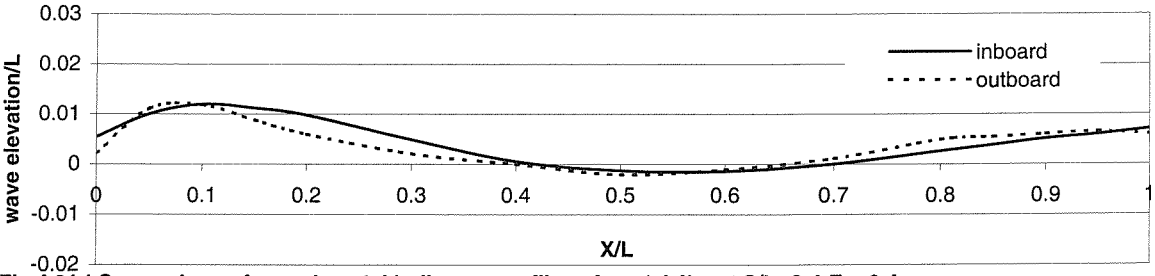

Fig.4.31d Comparison of experimental hull wave profiles of model 4b cat S/L=0.4 Fn=0.4

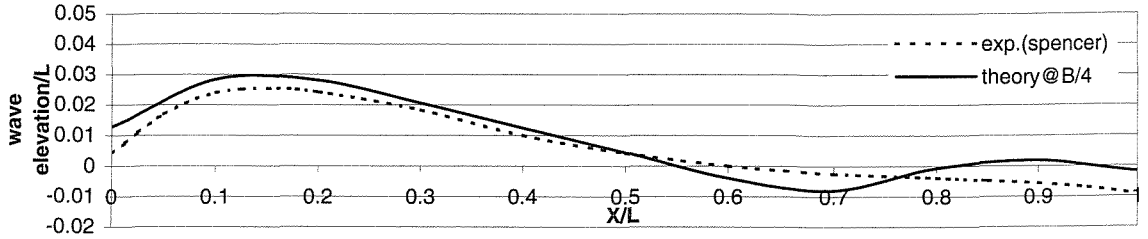

Fig.4.32 Comparison of hull wave profiles of model 4b cat S/L=0.4 Fn=0.6 (outboard)

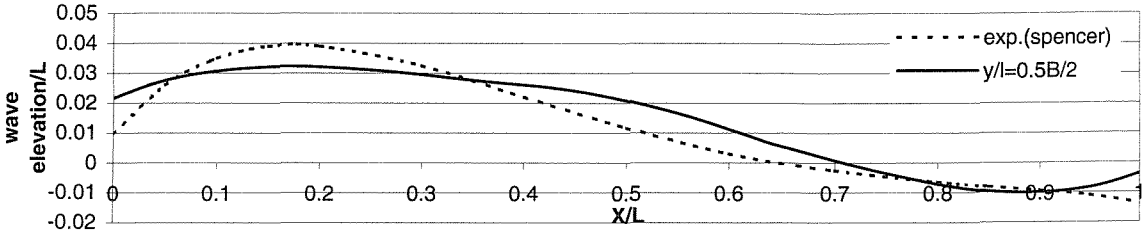

Fig.4.33 Comparison of hull wave profiles of model 4b cat S/L=0.4 Fn=0.9 (outboard)

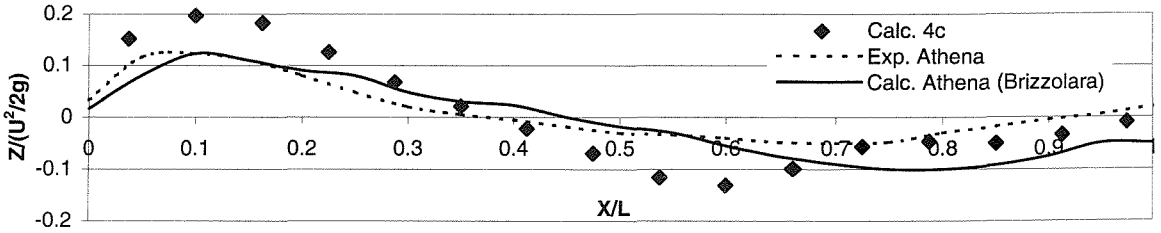

Fig.4.34 Comparison of hull wave profiles between model 4c and Athena, monohull Fn=0.48

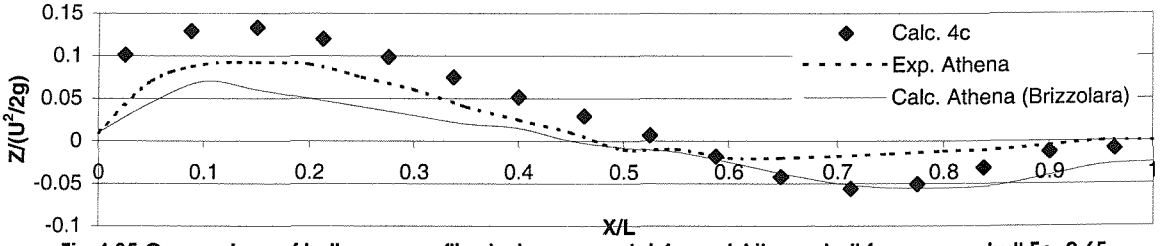

Fig.4.35 Comparison of hull wave profiles between model 4c and Athena hull form, monohull Fn=0.65

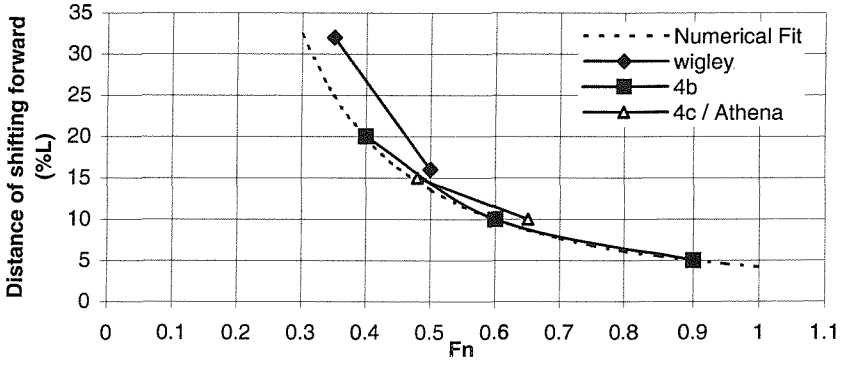

Fig.4.36 Theoretical shifting distance of wave profile along the hull

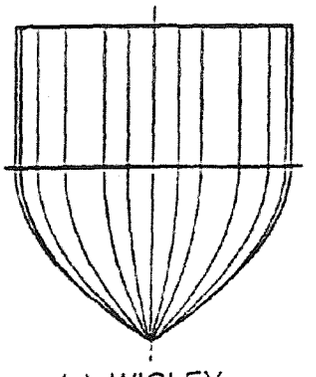

(a) WIGLEY

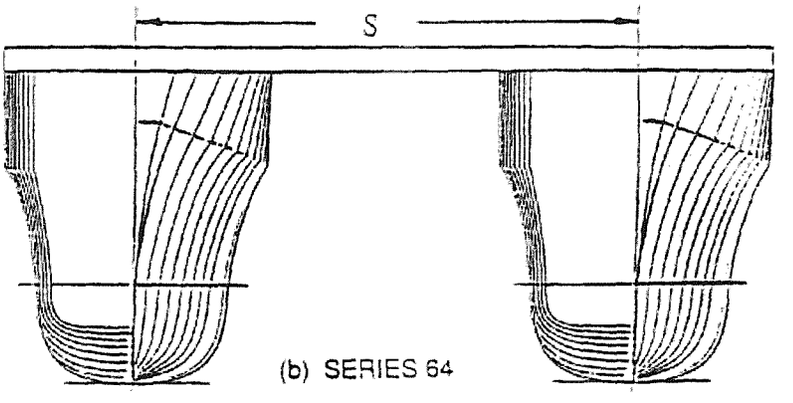

(b) SERIES 64

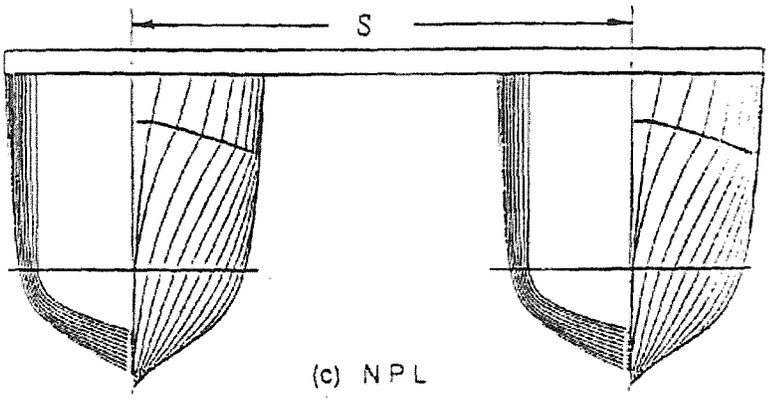

(c) N P L

Fig.5.1 Hull Forms used for validation and example applications

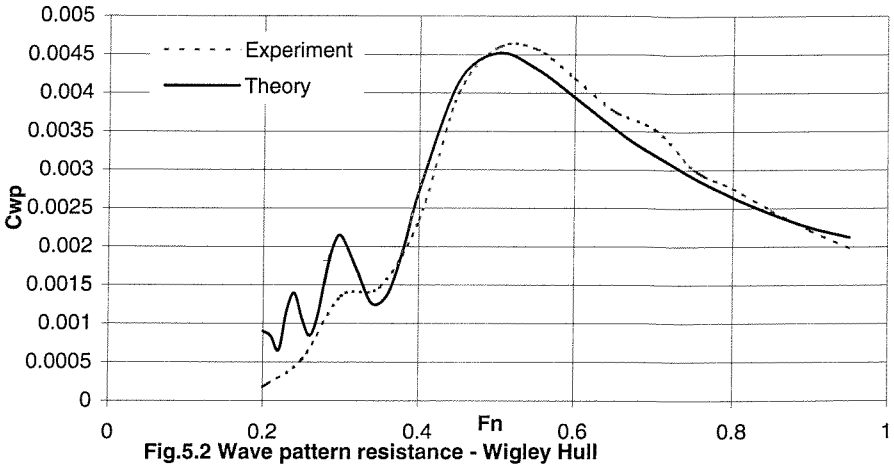

Fig.5.2 Wave pattern resistance - Wigley Hull

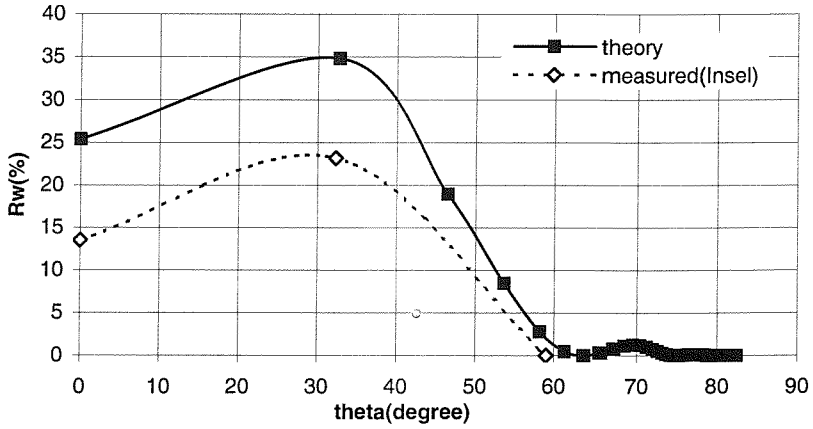

Fig.5.3a Distribution of wave pattern resistance: Wigley Monohull Fn=0.5

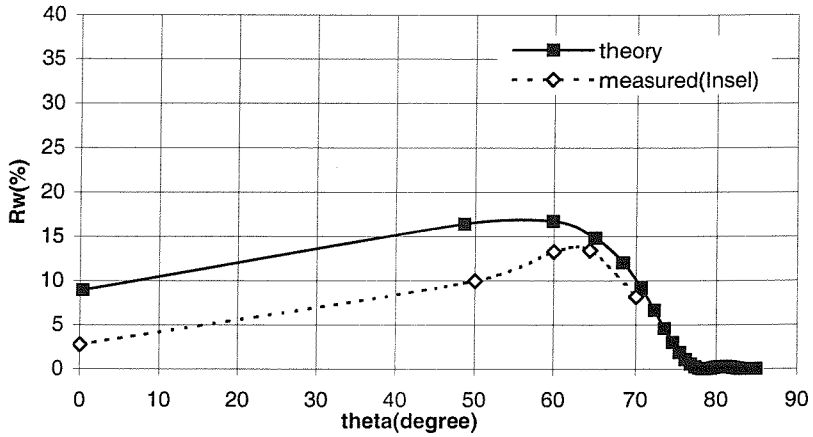

Fig.5.3b Distribution of wave pattern resistance: Wigley Monohull Fn=0.75

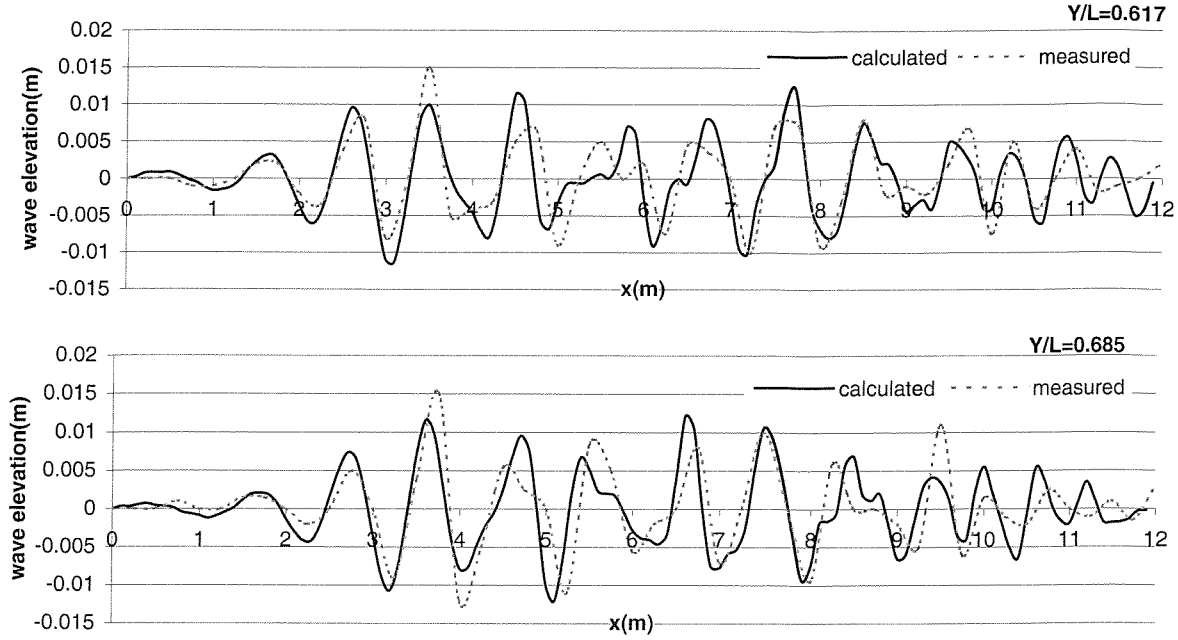

Fig.5.4 Comparison of wave cuts between Theory and Experiment – Wigley Hull

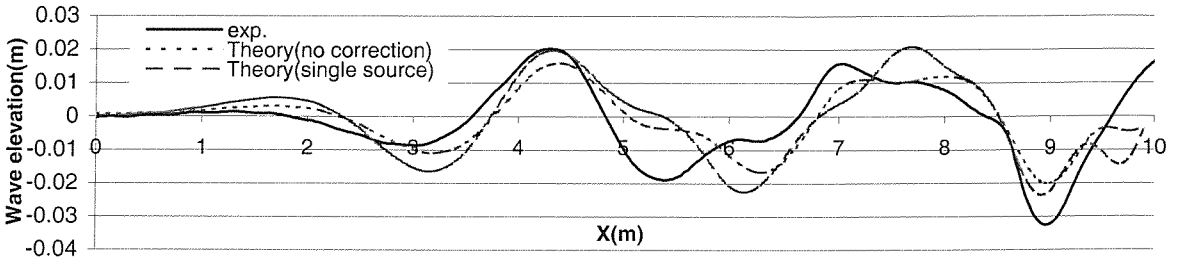

Fig.5.5 Comparison of wave profiles: Model 5s Catamaran S/L=0.3 Fn=0.59 H=1.85m Fn_H=0.55 Y/L=0.86

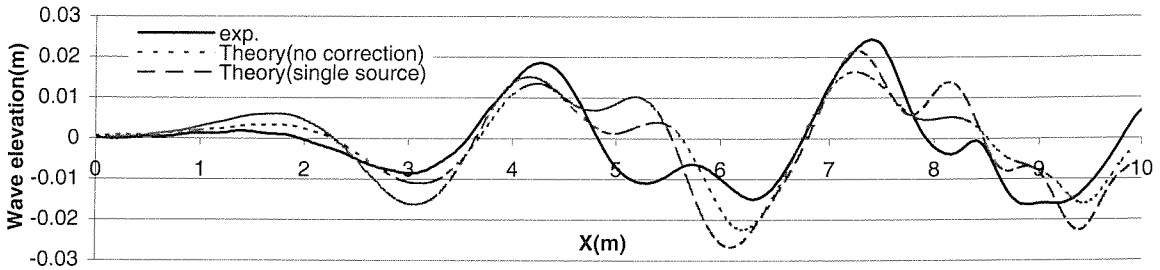

Fig.5.6 Comparison of wave profiles: Model 5s Catamaran S/L=0.4 Fn=0.59 H=1.85m Fn_H=0.55

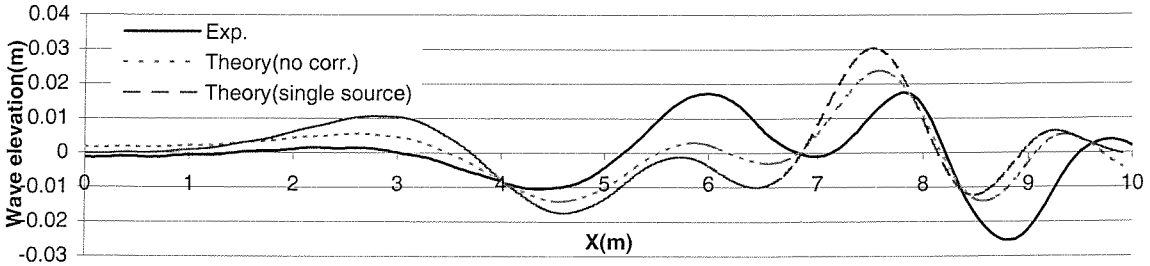

Fig.5.7 Comparison of wave profiles: Model 5s catamaran S/L=0.4 Fn=0.79 H=1.85m Fn_H=0.73 Y/L=0.86

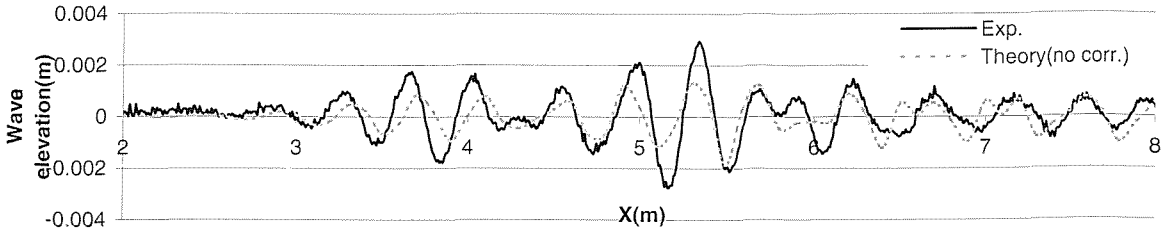

Fig:5.8a Comparison of wave profiles: 5b monohull Fn=0.22 H=0.4m Fn_H=0.44 Y/L=0.93

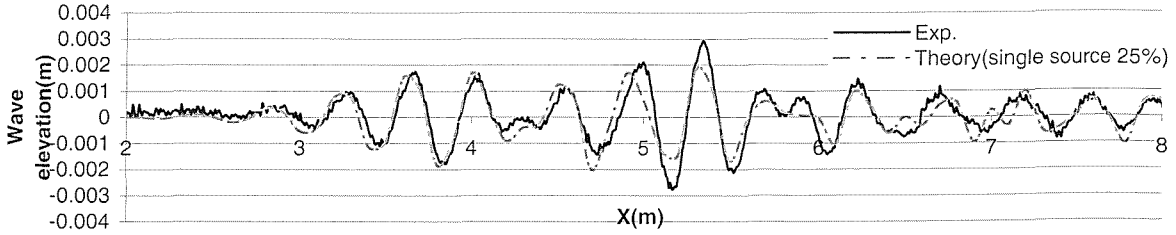

Fig:5.8b Comparison of wave profiles: 5b monohull Fn=0.22 H=0.4m Fn_H=0.44 Y/L=0.93

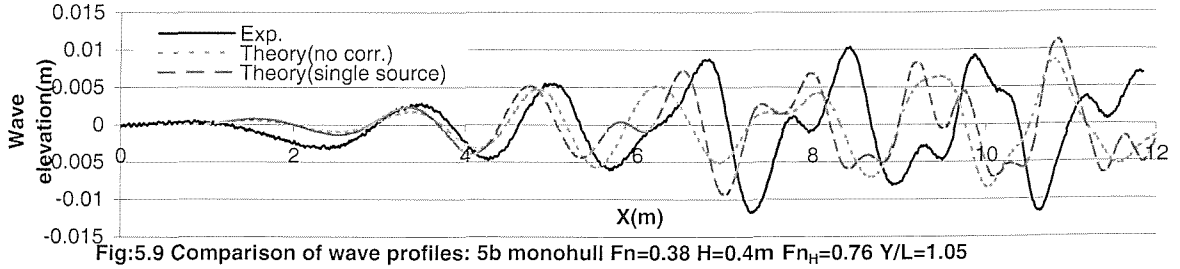

Fig:5.9 Comparison of wave profiles: 5b monohull Fn=0.38 H=0.4m Fn_H=0.76 Y/L=1.05

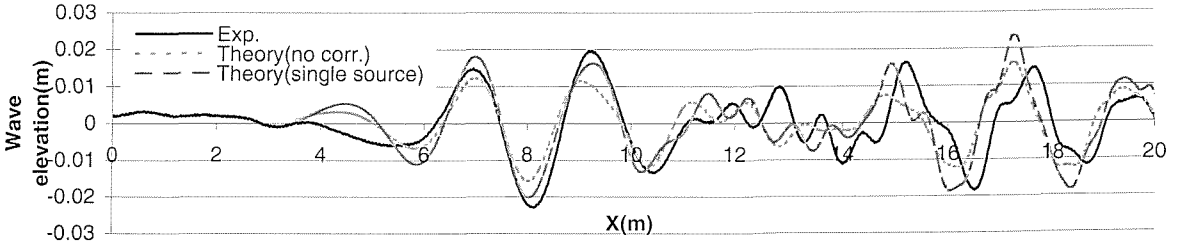

Fig:5.10 Comparison of wave profiles: 5b monohull Fn=0.44 H=0.4m Fn_H=0.89 Y/L=1.18

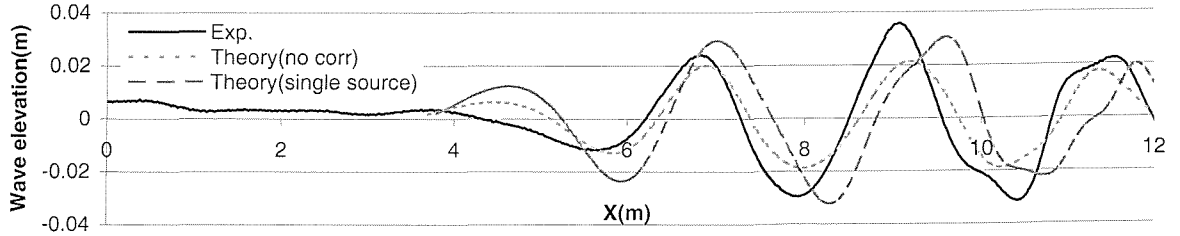

Fig:5.11 Comparison of wave profiles: 5b catamaran S/L=0.4 Fn=0.435 H=0.4m Fn_H=0.87 Y/L=1.05

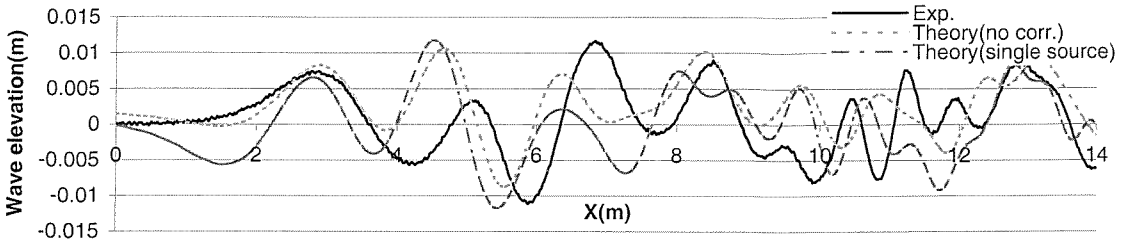

Fig:5.12 Comparison of wave profiles: 5b monohull Fn=0.511 H=0.2m Fn_H=1.45 Y/L=1.05

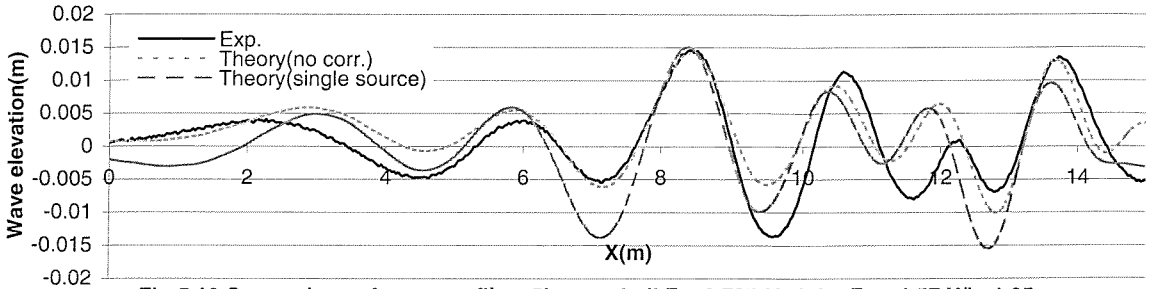

Fig:5.13 Comparison of wave profiles: 5b monohull Fn=0.785 H=0.4m Fn_H=1.57 Y/L=1.05

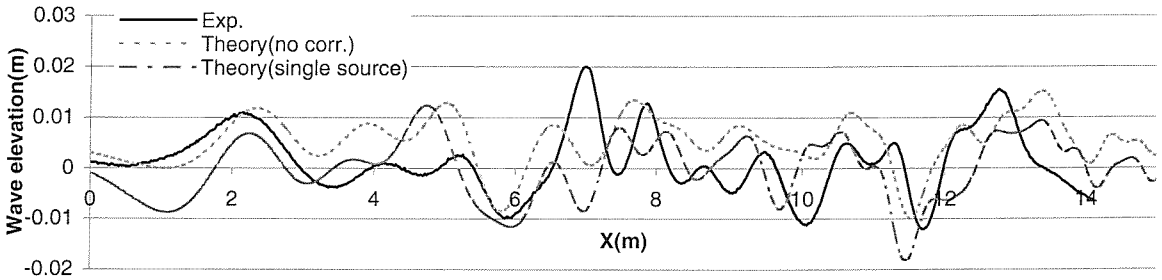

Fig:5.14 Comparison of wave profiles: 5b cat S/L=0.4 Fn=0.515 H=0.2m Fn_H=1.46 Y/L=0.93

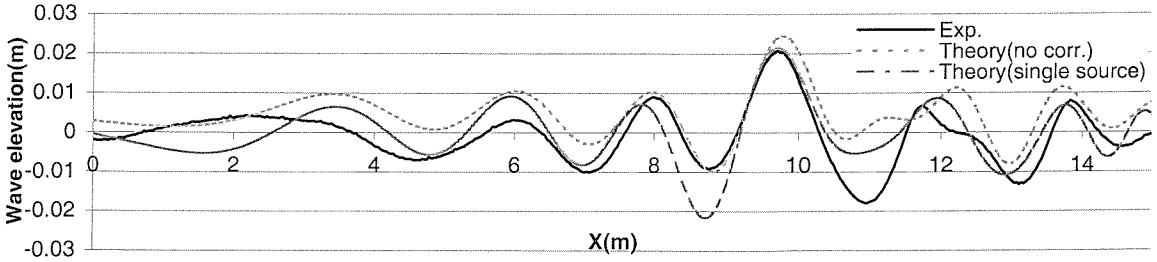

Fig:5.15 Comparison of wave profiles: 5b catamaran S/L=0.4 Fn=0.785 H=0.4m Fn_H=1.57 Y/L=0.93

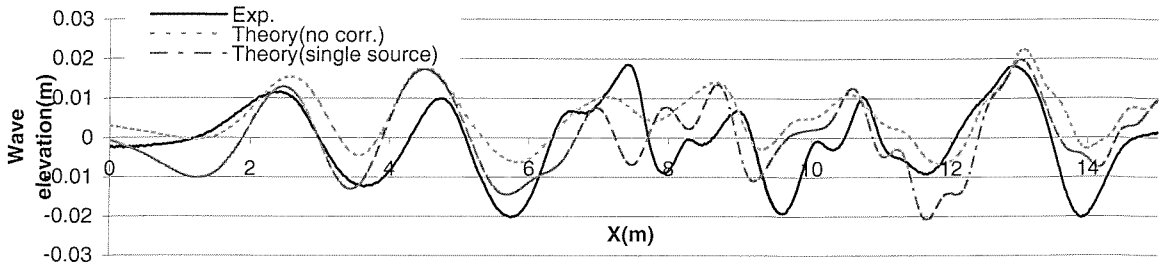

Fig:5.16 Comparison of wave profiles: : 5b S/L=0.2 Fn=0.515 H=0.2m Fn_H=1.46 Y/L=0.93

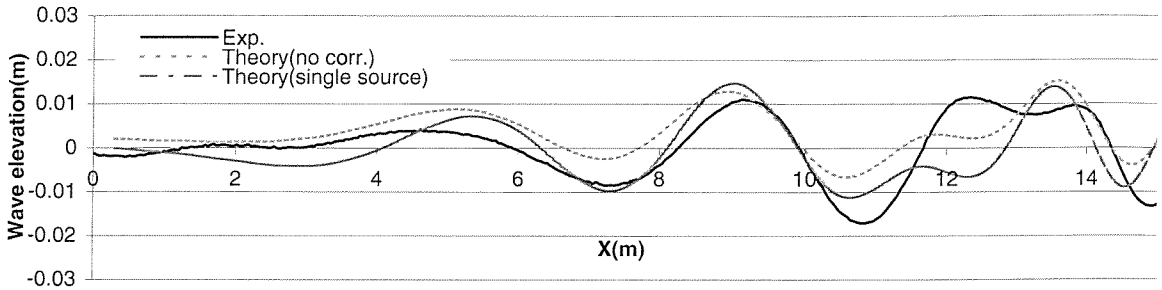

Fig:5.17 Comparison of wave profiles: 5b S/L=0.2 Fn=1.02 H=0.4m Fn_H=2.04 Y/L=0.93

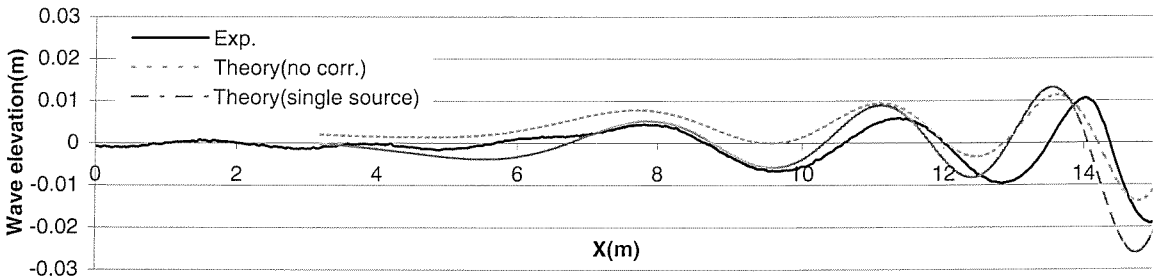

Fig:5.18 Comparison of wave profiles: 5b S/L=0.4 Fn=1.02 H=0.4m Fn_H=2.04 Y/L=0.93

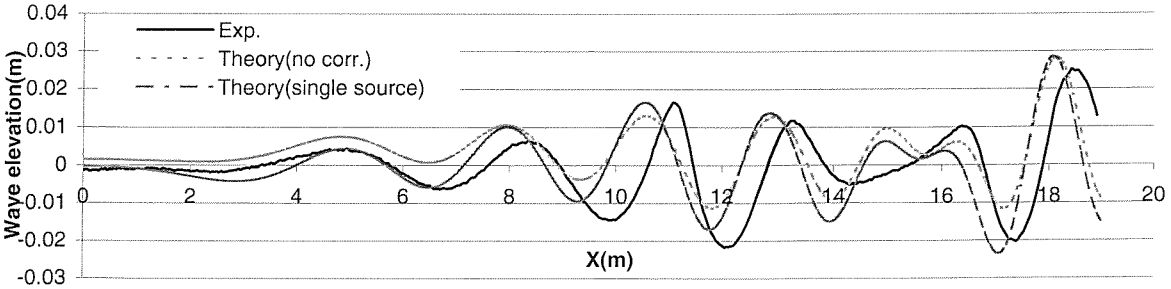

Fig:5.19 Comparison of wave profiles: 5b catamaran S/L=0.4 Fn=1.02 H=0.2m Fn_H=2.89 Y/L=1.05

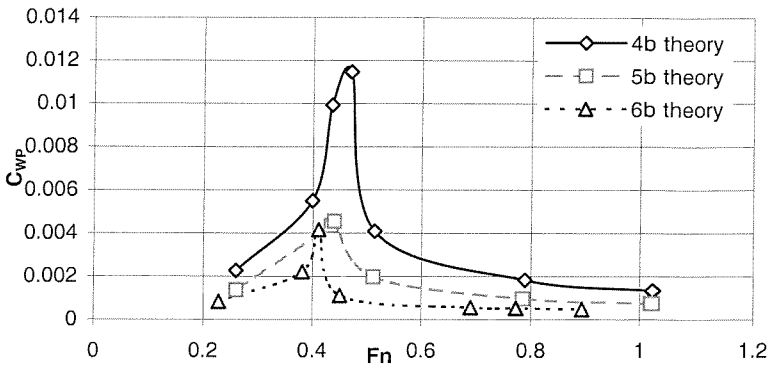

Fig.5.20 Theoretical wave pattern resistance: effect of length to displacement ratio, H=0.4m

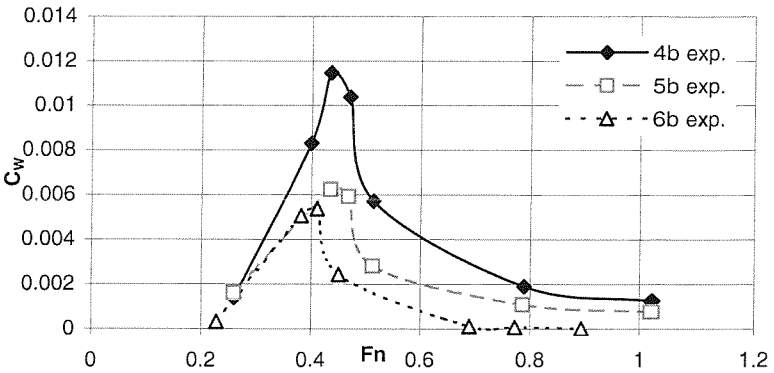

Fig.5.21 Experimental wave resistance: effect of length to displacement ratio, H=0.4m

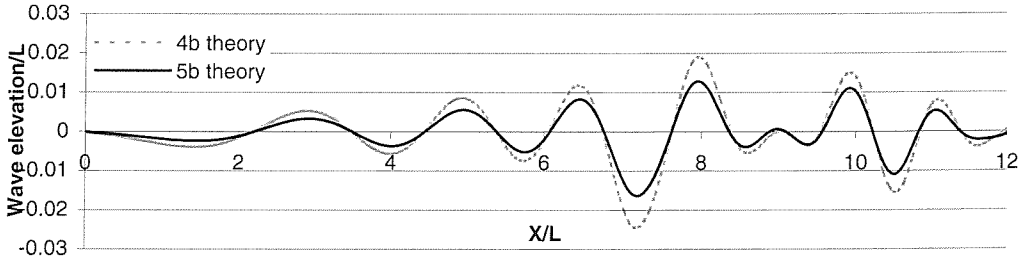

Fig.5.22a Theoretical wave profiles: catamaran S/L=0.4 Fn=1.02 H=0.4m Fn_H=2.04 Y/L=0.93

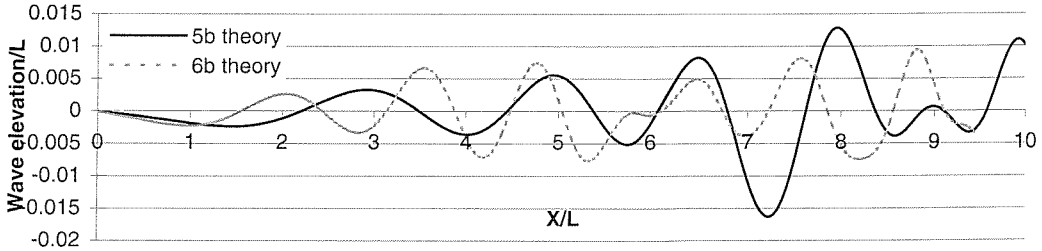

Fig.5.22b Theoretical wave profiles: catamaran S/L=0.4 Fn=1.02/0.89 H=0.4m Fn_H=2.04 Y/L=0.93/0.71

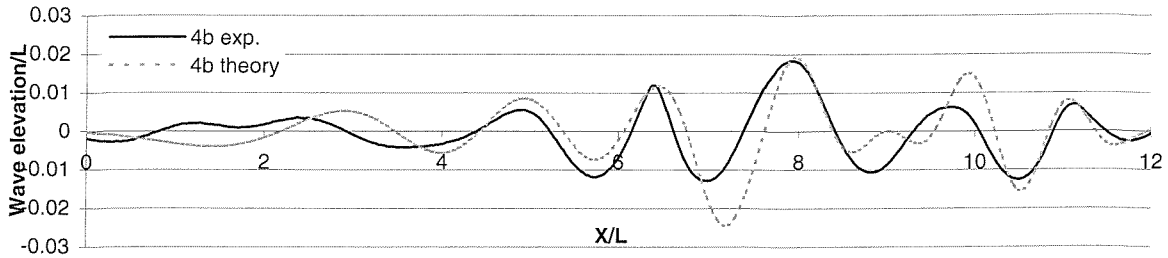

Fig.5.23 Comparison of wave profiles: model 4b catamaran S/L=0.4 Fn=1.02 H=0.4m Fn_H=2.04 Y/L=0.93

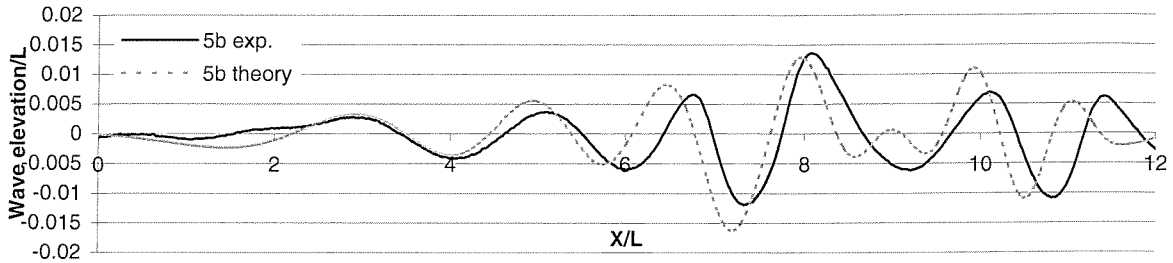

Fig.5.24 Comparison of wave profiles: model 5b catamaran S/L=0.4 Fn=1.02 H=0.4m Fn_H=2.04 Y/L=0.93

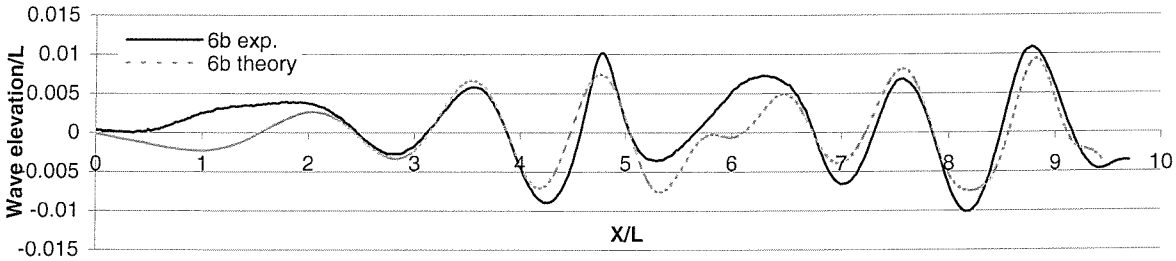

Fig.5.25 Comparison of wave profiles: model 6b catamaran S/L=0.4 Fn=0.89 H=0.4m Fn_H=2.04 Y/L=0.71

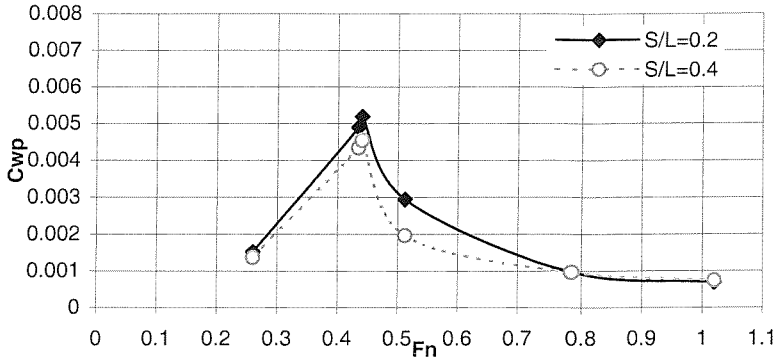

Fig.5.26 Theoretical wave pattern resistance: H=0.4m

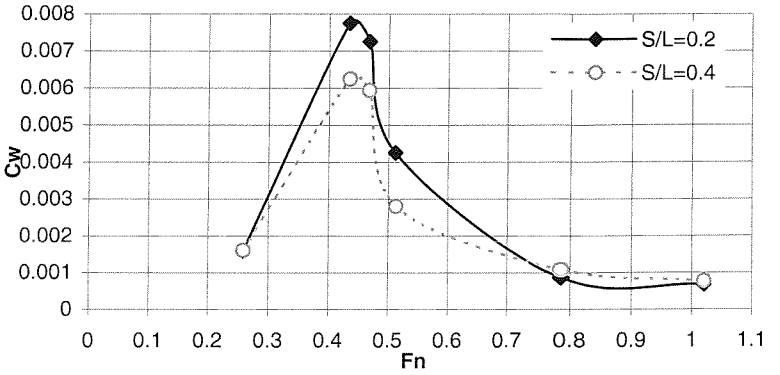

Fig: 5.27 Experimental wave resistance: H=0.4m

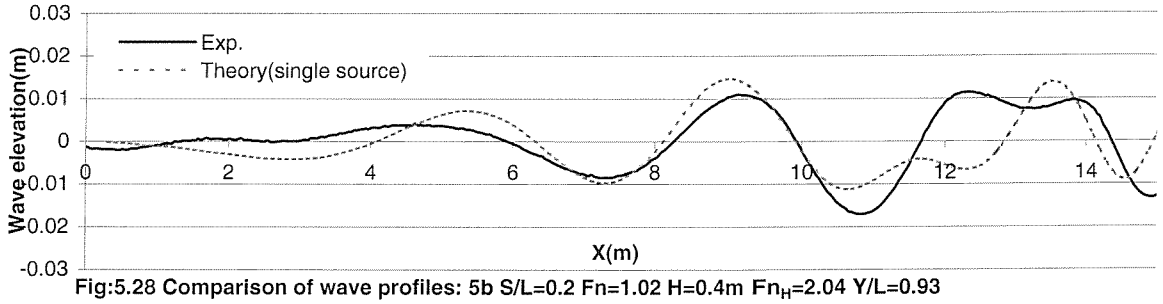

Fig:5.28 Comparison of wave profiles: 5b S/L=0.2 Fn=1.02 H=0.4m Fn_H=2.04 Y/L=0.93

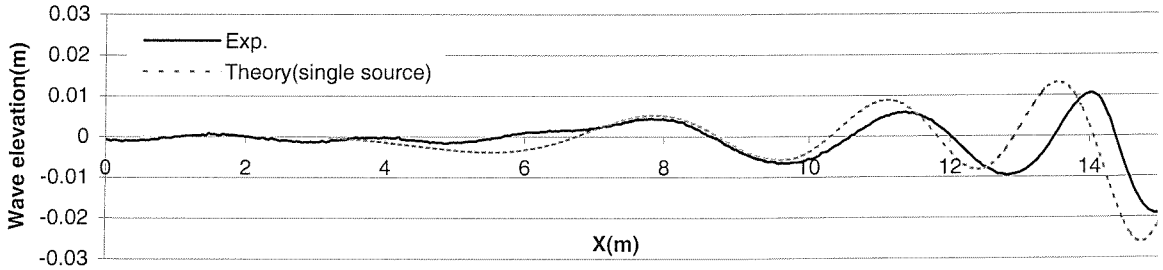

Fig:5.29 Comparison of wave profiles: 5b S/L=0.4 Fn=1.02 H=0.4m Fn_H=2.04 Y/L=0.93

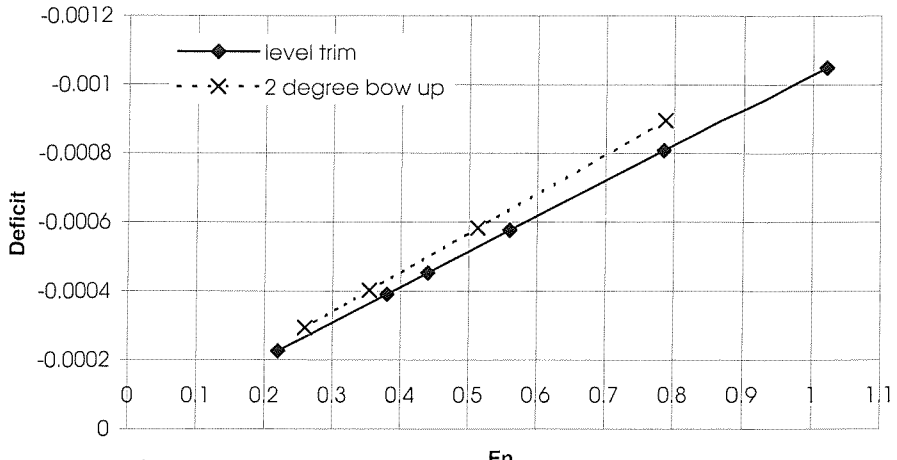

Fig.5.30 Deficit required to balance net source strength of zero: model 5b at level trim and 2 degree bow up

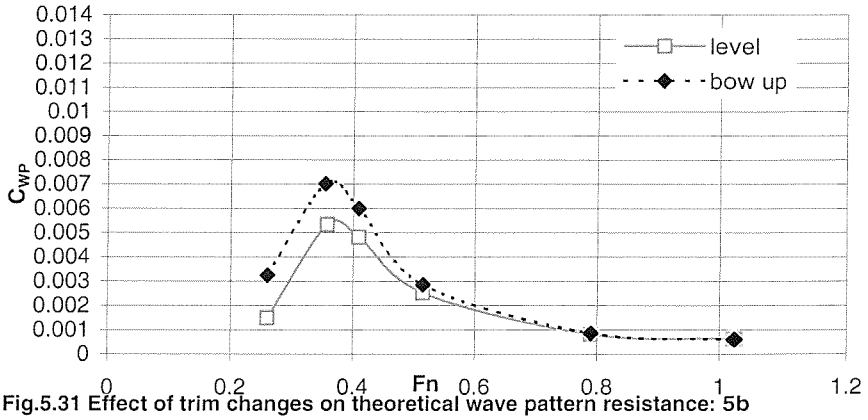

Fig.5.31 Effect of trim changes on theoretical wave pattern resistance: 5b catamaran S/L=0.2 H=0.2m

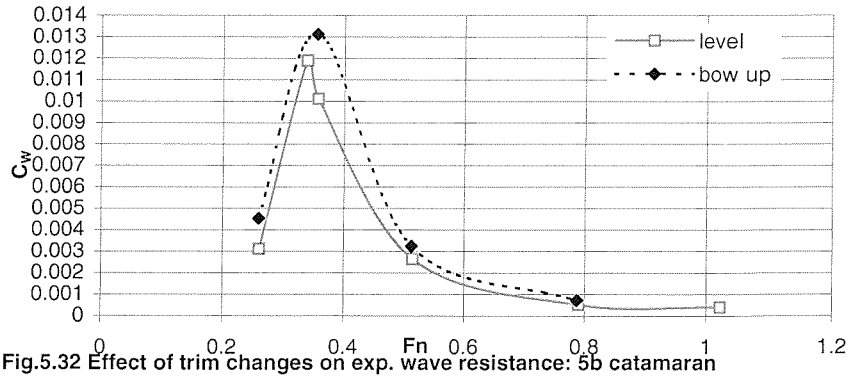

Fig.5.32 Effect of trim changes on exp. wave resistance: 5b catamaran S/L=0.2 H=0.2m

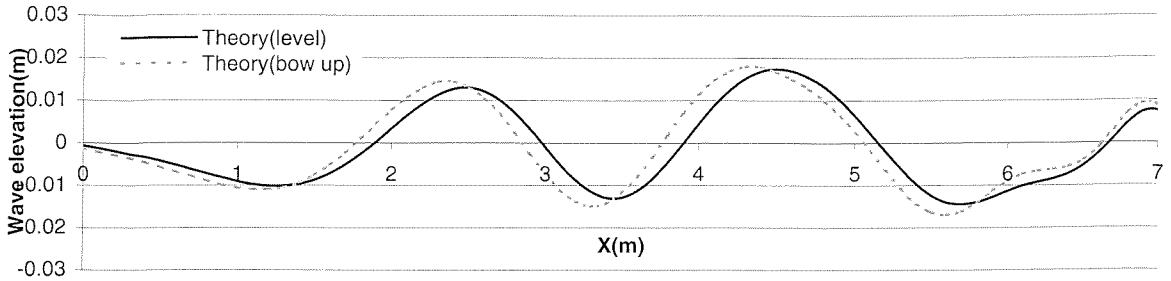

Fig.5.33 Theoretical wave cuts: 5b catamaran S/L=0.2 Fn=0.51 H=0.2m Fn_H=1.45 Y/L=0.93

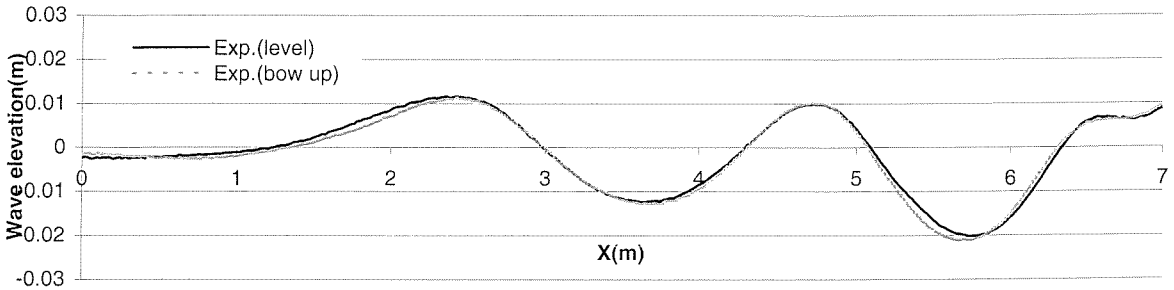

Fig.5.34 Experimental wave cuts: 5b catamaran S/L=0.2 Fn=0.51 H=0.2m Fn_H=1.45 Y/L=0.93

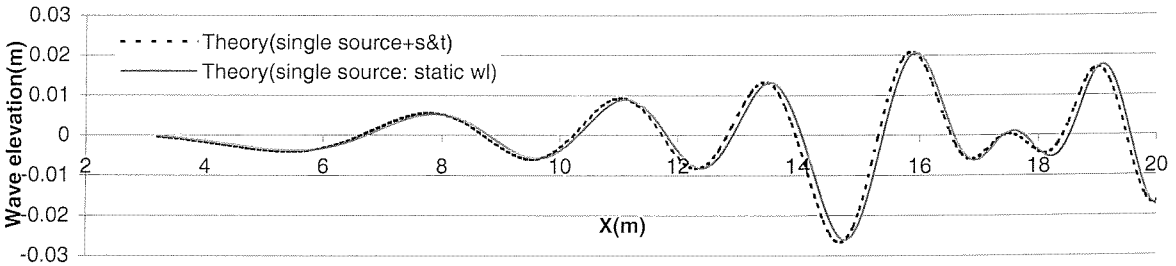

Fig.5.35 Theoretical wave cuts: 5b S/L=0.4 Fn=1.02 H=0.4m Fn_H=2.04 Y/L=0.93

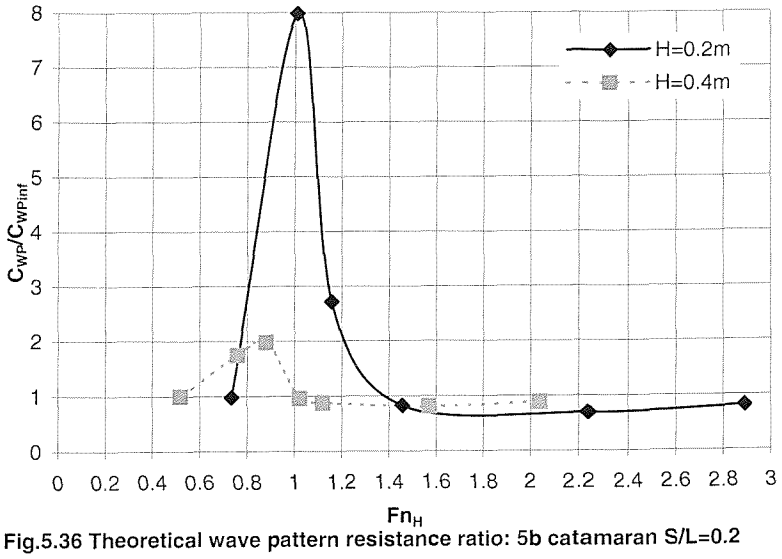

Fig.5.36 Theoretical wave pattern resistance ratio: 5b catamaran S/L=0.2

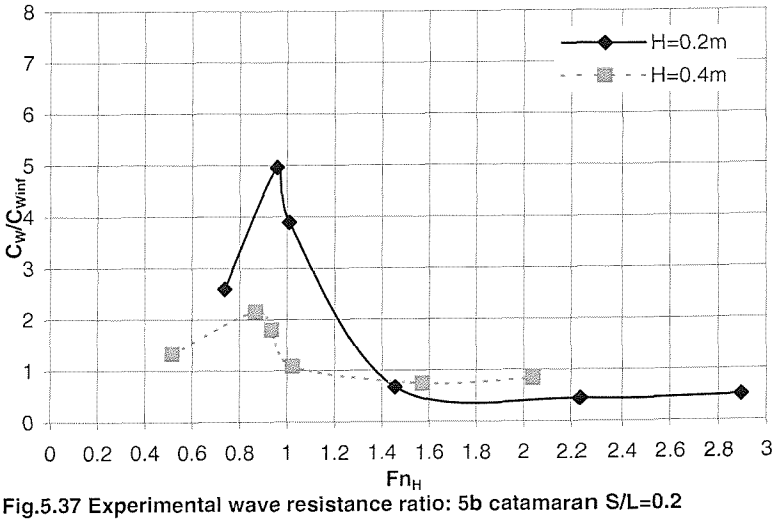

Fig.5.37 Experimental wave resistance ratio: 5b catamaran S/L=0.2

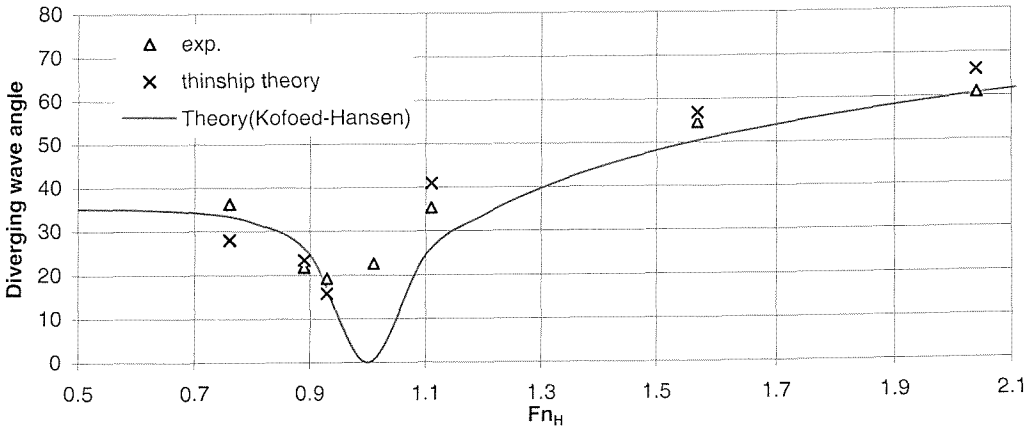

Fig.5.38 Diverging wave angle

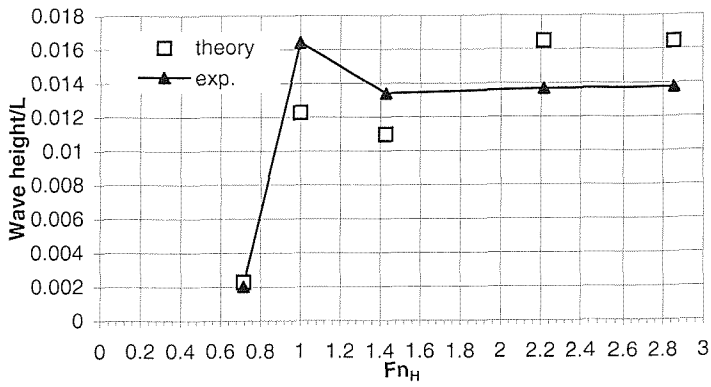

Fig.5.39a 1st Leading wave height, 5b monohull H=0.2m

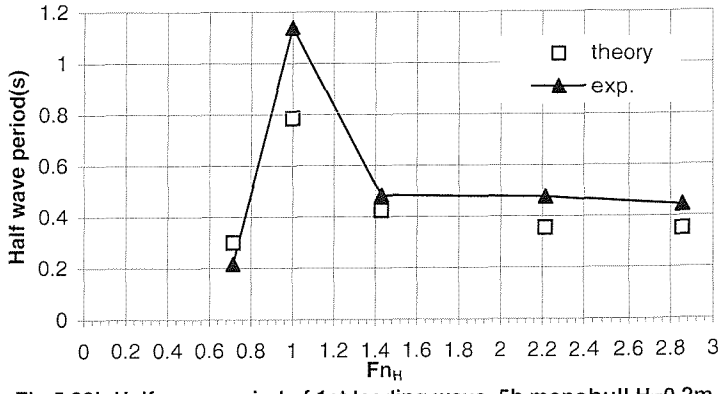

Fig.5.39b Half wave period of 1st leading wave, 5b monohull H=0.2m

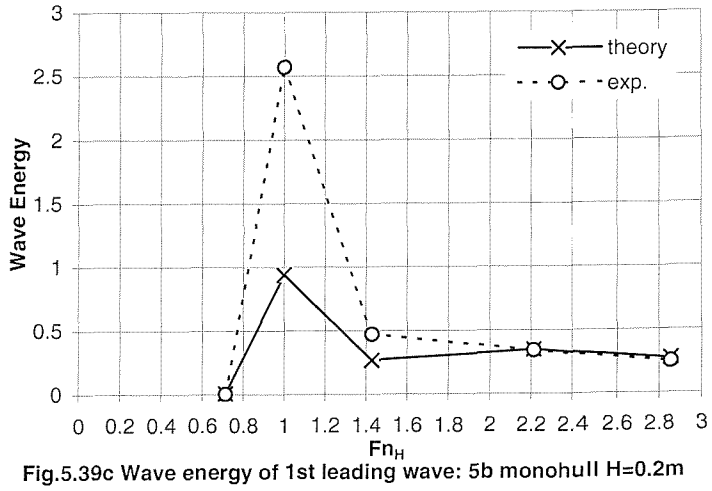

Fig.5.39c Wave energy of 1st leading wave: 5b monohull H=0.2m

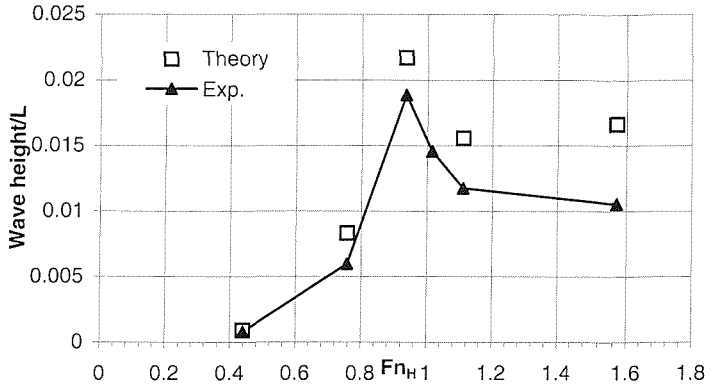

Fig.5.40a 1st Leading wave height, 5b monohull H=0.4m

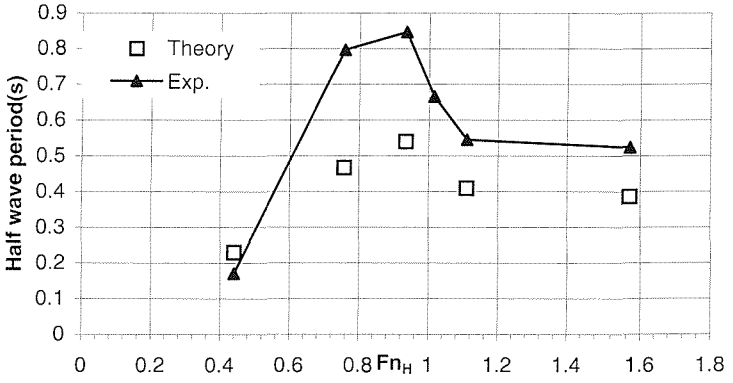

Fig.5.40b Half wave period of 1st leading wave, 5b monohull H=0.4m

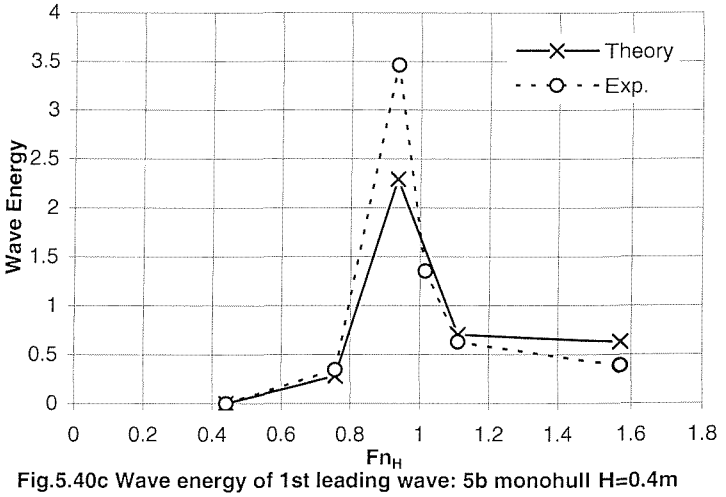

Fig.5.40c Wave energy of 1st leading wave: 5b monohull H=0.4m

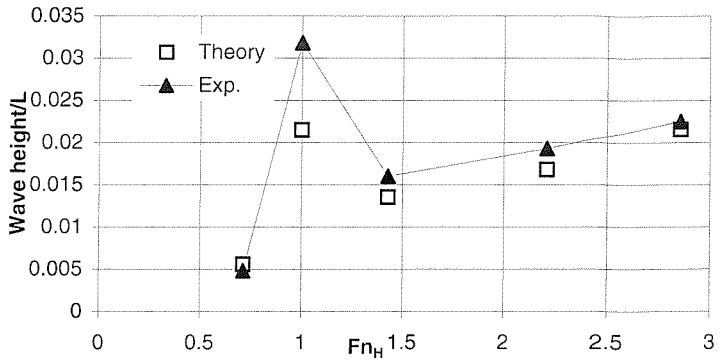

Fig.5.41a 1st Leading wave height: 5b catamaran S/L=0.4 H=0.2m

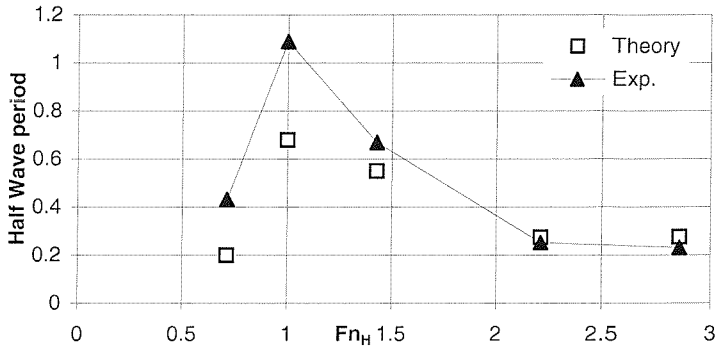

Fig.5.41b Half wave period of 1st leading wave: 5b catamaran S/L=0.4 H=0.2m

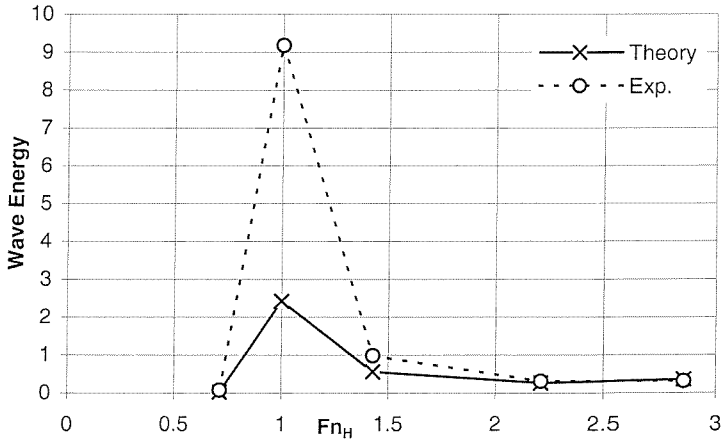

Fig.5.41c Wave energy of 1st leading wave: 5b catamaran S/L=0.4 H=0.2m

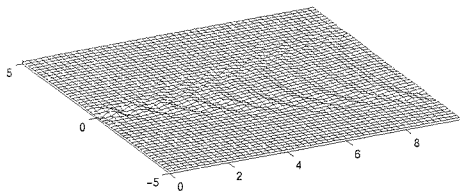

Fn=0.3

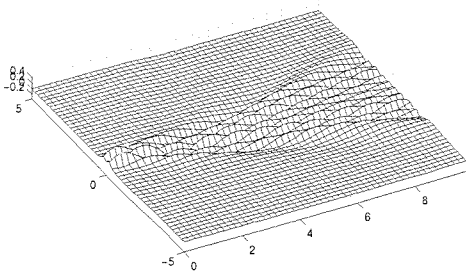

Fn=0.9

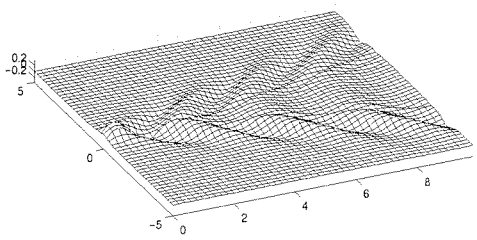

Fn=0.5

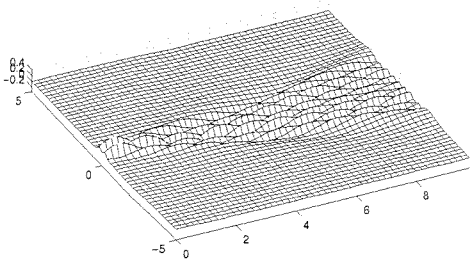

Fn=1.0

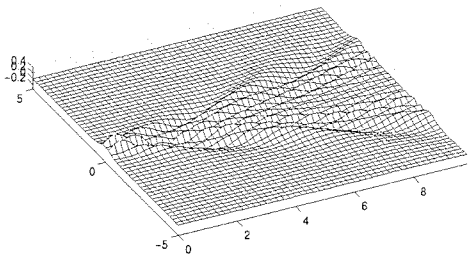

Fn=0.7

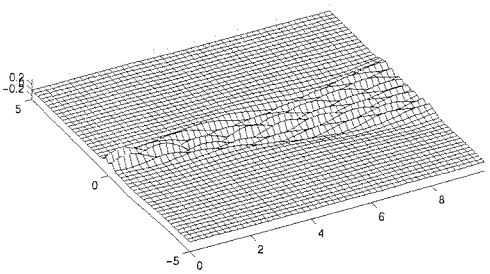

Fn=1.2

Fig.5.42 Wave patterns – NPL Catamarans S/L=0.25 (Deep water)

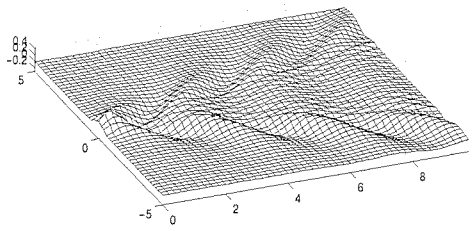

Fn_H=0.8

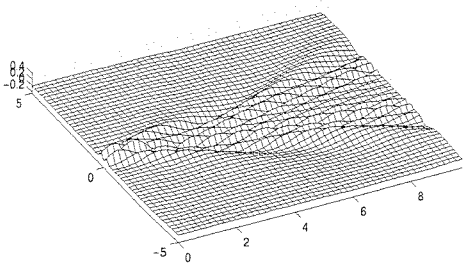

Fn_H =0.8

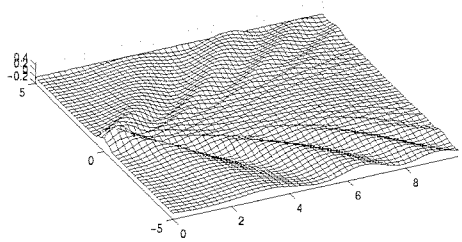

Fn_H =1.0

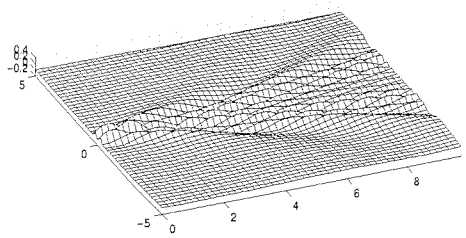

Fn_H =1.0

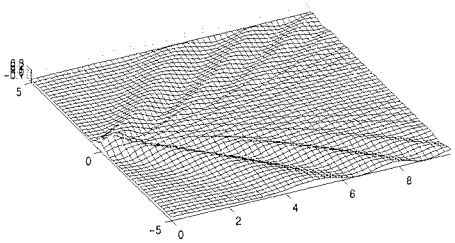

Fn_H =1.2

Fn=0.5

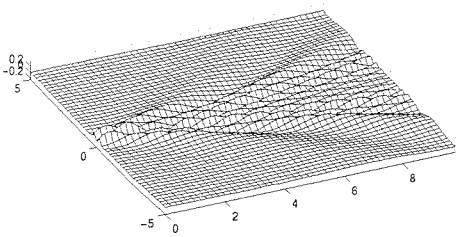

Fn_H =1.2

Fn=0.8

Fig.5.43 Wave patterns :NPL Catamaran S/L=0.25: Change in depth Froude number at given speeds

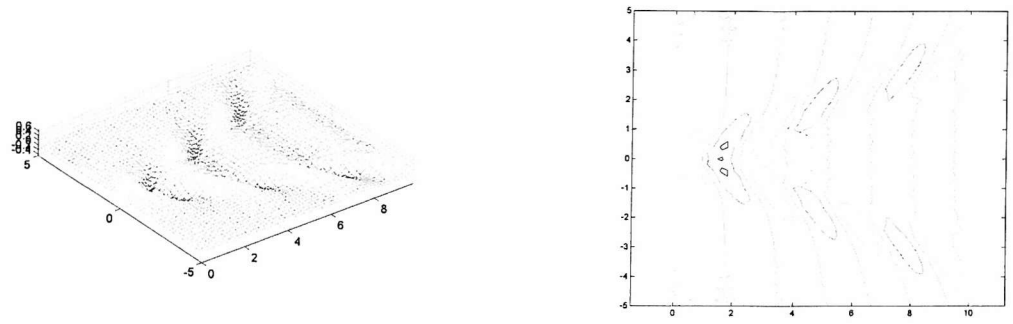

Figure 5.44a: Model 5b S/L=0.25, Fn=0.5, Fn_H=0.8

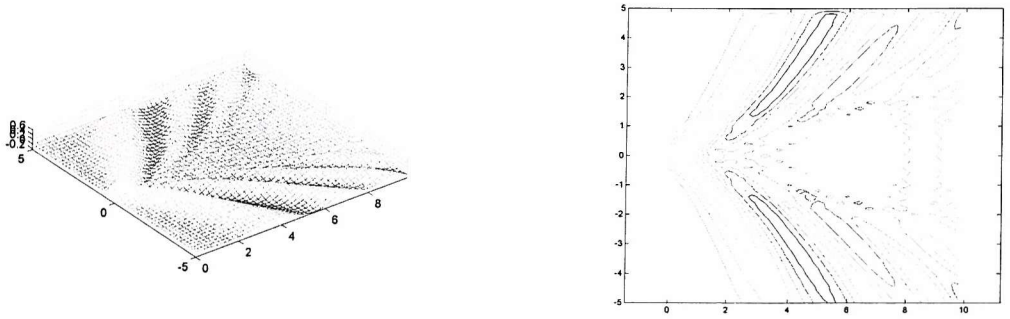

Figure 5.44b: Model 5b S/L=0.25, Fn=0.5, Fn_H=1.05

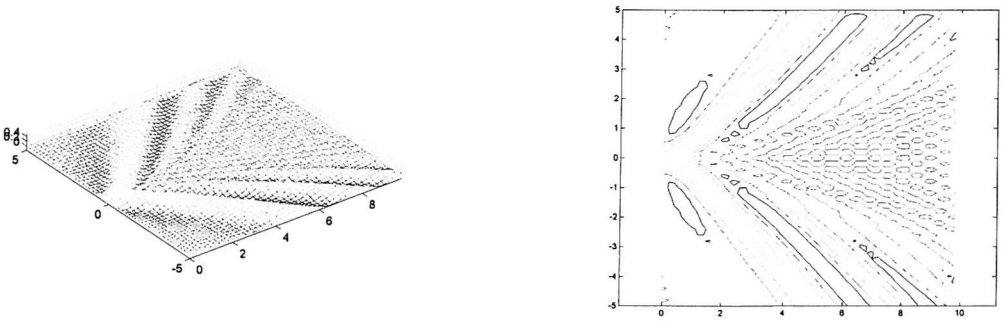

Figure 5.44c: Model 5b S/L=0.25, Fn=0.5, Fn_H=1.2

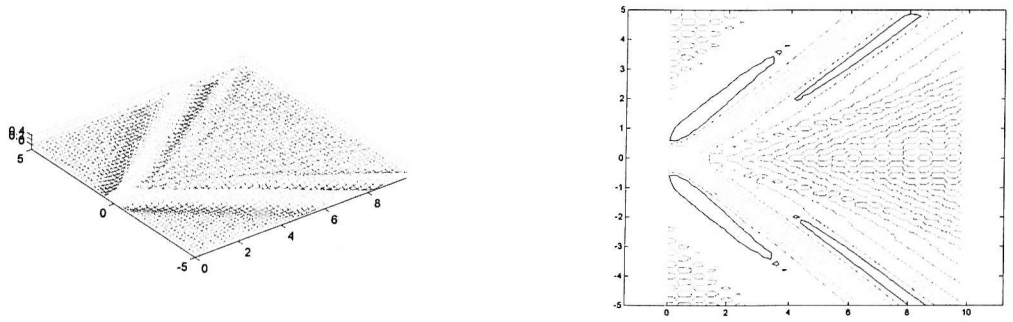

Figure 5.44d: Model 5b S/L=0.25, Fn=0.5, Fn_H=1.5

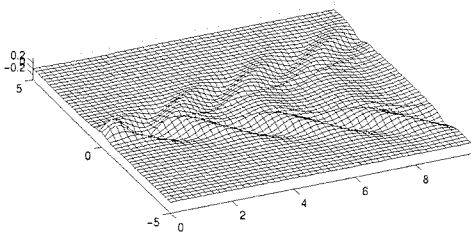

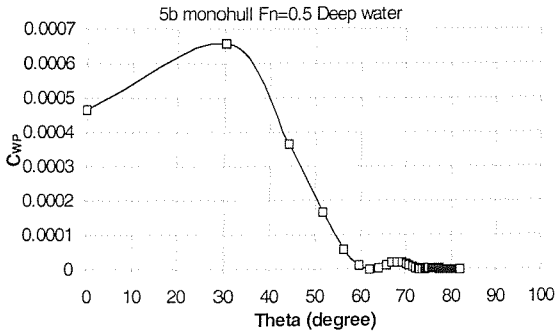

Fn=0.5

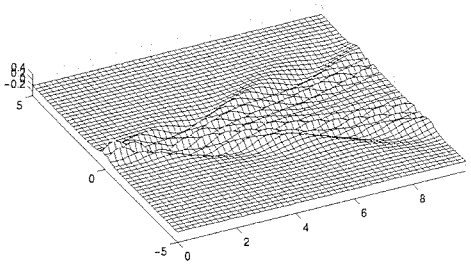

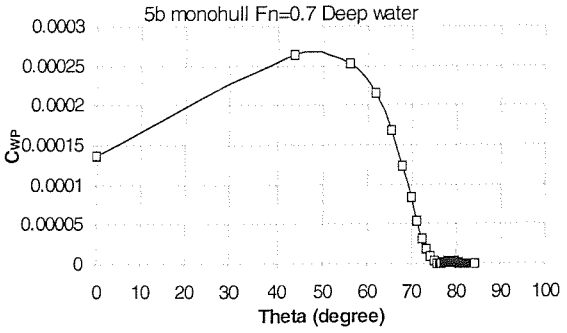

Fn=0.7

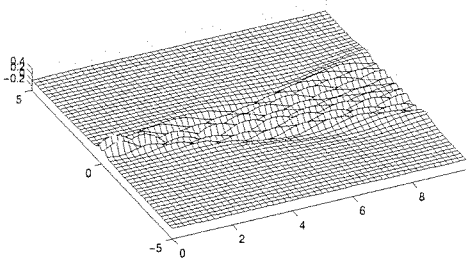

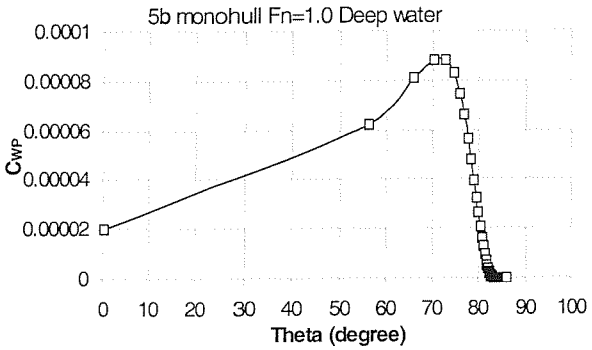

Fn=1.0

Fig.5.45 Wave pattern & distribution of wave pattern resistance: change in Fn at a given water depth, 5b monohull

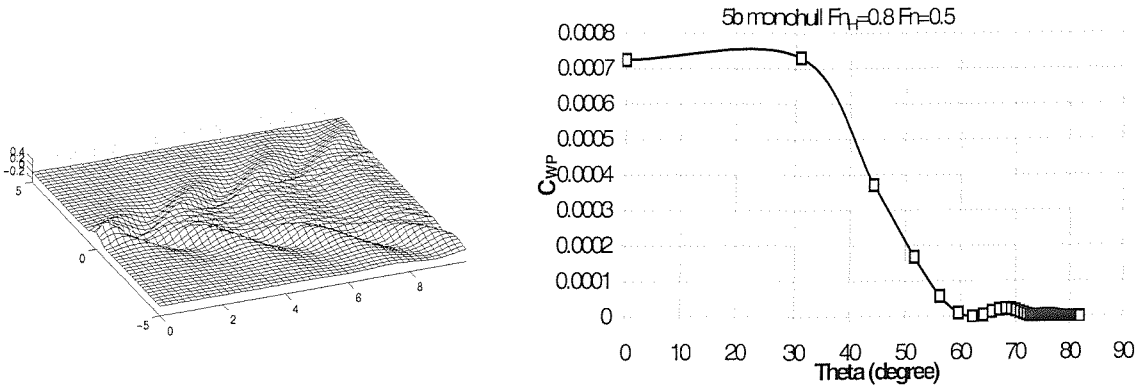

Fn_H =0.8

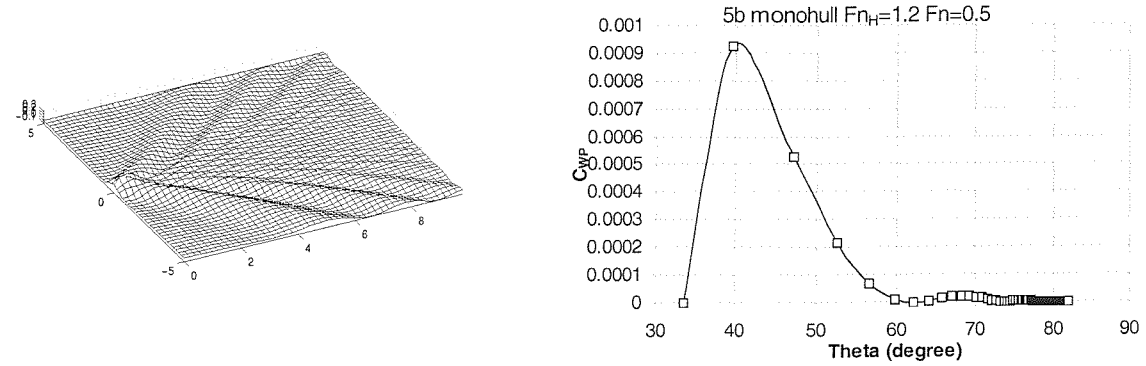

Fn_H =1.2

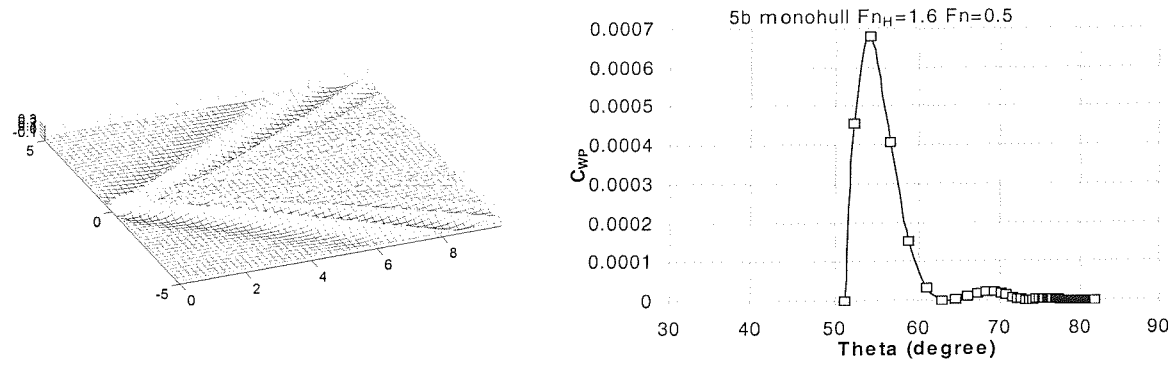

Fn_H=1.6

Fig.5.46 Wave pattern & distribution of wave pattern resistance: change in depth Froude number at a given speed (Fn=0.5), 5b monohull

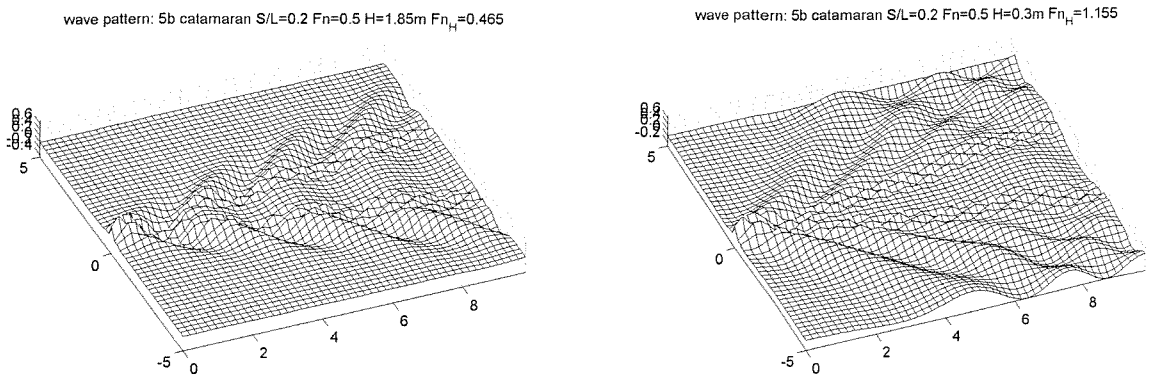

Fig.5.47 Comparison of wave pattern at the same speed but different water depth

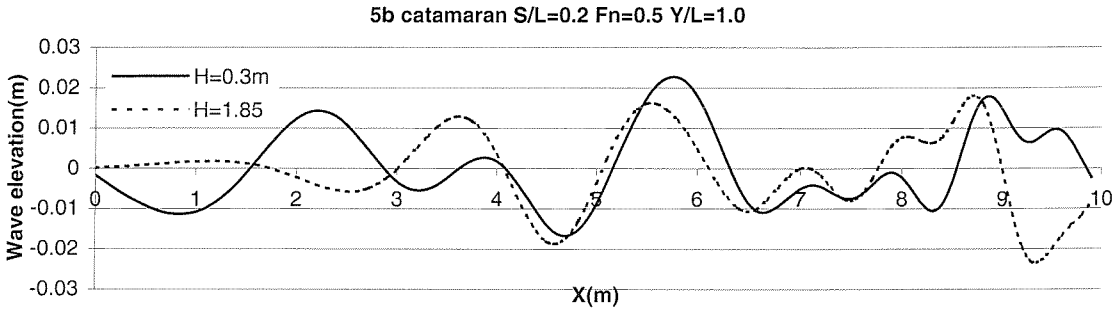

Fig.5.48 Comparison of wave cuts at the same speed but different water depth

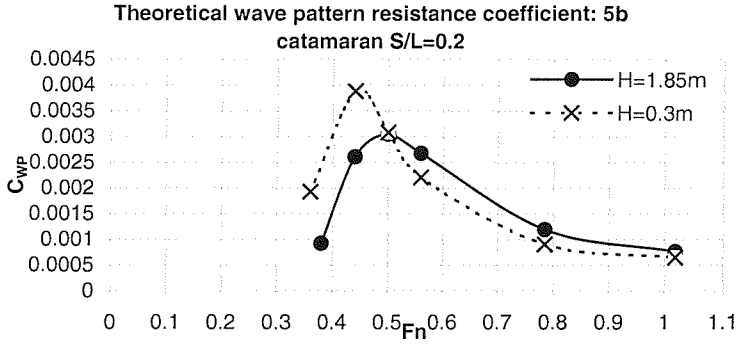

Fig.5.49 Comparison of wave pattern resistance at the same speed but different water depth

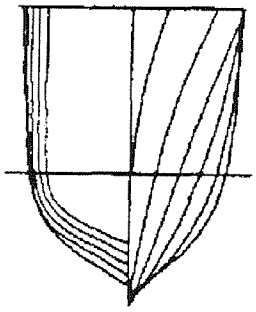

Model: 5a

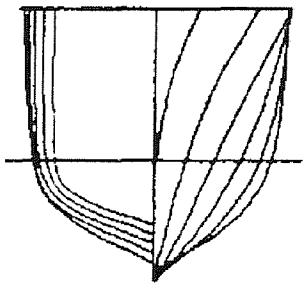

Model: 5b

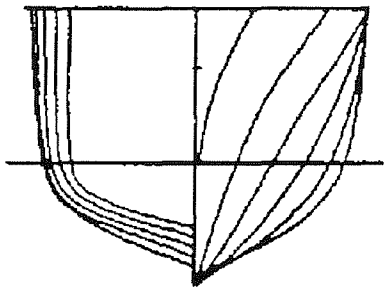

Model: 5c

Fig.5.50 Three NPL Hull Forms used for example applications

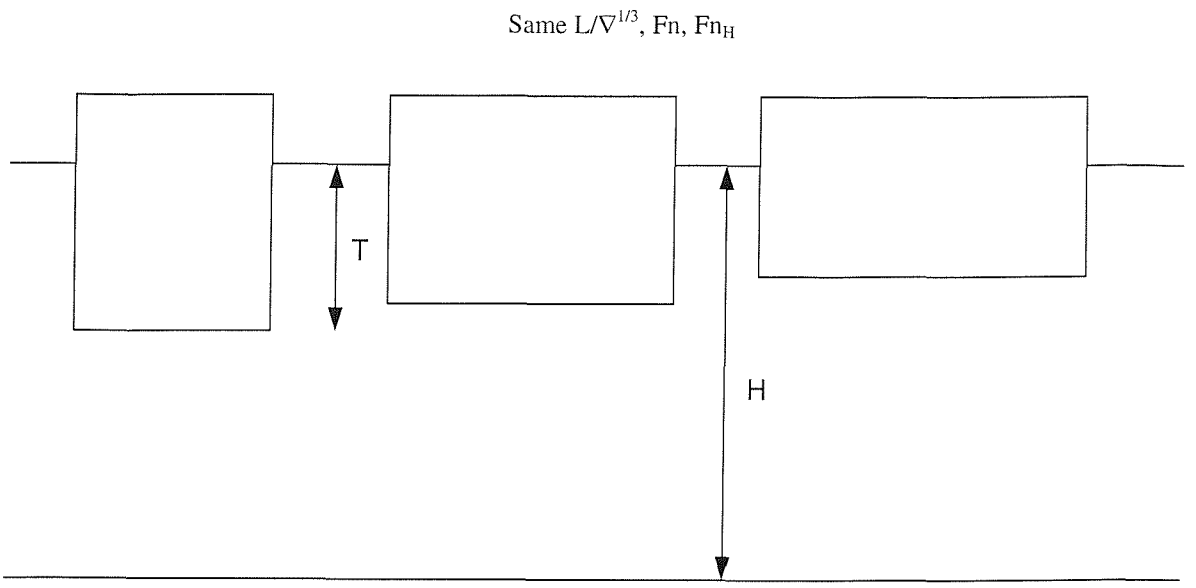

Fig.5.51 Diagram of model 5a, 5b, and 5c: effect of clearance under hull

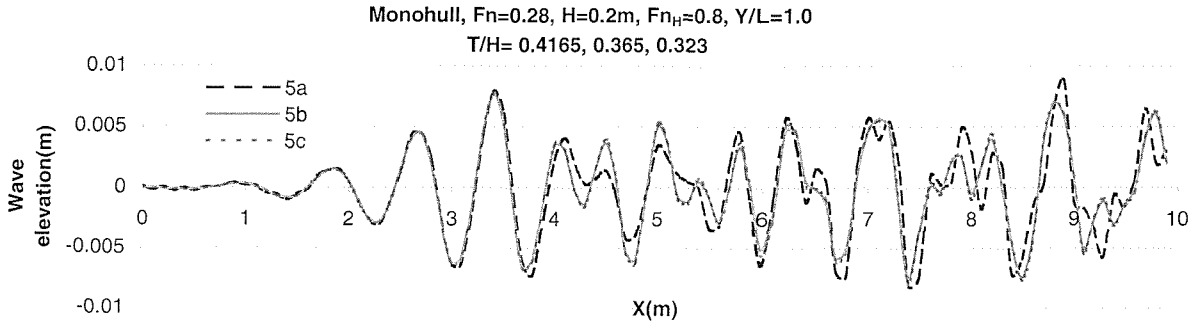

Fig.5.52 Theoretical wave cuts: NPL Monohull: 5a, 5b, 5c at Fn_H=0.8, Fn=0.28

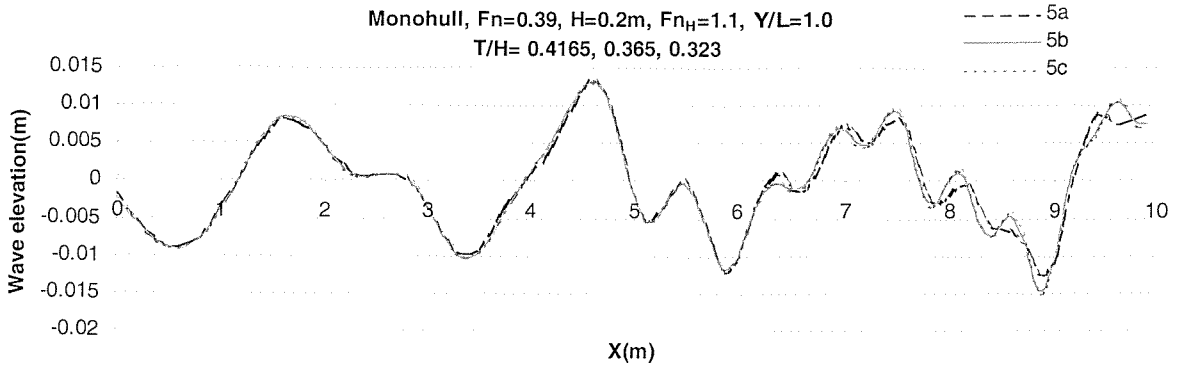

Fig.5.53 Theoretical wave cuts: NPL Monohull: 5a, 5b, 5c at Fn_H=1.1, Fn=0.39

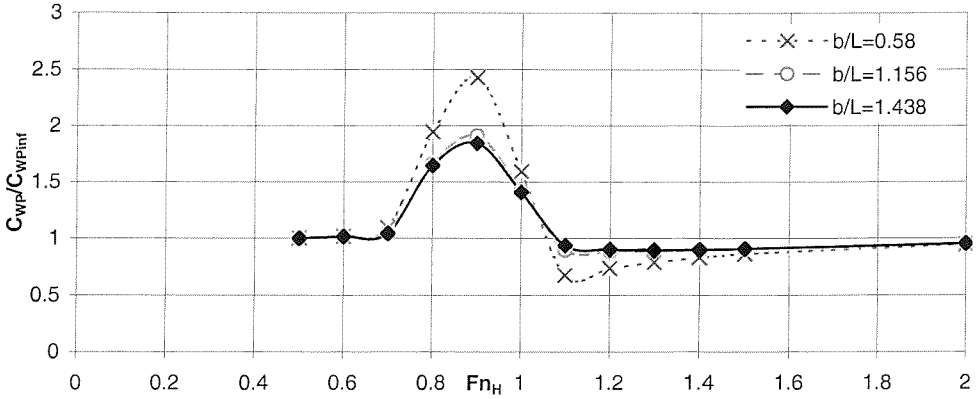

Fig.5.54 The effect of tank breadth on wave pattern resistance: 5b monohull H=0.4m

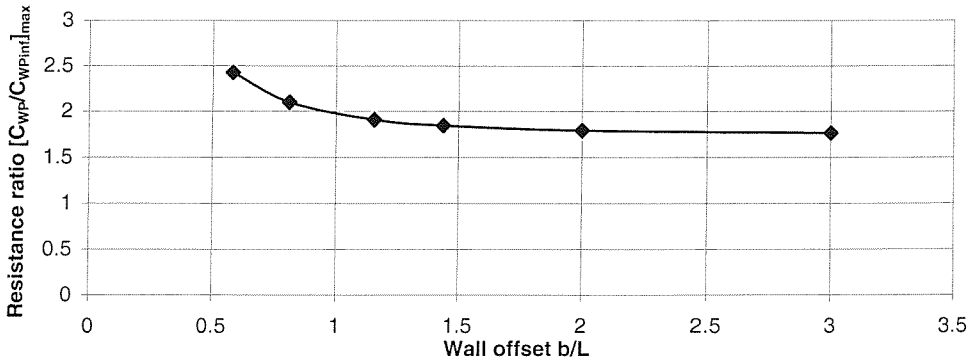

Fig.5.55 A comparison of the variation of maximum resistance ratio with distance from a wall in shallow water: 5b monohull H=0.4m Fn_H=0.9

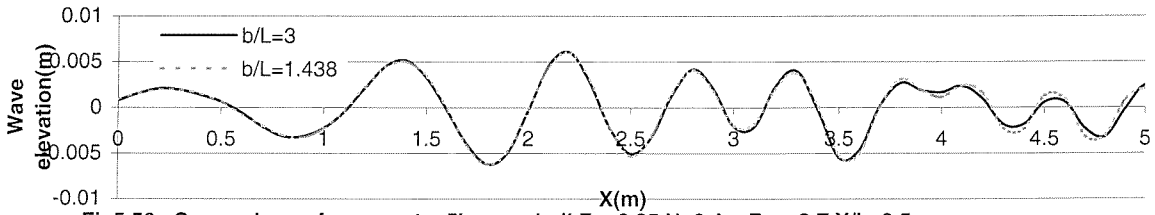

Fig5.56a Comparison of wave cuts: 5b monohull Fn=0.35 H=0.4m Fn_H=0.7 Y/L=0.5

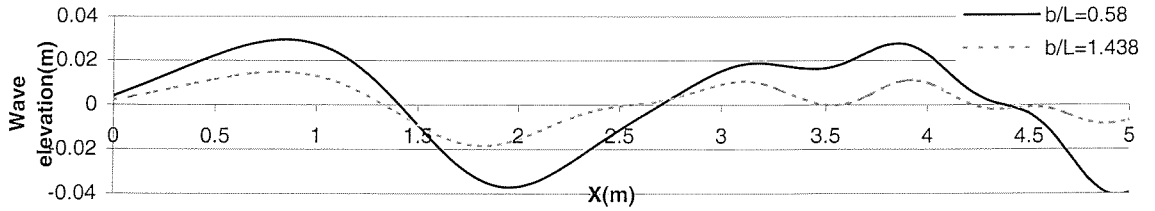

Fig5.56b Comparison of wave cuts: 5b monohull Fn=0.45 H=0.4m Fn_H=0.9 Y/L=0.5

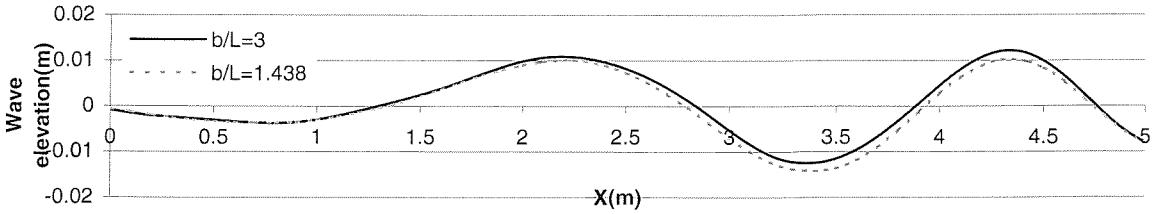

Fig5.56c Comparison of wave cuts: 5b monohull Fn=0.7 H=0.4m Fn_H=1.4 Y/L=0.5